Gélifiants supramoléculaires : synthèse, auto-assemblage, biocompatibilité et application pour la culture de cellules neuronales

Anaïs Chalard

Université Fédérale
Toulouse Midi-Pyrénées

THÈSE

En vue de l'obtention du

DOCTORAT DE L'UNIVERSITÉ DE TOULOUSE

Délivré par :

Université Toulouse 3 Paul Sabatier (UT3 Paul Sabatier)

Présentée et soutenue par :
Anaïs CHALARD

le 12 mars 2019

Titre :

Gélifiants supramoléculaires : synthèse, auto-assemblage, biocompatibilité et application pour la culture de cellules neuronales

---

École doctorale et discipline ou spécialité :
ED SDM : Chimie macromoléculaire et supramoléculaire - CO044

Unité de recherche :
IMRCP - Laboratoire des Interactions Moléculaires et Réactivité Chimique et Photochimique

Directeur/trice(s) de Thèse :

Juliette FITREMANN et Pierre JOSEPH

Jury :
M. Guy SCHLATTER, Rapporteur
M. Philippe BARTHELEMY, Rapporteur
Mme Isabelle MARIDONNEAU-PARINI, Examinateur
M. Vincent STUDER, Examinateur
Mme Laurence VAYSSE, Invité
M. Laurent MALAQUIN, Invité
Mme Juliette FITREMANN, Directeur de thèse
M. Pierre JOSEPH, Co-directeur de thèse

Supramolecular gels: synthesis, self-assembly, biocompatibility and application as scaffold for neuronal cell culture

Anaïs Chalard

A thesis submitted for the degree of Doctor of Philosophy

Université Toulouse 3 - Paul Sabatier

March 2019

PROJET FINANCÉ PAR L'ANR - PROJECT FUNDED BY THE ANR

Remerciements

Je remercie d'abord l'Agence Nationale de la Recherche pour avoir financé cette thèse dans le cadre du projet « Neuraxe ».

Je remercie ensuite les professeurs Philippe Barthélémy et Guy Schlatter d'avoir accepté d'être rapporteurs dans mon jury de thèse. Merci également à Isabelle Maridonneau-Parini et Vincent Studer d'avoir accepté les rôles d'examinateurs.

Je tiens ensuite à remercier mes deux directeurs de thèse, Juliette Fitremann et Pierre Joseph, de m'avoir donné l'opportunité de faire cette thèse sous leur encadrement. Je les remercie également pour la confiance qu'ils m'ont accordée durant ces trois années ainsi que pour leur bienveillance et leur enthousiasme. Ce fut un véritable plaisir de travailler au quotidien avec vous sur ce projet qui n'a cessé de me fasciner. Encore merci.

Je remercie également Laurence Vaysse auprès de qui moi, simple chimiste, j'ai appris les rudiments de la culture cellulaire. Grâce à elle, j'ai acquis une rigueur scientifique indispensable en recherche, mais également un goût pour l'étude des neurones. J'ai beaucoup apprécié travailler à ses côtés et son aide a été des plus précieuses pendant cette thèse. Pour cela, je la remercie encore chaleureusement.

Merci à tous les membres du laboratoire des IMRCP, à son directeur Christophe Mingotaud pour m'avoir permis de travailler dans son laboratoire, et à l'équipe IDeAS au sein de laquelle j'ai été accueillie. Un merci particulier à Barbara Lonetti pour les analyses en SAXS mais aussi à Clément Roux, Stéphane Gineste et Christophe Coudret qui nous ont souvent aidé sur le projet avec leur précieux conseils et expertise. Merci également à Delphine Bordignon pour toutes les synthèses et autres expérimentations qu'elle a réalisées au sein du projet.

Je remercie également les membres du LAAS-CNRS avec qui j'ai pu travailler ou interagir au cours de ma thèse, et en particulier à ceux de l'équipe MILE. Un grand merci aussi à Laurent Malaquin et Sandrine Assié-Souleille qui ont été d'une aide précieuse pour l'élaboration de ce projet, et merci à Xavier Dollat pour avoir confectionné certains de nos précieux outils pour nos recherches. Merci à Charline Blatché pour m'avoir formée et aidée au sein de la plateforme caractérisation.

Je remercie Isabelle Loubinoux de l'unité ToNIC à l'INSERM de Purpan pour m'avoir accueillie au sein de son équipe, mais également pour ses conseils en biologie.

Je remercie les personnes du CMEAB qui nous ont permis d'obtenir de magnifiques images de microscopie électronique au sein de leur plateforme. Merci également à Stéphanie Bosch et Brice Ronsin de la plateforme d'imagerie CBI-LITC constitutive de TRI qui nous ont permis d'avoir accès à leurs microscopes confocaux, ainsi que pour leurs ingénieuses astuces d'imagerie. Merci aux personnes de la plateforme de caractérisation de l'Institut de Chimie de Toulouse, en particulier à Nathalie Saffon-Merceron pour les analyses RX. Merci à Cyrille Rebout du LCC pour les analyses en ATG.

Je remercie également l'Institut National Polytechnique de Toulouse de m'avoir permis de m'exercer au tutorat et à l'enseignement et de m'avoir fait confiance deux années de suite pour encadrer les TP de Chimie à la Prépa des INP. Merci en particulier à Nathalie Beltran-Puel, Morgane Kopitsch et mes anciennes professeures, Marie-Claude Betbeder et Christine Cecutti, que j'ai eu le plaisir de retrouver cette fois-ci en tant que collègues.

Un grand merci également aux stagiaires que j'ai pu encadrer au LAAS au cours de ma thèse : Nathan Trouvain, Chloé Oneda et Morgane Mauduit. Votre travail a été d'une grande valeur pour moi et je vous dois une fière chandelle. Je vous souhaite à tous les trois une très bonne continuation dans vos études et plein de réussite.

Un merci tout particulier à Odile Dechy-Cabaret du LCC qui fut ma professeure pendant 2 ans à l'ENSIACET, mais qui surtout est le point de départ de cette histoire car sans elle je n'aurais jamais eu vent de ce sujet de thèse.

Vient enfin le tour des copains, de tous les gens avec qui j'ai passé de très bons moments dans mes deux labos et qui ont fait en sorte que ces trois années de dur labeur soient un peu plus douces. Je commence avec les non-permanents des IMRCP : merci à Baptiste, Delphine, Aurélie, Marvin, Maxime, Vivien, Laurent, Charlène, « Chin-Chin », Cécile, Lucie, Jordi, Baptiste M., Claire, Simon et tous les autres que j'oublie probablement (et je m'en excuse). Merci pour ces interminables parties de tarot entre midi et deux, au cours desquelles ma « poker face » vous aura certainement marqué à jamais, et pour le curling dans les couloirs (ça sera difficile maintenant de trouver quelqu'un qui passe aussi bien dans les cartons…) ! Au LAAS je remercie mes « copinettas » de bureau, Marianne et Inga avec qui j'ai beaucoup (trop ?) discuté de sujets « philosophiques » divers et surtout beaucoup rigolé ! Ces moments passés à vos côtés et votre soutien ont beaucoup compté pour moi. Merci à vous et à Jeffrey (et YouTube) pour la précieuse formule de trigonométrie ! Merci également à Bayan, Marion, Lyne, Amani, Nicolas, Léo avec qui j'ai également passé de très bons moments. A tous, je vous souhaite plein de réussite et de bonheur pour la suite.

Merci également à tous mes autres copains et proches d'ici et d'ailleurs pour votre soutien et vos encouragements.

Je remercie bien évidemment ma famille pour m'avoir toujours encouragée et cru en moi. Merci en particulier à ma sœur Céline, qui d'abord a gentiment corrigé l'anglais de ce manuscrit, mais surtout qui m'a toujours poussé à donner le meilleur de moi-même. Je ne serais probablement jamais arrivée jusque-là sans elle.

Enfin, un des plus beaux mercis pour mon chéri, Hugo, à mes côtés depuis déjà 6 ans. Tu as été d'un soutien des plus importants, dans les bons et surtout dans les mauvais moments… Merci pour la vaisselle, mais surtout merci pour tout l'amour que tu m'apportes au quotidien depuis tout ce temps. J'espère un jour te rendre tout ce que tu m'as donné. Je t'aime.

Table of content

REMERCIEMENTS **1**

TABLE OF CONTENT **1**

TABLE OF ABBREVIATIONS **5**

GENERAL INTRODUCTION **9**

I. MOLECULAR GELS **13**

I.1 SUPRAMOLECULAR ASSEMBLIES AND MOLECULAR GELS: DEFINITION AND STATE OF THE ART 13

I.1.1 Molecular hydrogels *15*

I.1.1.1 Definition and properties 15

I.1.1.2 Gelation triggers 17

I.1.1.2.1 Temperature 18

I.1.1.2.2 pH 18

I.1.1.2.3 Ion exchange 19

I.1.1.2.4 Solvent exchange 19

I.1.1.3 Characterization of hydrogels 20

I.1.1.3.1 Transition temperatures 20

I.1.1.3.2 Investigation of the microscopic structure 21

I.1.1.3.3 Spectroscopic methods 23

I.1.1.3.4 Mechanical properties 23

I.1.2 Examples of low molecular weight hydrogels *24*

I.1.2.1 Peptide derivative hydrogels 24

I.1.2.2 Simple amino acids and Fmoc derivatives 28

I.1.2.3 Sugar and nucleoside-derived low molecular weight gelators 29

I.1.2.3.1 Carbohydrate derivatives in general 30

I.1.2.3.2 Carbohydrate derivatives for cell culture applications 33

I.1.2.3.3 Nucleoside derivatives for cell culture applications 34

I.1.3 Conclusion *37*

I.2 SYNTHESIS AND CHARACTERIZATION OF CARBOHYDRATE-DERIVED HYDROGELATORS 39

I.2.1 Synthesis of the gelators and gelation ability *39*

I.2.1.1 Alkylgalactonamides and alkylgluconamides 40

I.2.1.2 Alkanoylglucamines and *N*-alkanoyl-*N*-methyl-glucamines 42

I.2.1.3 Selection of the molecules of interest 44

I.2.2 Gelation of alkylgalactonamides: modulation of the gelation conditions and characterization of the resulting gels *44*

I.2.2.1 Gelation of alkylgalactonamides at room temperature 44

I.2.2.2 Gelation under controlled cooling rates 45

I.2.2.2.1 Influence of the cooling rate on the gelation point density 45

I.2.2.2.2 Influence of the cooling rate on the fiber length 47
I.2.2.2.3 Influence of the cooling rate on the fiber width 48
I.2.2.3 Molecular organization in the fibers 51
I.2.2.4 Mechanical properties 52
I.2.2.5 Determination of the gelation points 54
I.2.2.6 Solubility of the molecules 55
I.2.2.7 Surface tension measurements 55
I.3 CONCLUSION 57
REFERENCES 58

II. APPLICATION AS CELL CULTURE SCAFFOLDS FOR THE GROWTH OF NEURONS 65

II.1 NEURAL STEM CELLS: GROWTH MECHANISMS AND ARTIFICIAL MATRICES 65
II.1.1 Neural stem cells: definitions, structure and growth mechanisms 66
II.1.1.1 Specificities of neuronal and glial cells 66
II.1.1.2 Neural stem cells 68
II.1.1.2.1 Formation of neurons and glial cells 68
II.1.1.2.2 Location in the adult brain and hNSCs retrieval 70
II.1.1.3 The growth of neurons 72
II.1.1.3.1 Growth factors 72
II.1.1.3.2 Neurite outgrowth 73
II.1.1.3.3 Guidance cues 75
II.1.1.3.4 Adhesion molecules 76
II.1.1.3.5 Substrate mechanics 77
II.1.2 In vitro growth of neural stem cells 78
II.1.2.1 Hydrogels 79
II.1.2.1.1 ECM derived hydrogels 79
II.1.2.1.2 Polysaccharide-derived hydrogels 81
II.1.2.1.3 Commercial hydrogels 81
II.1.2.2 Other types of scaffolds 82
II.1.2.3 Organoids 84
II.1.3 Conclusion 85
II.2 STUDY OF BIOCOMPATIBILITY AND CELL GROWTH WITH THE ALKYLGALACTONAMIDE HYDROGELS 87
II.2.1 Hydrogel preparation for biological assays 87
II.2.2 Biocompatibility assays with the alkylgalactonamide hydrogels 88
II.2.2.1 Cell survival study 89
II.2.2.2 Cell growth assessment 89
II.2.2.3 Determination of cell penetration inside the scaffolds: 3D cell growth 92
II.2.3 Characterization of cell growth and differentiation of hNSCs on Gal-C7 hydrogels 93
II.2.3.1 Development of immunolabeling techniques on hydrogels 94
II.2.3.2 Growth and differentiation of human neural stem cells 95
II.2.4 Biocompatibility tests with other hydrogels 96

II.3 DISCUSSION ON THE HYDROGELS AND THE BIOLOGICAL RESULTS 99
II.4 CONCLUSION 102
REFERENCES 103

III. SHAPING OF HYDROGELS 109

III.1 SHAPING OF HYDROGELS: TOWARDS 3D BIOPRINTING 109
III.1.1 3D printing and bioprinting 109
III.1.1.1 Different types of printing processes 110
III.1.1.2 3D printing and bioprinting of hydrogels 111
III.1.2 Wet spinning 114
III.1.2.1 Definition and principles 114
III.1.2.2 Applications: wet spinning of hydrogels 118
III.1.3 Objectives – Fiber alignment in the hydrogels 120
III.2 SHAPING AND FIBER ALIGNMENT OF THE ALKYLGALACTONAMIDE HYDROGELS AND OTHER FAMILIES 122
III.2.1 Extrusion tests 122
III.2.1.1 Gelation under a strain 122
III.2.1.2 Gel extrusions 124
III.2.2 Wet spinning of Gal-C7 hydrogels 127
III.2.2.1 Determination of the conditions leading to the formation of a filament: establishment of the phase diagrams 128
III.2.2.2 Physical characterization of the spinning process 130
III.2.2.2.1 Jet velocity 130
III.2.2.2.2 Analyses of the jet and filament diameters 132
III.2.2.3 Microscopic characterization and composition of the filaments 134
III.2.2.3.1 Optical and electronic microscopy observations 134
III.2.2.3.2 Thermogravimetric analysis 135
III.2.2.4 Lifetime of the wet spun filaments 136
I.3.1.1.1 Morphological transformation of the filaments into crystals 136
I.3.1.1.2 X-Ray analysis of the morphological transformation 139
III.2.2.5 Conclusion 141
III.3 APPLICATION OF WET SPINNING TO 3D PRINTING OF HYDROGELS 143
III.3.1 Printing set-up and phase diagrams 143
III.3.2 Width of the deposits 146
III.3.3 Thickness of the deposits 147
III.3.4 Microscopic structure of the hydrogel 150
III.3.4.1 Conclusion 151
III.4 CONCLUSION 152
REFERENCES 153

GENERAL CONCLUSION AND PROSPECTS 157

MATERIALS AND METHODS 159

Table of content

SCIENTIFIC CONTRIBUTIONS **179**

APPENDIXES **181**

RESUME DE LA THESE **191**

INTRODUCTION 191

I. SYNTHESE ET CARACTERISATION DE GELIFIANTS DERIVES DE COMPOSES SACCHARIDIQUES 196

II. ETUDE DE LA BIOCOMPATIBILITE ET DE LA CROISSANCE DE CELLULES NEURALES AVEC LES GELS D'ALKYLGALACTONAMIDES 200

III. MISE EN FORME DES HYDROGELS DE *N*-HEPTYL-D-GALACTONAMIDE 205

CONCLUSION 209

Table of abbreviations

2D	Two-dimensional
3D	Three-dimensional
AFM	Atomic force microscopy
BDNF	Brain-derived neurotrophic factor
bFGF	Basic fibroblast growth factor
BrdU	Bromodeoxyuridine
$CaCl_2$	Calcium chloride
CAM	Cell adhesion molecule
CNS	Central nervous system
Cryo-SEM	Cryo-scanning electron microscopy
DAPI	4′,6-diamidino-2-phenylindole
DMEM	Dulbecco's modified Eagle's medium
DMF	Dimethylformamide
DMSO	Dimethyl sulfoxide
DNA	Deoxyribonucleic acid
DSC	Differential scanning calorimetry
ECM	Extra-cellular matrix
EDC	1-Ethyl-3-(3-dimethylaminopropyl)carbodiimide
EDTA	Ethylenediaminetetraacetic acid
EGF	Epidermal growth factor
eq.	Equivalent
Et_3N	Triethylamine
EtOAc	Ethyl acetate
EtOH	Ethanol
FBS	Fetal bovine serum
FF	Diphenylalanine
FITC	Fluorescein isothiocyanate
Fmoc	Fluorenylmethyloxycarbonyl
G′	Elastic modulus
G″	Viscous modulus
GDNF	Glial cell line derived neurotrophic factor
GF	Growth factor
GFAP	Glial fibrillary acidic protein

Table of abbreviations

GFP	Green fluorescent protein
HA	Hyaluronic acid
HCl	Hydrogen chloride
HFP	Hexafluoropropan-2-ol
hMSC	Human mesenchymal stem cell
hNSC	Human neural stem cell
HPLC	High-performance liquid chromatography
ID	Inner diameter
IKVAV	Isoleucine-lysine-valine-alanine-valine
LMWG	Low molecular weight gelator
MA	Methacrylate
MAP2	Microtubule-associated protein 2
MeOH	Methanol
MTT	3-(4,5-dimethylthiazol-2-yl)-2,5-diphenyltetrazolium bromide
Na_2CO_3	Sodium carbonate
NaOH	Sodium hydroxide
NeuN	Neuronal nuclei marker
NGF	Nerve growth factor
NHS	*N*-Hydroxysuccinimide
NMR	Nuclear magnetic resonance
NPC	Neural progenitor cell
NSC	Neural stem cell
O4	Oligodendrocyte marker
OD	Optical density
PA	Peptide amphiphile
PB	Phosphate buffer
PBS	Phosphate buffered saline
PC	Polycarbonate
PDMS	Polydimethylsiloxane
PEG	Polyethylene glycol
PLGA	Poly(lactic-co-glycolic acid)
PTFE	Polytetrafluoroethylene
RADA	Arginine-alanine-aspartic acid-alanine
RGD	Arginine-glycine-aspartic acid
RNA	Ribonucleic acid
SAFiN	Self-assembled fibrillar network

SAP	Self-assembling peptide
SAXS	Small-angle X-ray scattering
SEM	Scanning electron microscopy
SGZ	Subgranular zone
SVZ	Subventricular zone
TEM	Transmission electron microscopy
TGA	Thermo-gravimetric analysis
$T°_{amb}$	Room temperature
$T°_{gel \rightarrow sol}$	Transition temperature from gel to solution
$T°_{sol \rightarrow gel}$	Transition temperature from solution to gel
Tuj-1	Anti-β3-tubulin antibody
WAXS	Wide-angle X-ray scattering
wt %	Weight percent
Y_0	Initial modulus

General introduction

The brain is probably the most complex organ in biology, in terms of understanding, architecture and structure. This is why when a lesion such as a stroke or a brain trauma happens, it is particularly difficult to fully recover all motor and cognitive functions potentially resulting in heavy handicaps. To repair the damaged connections these lesions incur, stem cells, that can produce neurons and glial cells, colonize the injured zone. However, it is a long process for it takes a while for those cells to migrate, divide and differentiate. Most of the time they are also not enough to regenerate a functional tissue. Moreover, the biological environment induced by a lesion is very unfavorable for stem cells as it inhibits their growth and their differentiation, most of the time resulting in cell death. This is why regeneration of brain lesions is particularly complicated. A solution to this problem could be the direct post-traumatic transplantation of pre-differentiated neural stem cells into the patient's brain to directly provide functional neurons inside the lesion and accelerate recovery. Stem cells could even originate from the patient himself having been collected prior to the lesion as a preventive measure to proceed to autologous grafts that cause less immune response and less complications.

Together with the repair of brain lesions, another great advance in biology would be the possibility to recreate *in vitro* brain models. This could be helpful to study some of its functions and pathologies, but also to study drug-delivery or of the effects of some drugs on cells, etc. These brain models could then be coupled to other models of organs and these *in vitro* biological systems could even one day replace the use of animals for *in vivo* biological trials.

Tissue engineering brings answers to these challenges. This scientific discipline has been developing for about 30 years and can be described as "an interdisciplinary field that applies the principles of engineering and the life sciences toward the development of biological substitutes that restore, maintain, or improve tissue function" by Langer and Vacanti[a] in 1998. Living cells alone or put together with artificial scaffolds are developed to recreate biological tissues as close as possible to *in vivo* conditions. One of the main goals of tissue engineering is to later be able to develop *in vitro* tissues in order to reduce the need of organs for transplant. This discipline is therefore particularly suited for the issues described above.

[a] Langer, R.; Vacanti, J. P. Tissue Engineering. *Science* **1993**, *260* (5110), 920–926. https://doi.org/10.1126/science.8493529.

In order to cure brain lesions, a possible strategy would be to grow neural stem cells *in vitro* on a hydrogel scaffold so that they start to differentiate and organize as functioning cells, and then to implant the said scaffold directly into the patient's brain (Figure 0-1).

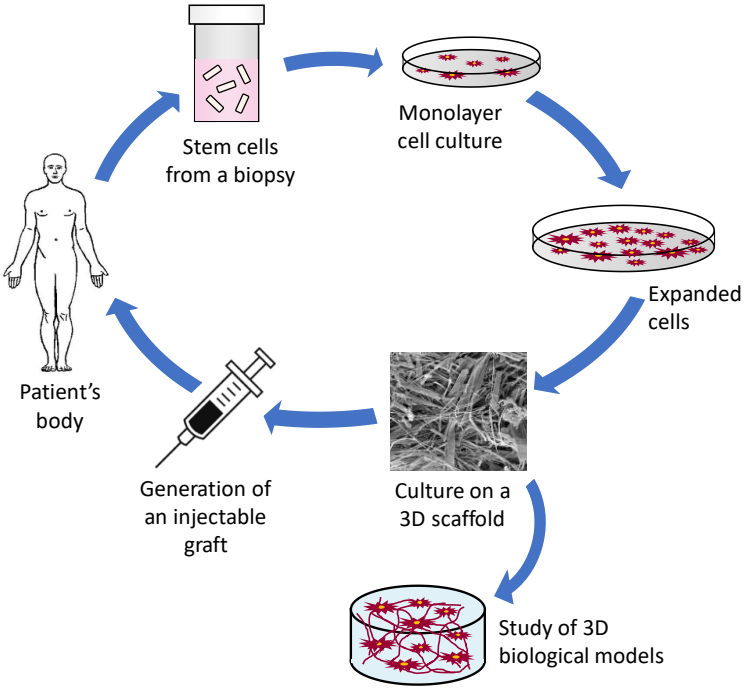

Figure 0-1: Tissue engineering approach for the generation of injectable grafts out of stem cells or for the production of 3D in vitro models.

To obtain a biocompatible material, preferably injectable, the main focus of research should be the scaffold's properties so that neural cells can grow inside. Such a scaffold could also be used for the study of three-dimensional *in vitro* biological models.

On top of that, tissue engineering could help mimic the *in vivo* organization of neurons. As a matter of fact, they form aligned bundles inside the cortex, with their cellular bodies at the surface and their axons plunging into the depth of the tissue. The developed biomaterial could reproduce that anisotropic structure of the cortex in order to obtain aligned axons inside the scaffold. Artificially recreating this organization could enable us to get a more accurate model but also, if implanted *in vivo*, this could improve the efficiency of the connections between the host tissues and the graft. This organization of the material could be obtained by various strategies. Moreover, structures with very precise and even personalized design could be built thanks to three-dimensional printing.

The goal of this present work is to develop a novel biomaterial for the growth and differentiation of neural stem cells with the aim of reproducing best the *in vivo* conditions for the cells in order to develop artificial brain tissue. Most importantly, there is a need to find a biomaterial with mechanical properties adapted to the growth of neurons. It is now well known that, in order to

differentiate, neural stem cells need very soft materials, with a rigidity close to that of brain tissue. The second objective is also to explore different strategies to shape the gel in order to create aligned patterns and/or to be 3D printed. The final aim of this research is to implant grafts made out of this material and stem cells for the repair of brain lesions.

This manuscript will be divided in three distinct chapters. The first one will deal with the design, the synthesis and the characterization of supramolecular hydrogels with very simple chemical structures that should be suited for the growth of neural stem cells. In this chapter, after introducing and reviewing the different types of low molecular weight hydrogels developed by the scientific community, the hydrogels that we developed will be described and discussed. The second chapter will focus on the biocompatibility and biological assays of our hydrogels with cells of a neuronal cell line and with adult human neural stem cells. In the introduction of this chapter, the specificities of the growth of neural stem cells and which strategies are implemented nowadays to address this issue will be tackled. Finally, the shaping of these hydrogels will be described in the third part after seeing beforehand which methods could be employed in our case.[b]

[b] N.B.: Some parts of this thesis are directly quoted from our published article: Chalard, A.; Vaysse, L.; Joseph, P.; Malaquin, L.; Souleille, S.; Lonetti, B.; Sol, J.-C.; Loubinoux, I.; Fitremann, J. Simple Synthetic Molecular Hydrogels from Self-Assembling Alkylgalactonamides as Scaffold for 3D Neuronal Cell Growth. *ACS Applied Materials & Interfaces* **2018**, *10* (20), 17004–17017. https://doi.org/10.1021/acsami.8b01365.

I. Molecular gels

I.1 Supramolecular assemblies and molecular gels: definition and state of the art

By definition, a supramolecular assembly is "the formation of a well-defined complex of molecules held together by noncovalent bonds" (from Nature website). Supramolecular assemblies also result from more flexible molecular organizations without very specific interactions between them. They can be found everywhere in nature and living organisms. Every single cell is actually in itself a supramolecular assembly: its membrane results from the association of many small molecules called phospholipids, which self-assemble by weak interactions to form a double layer of molecules that then consists in the final membrane (Figure I-1). Organelles inside the cell are also a result of self-assembling molecules.

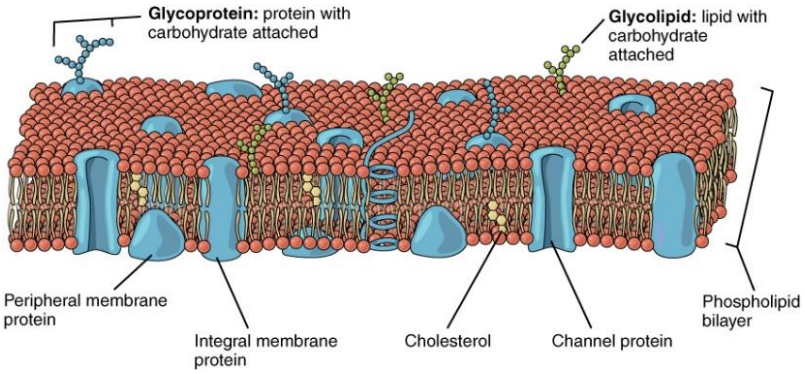

Figure I-1: Representation of the phospholipid bilayer that – amongst other components – forms the cell membrane (source: Wikipedia).

Self-assembly mechanisms govern many other domains. Proteins are formed, shaped and interact through supramolecular mechanisms. The extra-cellular matrix (ECM) is composed of many proteins such as collagen that self-assemble to form a network supporting the cells. In different domains, soaps for instance are amphiphilic molecules (molecules composed of a polar hydrophilic head and an apolar hydrophobic tail) called "surfactants" that form micelles once in solution in water by self-assembling mechanisms.

Self-assembly can also result in the formation of gels. Gels can be qualified as semi-solids: a liquid phase is trapped by a three-dimensional solid network thanks to surface tensions and capillary forces. This three-dimensional network is formed by the intertwining of long and unidimensional molecular structures such as macromolecules, fibers, colloidal strings, etc. The structures

composing this network can be reticulated either physically (physical gels) or chemically (chemical gels) and can range from the nanometric to the micrometric scale.

We call hydrogels the ones made of water and organogels the ones that result from organic liquids. Hydrogels can result from the self-assembly of small molecules (low molecular weight gelators or LMWGs) but also from polymers (Figure I-2).[1] The firsts are called "molecular gels" whereas the others are polymeric gels, which either can be the result of entangled polymer chains or be reticulated by covalent bonds (cross-linked gels)[2].

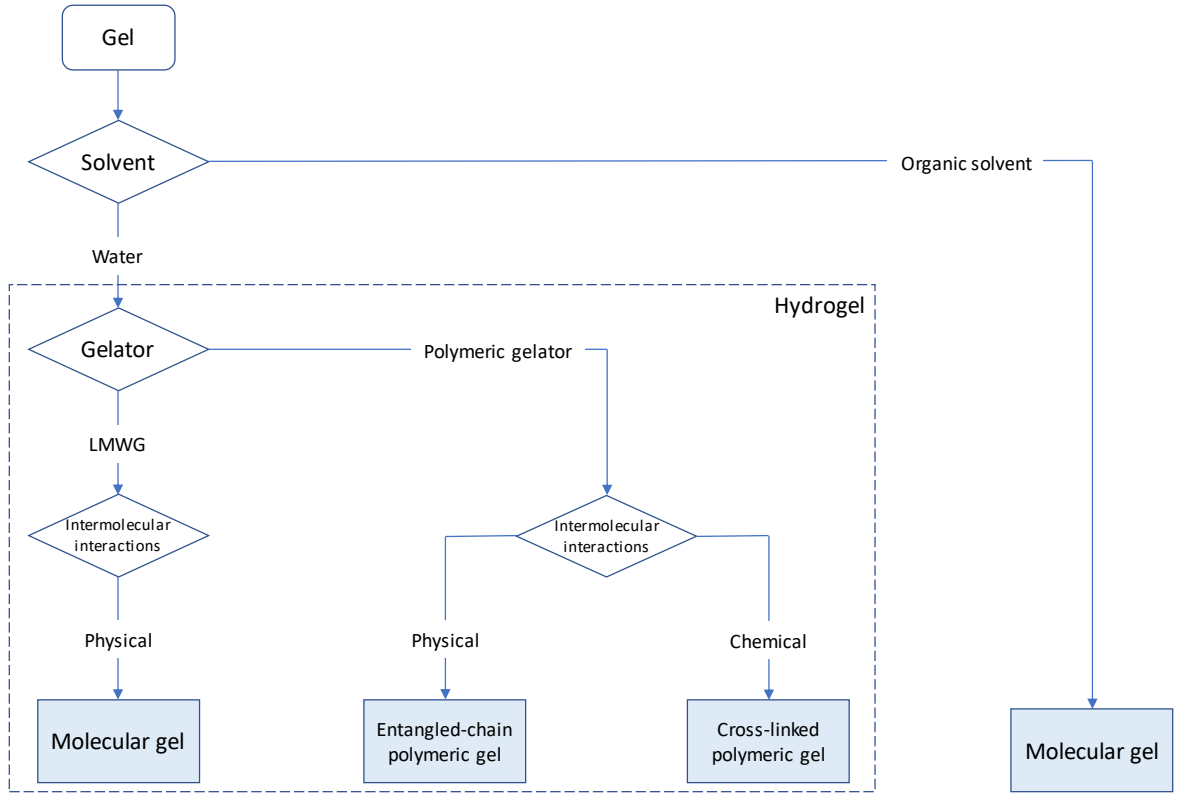

Figure I-2: Classification of the different classes of gels (adapted from [1] and [3]).

This specific application of supramolecular assemblies has gained much interest in the past decades because of the various applications of gels in many scientific domains and the interesting properties of self-assemblies. Because of its application to biological systems where aqueous mediums are preferred, our work focuses specifically on molecular hydrogelators.

After detailing their formation and their characterization, we are going to discuss the state of the art concerning molecular hydrogels, with an emphasis on cell culture applications.

I.1.1 Molecular hydrogels

I.1.1.1 Definition and properties

In the case of molecular gels, the small molecules called "gelators" self-assemble to form fibers that then entangle to form a three-dimensional network that is able to hold a liquid, and thus form a gel (Figure I-3). This self-assembled fibrillar network (SAFiN) is held together by noncovalent intermolecular interactions such as hydrogen bonding, van der Waals interactions, π-π stacking in the case of molecules containing aromatic moieties, or hydrophobic interactions in the case of hydrogels.[4]

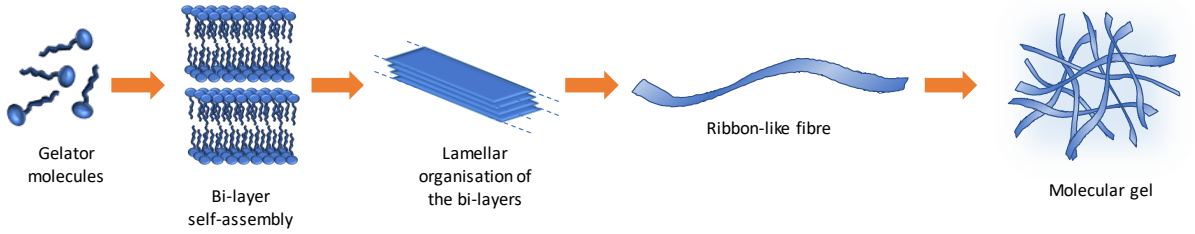

Figure I-3: Description of the self-assembly of small gelator molecules leading to the formation of a molecular gel.

The gelator molecules form supramolecular assemblies because intermolecular interactions with each other are favored against interactions with the solvent. That is why hydrogelator molecules contain most of the time hydrophobic groups in order to reduce their solubility and thus their affinity with water. Indeed, hydrogen bonding is an efficient mean for molecules to interact with each other, but it also occurs with water molecules. A hydrogelator thus needs to contain hydrophobic moieties to form hydrophobic interactions for the molecules to self-assemble, otherwise the hydrogen bonds would only occur with water and the molecule would just be dissolved.[5] Certain chemical groups favor the formation of molecular assemblies such as aromatic rings for π-π stacking, carbonylated functions like amides or ureas and alcohols or amines to create hydrogen bonds, etc. In order to obtain hydrogelators, hydrophobic moieties should also be included with the use of alkyl chains to create Van der Waals interactions. However, even if the requirements for obtaining a gelator are well understood, it is still very hard to predict if a molecule will gel a solvent or not. Adapting molecules from known gelators often result in new ones, but synthesizing a new one "out of thin air" is often more complicated.[6] Indeed, self-assemblies rely not only on intermolecular bonds but also on molecular arrangements and conformation. For instance, two diastereomeric compounds can have completely different gelling properties: one can easily give a hydrogel at very low concentration, whereas its diastereomer will be soluble (see I.2.1.1). Nevertheless, chemical modelling is more and more employed

complementarily with organic chemistry, and it is sometimes possible to accurately predict the gelling properties of a molecule.[7]

Moreover, for the fibers to be formed, the concentration of gelator in solution should be higher than the critical aggregation concentration (CAC), which is the minimum concentration for which self-assembled aggregates can form. Above this concentration, the self-assemblies can further grow to become lamellar structures[8] that then extend and form fibers of the SAFiN[9] (Figure I-3). In addition, despite its reduced interaction with the solvent, the self-assembly of the molecules should not result in the recrystallization or precipitation of the compound. Convenient interactions between the supramolecular fibers and the solvent must take place so that the solvent can swell the network and form the gel. Finally, one direction should be favored for the growth of the self-assembly in order to obtain fibers and not micelles.

Molecular hydrogels have different specificities compared to polymeric gels that can turn to advantages for some applications. First, because of the weak interactions that govern their formation, the dynamics of molecular hydrogels are different compared to polymeric gels.[1] In the context of using them as biomaterials, this should affect the clearance. There is an equilibrium between the free molecules and the ones in the assembly which explain a faster degradation as well as a different bioavailability/toxicity compared with polymers. This is particularly interesting for the fabrication of biological implants for instance, since once inside the body, they can then rapidly degrade within several days to months. This also affects their rheological behaviors such as self-healing properties: because of the dynamics of molecular gels, these can sometimes undergo strain and reform afterwards in their initial organization. This property is particularly desired for injectable materials, for example. However, it also results in a weaker mechanical strength, which can sometimes actually be an advantage for the culture of cells that need softer gels to grow, as it is the case for neurons.[10]

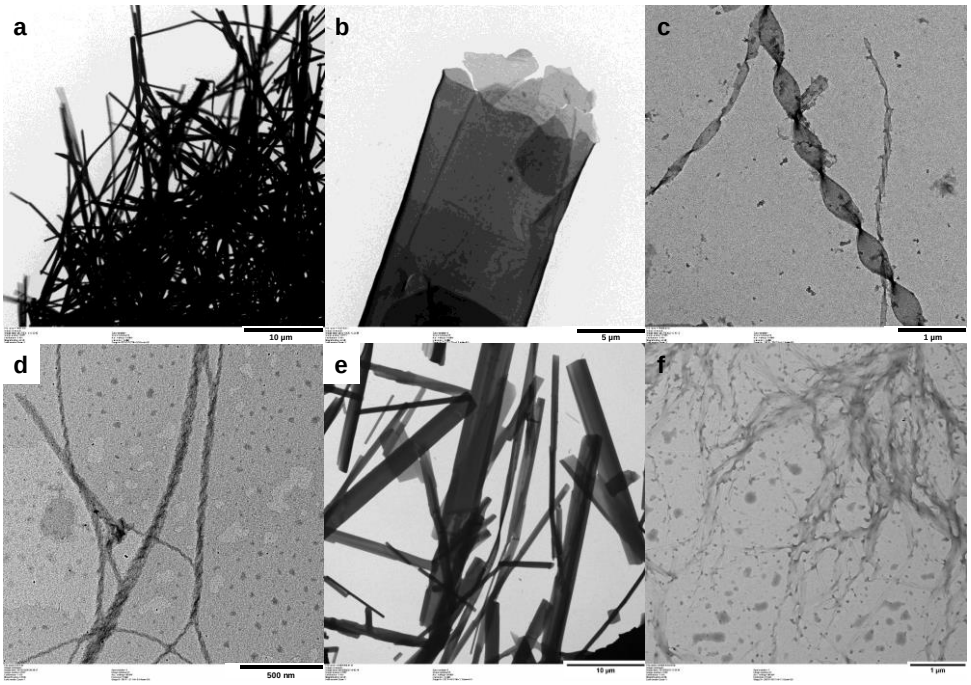

Figure I-4: Examples of self-assembled structures obtained from various small gelator molecules synthesized in our laboratory. a. N-hexyl-D -glucoheptonamide (scale bar: 10 µm). b. N-dodecyl-D-glucoheptonamide (scale bar: 5 µm). c. N-dodecanoyl-D-glucamine (scale bar: 1 µm). d. Lact-Tz-C16 (scale bar: 500 nm). e. N-heptyl-D-galactonamide (scale bar: 10 µm). f. N-methyl-N-dodecanoyl-D-glucamine (scale bar: 1 µm).

Secondly, contrary to polymers where the gels network is composed of macromolecules, with molecular gels, the composing fibers can have various nano-/microscopic structures: grooved fibers, ribbons, helixes, etc. (Figure I-4). These different structures can influence their applications, like in the case of cellular alignment in hydrogels for instance. Finally, molecular gels also have a better "intrinsic reproducibility", meaning that the fibers are composed of the same identical molecules. If the gelator molecules are well purified, the gels will always have the same composition. With polymers, the distribution in the macromolecules' lengths can vary from one batch to another, which can result in variations in the gelling properties. However, in the case of molecular gelators, their chemical functionalization is much more complicated than for polymers, because it can alter a lot the self-assembling properties.

For all these reasons, we got particularly interested in molecular hydrogels rather than polymeric ones. Molecular hydrogelators can be of different natures such as peptides or various small organic molecules. They can be based on natural derivatives as well as being entirely synthetic. Nevertheless, whatever their nature, their properties and structures are somehow very similar.

I.1.1.2 Gelation triggers

Here is a brief presentation of several gelation triggers such as temperature, pH, ion or solvent exchange. What triggers the gelation is actually a change in the affinity of the molecule with the

solvent, which makes it less soluble and provokes self-organization. Other gelation mechanisms exist such as sonication or chemical or enzymatic reactions leading to the formation of gels.[11] Yet, these methods are less common in the literature in the case of molecular gels so we chose not to describe them here.

I.1.1.2.1 Temperature

One of the most common mechanism that can trigger gelation of molecular gelators is a change in temperature. The gelator molecules are dissolved in water at high temperature and by cooling down the solution, the gel is formed. Indeed, temperature affects the strength of intermolecular bonds: at high temperature, the hydrogen bonds are easily broken because of the high energy but when the temperature lowers, the intermolecular interactions become more persistent and the molecules can self-assemble. Most hydrogels can be formed through such mechanism. The transition temperature to go from the solution (sol) to the gel is called $T°_{sol \rightarrow gel}$ whereas the temperature for the opposite phenomenon is $T°_{gel \rightarrow sol}$. Usually these two temperatures are not the same: a hysteresis is often observed in the cycles of sol→gel and gel→sol transitions with most of the time $T°_{gel \rightarrow sol} > T°_{sol \rightarrow gel}$. This inherent property of a gelator has to be taken into account for its further application. For biological application for instance, the $T°_{gel \rightarrow sol}$ should not be lower than 37 °C, otherwise the gel can be dissolved at biological temperatures.

I.1.1.2.2 pH

pH is also often a trigger for gelation thanks to protonation/deprotonation mechanisms which modifies the intermolecular interactions and thus the fibrillar network via hydrogen bonding and van der Waals interactions. Gelators containing carboxylate or amine groups often result in pH-triggered hydrogels for those moieties can easily be (de)protonated. The charged compounds are more soluble in water compared to the protonated ones, resulting in a difference of interaction with the solvent and thus in the self-assembly of the protonated molecules (Scheme I-1).

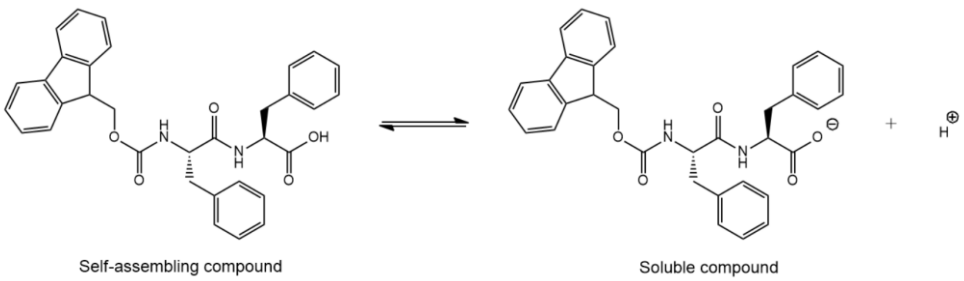

Scheme I-1: Equilibrium between the two species of a self-assembling compound containing a carboxylic group, example of a Fmoc-diphenylalanine gel.

It is a very convenient way for gelation because it does not require heating – which sometimes could deteriorate the gelators – and a small addition of a base or an acid can consequently and precisely change the pH. The gelation can then occur in a very controlled manner, especially in the case of controlled release of protons. For some hydrogels, gelation can be triggered by both temperature and pH.

I.1.1.2.3 Ion exchange

For some hydrogels, gelation can also occur with the presence of some ionic species. Those gels are often prepared by mixing the gelator with an ionic medium such as an aqueous solution of $CaCl_2$ for instance.[12] In this case, it is the ionic interactions between the salts and the charged parts of the gelator that allow the formation of molecular assemblies. This preparation technic is very interesting for applications such as drug delivery[13] or cell encapsulation. Indeed, cells are particularly sensitive to pH and temperature and in order to encapsulate them in a hydrogel, ion exchange is a convenient and rather harmless method. The only limitation here is that you have to have charged gelator molecules.

On the same trend, the ionic force of the solvent can influence a lot the state of a hydrogel. For instance, a gelator can be well soluble in pure water, but once PBS is added to the solution, the ionic force of the solvent is modified as well as the solubility of the gelator in this new medium. Since the solubility is decreased, the self-assembly of the molecules and thus the gelation occur. Here again, many hydrogelators for biological applications are prepared this way for the encapsulation of live cells.[14]

I.1.1.2.4 Solvent exchange

Another and less employed way to form hydrogels is with the exchange of solvents. The gelator molecules are first dissolved in a solvent where it is particularly soluble and which is miscible to water (most of the time an organic solvent). Then water is added to the solution, and the gelation occurs.[15,16] Indeed, once the gelator molecules are in contact with water, the solubility decreases and these ones self-assemble following the same mechanisms as previously described to form the gel. The organic solvent being miscible with water, this one is easily rinsed from the gel and a solvent-free hydrogel can thus be obtained. The gelator concentration in the solvent can be higher than the one usually employed in water for the formation of the gel by temperature changes. Direct cell encapsulation can be achieved thanks to this technique as well, by mixing a gelator solution in a solvent with cells dispersed in cell culture medium for instance. Dimethyl sulfoxide (DMSO) is a good example of an organic solvent for this application because it is tolerable for cells in a certain concentration range.[17]

However, the disadvantages of this technique are that sometimes some solvent can remain in the gel if it is not rinsed enough, which can then be detrimental if used for cell culture. Moreover, the gelation occurs only at the interface between the two solvents. Thanks to diffusion, the water can gel the system further but it is often hard to get homogenous gels with this technique.

I.1.1.3 Characterization of hydrogels

One of the first visual tests to know if a gel is obtained is traditionally flipping the preparation vial in order to see if the gelator solution hangs to the bottom or if it drops. This test being helpful for a first assessment, yet other characterization techniques exist in order to assess a gel's properties.

I.1.1.3.1 Transition temperatures

Transition temperatures between the gel and the solution states are key parameters for a gelator molecule, especially for the gel's further application. In order to determine $T°_{sol \rightarrow gel}$ and $T°_{gel \rightarrow sol}$, differential scanning calorimetry (DSC) can be used. It relies on the measurement of the difference of enthalpy between a sample and a reference through temperature cycles. According to the sign of the measured enthalpy, we can know if the phenomenon is exothermic or endothermic. This way, the sample's physical changes such as melting, solidification or gelation and their corresponding temperature can be determined (Figure I-5).

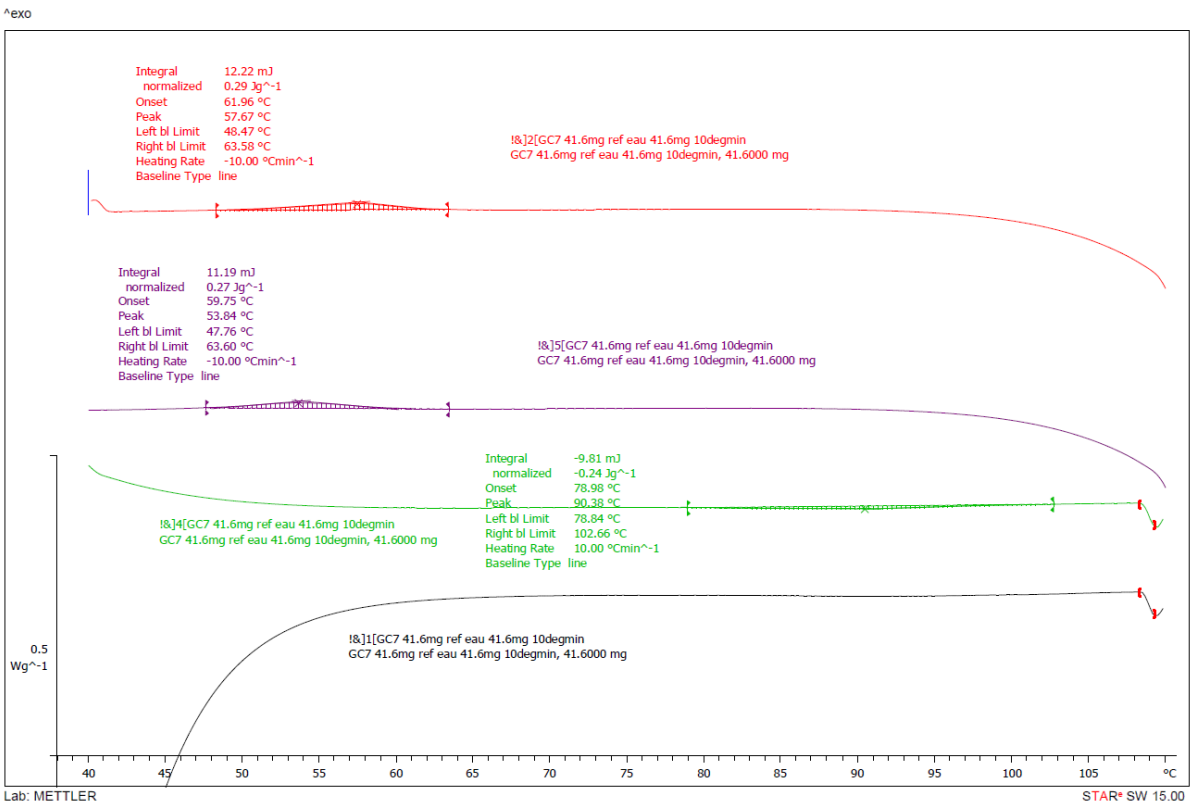

Figure I-5: Example of a hydrogel thermogram obtained by DSC.

I.1.1.3.2 Investigation of the microscopic structure

In order to have an insight into the microscopic and self-assembled structures of hydrogels, several techniques enable us to explore these at different scales.

First of all, transmitted light optical microscopy observations give a first overview of the gels architecture. If the hydrogel is translucent enough so that the light can pass through, its fibers can be observed on the condition that their size permits it. Typically, the threshold under which fibers cannot be observed is around 4 µm. For this reason, this technique is rarely used because in most cases, molecular gels are composed of rather nanometric fibers.

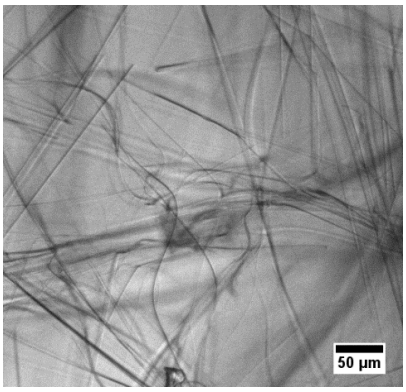

Figure I-6: Optical microscopy observation of an N-heptyl-D-galactonamide hydrogel.

If optical microscopy has insufficient magnification, electronic microscopy usually gives better tools for observation. Being a transmitted or scanning electron beam, electronic microscopy can achieve magnifications more than 30 000 x and even resolutions up to 50 pm[18]. For transmission electron microscopy (TEM), the sample has to be deposited on a grid in a very thin layer (see Figure I-4). For scanning electron microscopy (SEM), the electron beam scans the surface of the sample. Since not all surfaces reflect electrons, a thin metal layer is usually deposited on the sample. Yet, for most of hydrogels, cryo-SEM is usually preferred because the sample drying during regular SEM can alter the microscopic structure a lot. In order to keep the native network of the hydrogel as much as possible, this one is first frozen to cryogenic temperature, fractured and then metallized after a small layer of ice is freeze-dried. This technique still displays some freezing artefacts because of the volume increase of the ice that tends to push on the microstructures. Nevertheless, most of the microscopic organization is preserved.

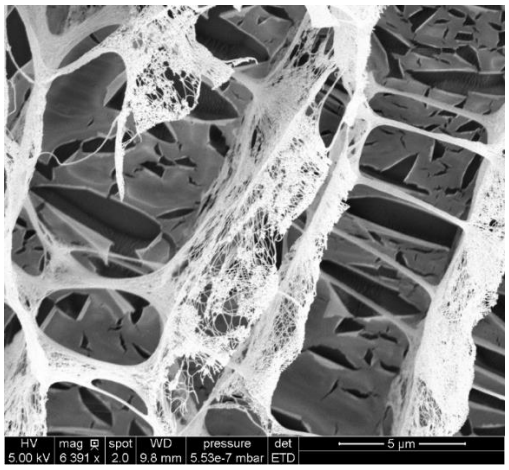

Figure I-7: Example of a cryo-SEM observation of a hydrogel (Lact-Tz-C16 from 19) showing ice artefacts with their typical alveolar pattern.

Atomic force microscopy (AFM) or scanning force microscopy (SFM) can be another technique used to characterize the structure of molecular gels, especially in the case of very thin nanometric fibers. Indeed, the principle of this kind of microscopy is the scanning of a surface with a probe. A resolution of about fractions of a nanometer can be achieved through this non-optical technique. It also provides an insight into the roughness of the material, as well as local mechanical properties. However, AFM does not provide the inner structure of a hydrogel, which can be different from the one on the surface. The scanned area is also much reduced compared to other microscopic techniques and the acquisition can take longer. What is more, many artefacts can be generated by this method, because of the probe, the operating environment or the sample itself. Thus, AFM gives interesting information about the gel's properties, but it has to be used complementary to other microscopies.

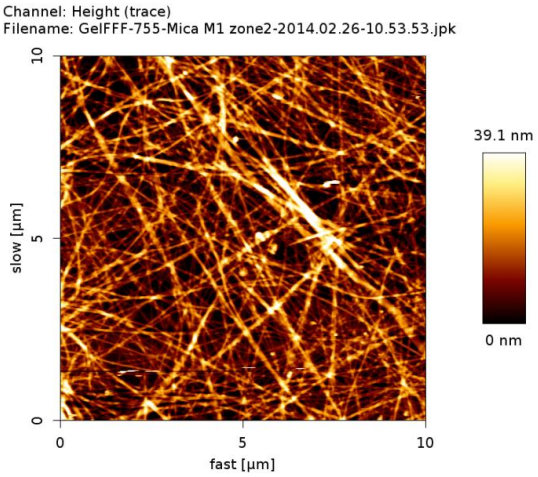

Figure I-8: Example of an AFM image of an air-dried Fmoc-diphenylalanine gel (contact mode, channel height).

I.1.1.3.3 Spectroscopic methods

For the determination of the molecular organization in hydrogels, other techniques have to be implemented. Small-angle X-ray scattering (SAXS) allows us to have an insight into the molecular organization in the hydrogel's SAFiN and thus to understand better how the gelator molecules self-assemble to form the fibers. It gives information on the size of the stacked structures forming the self-assemblies. Infrared spectroscopy (IR) can also be used and gives information about the intermolecular interactions, such as hydrogen bonds that are easily characterized through this method. Nuclear magnetic resonance (NMR) can also help detect which intermolecular interactions occur in the self-assemblies, again especially with hydrogen bonds.

I.1.1.3.4 Mechanical properties

Characterization of hydrogels does not only rely on the determination of the microscopic structure. Their rheological and mechanical behaviors can also be assessed which are rather specific in the case of gels. In oscillatory dynamic rheology, by definition a gel has an elastic modulus (G′) superior to its viscous modulus (G″) over a large frequency range, from high frequency oscillations (typically 10-100 Hz) to low frequency oscillations (typically 10-2 / 10-3 Hz). Concretely, it means that when a sinusoidal strain (or sinusoidal stress) is applied to the gel, within the limits of the linear viscoelastic region, this one must behave like an elastic solid (featured by G′) and not flow like a liquid (featured by G″), and this is expressed by $G' > G''$.[7] It has to include low frequencies because when at rest (when $f \rightarrow 0$, i.e. on the long term), the gel has to remain "solid" and must not flow. Also, G′ and G″ should remain constant over this range of frequencies. These rheological behaviors are characteristic of gels and should be assessed when hydrogels are prepared.

Another way to access the mechanical properties of hydrogels is by doing uniaxial compression tests. Here the stress underwent by the sample is measured against the displacement of the mobile. A strain ramp (from 0 to less than 10 % of the height of the sample) is applied on a cylinder of the sample and the resulting stress is then measured. The sample can be confined during the test, but then wall effects have to be taken into account with specific equations. Within the linear elastic regime (i.e. for low strains), the resulting curve has a linear part. The slope of this linear region corresponds to the Young's modulus of the material, which characterizes its stiffness.

Researchers in the domain of biomaterials have been more and more interested in the mechanical properties of their materials. Indeed, it has been shown that the rigidity of a biomaterial can influence significantly the development of the cells cultured on them. The studies demonstrated that the stiffness of a biomaterial should be similar to the tissue it tries to imitate. For instance,

for the growth of neurons, the biomaterials used should have a rigidity close to that of the brain, which is a very soft tissue (see chapter II.1.1.3.5). For this reason, mechanical strength of hydrogels is an important property to characterize.

I.1.2 Examples of low molecular weight hydrogels

In this part, we will describe LMWGs that are the most described in literature, with a focus on cell culture applications. We will first review peptide then amino acid and Fmoc-derivatives gelators, and then we will particularly discuss hydrogelators based on carbohydrates.

I.1.2.1 Peptide derivative hydrogels

One class of molecules that, according to their length, can sometimes belong to both polymer and molecular gels is that of peptide derivatives. Peptides are composed of at least two amino acids linked by a peptide bond and up to fifty amino acids (if more than that, they are considered as proteins). When a peptide contains many amino acids, we talk about polypeptide and these molecules can belong to the polymer class, or are at least referred to as "macromolecules". The gels formed by these polypeptides can thus be considered as polymer gels. Peptides formed from a smaller number of amino acids are called "oligopeptides" (up to twenty amino acids). As a result, some oligopeptides can belong to the low molecular weight hydrogelators.

Amino acid derivatives and oligopeptides can easily form gels thanks to the well-defined fibrillar structures formed by the various intermolecular interactions created by hydrogen bonding, electrostatic interactions and aromatic stacking for instance. The resulting fibrillar network then traps water and thus forms hydrogels.[20] These compounds are called self-assembling peptides (SAPs). There are various ways of preparing hydrogels out of them: temperature cycles, solvent exchange, pH changes, etc. This kind of hydrogelators is of great interest because of the inherent biocompatibility of amino acids compounds. They are widely studied for cell culture and tissue engineering applications and some of them are now commercialized, such as PuraMatrix or PepGel.[21–23] Considering the variety of applications of these gelators and the aim of the project to cell culture applications, here, we will only focus on amino acid and peptide hydrogels used for cell culture applications.

One of the great challenges for biomaterials is cell adhesion. Indeed, it is important for the cells survival and proliferation to adhere to the scaffold. One way to promote cell adhesion to the scaffold in the case of peptide-derived hydrogel is to use the RGD amino sequence (Arginine-Glycine-Aspartic acid). This sequence is actually a peptide motif found responsible for cell

adhesion in the ECM. Cell adhesion proteins located on the cell membrane called "integrins" bind specifically to this sequence.[24] RGD is actually derived from fibronectin, which is an integrin-binding protein. Many studies have thus tried to integrate this sequence to their peptide gelators in order to promote cell adhesion to the scaffold. Hogrebe *et al.* recently developed a system of small SAPs (base on the KFE-8 peptide) containing in their sequence the RGD motif or a non-adherent derivative like RDG. When KFE-RGD, KFE-RDG and unmodified KFE-8 are combined together (Figure I-9), hydrogel stiffness and human mesenchymal stem cells (hMSCs) adhesion and differentiation can be tuned thanks to the total peptide and the RGD concentrations.[25] Many other studies tried to integrate the RGD sequence at the end of their SAPs to promote cell adhesion and differentiation for various tissue engineering applications[26–28]: myocardium reconstruction[29], liver[30] or dental pulp reconstruction[31], etc.

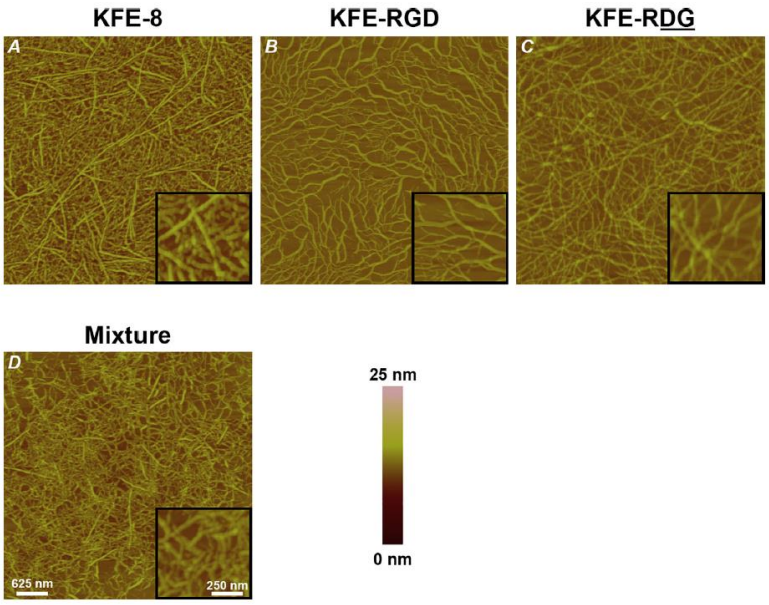

Figure I-9: AFM images of KFE-8 (A), KFE-RGD (B), KFE-RDG (C) and a mixture of the three SAPs (D) hydrogels developed by Hogrebe et al., revealing their nanometric fibrillar structure. Main image scale bar = 625 nm. Insert scale bar = 250 nm. Colored bar indicates image height from 0 to 25 nm. From [25].

In one of their studies, Berns *et al.* (from Samuel I. Stupp's research team) also included the RGD sequence into the structure of a peptide amphiphile based on Palmitoyl-VVAAEE-NH_2, but they also combined this latter with another peptide sequence of interest, which is the IKVAV motif (Ile-Lys-Val-Ala-Val).[32] This sequence is actually derived from laminin, which is a protein found in the ECM. Its use for the synthesis of cell culture scaffolds trying to mimic the ECM thus seems obvious. In this study, thanks to these RGD and IKVAV sequences, Berns *et al.* succeeded in promoting neurite outgrowth of the neuronal cells they encapsulated inside their hydrogels. Moreover, they were able to align the gel fibers simply by annealing their peptide solution and then extruding it during gelation (Figure I-10). They already described this phenomenon in a previous study with a similar SAP.[33] These aligned-fibers scaffolds then induced a cell growth along the fibers and a

general orientation of the neurites. Similarly, Matsuoka *et al.* developed a 13-amino acid peptide hydrogel including the IKVAV sequence for inner ear reconstruction.[34]

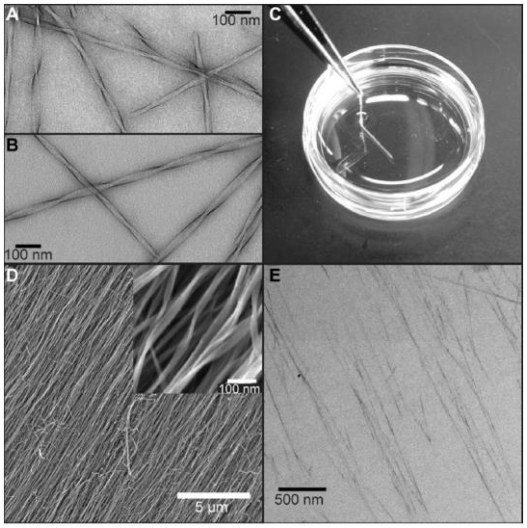

Figure I-10: Hydrogel fibers of a self-assembling peptide containing the IKVAV sequence. Alignment of the fibers could be achieved thanks to a simple extrusion through a pipette. From [32].

Cheng *et al.* also used the IKVAV sequence to grow neural stem cells, but they combined it to another widely used amino acid sequence: RADA (Arginine-Alanine-Aspartic acid-Alanine).[35] This one is derived from a segment found in a yeast protein. It is actually used to mimic the RGD sequence. When used to form hydrogels, this motif is usually repeated several times such as with RADA16-I (Ac-$[RADA]_4$-$CONH_2$). It is actually already commercialized as PuraMatrix™ and often used as cell culture scaffolds for various studies. Indeed, this peptide motif is very efficient for self-assembling as nanofibrillar hydrogels. PuraMatrix™ is thus frequently used for tissue engineering applications such as cardiac[36] or mucosal[37] regeneration where cells can directly be encapsulated into the scaffold. Many other studies for neural regeneration try to use the RADA16 sequence.[14,38] Ellis-Behnke *et al.* actually found that the injection of PuraMatrix™ into the lesion of severed optical nerves on hamsters enable axonal regeneration and the return of vision functions.[39] The resulting hydrogel is indeed permissive enough so that the axons could penetrate the scaffold and reconnect with native tissues.

Other, less recurrent, peptide sequences can be used to form hydrogels for cell culture scaffolds. Gelain *et al.* for instance have investigated the use of LDLK12 (Leucine-Aspartic acid-Leucine-Lysine) derivatives for the growth of neural stem cells.[40] They also tried to functionalize the LDLK12 sequence with a KLPGWSG motif, which is found in proteins involved in stem cell maintenance and differentiation.[41] They also developed a series of thirty-two peptides derived from the PFSSTKT motif, which is the Bone Marrow Homing Peptide 1 (BMHP1) functional sequence that promotes neural stem cells viability and differentiation. Several of those SAPs were

also functionalized, notably with the RGD motif. The resulting hydrogels displayed various fiber structures and expressed self-healing properties, which is particularly interesting for injectable materials. Several of them promoted the survival, adhesion and differentiation of hNSCs.[42] Recently, Arioz *et al.* developed electroactive materials for the growth of neuronal cells out of peptide nanofibers containing tetra-aniline. They actually synthesized two non-electroactive materials, lauryl-VVAGEE-$CONH_2$ and lauryl-VVAGKK-$CONH_2$ and they found out that when they replaced the lauryl moiety by tetra-aniline, the nanofibers became electroactive and the neural outgrowth and differentiation were improved compared to the non-electroactive ones.[43] Furthermore, Restu *et al.* used the P1 peptide (Ac-FFFGK-OH), which is an integrin recognition sequence, to culture HeLa and fibroblast cells. The resulting hydrogel was proved to be biocompatible as well as easily degraded by enzymatic hydrolysis, and it can also be used for drug-release applications.[44]

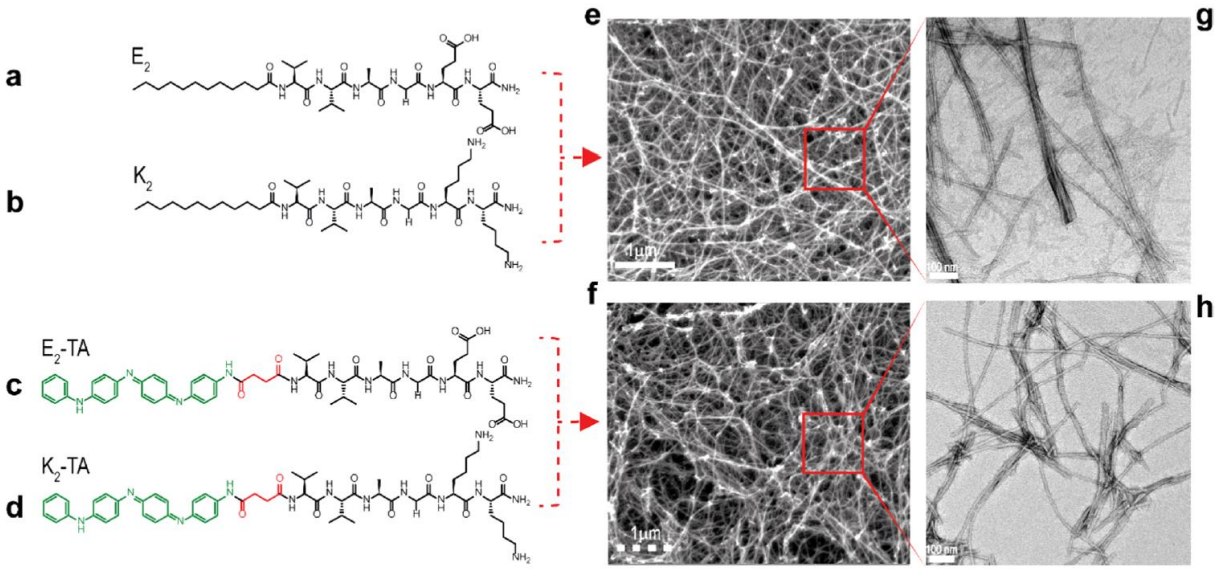

Figure I-11: "Chemical structures of non-electroactive (a) lauryl-VVAGEE-Am (E2) and (b) lauryl-VVAGKK-Am (K2) and electroactive (c) TAVVAGEE-Am (E2-TA) and (d) TA-VVAGKK-Am (K2-TA) peptide amphiphiles. Scanning electron microscopy (SEM) images of (e) E2/K2 and (f) E2-TA/K2-TA gels reveal a mesh-like structure. Transmission electron microscopy (TEM) images of (g) E2/K2 and (h) E2-TA/K2-TA gels show a nanofibrous structure." From [43].

Peptides thus offer a large panel of possible combinations to form self-assembling materials. The various amino acids containing aromatic and carbonylated moieties can easily form hydrogen bonding and organize as self-assemblies. Nevertheless, even with this class of molecules, the design of hydrogelators relates most of the time on serendipity more than real molecular design; often several trials have to be done to synthesize a brand-new peptide hydrogelator. Moreover, except for the ones that are commercialized, the main problem with this kind of gelators is most of the time the complexity of their synthesis. Indeed, peptide synthesis can be achieved in an automated way with the solid phase peptide synthesis (SPPS) method. But this technique still results in a quite expensive synthesis.

I.1.2.2 Simple amino acids and Fmoc derivatives

Shorter gelators can also be obtained out of simple amino acids. Suga *et al.* for instance developed lysine-based hydrogels as a coating to promote cell attachment to plastic surfaces.[45] Dou *et al.* synthesized a phenylalanine-derived hydrogel in which they encapsulated the cells and formed 3D scaffolds. They can control the wettability of the latter to tune cell adhesion and growth.[17] Liu *et al.* also worked on phenylalanine-derived hydrogels and they found out that the nanofibers' chirality changed according to the molecule's chirality. Interestingly, they also showed that the cells developed a better adhesion and differentiation on left-handed helical fibers.[46]

In the course of peptide synthesis, one of the terminal protecting groups often used is the fluorenylmethyloxycarbonyl group, abbreviated as Fmoc. With its conjugated aromatic groups, this moiety actually enables the formation of π-π interactions, helping the self-assembly when combined with amino acids for instance. Many studies actually employ gelators made out of Fmoc coupled to one or several amino acids, for the synthesis of these molecules is relatively simple and often results in molecular gels.

For cell culture applications, the Fmoc-diphenylalanine (FmocFF) which forms hydrogels has been used in several studies. Jayawarna *et al.* (Ulijn's research group) for instance developed hydrogels that are a mixture of Fmoc-FF and Fmoc coupled to either lysine, glutamic acid or serine in order to adapt the compatibility of the gelator with different cell types (Figure I-12). Bovine chondrocyte cells have been successfully grown on the scaffolds as well as 3T3 fibroblast cells and human dermal fibroblasts for some of the hydrogel combinations.[47] Still with the use of phenylalanine, Chronopoulou *et al.* reported the enzymatic synthesis of a Fmoc-Phe_3 hydrogel in ten minutes, from Fmoc-Phe and Phe_2 precursors mixed with the *Pseudomonas fluorescence* lipase. Rat microglial cells were cultured on the resulting scaffolds that promoted cell adhesion and enhanced the production of nerve growth factors.[48] Wang *et al.* demonstrated that halogenated phenylalanine coupled to Fmoc had better gelation properties in water than regular Fmoc-Phe gelators. They showed that Fmoc-fF (fF = fluorinated phenylalanine) was the most efficient gelator, for it gelled water at very low concentration (0.15 wt %). However, none of the halogenated gelators was suitable for cell culture applications. To overcome this, they developed another gelator which is the Fmoc-fFfFRGD. This hydrogel was thus able to promote the adhesion and the proliferation of NIH3T3 cells.[49]

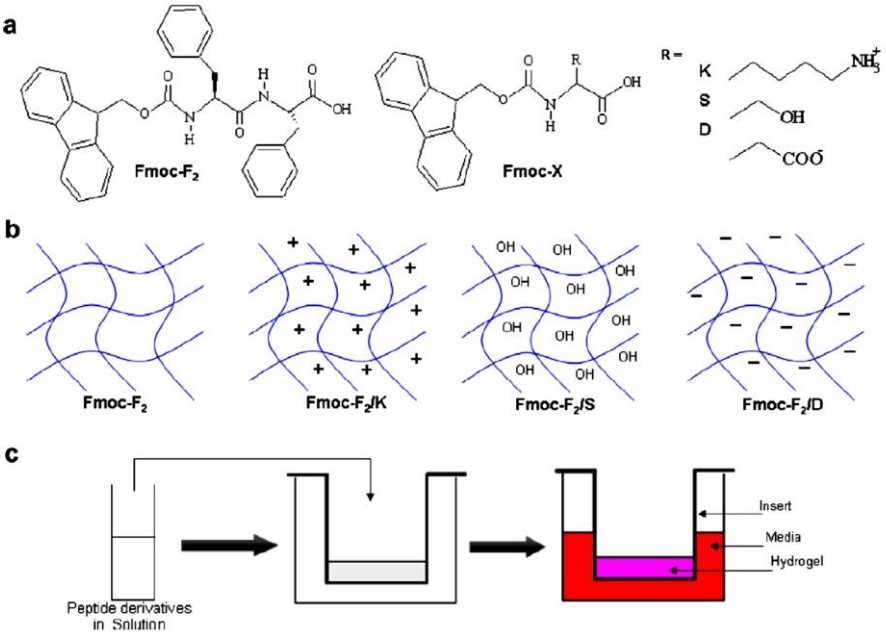

Figure I-12: a. Chemical structures of the four hydrogel systems studied by Jayawarna et al. "b. A representation of the four structures. c. A schematic of hydrogel formation in cell culture inserts." From [47].

Here again, the RGD motif was employed in order to adapt the hydrogel properties to cell culture application. Similarly, Cheng *et al.* simply developed a Fmoc-RGD self-assembling peptide and were able to grow fibroblast cells on the Fmoc-RGD hydrogels, but not on the Fmoc-RDG one that they used as a control.[50] Rodriguez *et al.* also reported the use of Fmoc-FRGDF hydrogels for *in vivo* trials. In this same study, they also developed a Fmoc-DIKVAV hydrogel and a Fmoc-DYIGSRF; YIGSR being another peptide sequence, like IKVAV, derived from laminine. Those three hydrogels were able to enhance the neural tissue repair after cell transplantation *in vivo*.[51] In a more recent study too, this same research group reported the use of Fmoc-DIKVAV hydrogel in which glial cell line derived neurotrophic factors (GDNF) were encapsulated. They found out that even 172 hours after *in vivo* transplantation, the GDNF were still released in the tissues and promoted the growth of the neural cells.[52]

This simple combination of Fmoc with small peptides again offers multiple possibilities to form hydrogels that appear to be biocompatible materials for cell culture and tissue engineering applications.

I.1.2.3 Sugar and nucleoside-derived low molecular weight gelators

Another family of molecules that can form molecular hydrogels are sugar- or carbohydrate-derived compounds. We will develop this part more in details since carbohydrate gelators have been selected in this thesis for cell culture. In sugar amphiphiles, the segregation of the hydrophilic part (multiple hydroxyl functions of the carbohydrate group) and the hydrophobic

part provokes the self-assembly of molecules. Most often, they behave as surfactants and form micelles, but some of them are able to self-assemble on a long range into fibers or ribbons and are able to form hydrogels. One interesting point about the use of sugar-derived molecular gels is also that many carbohydrates are building blocks of living organisms' components. They are constituents of macromolecules of the extracellular matrix (e.g. hyaluronic acid), of glycoproteins and glycolipids that play important structural, energetic and recognition roles in living organisms.[53] Nucleic acids (DNA and RNA) also involve carbohydrate groups in their structure, a desoxyribose in the case of DNA, a ribose in the case of RNA. Thus, the elemental bricks of DNA or RNA, i.e. the nucleosides, also constitute an interesting building block for the design of molecular gels. In addition to the carbohydrate part, the nucleobases provide several functions able to form strong directional hydrogen bonds that will trigger self-assembly.

I.1.2.3.1 Carbohydrate derivatives in general

Carbohydrate-derived LMWGs are not so widespread. AS for other molecular hydrogelators, obtaining the right balance of building block to provide the self-assembly into fibers swollen in water, instead of getting micelles or precipitates, is not so easy. In addition, the preparation of carhohydrate derivatives require many protection and deprotection steps, with intermediate purification steps, leading to time-consuming synthesis and tedious yields. Contrary to peptide derivatives, there are still no high throughput carbohydrate-based syntheses. However, some very simple molecular gelators based on carbohydrate were described early in the literature. Pfannemüller and Welte in 1985 described the preparation of several "synthetic glycolipids"[c] that form hydrogels once cooled down after dissolution in water at high temperature.[54] These carbohydrate gelators are alkylaldonamides obtained by a one-step synthesis by opening sugar lactones with an alkylamine. The synthesized compounds were *N*-alkylgluconamides, *N*-alkanoyl-*N*-methylglucamides or *N*-Alkanoyl-*N*'-gluconoyl-ethylenediamines among others. Fuhrhop *et al.* as well studied in detail the microscopic structure and the self-assembly of *N*-octylaldonamides obtained from sugar lactones with different configurations (glucose, galactose, mannose, etc.).[9] They were described as forming coarse white gels, obtained after dissolution of the solid at high temperature and cooling down to room temperature. Fuhrhop reported that the gels resulting from galactonamides were more stable than the ones from gluconamides compounds, for these latter often recrystallized after a few days (Scheme I-2).

[c] The term "glycolipid" is often used by authors to describe all sorts of amphiphile derivatives composed of a carbohydrate and a hydrophobic part such as an alkyl chain. This designation is used because of the comparison with the structure of natural glycolipids. However, the various structures and functions of these synthetic compounds can be different from the ones of natural glycolipids.

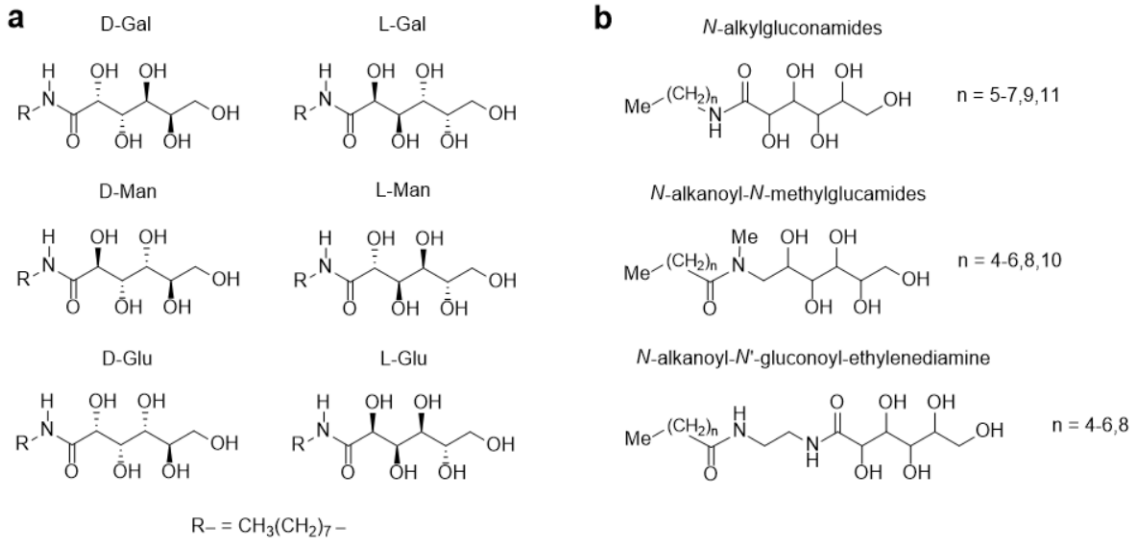

Scheme I-2: Examples of molecules synthesized by Fuhrhop who used derivatives of the L and D enantiomers of galactose (Gal), mannose (Man) and glucose (Glu) as polar heads (a) and by Pfannemüller and Welte (b). Adapted from [54] and [9].

More recently, Mizrahi *et al.* also synthesized the *N*-hexyl-D-galactonamide and used its hydrogel as an electrophoresis gel. They synthesized this molecule with the idea of decreasing the gelation point compared to the *N*-octyl-D-galactonamide described by Fuhrhop *et al.* This molecule is actually non-charged but they found that hydrogen bonding between the molecules actually lowers the pK_a of the hydroxyl functions, resulting in the deprotonation and the charging of the gelator molecules, which makes it usable for electrophoresis.[55]. Ávalos *et al.* described the gelation of carbohydrate amphiphiles and bolaamphiphiles in water, with structures quite close from alkylaldonamides. In this case, the molecules are derived from D-glucamine and *N*-methyl-D-glucamine, linked to an alkyl chain by a urea moiety. Different gelation properties were observed for methylated and non-methylated molecules.[56] Indeed, the presence of a methyl group on the amide or urea group in carbohydrate gelators often increases the solubility of the molecule in water and can sometimes prevent their gelation.[57]

Several gelators were built on this basis, with a carbohydrate polar head linked to an alkyl chain by a urea or amide group. Capicciotti *et al.* developed ice recrystallization inhibitors based on alkylaldonamides (Figure I-13). For this study, they used the two forms of glucose and galactose: the pyranose form, which is the cyclic form, and the open form. They found that the *n*-octyl-β-D-galactopyranose (a surfactant) and the *N*-octyl-D-gluconamide (a LMWG) molecules were efficient for ice recrystallization inhibition. However, they did not correlate the formation of a hydrogel to the ice recrystallization inhibition activity. Nevertheless, these hydrogels can be interesting for the encapsulation of cells in a cryopreservation environment.[58]

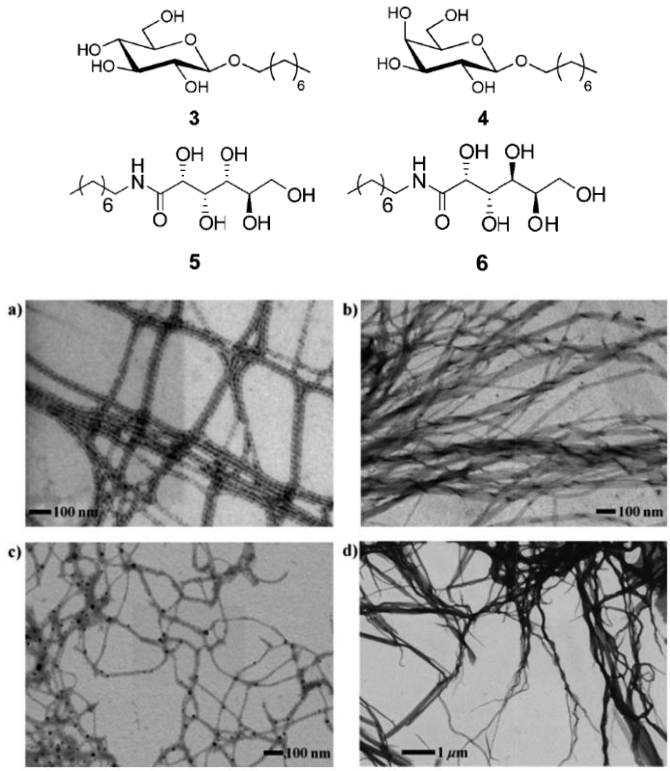

*Figure I-13: The molecules synthesized by Capicciotti et al. 3: n-octyl-β-D-glucopyranoside; 4: n-octyl-β-D-galactopyranoside; 5: N-octyl-D-gluconamide and 6: N-octyl-D-galactonamide. TEM images of the hydrogels resulting from **5** (a) and **6** (b) in water and from **5** (c) and **6** (d) in PBS. From [58].*

Ohsedo *et al.* showed that interestingly, the mix of two fragile alkylaldonamide hydrogels can result in a stable and self-healing hydrogel.[59] In another study they also described self-healing hydrogels out of D-glucamine linked to an alkyl chain by a glycine moiety (Figure I-14).[60] On this same scheme, Minakuchi *et al.* also tried to include an amino acid as a linker in an alkylgluconamide molecule. They used different amino acids such as Val, Phe, or Gly and they found out that the ones forming hydrogels were the molecules containing Val, Leu or Ile. Moreover, these molecules can gel water, but also other organic solvents as well as ionic liquids at low concentrations (> 1 wt %).[61] Cano *et al.* synthesized two-headed thiolactose amphiphiles with a flexible ethylene glycol linker that are able to gel water from 0.1 wt %.[62]

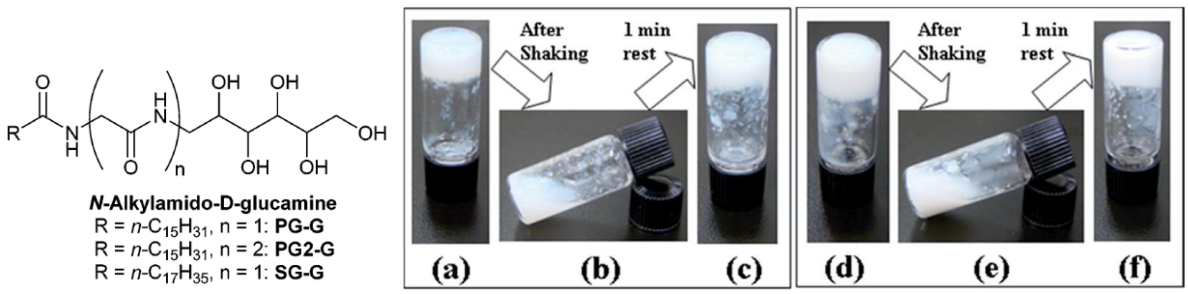

Figure I-14: The D-glucamine derivatives containing a glycine moiety synthesized by Ohsedo et al. Self-healing tests of PG-G (a-c) and PG2-G (d-f) hydrogels. From [60].

Clemente *et al.* synthesized a series of carbohydrate-based gelators by click-chemistry, composed of a disaccharide head (lactose, cellobiose or maltose), a triazole and an amide linker connected to an alkyl chain of sixteen carbons. They studied the influence of the sugar head of the glycoamphiphiles on the micro and nano-structure of the resulting hydrogels. The amphiphiles self-assemble into twisted ribbons in water and it was found that the torsion direction of the ribbons depended on the disacharide head employed. Thanks to cryo-TEM and circular dichroism, they were able to establish a model for the molecular arrangement inside the fibers (Figure I-15).[63]

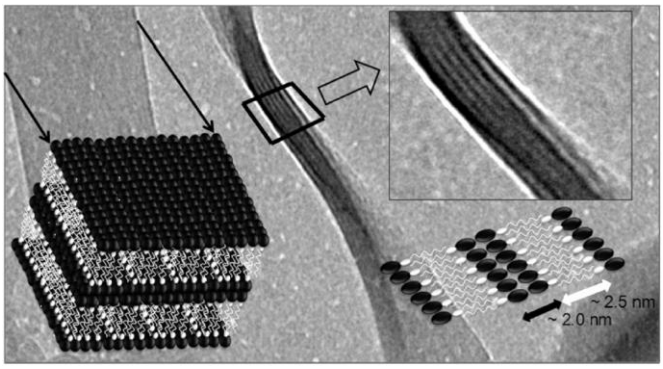

Figure I-15: Cryo-TEM observations of twisted ribbon fibers and the model of the molecular arrangement inside. From [63].

I.1.2.3.2 Carbohydrate derivatives for cell culture applications

In this section more particularly, we gathered the carbohydrate-based molecular gelators that have been tested for cell culture. Only few of them have been described for this purpose. Most of the time, the carbohydrate part is coupled to other biocompatible moieties such as amino acids. Wang *et al.* for instance coupled an *N*-acetylgalactosamine head to lysine and naphthalene groups and the resulting molecule forms a hydrogel at very low concentration. 2D cultures were performed on this gel with different cell lines (NIH3T3, HepG2, AD293 and HeLa cells) and they showed good adhesion and proliferation.[64]

Xiao *et al.* developed photoresponsive hydrogels based on spyropyran and galactose that are able to deliver micro-RNA into hepatocytes. Indeed, galactose is particularly suited for hepatocytes since these cells have galactose receptors on their membrane (Figure I-16).[65] Hydrogel capsules of an *N*-acetylgalactosamine coupled to a double cyclopentane chain by an amide linker were synthesized by Ikeda *et al.* for their use in targeted drug delivery. Those capsules are enzyme and cell responsive and are used to detect prostate cancer cells. However this hydrogel is quite stiff, which explains its use as capsules, and a high concentration of gelator has to be used to form a gel (5 to 10 wt % in water).[66] Still from this research group, they used the same hydrogel this time to create molds for collagen cell culture scaffolds.[67]

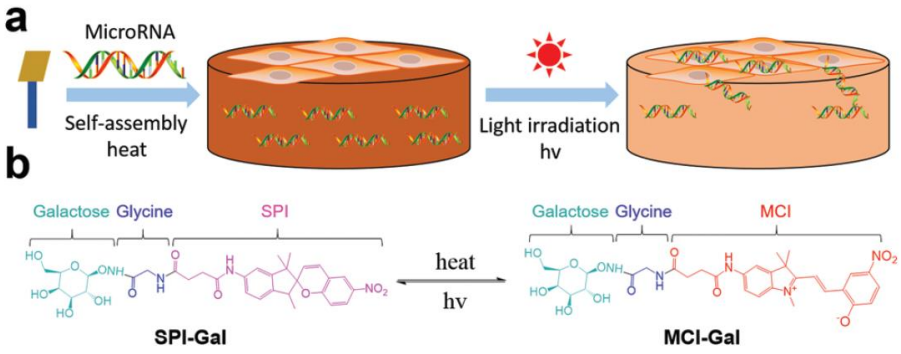

Figure I-16: "a. Schematic illustration of the dual-functional supramolecular hydrogel for targeted and light-controlled delivery of miRNA into cells cultured on top of the gel. b. Structure transformation between SPI–Gal and MCI–Gal under heat or light control." From [65].

Other studies tried to link sugars with amino acids in order to improve the biocompatibility of their gelators. Yang *et al.* for instance, synthesized the two enantiomers of a D-glucosamine-based hydrogelator: Nap-D-Phe-D-glucosamine and Nap-L-Phe-D-glucosamine. Though there is no difference on the gelation properties of the molecules, the microscopic structures of the gel fibers are different as well as the biocompatibilities. Indeed, the Nap-D-Phe-D-glucosamine seems to have better wound-healing properties than the other.[68] Similarly, Liu *et al.* developed glycopeptide gelators for the culture of NIH3T3 and human umbilical vein endothelial cells. They used naphthalene coupled to phenylalanine and aspartic acid with one, two or three glucose moieties and they compared it to peptides with no glucose. The result is that the sugar moieties improve the biophysical and biofunctional properties of the scaffolds.[69]

I.1.2.3.3 Nucleoside derivatives for cell culture applications

As previously mentioned, DNA has also sugar moieties in its skeleton called desoxyriboses. Nucleosides are the building blocks of DNA, and this latter is one of the building bricks of life. More and more studies are thus including nucleosides in their biomaterials, considering that these bricks are biocompatible. Moreover, nucleosides are very efficient to form self-assembling materials thanks to the many hydrogen bonds they can display. It can be expected that many molecular hydrogelators should be derived from nucleosides. In fact DNA alone can form an ECM-like network but it has been shown that the cells do not grow on DNA only scaffolds.[70]

Buerkle *et al.* for instance used guanosine derivatives to form molecular gels in water as well as in cell culture medium. The resulting hydrogels are found to be non-toxic, injectable and their stiffness can be tuned by mixing them with an analogue compound. Cell culture trials have also been done on a human endothelial cell line, but in order to promote cell adhesion, the initial scaffold had to be mixed with gelatin.[71] Rotaru *et al.* also worked on guanosine-derived hydrogels. They coupled the guanosine with benzene-1,4-diboronic acid (through the complexation of the

ribose-diol with boronic acid) and this resulting compound formed a hydrogel once mixed with K^+ ions. This hydrogel was further cross-linked, again via electrostatic bonds, with Mg^{2+}. Cell culture assays have been made on fibroblast cells, but they resulted in a cell viability of 73 % after only 24h.[72]

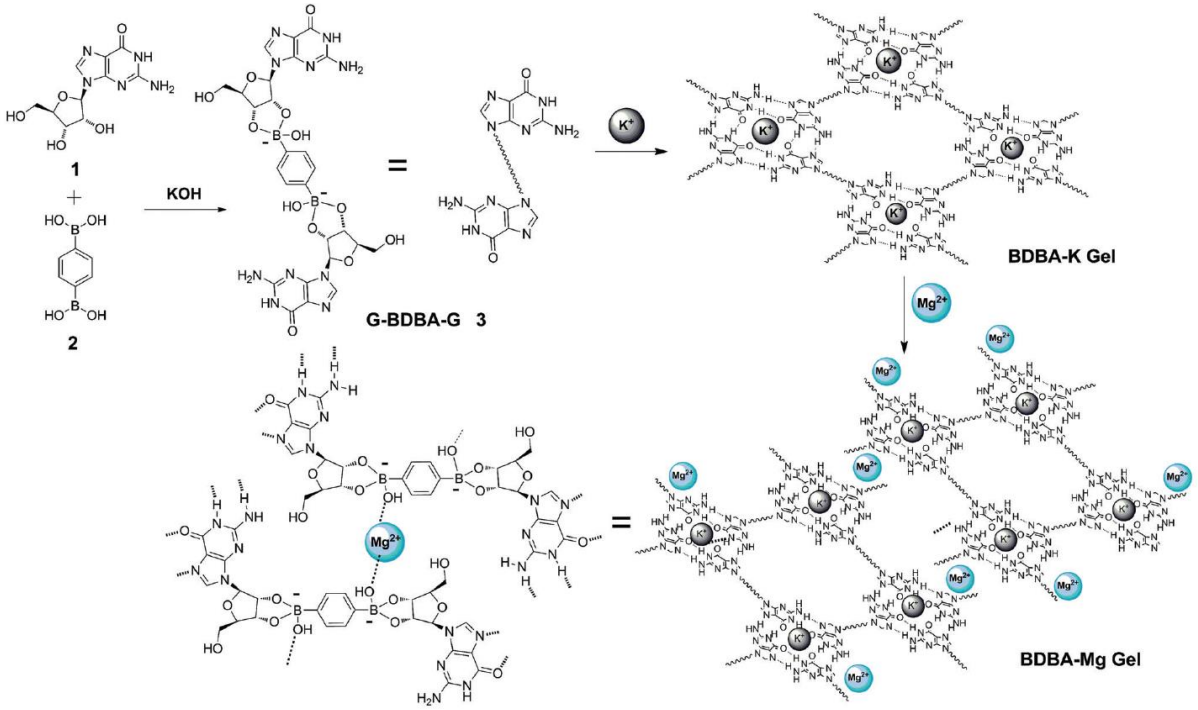

Scheme I-3: Reaction pathways for the hydrogels described by Rotaru et al., the G-BDBA-G 3 molecule is stabilized with K^+ via G-quartet formation and with Mg^{2+} via external cross-linking. From [72].

Barthelemy's research group has also worked on hydrogels derived from nucleobase for cell culture applications. They first studied a glycosyl-nucleosyl-fluorinated compound for the growth of osteoblasts. It is composed of a polar glycosyl head group, a thymidine moiety and a hydrophobic fluorinated aliphatic chain and it is prepared by cooling down a hot solution of the gelator in PBS. It degrades slowly in cell culture medium as well as when implanted subcutaneously. Encapsulated cells show a good growth and adhesion to the scaffold, both *in vitro* and *in vivo*. *In vivo*, host cells and blood vessels even penetrate the gel.[73] Similarly, Barthelemy's team also developed bolaamphiphiles based on the same glycoyl-thymidine-triazole derivatives (Figure I-17). Contrary to the amphiphile analogues, this bolaamphiphile gelator presents interesting characteristics such as injectabilty. It was used for the culture of human adipose tissue stem cells.[74]

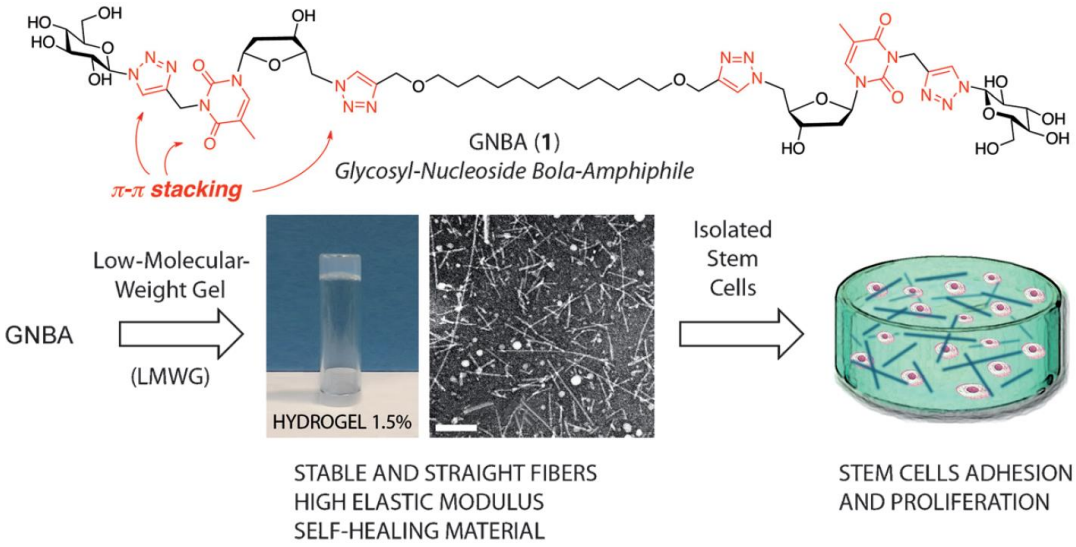

Figure I-17: Glycosyl-nucleosyl-derived bolaamphiphile developed by Barthelemy's group for the growth of stem cells. From [74].

In a more recent study, they added an amide or urea moiety after the triazole group in their bolaamphiphile compounds. They showed that these series of compounds still have self-healing properties but one of the urea derivatives has faster gelation kinetics and a higher elastic module compared to the other urea and amide derivatives. It is also biocompatible and is slowly degraded when implanted *in vivo*.[75]

Other studies employ a combination of carbohydrates and nucleobases (nucleoside without the deoxyribose moiety). Li et al for instance synthesized a series of gluco-phenylalanine-nucleobase hydrogelators that are biocompatible and biostable but that are also able to bind and to deliver nucleic acid directly in the nucleus of cells.[76] Yuan *et al.* synthesized as well various molecules derived either from glucuronic acid-amino acids-nucleobase compounds, or from amino acids-nucleobase conjugates, the nucleobase being thymine or adenine (Scheme I-4). Although being biocompatible, none of these molecules were able to form a hydrogel.[77] In the same way, they later developed other biocompatible molecules and they were able to form hydrogels only when mixing two amino acids-nucleobase compounds this time.[78]

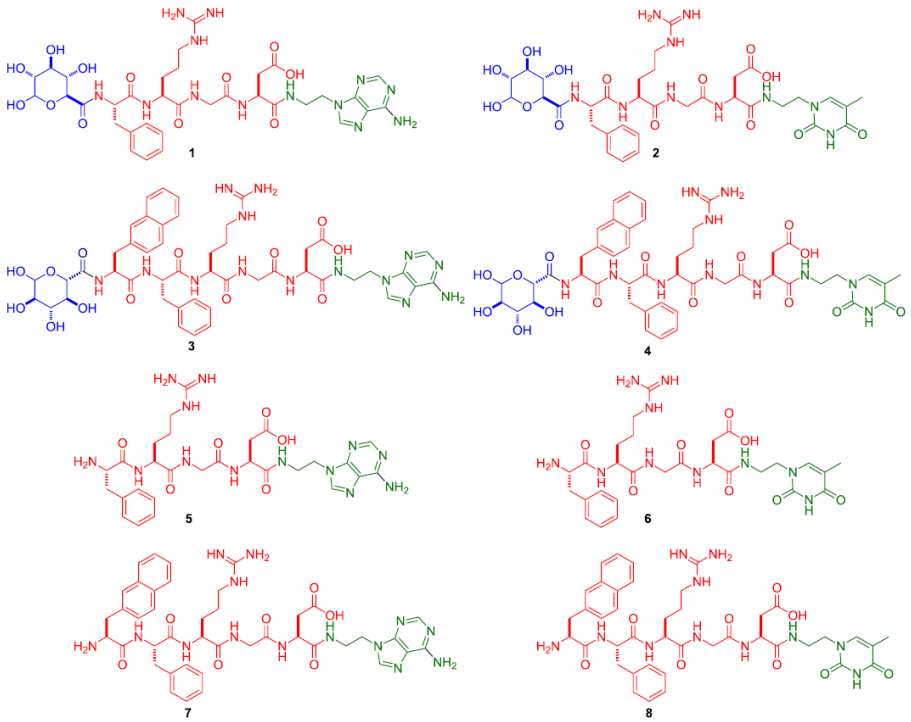

Scheme I-4: Molecules synthesized by Yuan et al. derived either from glucuronic acid-amino acids-nucleobase compounds (1-4), or from amino acids-nucleobase conjugates (5-8). From [77].

This inclusion of different chemical species such as amino acids, sugars and nucleobase results in various gelling molecules, but also to easily functionalize the molecules in order to adapt their properties to their future function.

I.1.3 Conclusion

Low molecular weight gelators offer vast possibilities of compounds to make biocompatible scaffolds that can be adapted specifically to their further application. In order to obtain self-assembling material, the LMWGs should contain chemical groups that favor aromatic and hydrophobic interactions, hydrogen bonding, etc. Fortunately, for biological applications, many biocompatible moieties such as amino acid, peptide and sugar derivatives can be used to build such self-assemblies.

The main advantage of molecular gels is that they produce soft, loose and degradable hydrogels. Contrary to polymer gels, with LMWGs an equilibrium between the aggregated and the free molecules allows a better *in vivo* clearance. However, this can also induce a higher toxicity if the molecules are not easily integrated/degraded by the organism. Another specificity of molecular gels is the variety of fiber structures that they display. The fibers can range from nanometric to micrometric scale, they can have a helical shape or look like wide flat ribbons for instance. Moreover, the formation of a hydrogel by a LMWG is quite reproducible in the way that all the

molecules are exactly the same and they always self-assemble in the same pattern. In addition, hydrogels can be formed via different methods (temperature change, ion or solvent exchange, etc.) that can enable cell encapsulation for biological application for instance.

Yet, the synthesis of LMWGs is not so straightforward. Indeed, many protection/deprotection steps can be needed and the desired molecule is often obtained after several intermediaries, especially with carbohydrate derivatives. Furthermore, the purification steps can sometimes be complicated. For example, reactions involving click chemistry are very easy to implement, but the post-synthesis removal of the cupper necessary for the reaction is more difficult. Moreover, obtaining a gelator with this class of molecules often relies on serendipity more than on real molecular design for the intermolecular interactions are not so easy to predict. Again, contrary to polymer gels, functionalization of the LMWGs is not possible after self-assembly. The inclusion of groups of interest (such as the RGD peptide sequence for instance) has to be done during the synthesis, and yet this addition can completely change the self-assembling behavior of the initial compound. As previously mentioned, molecular gels can also display a much faster degradation and/or a higher toxicity compared to polymer gels. Their particular softness can also be an inconvenient for some applications. Thus, LMWGs are a very specific kind of gelators with very different properties from polymer gels. These specificities can then be used for particular applications that polymeric gels could not fulfill.

In this study, we became interested in the synthesis of very simple carbohydrate derivatives as LMWG. Previously in our laboratory, several LMWGs had already been tried for biological applications, such as Fmoc dipeptides, molecules containing triazole moieties or dipalmitoyl saccharose esters. Unfortunately, these molecules were poorly biocompatible. Simpler compounds made out of biocompatible building blocks had to be investigated. For this reason, very simple molecules with a saccharide head and a short lipid chain were synthesized and studied as potential biocompatible hydrogel scaffolds.

In the next part, we are going to report the results on the synthesis of the carbohydrate-derived gelators and the characterization of their hydrogels.

I.2 Synthesis and characterization of carbohydrate-derived hydrogelators

The first step during this PhD was the synthesis of several carbohydrate-based molecular gelators and the characterization of their hydrogels. Several molecules of different types were prepared in order to find which ones presented the best properties relative to their further application. This part thus describes the synthesis of the different molecules and the chemical and physical characterization of the resulting hydrogels.

I.2.1 Synthesis of the gelators and gelation ability

Throughout this work, several low molecular weight hydrogelators have been synthesized, all of them having the same base structure: a polar head derived from glucose or galactose and a short alkyl chain (less than 18 carbons). Some of these molecules have already been described in the literature as hydrogelators (see I.1.2.3.1), and some of them are new molecules (Table I-1). Their structures have been slightly modified in order to have the highest chance to keep their gelling properties. In all the cases, very simple structures were designed in order to obtain a library of gelators accessible in one step and easy to purify. Here we describe the different families of molecules that were synthesized.

Table I-1: Chemical structures and properties of the different molecules synthesized

Name	Chemical name	Structure	Gel concentration	Gel aspect	References
Alkylgluconamides					
Glu-C7	*N*-heptyl-D-gluconamide	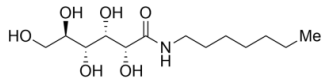	2 wt %	White gel unstable after a few hours	9,54,59
Alkylgalactonamides					
Gal-C9	*N*-nonyl-D-galactonamide	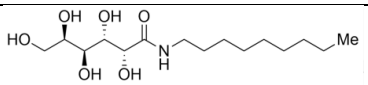	0.5 wt %	Heterogeneous white gel	This work
Gal-C8	*N*-octyl-D-galactonamide	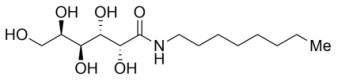	0.5 wt %	Coarse white gel	9
Gal-C7	*N*-heptyl-D-galactonamide	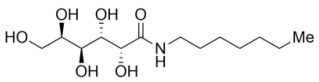	0.45 wt %	Coarse white gel	This work
Gal-C6	*N*-hexyl-D-galactonamide	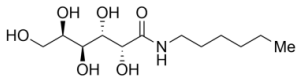	1 wt %	Coarse white gel	55
Gal-C5	*N*-pentyl-D-galactonamide	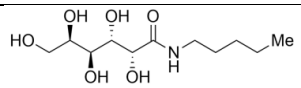	1.75-2 wt %	Very fragile white gel	This work
Alkanoylglucamines					
Gluca-C12	*N*-dodecanoyl-D-glucamine	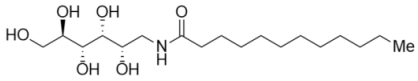	2-3 wt %	Stable opaque white gel only if HFP is used	This work
N-alkanoyl-N-methyl-glucamines					
Me-Gluca-C12	*N*-methyl-*N*-dodecanoyl-D-glucamine	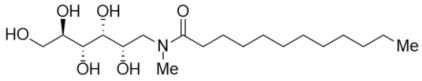	3-5 wt %	Transparent thixotropic gel	79,80
Me-Gluca-C14	*N*-methyl-*N*-tetradecanoyl-D-glucamine	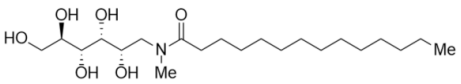	No gel	_	This work

I.2.1.1 Alkylgalactonamides and alkylgluconamides

The first carbohydrate-based gelator family we became interested in was that of alkylaldonamides. These molecules are prepared by reacting an alkylamine with a sugar lactone. In our case, the lactones are galactonolactone and gluconolactone (Scheme I-5 and Scheme I-6: Synthesis scheme of Glu-C7.). Here their structure has been slightly adapted compared to the literature. Indeed, their final application being their use as cell culture scaffolds with the possibility of cell encapsulation, the gel has to keep its structure at 37 °C and it should ideally have

a gelling temperature close from 40 °C. Thus, different variations of the chain length and the sugar part have been made to possibly modulate the solubility in water and their gelling temperature.

Five molecules called alkylgalactonamides have been synthesized with a galactonolactone and a fatty amine (Scheme I-5)Scheme I-5: Synthesis schemes of the five alkylgalactonamides. They are abbreviated as Gal-Cn, with n being the number of carbons in the alkyl chain (5≤n≤9).

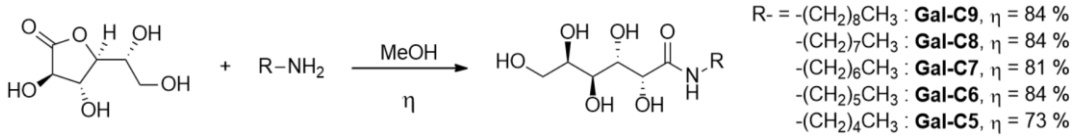

Scheme I-5: Synthesis schemes of the five alkylgalactonamides.

In the alkylgluconamide family, *N*-heptyl-D-gluconamide has also been synthesized following the same protocol as the alkylgalactonamides but with gluconolactone instead of galactonolactone (Scheme I-6).

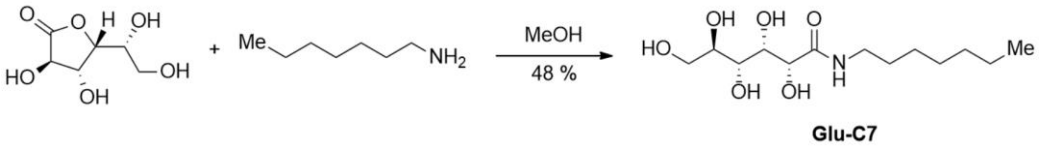

Scheme I-6: Synthesis scheme of Glu-C7.

The syntheses as well as the purifications were straightforward for these compounds. Only one step was necessary to obtain the desired molecule and a simple recrystallization enable us to purify it. The molecules have then been characterized with several techniques to validate their structures and check their purity: ^{1}H,^{13}C and 2D NMR, mass spectrometry and elemental analysis.

To form the gels, the resulting solids were dissolved in water at high temperature and the gelation occurred when the solution was cooled down to room temperature (for the gel concentrations: 1 wt % = 10 mg of solid dissolved in 1 ml of water). Gal-C8 was already described in the literature as being a poorly soluble molecule in water, even at low concentrations.[9] To solubilize the molecule, a solution with a concentration of 0.5 wt % (the maximum concentration that can be reached) had to be heated at least at 120 °C (under pressure) and the resulting gelling temperature was around 95 °C (assessed by DSC). If we replace the alkyl chain by a five-, six- or seven-carbon chain, the molecule should become more hydrophilic and thus more soluble. Gal-C7, Gal-C6 and Gal-C5 were then synthesized. They were more easily solubilized in water and their gelling points, determined by DSC were indeed reduced (see I.2.2.5). Gal-C9 has also been synthesized to complete the series of alkylgalactonamides.

The concentration used for preparation of Gal-C7 gels (0.45 wt %) was the maximal solubility of the molecule in water at high temperature. For Gal-C6, the concentration used (1 wt %) was the lowest concentration for which the gel was found resistant enough for cell culture. For Gal-C5, the molecule was soluble at 2 wt % and the gel was formed rapidly but if we used lower concentrations, the gelation time was much longer: at 1 wt %, the solution had to be put at 4 °C to gel for two days, at 1.5 wt % the solution gelled within one night at room temperature. With gal-C9, the highest concentration we could achieve was 0.5 wt % when heating the solution at 130 °C for several hours. After cooling down the solutions, all of these molecules formed opaque white gels that were very brittle (Figure I-18). Gal-C9 formed a quite heterogeneous gel and Gal-C5 gave very fragile gels. Alkylgalactonamide hydrogels are all very sensitive to what is called synaeresis, which is the expulsion of water from the gel when this one undergoes mechanical stain. This phenomenon is detrimental to the gel since this one cannot retrieve its initial structure once the water is expelled.

Figure I-18: Alkylaldonamide gels obtained after cooling down of the hot solutions.

As for Glu-C7, it formed a very unstable gel at 2 wt % in water: after a few hours, the molecule recrystallized and the gel lost its structure. This phenomenon was actually already described in the literature, which is why this molecule was not further exploited, neither were its analogues.[9,54,59]

I.2.1.2 Alkanoylglucamines and *N*-alkanoyl-*N*-methyl-glucamines

Another type of supramolecular gelators was designed by changing the sugar head and slightly modifying the chemical function between the polar head and the fatty chain. For these molecules, glucamine and derivatives of fatty acids (containing 12 or 14 carbons) were used as reactants, which reversed the amide bond compared to aldonamide molecules: this time the polar head is linked to the alkyl chain by the nitrogen atom from the amide group. Different protocols were used to synthesize the molecules (Scheme I-7). They underwent one or several recrystallizations as purification steps and the molecules were characterized by the same spectroscopic methods as for alkylgalactonamides. Here again, the syntheses and purifications were easily implemented.

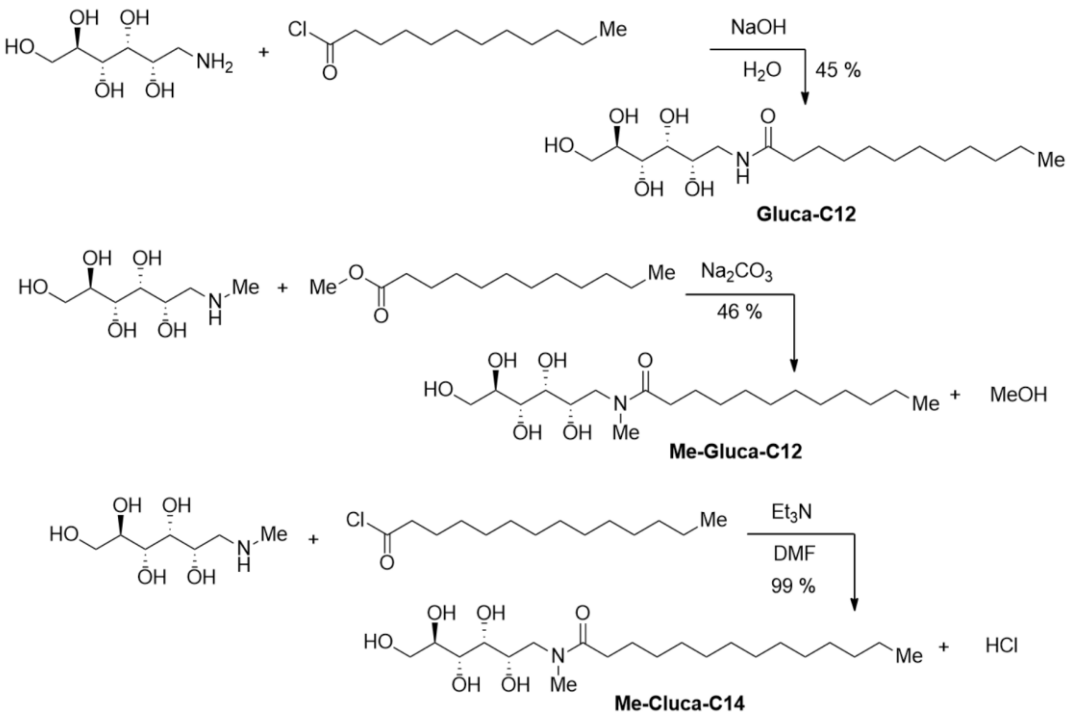

Scheme I-7: Synthesis schemes of Gluca-C12 (top), Me-Gluca-C12 (center) and Me-Gluca-C14 (bottom).

First gelation trials had already been made with *N*-octanoyl-D-glucamine, which only recrystallized after dissolution in water. Gluca-C12 was then synthesized in order to improve the gel stability by increasing the carbon chain length. At concentrations between 0.33 and 3 wt % in pure water, this molecule gave a very opaque white gel forming at approximately 70 °C but this one was very loose and fragile. If we added a small amount (0.7 wt %) of hexafluoropropan-2-ol (HFP) in the water and we heated a 3 wt % solution of gelator in this mix at 100 °C, a more cohesive gel was obtained. Then the HFP could be rinsed from the gel by soaking it in several water baths. This point is crucial if we want to exploit this hydrogel for cell culture applications. What is also interesting with this gel is that it did not really undergo synaeresis when mechanically solicited, the gel still lost its shape, but it did not really expel water.

On the same template as Gluca-C12, Me-Gluca-C12 was synthesized. This molecule had already been described in the literature as forming a transparent gel.[79,80] Even though the carbon chain of this compound was longer than the ones previously synthesized, this molecule was found to be the most soluble in water and could be easily dissolved at 70 °C. Indeed, the addition of the methyl on the amine prevents the formation of hydrogen bonds between the amide groups: instead of having an insoluble molecule resulting from very strong intermolecular interactions, this one behaves like a surfactant and can be dissolved in water. However, Me-Gluca-C12 was still able to gel, with a gel point of a 5 wt % solution visually estimated between 5 and 10 °C. Around 32 °C, the gel liquefied again, which makes it incompatible with cell culture applications. Nevertheless, this gel had a very interesting property: when mechanically solicited, its viscosity decreased but

once at rest, the gel retrieved its initial structure. This phenomenon is called thixotropy and it is particularly interesting for injectable materials. As a way to improve its gel point which is too low, two more carbons were added to the alkyl chain resulting in Me-Gluca-C14. Several gelling trials were done at various concentrations as well as with some HFP in the water, but no condition was found to produce a gel with this molecule for it systematically recrystallized without forming a gel.

I.2.1.3 Selection of the molecules of interest

After these first gelation trials, one particular family of gels already seemed to stand out. Indeed, the alkylgalactonamide family was the one that forms gels the most easily despite a poor solubility of the gelators in water, and the alkylgluconamide (Glu-C7) formed very unstable gels that recrystallize after a few hours. Within the alkylgalactonamide family, Gal-C9 was too poorly a soluble molecule to work easily with, and Gal-C5 was found to be excessively fragile for biological applications. Those two were then no further exploited. In the end, only Gal-C8, Gal-C7 and Gal-C6 were characterized and tried for cell culture applications.

Concerning the alkanoylglucamine family, their gelation was a bit more complicated. Indeed, Gluca-C12 formed a gel but it was only stable if a small fraction of HFP was added in the water. Nevertheless, after a few washes with water, this one could be easily eliminated, and the gel's biocompatibility could still be tested (see chapter II.2.4). Me-Gluca-C12 formed a nice thixotropic gel at a 5 wt % concentration but the problem was that it melted at 32 °C, which made it definitely unusable for cell culture. Me-Gluca-C14 was not able to form a gel.

I.2.2 Gelation of alkylgalactonamides: modulation of the gelation conditions and characterization of the resulting gels

In this part, we will describe how temperature rates can critically affect the morphology and the reproducibility of our hydrogels. Then the characterization of the resulting gels will be reported.

I.2.2.1 Gelation of alkylgalactonamides at room temperature

For the first gelation trials with the alkylgalactonamide molecules, the simplest way to obtain the hydrogels was to heat the gelator aqueous solution at high temperature around 100 °C and, once the gelator was dissolved, put it back at room temperature by directly letting it rest on the bench (referred as "0 min" cooling). Performed into vials of large volumes (at least 1 or 2 ml) the gels obtained appeared stable and homogeneous visually. But for smaller volumes, especially less than

500 µl, we noticed that it was hard to obtain reproducible gels. Indeed and especially when preparing the trials for cell culture, the gels were sometimes homogeneous and white whereas other times they were somehow fragmented and more translucent as it can be seen on Figure I-19 on the left picture.

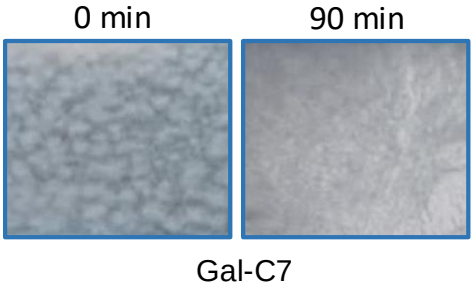

Figure I-19: Differences in macroscopic aspect of Gal-C7 gels. The one from the left was instantaneously cooled to room temperature; the one on the right underwent a controlled cooling (see I.2.2.2).

On the heterogeneous gels, the nucleation points could be clearly outlined with the naked eye as well with optical microscopy. All the matter actually concentrated on small distinct parts of the gel, which made it very fragile. Actually, with the alkylgalactonamides, the gelation occurs by nucleation similarly as a crystallization phenomenon.[81] In these conditions, they were not suitable for cell culture, because they did not withstand several rinses with culture media or phosphate buffer.

I.2.2.2 Gelation under controlled cooling rates

It is well known that with hydrogels, the gelation process can influence a lot the final aspect and properties of the gel.[82,83] In particular, gels formed by temperature changes can be affected by the cooling rate imposed on the hot solutions.[84] Thus, we adapted this reasoning to our systems in the hope of making gels in a reproducible way. We used a programmable oven to control the cooling rate during the gelation. We placed hot solutions of gelator in water in the oven at 100 °C and they were cooled down to 25 °C at different rates: either within 15, 30, 60 or 90 minutes. The gels referred as "0 min" are the ones directly cooled at room temperature without a controlled rate.

With optical and electronic microscopy observations, we have been able to characterize the microscopic structures of the hydrogels that underwent the different cooling conditions. We later also studied their rheological and mechanical properties.

I.2.2.2.1 Influence of the cooling rate on the gelation point density

As a first means of characterization, we tried to measure the nucleation point density on optical microscopic observations of the gels for the several cooling rates. Indeed, the more nucleation

points there were in the gel, the less resistant it was, for the gel could easily break in-between the spherulitic aggregates. If we can find a condition for which we obtain the least nucleation points, then the gel should be more homogeneous and less fragile.

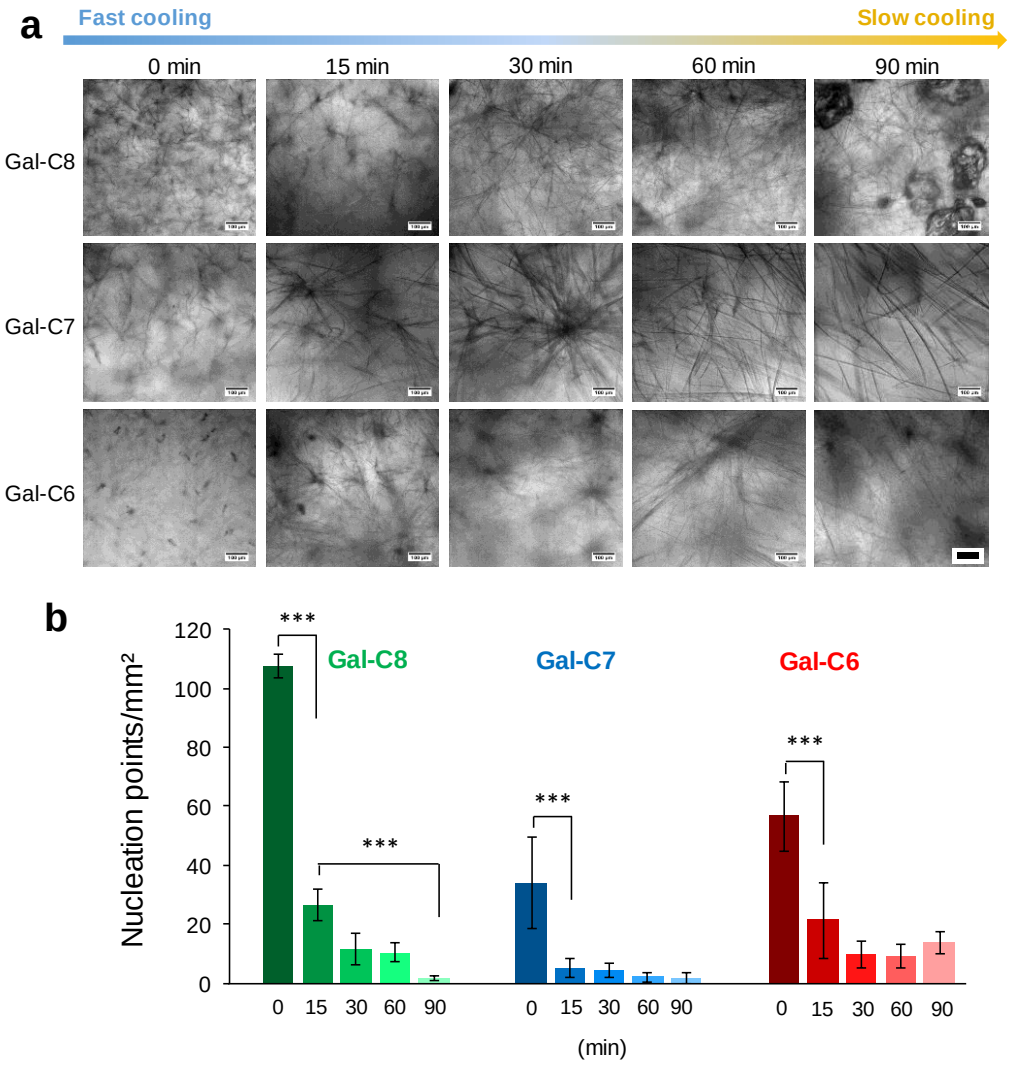

*Figure I-20: Influence of the controlled cooling rate on the gels aspect. (a) Bright-field microscopy observations of the three different gels prepared with different cooling rates, from an instantaneous cooling ("0 min") to slower cooling rates (time in min to go from 100 °C to 25 °C) (scale bars: 100 µm). (b) The nucleation point density was then quantified on each microscopy image and reported as a graph. The data represents the mean +/- SD of the number of nucleation points per mm² (n=6 per gel for the different cooling rates). Asterisks represent statistical significance between 0 and 15 min cooling rate or 15 and 90 min for the different gels (***: p < 0.0001).*

Figure I-20a shows the aspect of the alkylgalactonamide hydrogels that underwent the controlled cooling rates compared to the "0 min" condition in which they were instantly put to room temperature. The bottom of the gels was observed by inverted optical transmission microscopy (×10 magnification). It can clearly be seen on this figure that the cooling conditions affected the macroscopic and microscopic aspect of the gels. The difference could even be seen with the naked eye (see Figure I-19). With these bright field microscopy pictures, the nucleation point density

was visually assessed for each condition and each gel; the mean values of the densities were reported on the graph from Figure I-20b.

As a result, for each gel, there was a significant drop in the nucleation point density when at least a 15 min controlled cooling rate had been applied. Moreover, the slowest was the cooling, the less nucleation points there were and the more homogeneous the gels were. What was also noticeable is that for each condition, Gal-C7 always had a nucleation point density lower than the other two, even for a "0 min" condition. A 90 min cooling significantly decreased the number of nucleation points in Gal-C8 hydrogels compared to a 15 min cooling. For that reason, 90 min cooling rates were further applied in cell culture trials with the alkylgalactonamide gels.

I.2.2.2.2 Influence of the cooling rate on the fiber length

The difference of microstructure depending on the gelation conditions can be analyzed more precisely by optical microscopy. Indeed, the gels are translucent enough and the size of the fibers composing the gels is quite substantial so that we are able to observe the mesh only with a 10X objective on an optical microscope (Figure I-21). Only fibers exceeding the threshold of 4 µm in length, below 550 µm (i.e. the frame maximal dimensions) and large enough have been counted with this technique. To extract quantitative information from the images, we thus compared the gels fibers length distribution within these ranges of magnitude and *apparent* lengths were extracted for the different gels and gelling conditions.

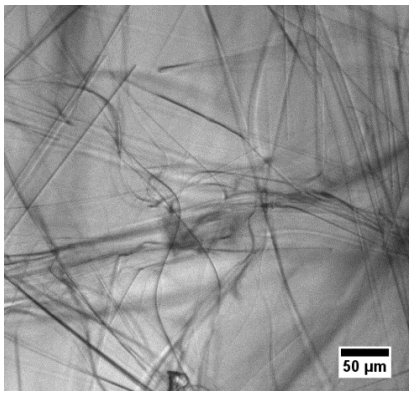

Figure I-21: Optical microscopy observation of a Gal-C7 gel.

At first sight, it looked like the longer the cooling rate was, the longer the fibers were. The *apparent* fiber lengths measurements are reported on the box chart from Figure I-22a.

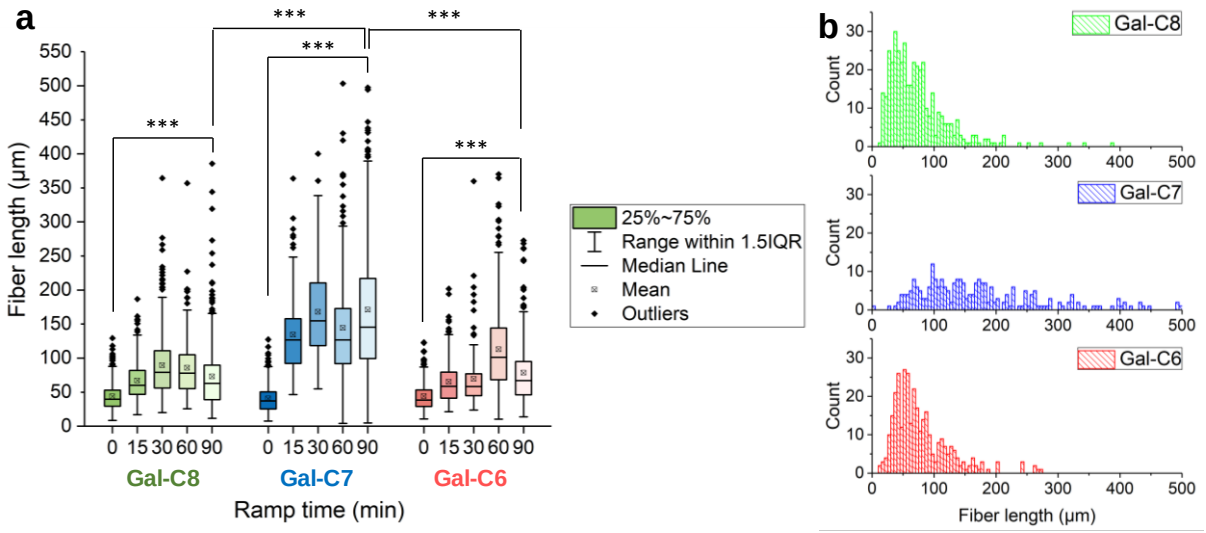

*Figure I-22: Fiber lengths analysis of gels prepared at different cooling rates. (a) Gal-C8,C7,C6 solution were allowed to gel at different cooling rate (time in min to go from 100 °C to 25 °C), the apparent fiber lengths were then analyzed on bright-field microscopy observation using ImageJ software (NeuronJ plugin). Asterisks represent statistical significance between 0 and 90 min cooling rate for each gel or between the 90 min cooling rates of the three gels (***: $p < 0.0001$). (b) Representative histogram of the fiber lengths obtained for the three gels for a 90-minute cooling rate.*

Concurrent with the decrease of the nucleation points, for all the gels, a significant increase in the fiber length was observed when a 90 min cooling time was applied compared to the "0 min" condition, and most of the effect occurred between 0 and 15 min. This means that just avoiding a sudden cooling of the hot solutions already enabled the development of much longer fibers.

In addition, several features were specific to Gal-C7. First, Gal-C7 had significantly longer apparent fibers than the two other gels when cooled over 90 min (Figure I-22a and b). Second, the length distribution for Gal-C7 was more widespread than for Gal-C8 and Gal-C6. Tertiary, Gal-C8 and Gal-C6 showed a much higher population of very short fibers, even with a 90 min cooling (Figure I-22b), and these gels looked much denser. Finally, Gal-C7 formed fibers that can reach up to 500 µm and over. The combination of all these factors - the nucleation point density and the fiber length - accounted for the aspect and the stability of the gels. Controlling the cooling rate during the gelation was thus a convenient method to obtain homogeneous and more stable gels in a reproducible way.

I.2.2.2.3 Influence of the cooling rate on the fiber width

To have more insight into the microscopic structure of the alkylaldonamide hydrogels, we used electronic microscopy. With this technique, smaller fibers embedded in the networks were observed (Figure I-23). With TEM clichés, measurements of the *apparent* fiber width were done in order to assess the size of the fibers. The results are represented on the graph of Figure I-23c in the case of "0 min" gels.

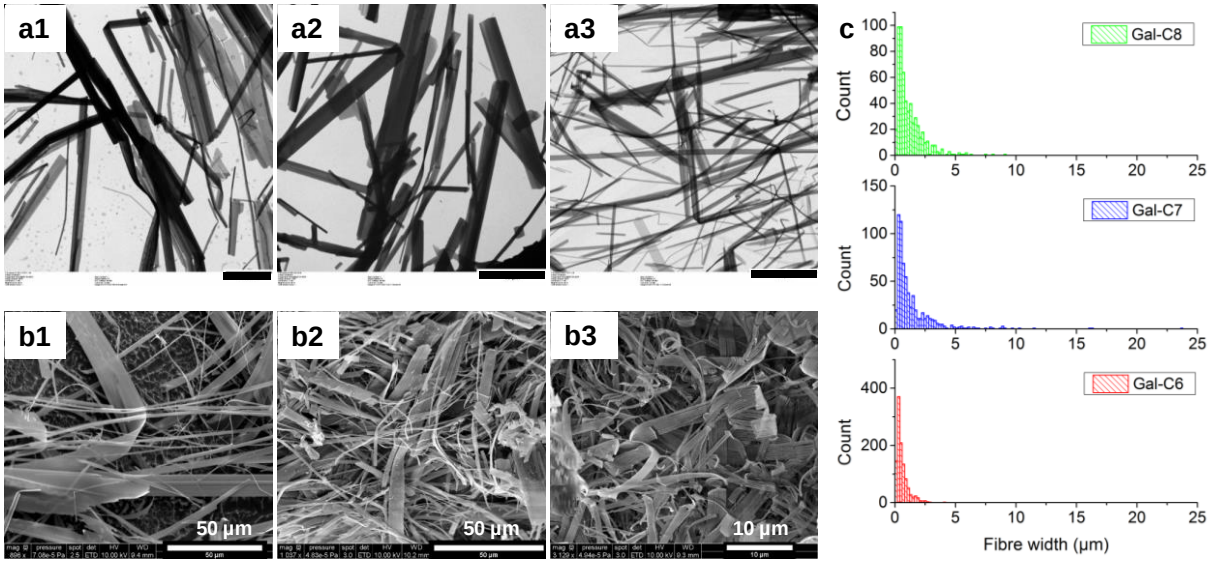

Figure I-23: Microscopic structure of the gel fibers. TEM images of Gal-C8, Gal-C7 and Gal-C6 gels (a1-a3, scale bar: 10 µm) and cryo-SEM images of Gal-C8, Gal-C7 and Gal-C6 gels prepared with a "0-min" cooling (b1-b3). (c) Histograms of the apparent fiber widths of the three gels for a "0 min" cooling time (measured on the TEM images).

What can be seen on the histograms is that indeed, there are very wide fibers in these hydrogels, but many of the fibers are actually less than 1 µm. The latter cannot be outlined with optical microscopy. The actual median width for Gal-C8 is 1.3 µm, for gal-C7 1.1 µm, and 0.3 µm for Gal-C6. Moreover, the ribbon-like shape of the aldonamide gelators' fibers appears clearly on the TEM pictures, as well as on the cryo-SEM pictures. Those ribbons can be very large; up to 35 µm for Gal-C7 or Gal-C8 gels is certain conditions. Gal-C6 fibers are narrower than the two others with a maximum width of 12 µm. This also appears clearly on optical microscopy observations where it is more difficult to distinguish Gal-C6 fibers than Gal-C7 or Gal-C8. From these first observations, we can already clearly distinguish Gal-C6 from Gal-C8 and Gal-C7 gels for their microscopic structures are quite different. Even though Gal-C6 is the most concentrated in gelator, its fibers are significantly thinner which may result in different properties.

Since the cooling rates had a significant influence on the fiber length within the hydrogels, we wanted to see if it had an influence on the fiber widths as well. For that, we used TEM clichés on which the *apparent* fiber widths were measured (such as it can be seen on Figure I-23a). Those measurements are reported on Figure I-24.

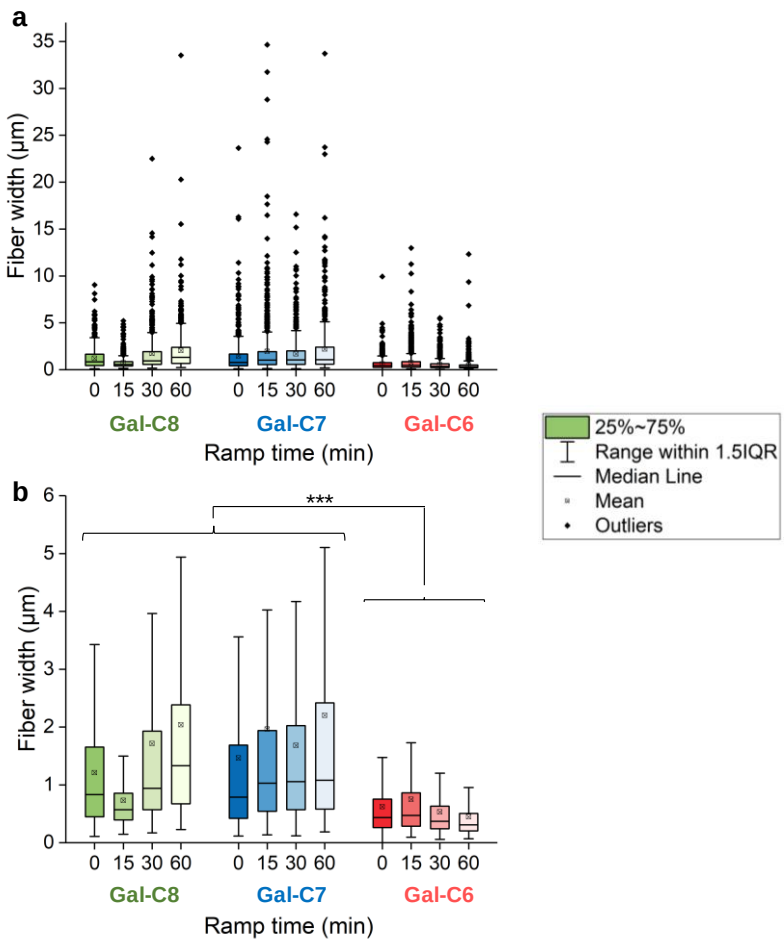

Figure I-24: Distribution of the fiber widths measured on TEM clichés with (a) and without outliers (b) at the different cooling times.

First, the controlled cooling rates did not seem to affect much the apparent fiber widths. A slight effect was however observed for Gal-C8 and Gal-C7, the widths seemed to increase with the longest cooling times whereas they decreased for Gal-C6. Nevertheless, for each gel, the median fiber widths remained approximately the same whatever the condition (Figure I-24b).

What was noticeable though is that, again and whatever the condition, Gal-C8 and Gal-C7 had significantly wider fibers than Gal-C6. Their size distribution was wider than the one of Gal-C6 (Figure I-24a). Very wide fibers (up to 35 µm) could be obtained with Gal-C8 and Gal-C7 whereas the maximum width for Gal-C6 was only of 13 µm. This difference between the gelators may later have an influence on the biological assessments of the hydrogels, for a difference in fiber width may induce a difference in local rigidity, topography or in interaction surface with the cells.

I.2.2.3 Molecular organization in the fibers

The three gels (90 min cooled) have also been analyzed by small angle X-ray scattering (SAXS) providing an insight in the molecular packing of the gelator molecules into the fibers and a measure of the fiber thicknesses.

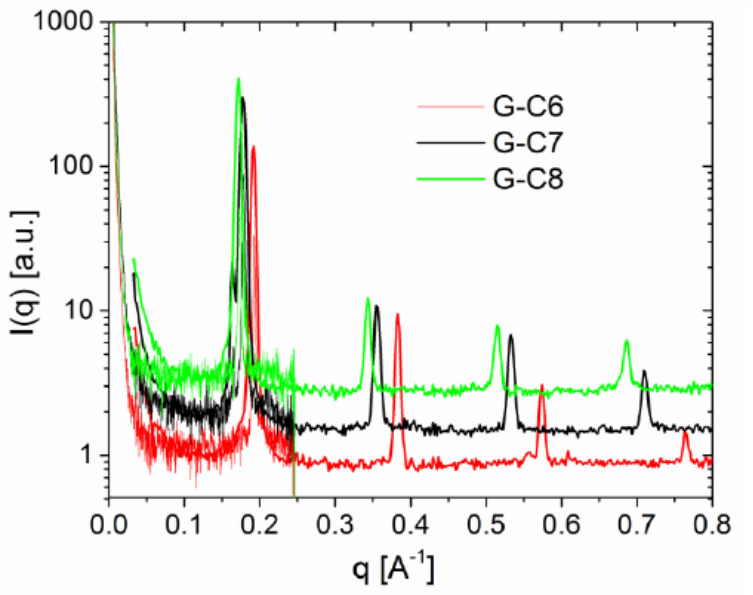

Figure I-25: Small Angle X-ray Scattering (SAXS) intensity as a function of the scattering vector, q, for the tree samples, Gal-C6, Gal-C7 and Gal-C8.

The curves for the three gels are shown in Figure I-25. The low q region presents a power law trend, $I(q) \propto q^{-4}$, which corresponds to the Porod region for the sharp interface of the large ribbons observed in TEM. At larger q values, the SAXS curves present strong scattering peaks at relative position ratios 1:2:3:4 and evidence well-defined lamellar organization. In the case of Gal-C7 an additional interaction peak is observed at lower q values, q_1^*=0.164 Å^{-1}, which corresponds to an interaction distance of 38.3 Å. There are not higher order peaks whose position can be related to it. This peak is indicative of the coexistence of two different arrangements. From the positions of the first order peaks (q_0^*=0.192 Å^{-1}, 0.178 Å^{-1} and 0.172 Å^{-1} for Gal-C6, Gal-C7 and Gal-C8 respectively), it is possible to calculate the long period spacing of the lamellar structure (Table I-2). In the three samples, it increases with the hydrophobic chain length from Gal-C6 to Gal-C8. The difference in the case of Gal-C6 and Gal-C7 (2.5 Å) is roughly twice the C-C bond length (1.5 Å). Conversely, the change in the lamellar spacing in Gal-C7 and Gal-C8 gels (1.3 Å), can't be only attributed to the different chain length, a variation in the sugar conformation or chain interdigitation could be the reason.

Table I-2: Spacing of the lamellar structure and mean thickness of the fibers for Gal-C6, Gal-C7 and Gal-C8 gels, determined by SAXS. Length difference for a C-C bond increment = 1.5 Å. FWHM = Full width at the half maximum.

	Q ($Å^{-1}$)	FWHM ($Å^{-1}$)	Lamellar spacing (Å)	Mean Thickness (Å)
G-C6	0.192	0.00238	32.7	2600
G-C7	0.178/0.164	0.00273/0.00363	35.2/38.3	2300/1730
G-C8	0.172	0.00251	36.5	2500

The crystalline structure of Gal-C8 has been described in the literature[85] as tail-to-tail bimolecular arrangements of extended octyl chain conformations. For the spacing between the lattice planes in the case of Gal-C8, we find values of 36.5 Å for the first order peak, which is well in accordance with the 37 Å already reported. The differences are probably to be attributed to different conformations of the sugar hydrophilic head: a *gauche* bend is 1.2 Å shorter than an *anti* conformation[85]. As the lamellar spacing in Gal-C8 gels is very similar to that found in the crystalline form, its fibers can be then considered as solid-like. The same solid-like phase can be reasonably assumed for the other samples. As a consequence, the distance between the correlated planes can be deduced from the linewidth of the Bragg peak, as frequently done for bilayers, providing a more precise measure of the ribbons thickness[86]. The thicknesses measured are reported in Table I-2. They are around 250±50 nm, for all the gels, that correlates quite well with the thicknesses estimated by cryo-SEM.

I.2.2.4 Mechanical properties

To complete their characterization, the mechanical properties of the gels have been assessed by dynamic rheology and by uniaxial and unconfined compression tests. The rheological tests could not be performed on gels that underwent controlled cooling but only on “0 min” cooled gels. Conversely, the mechanical properties of the gels could be measured by uniaxial and unconfined compression tests, and in this case, they could be performed with gels that underwent controlled cooling. Thus, both methods have been used.

The rheograms (Figure I-26) typically displayed the characteristics of a gel: both the elastic modulus (G′) and the viscous modulus (G″) exhibited plateaus, and G′ is about 10 times larger than G″, over the full range of frequency probed (10 to 0.1 Hz). Moduli were quite low, from 2 to 50 kPa (Table I-3), showing that they are very soft gels. There was a significant difference of elastic moduli G′ for the three gels that decreased in the order: Gal-C6 (50 kPa) ≫ Gal-C7 (7 kPa) > Gal-C8 (3 kPa) (Table I-3). Gal-C6 appeared to be a much stronger gel, ten times more rigid compared with Gal-C7 and Gal-C8.

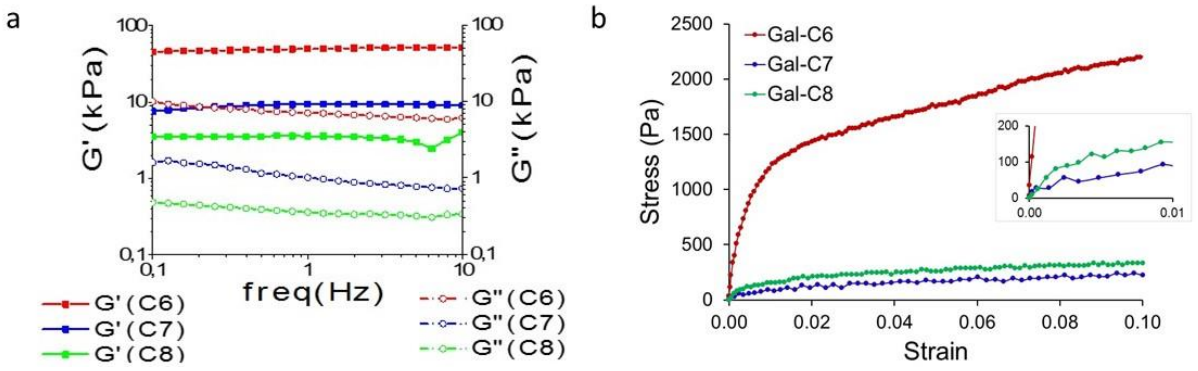

Figure I-26: (a) Rheology analysis of the three gels ("0-min" cooling): variation of the elastic (G') and viscous (G") modulus with the frequency (strain = 2.10^{-3} (0.2%), T° = 37°C). (b) Uniaxial compression of gels cylinders (90-min cooling; fast compression speed: 5 mm/s, T° = 20°C). Gel concentrations for both rheology and compression tests: Gal-C6: 1 wt %; Gal-C7: 0.45%; Gal-C8: 0.5%.

Table I-3: Elastic (G') and viscous (G") moduli measured by dynamic rheology, at 1 Hz, 0.2% strain, 37°C. Y_0: Initial moduli of the gels measured by uniaxial compression tests at different compressive rates, 20°C. 5 mm/s reflects an intermediate loading rate condition, 0.1 mm/s reflects a quasi-static loading rate condition.

Gel	**G' (1 Hz) kPa 37°C**	**G'' (1 Hz) kPa 37°C**	**Y_0 (5 mm/s) kPa 20°C**	**Y_0 (0.1 mm/s) kPa 20°C**
Gal-C6	50	3	153±31	39±7
Gal-C7	7	1	14±3	8±2
Gal-C8	3	0.5	24±3	12±4

In the case of uniaxial unconfined compression tests, a controlled cooling of 90 min has been applied to the gel solutions into sealed molds. Those tests were performed at low strain, from 0 to 10 % strain, at two compressive rates (5–0.1 mm/s) (Figure I-26). The curves displayed the features of stress–strain curves of cellular solids, such as foams or sponges at low strains.[87] The general trend on the Gal-C6, Gal-C7, and Gal-C8 stress–strain curves was a softening when the strain increased. Two regimes have been identified. At very low strain, the curves displayed a higher slope, from which the initial moduli (Y_0) were measured. They were quite similar for Gal-C7 (14 ± 3 kPa at 5 mm/s) and Gal-C8 (24 ± 3 kPa at 5 mm/s) and much higher for Gal-C6 (153 ± 31 kPa at 5 mm/s) (Figure I-26b, Table I-3).

These results were in accordance with the macroscopic observations: during handling, Gal-C6 gels were able to sustain a higher stress or strain before collapsing compared with Gal-C7 and Gal-C8 gels. When compression increased, fibers tended to bend, buckle and pack, and a fraction of water was also expulsed. These different phenomena lead to a progressive decrease of the gel resistance (softening), measured by a decrease of the modulus for all the gels. They were partly reversible

upon unloading. As a result, a second regime was observed at higher strain, with a very low modulus, between ≈1 and 5 kPa for all the gels. It corresponded to the residual stiffness of a gel partly compressed.

Both rheology and compression tests showed that these gels are very soft. On all measurements, Gal-C6 was clearly stiffer. As explained above, a higher concentration for Gal-C6 gels (1%) had to be selected in order to get gels that are able to withstand cell culture conditions. At lower concentrations, the gel was broken up during biological tests. However, for mechanical testing purposes, it was possible to make self-standing Gal-C6 gel cylinders at a lower concentration (0.65%) by slow cooling. Their moduli were respectively 25 ± 1 kPa (5 mm/s) and 19 ± 2 kPa (0.1 mm/s), close to the values obtained for Gal-C7 (at 0.45%) and Gal-C8 (at 0.5%) at similar concentrations. This supplementary data showed that the higher stiffness observed for Gal-C6 gels at 1% would be mainly related to its higher concentration. Finally, the moduli of Gal-C7 and Gal-C8 in quasi-static loading conditions (respectively 8 ± 2 and 12 ± 4 kPa at 0.1 mm·s−1) had the order of magnitude closest to the brain rigidity that is between 0.5 and 2.5 kPa in similar loading conditions.[88]

I.2.2.5 Determination of the gelation points

In order to have a better estimation of the gelation points of the different hydrogelators, DSC technique was used. They underwent several cycles of heating and cooling at different rates and their thermograms were obtained. Table I-4 references the different transition temperatures of the different gels for 3 and 10 °C/min rates.

Table I-4: Gel-sol transition temperatures T° (gel > sol) and sol-gel temperatures T° (sol >gel) at the peak of the three gels, for two heating-cooling rates.

Gel	Heating/cooling rate (°C/min)	$T°_{gel \rightarrow sol}$ (°C)	$T°_{sol \rightarrow gel}$ (°C)
Gal-C6	3	70	38
Gal-C6	10	79	35
Gal-C7	3	85	-
Gal-C7	10	94	58
Gal-C8	3	121	87
Gal-C8	10	120	95

The concentrations used were 1 wt % for Gal-C6, 0.45 wt % for Gal-C7 and 0.5 wt % for Gal-C8. The longer the carbon chain, the higher the transition temperatures are. There is a hysteresis in

the sol-gel transition since the solution forms a gel at a lower temperature ($T°_{sol \rightarrow gel}$) than the temperature at which the gel is melted ($T°_{gel \rightarrow sol}$). For the three molecules, the gelation point was above 37 °C and they could be used for cell culture applications.

I.2.2.6 Solubility of the molecules

The residual solubility of the gelators once in the form of hydrogel was also assessed. The hydrogels were prepared at their regular concentrations and after some time compressed in order to retrieve the water. This one was filtered and its composition was analyzed by thermogravimetric analysis, which gave us the water/gelator ratio. These results are represented in Table I-5. It indeed appears that the longer the alkyl chain is, the less soluble is the molecule.

Table I-5: Soluble fraction of the three gelators in pure water

Gel	Gal-C6 (1 wt %)	Gal-C7 (0.45 wt %)	Gal-C8 (0.5 wt %)
Solubility at 21h (wt % of gelator in the aqueous phase)	0.14 %	0.03 %	0.02 %
Solubility at 21h (µmol/ml)	5.0	1.2	0.7

I.2.2.7 Surface tension measurements

Surface tension measurements were also performed for the three alkygalactonamides in order to assess their surface activity. This piece of data is important for the further cell culture trials because if an amphiphilic molecule modifies too much the water surface tension, cell membranes could be altered and cell death could occur. In addition, what is quite specific to molecular hydrogels is that there is still an equilibrium between the aggregated gelator molecules (those embedded within the supramolecular ribbons or fibers) and the free gelator molecules. Depending on the structure of the gelator, the number of free molecules (its solubility) can be very different from one another. This may impact the bioavailability of the gelator and the way it interacts with the cells, and thus, its toxicity.

The measurements were performed on the filtrated residual water of crushed gels of Gal-C6, C7 and C8 at the concentrations of 1%, 0.45% and 0.5% respectively, as well as pure water by the pendant drop method. It was found that the three molecules modify up to 22 % the surface tension of pure water (9 % for Gal-C8, 22 % for Gal-C7 and 15 % for Gal-C6). In comparison, a 0.01 wt % solution of Triton X-100 in water, which is usually used for the permeation of cell membranes in

biology, decreases the surface tension of water by 58 % (data supplied by The Dow Chemical Company website). It means that, despite their amphiphile structure, the alkylgalactonamide molecules are quite poor surfactants, which may be an advantage for their use in cell culture.

I.3 Conclusion

Through this first stage of the project, several simple molecular gelators have been prepared and their conditions of gelation have been explored. More particularly, the alkylgalactonamide family has been revisited, with the introduction of an intermediate member, Gal-C7, that proved to have different gelling properties compared with GalC6 and GalC8, which were already known. They are very simple molecules that are very easy to synthesize at the gram scale as well as to purify. Based on this pattern of a polar sugar head linked to a short alkane chain, other molecules were synthesized but they resulted in less satisfying gels because of their poor stability or their complicated gelation conditions.

Gal-C6, Gal-C7 and Gal-C8 have thus been chosen to be fully exploited because they were the ones exhibiting the best gelation conditions and the best properties. Indeed, after dissolution in water at high temperature and cooling down, they form coarse white hydrogels that are composed of long and wide ribbon-like fibers. Their mechanical characterization indicates that they are quite soft gels but resistant enough to mechanical strain, even though they undergo synaeresis.

We introduced a new method to prepare the hydrogels in a reproducible way by applying a slow control of the cooling rate during gelation. It provided more homogeneous and stable gels, with longer apparent fiber length.

The biocompatibility of these gels has now to be assessed for their application to the growth of neurons and that is what we are going to see in the next chapter.

References

(1) Zhou, J.; Li, J.; Du, X.; Xu, B. Supramolecular Biofunctional Materials. *Biomaterials* **2017**, *129*, 1–27. https://doi.org/10.1016/j.biomaterials.2017.03.014.

(2) Keller, A. Introductory Lecture. Aspects of Polymer Gels. *Faraday Discussions* **1995**, *101*, 1. https://doi.org/10.1039/fd9950100001.

(3) Lukyanova, L. Préparation de Matrices Microporeuses d'organogel et Évaluation En Culture Cellulaire, Université Paul Sabatier-Toulouse III, 2009.

(4) Whitesides, G. M.; Mathias, J. P.; Seto, C. T. Molecular Self-Assembly and Nanochemistry: A Chemical Strategy for the Synthesis of Nanostructures. *Science* **1991**, *254* (5036), 1312–1319. https://doi.org/10.1126/science.1962191.

(5) Estroff, L. A.; Hamilton, A. D. Water Gelation by Small Organic Molecules. *Chemical reviews* **2004**, *104* (3), 1201–1218.

(6) Dastidar, P. Supramolecular Gelling Agents: Can They Be Designed? *Chemical Society Reviews* **2008**, *37* (12), 2699. https://doi.org/10.1039/b807346e.

(7) Weiss, R. G. The Past, Present, and Future of Molecular Gels. What Is the Status of the Field, and Where Is It Going? *Journal of the American Chemical Society* **2014**, *136* (21), 7519–7530. https://doi.org/10.1021/ja503363v.

(8) Kunitake, T.; Okahata, Y.; Shimomura, M.; Yasunami, S.; Takarabe, K. Formation of Stable Bilayer Assemblies in Water from Single-Chain Amphiphiles. Relationship between the Amphiphile Structure and the Aggregate Morphology. *Journal of the American Chemical Society* **1981**, *103* (18), 5401–5413. https://doi.org/10.1021/ja00408a021.

(9) Fuhrhop, J. H.; Schnieder, P.; Boekema, E.; Helfrich, W. Lipid Bilayer Fibers from Diastereomeric and Enantiomeric N-Octylaldonamides. *Journal of the American Chemical Society* **1988**, *110* (9), 2861–2867.

(10) Saha, K.; Keung, A. J.; Irwin, E. F.; Li, Y.; Little, L.; Schaffer, D. V.; Healy, K. E. Substrate Modulus Directs Neural Stem Cell Behavior. *Biophysical Journal* **2008**, *95* (9), 4426–4438. https://doi.org/10.1529/biophysj.108.132217.

(11) Du, X.; Zhou, J.; Shi, J.; Xu, B. Supramolecular Hydrogelators and Hydrogels: From Soft Matter to Molecular Biomaterials. *Chemical Reviews* **2015**, *115* (24), 13165–13307. https://doi.org/10.1021/acs.chemrev.5b00299.

(12) Zanna, N.; Focaroli, S.; Merlettini, A.; Gentilucci, L.; Teti, G.; Falconi, M.; Tomasini, C. Thixotropic Peptide-Based Physical Hydrogels Applied to Three-Dimensional Cell Culture. *ACS Omega* **2017**, *2* (5), 2374–2381. https://doi.org/10.1021/acsomega.7b00322.

(13) Kouchak, M. In Situ Gelling Systems for Drug Delivery. *Jundishapur J Nat Pharm Prod* **2014**, *9* (3).

(14) Koutsopoulos, S.; Zhang, S. Long-Term Three-Dimensional Neural Tissue Cultures in Functionalized Self-Assembling Peptide Hydrogels, Matrigel and Collagen I. *Acta Biomaterialia* **2013**, *9* (2), 5162–5169. https://doi.org/10.1016/j.actbio.2012.09.010.

(15) Mahler, A.; Reches, M.; Rechter, M.; Cohen, S.; Gazit, E. Rigid, Self-Assembled Hydrogel Composed of a Modified Aromatic Dipeptide. *Advanced Materials* **2006**, *18* (11), 1365–1370. https://doi.org/10.1002/adma.200501765.

(16) Ryan, D. M.; Anderson, S. B.; Senguen, F. T.; Youngman, R. E.; Nilsson, B. L. Self-Assembly and Hydrogelation Promoted by F5-Phenylalanine. *Soft Matter* **2010**, *6* (3), 475–479. https://doi.org/10.1039/B916738B.

(17) Dou, X.-Q.; Zhang, D.; Feng, C.-L. Wettability of Supramolecular Nanofibers for Controlled Cell Adhesion and Proliferation. *Langmuir* **2013**, *29* (49), 15359–15366. https://doi.org/10.1021/la4040276.

(18) Erni, R.; Rossell, M. D.; Kisielowski, C.; Dahmen, U. Atomic-Resolution Imaging with a Sub-50-Pm Electron Probe. *Physical Review Letters* **2009**, *102* (9). https://doi.org/10.1103/PhysRevLett.102.096101.

(19) Fitremann, J.; Lonetti, B.; Fratini, E.; Fabing, I.; Payré, B.; Boulé, C.; Loubinoux, I.; Vaysse, L.; Oriol, L. A Shear-Induced Network of Aligned Wormlike Micelles in a Sugar-Based Molecular Gel. From Gelation to Biocompatibility Assays. *Journal of Colloid and Interface Science* **2017**, *504*, 721–730. https://doi.org/10.1016/j.jcis.2017.06.021.

(20) Fichman, G.; Gazit, E. Self-Assembly of Short Peptides to Form Hydrogels: Design of Building Blocks, Physical Properties and Technological Applications. *Acta Biomaterialia* **2014**, *10* (4), 1671–1682. https://doi.org/10.1016/j.actbio.2013.08.013.

(21) Dou, X.-Q.; Feng, C.-L. Amino Acids and Peptide-Based Supramolecular Hydrogels for Three-Dimensional Cell Culture. *Advanced Materials* **2017**, 1604062. https://doi.org/10.1002/adma.201604062.

(22) Ryan, D. M.; Nilsson, B. L. Self-Assembled Amino Acids and Dipeptides as Noncovalent Hydrogels for Tissue Engineering. *Polym. Chem.* **2012**, *3* (1), 18–33. https://doi.org/10.1039/C1PY00335F.

(23) Matson, J. B.; Stupp, S. I. Self-Assembling Peptide Scaffolds for Regenerative Medicine. *Chemical Communications* **2012**, *48* (1), 26. https://doi.org/10.1039/c1cc15551b.

(24) Plow, E. F.; Haas, T. A.; Zhang, L.; Loftus, J.; Smith, J. W. Ligand Binding to Integrins. *Journal of Biological Chemistry* **2000**, *275* (29), 21785–21788. https://doi.org/10.1074/jbc.R000003200.

(25) Hogrebe, N. J.; Reinhardt, J. W.; Tram, N. K.; Debski, A. C.; Agarwal, G.; Reilly, M. A.; Gooch, K. J. Independent Control of Matrix Adhesiveness and Stiffness within a 3D Self-Assembling Peptide Hydrogel. *Acta Biomaterialia* **2018**, *70*, 110–119. https://doi.org/10.1016/j.actbio.2018.01.031.

(26) Tian, Y. F.; Devgun, J. M.; Collier, J. H. Fibrillized Peptide Microgels for Cell Encapsulation and 3D Cell Culture. *Soft Matter* **2011**, *7* (13), 6005. https://doi.org/10.1039/c1sm05504f.

(27) Huang, C.-C.; Ravindran, S.; Yin, Z.; George, A. 3-D Self-Assembling Leucine Zipper Hydrogel with Tunable Properties for Tissue Engineering. *Biomaterials* **2014**, *35* (20), 5316–5326. https://doi.org/10.1016/j.biomaterials.2014.03.035.

(28) Cheng, B.; Yan, Y.; Qi, J.; Deng, L.; Shao, Z.-W.; Zhang, K.-Q.; Li, B.; Sun, Z.; Li, X. Cooperative Assembly of a Peptide Gelator and Silk Fibroin Afford an Injectable Hydrogel for Tissue

Engineering. *ACS Applied Materials & Interfaces* **2018**, *10* (15), 12474–12484. https://doi.org/10.1021/acsami.8b01725.

(29) Wu, Z.; Chen, G.; Zhang, J.; Hua, Y.; Li, J.; Liu, B.; Huang, A.; Li, H.; Chen, M.; Ou, C. Treatment of Myocardial Infarction with Gene-Modified Mesenchymal Stem Cells in a Small Molecular Hydrogel. *Scientific Reports* **2017**, *7* (1). https://doi.org/10.1038/s41598-017-15870-z.

(30) Cheng, T.-Y.; Wu, H.-C.; Huang, M.-Y.; Chang, W.-H.; Lee, C.-H.; Wang, T.-W. Self-Assembling Functionalized Nanopeptides for Immediate Hemostasis and Accelerative Liver Tissue Regeneration. *Nanoscale* **2013**, *5* (7), 2734. https://doi.org/10.1039/c3nr33710c.

(31) Galler, K. M.; Hartgerink, J. D.; Cavender, A. C.; Schmalz, G.; D'Souza, R. N. A Customized Self-Assembling Peptide Hydrogel for Dental Pulp Tissue Engineering. *Tissue Eng Part A* **2012**, *18* (1–2), 176–184. https://doi.org/10.1089/ten.tea.2011.0222.

(32) Berns, E. J.; Sur, S.; Pan, L.; Goldberger, J. E.; Suresh, S.; Zhang, S.; Kessler, J. A.; Stupp, S. I. Aligned Neurite Outgrowth and Directed Cell Migration in Self-Assembled Monodomain Gels. *Biomaterials* **2014**, *35*, 185–195. https://doi.org/10.1016/j.biomaterials.2013.09.077.

(33) Zhang, S.; Greenfield, M. A.; Mata, A.; Palmer, L. C.; Bitton, R.; Mantei, J. R.; Aparicio, C.; de la Cruz, M. O.; Stupp, S. I. A Self-Assembly Pathway to Aligned Monodomain Gels. *Nat Mater* **2010**, *9* (7), 594–601. https://doi.org/10.1038/nmat2778.

(34) Matsuoka, A. J.; Sayed, Z. A.; Stephanopoulos, N.; Berns, E. J.; Wadhwani, A. R.; Morrissey, Z. D.; Chadly, D. M.; Kobayashi, S.; Edelbrock, A. N.; Mashimo, T.; et al. Creating a Stem Cell Niche in the Inner Ear Using Self-Assembling Peptide Amphiphiles. *PLOS ONE* **2017**, *12* (12), e0190150. https://doi.org/10.1371/journal.pone.0190150.

(35) Cheng, T.-Y.; Chen, M.-H.; Chang, W.-H.; Huang, M.-Y.; Wang, T.-W. Neural Stem Cells Encapsulated in a Functionalized Self-Assembling Peptide Hydrogel for Brain Tissue Engineering. *Biomaterials* **2013**, *34* (8), 2005–2016. https://doi.org/10.1016/j.biomaterials.2012.11.043.

(36) Soler-Botija, C.; Bagó, J. R.; Llucià-Valldeperas, A.; Vallés-Lluch, A.; Castells-Sala, C.; Martínez-Ramos, C.; Fernández-Muiños, T.; Chachques, J. C.; Pradas, M. M.; Semino, C. E.; et al. Engineered 3D Bioimplants Using Elastomeric Scaffold, Self-Assembling Peptide Hydrogel, and Adipose Tissue-Derived Progenitor Cells for Cardiac Regeneration. *Am J Transl Res* **2014**, *6* (3), 291–301.

(37) Akiyama, N.; Yamamoto-Fukuda, T.; Takahashi, H.; Koji, T. In Situ Tissue Engineering with Synthetic Self-Assembling Peptide Nanofiber Scaffolds, PuraMatrix, for Mucosal Regeneration in the Rat Middle-Ear. *Int J Nanomedicine* **2013**, *8*, 2629–2640. https://doi.org/10.2147/IJN.S47279.

(38) Holmes, T. C.; Lacalle, S. de; Su, X.; Liu, G.; Rich, A.; Zhang, S. Extensive Neurite Outgrowth and Active Synapse Formation on Self-Assembling Peptide Scaffolds. *PNAS* **2000**, *97* (12), 6728–6733. https://doi.org/10.1073/pnas.97.12.6728.

(39) Ellis-Behnke, R. G.; Liang, Y.-X.; You, S.-W.; Tay, D. K.; Zhang, S.; So, K.-F.; Schneider, G. E. Nano Neuro Knitting: Peptide Nanofiber Scaffold for Brain Repair and Axon Regeneration with Functional Return of Vision. *Proceedings of the National Academy of Sciences of the United States of America* **2006**, *103* (13), 5054–5059.

(40) Gelain, F.; Cigognini, D.; Caprini, A.; Silva, D.; Colleoni, B.; Donegá, M.; Antonini, S.; Cohen, B. E.; Vescovi, A. New Bioactive Motifs and Their Use in Functionalized Self-Assembling Peptides for NSC Differentiation and Neural Tissue Engineering. *Nanoscale* **2012**, *4* (9), 2946. https://doi.org/10.1039/c2nr30220a.

(41) Caprini, A.; Silva, D.; Zanoni, I.; Cunha, C.; Volontè, C.; Vescovi, A.; Gelain, F. A Novel Bioactive Peptide: Assessing Its Activity over Murine Neural Stem Cells and Its Potential for Neural Tissue Engineering. *New Biotechnology* **2013**, *30* (5), 552–562. https://doi.org/10.1016/j.nbt.2013.03.005.

(42) Gelain, F.; Silva, D.; Caprini, A.; Taraballi, F.; Natalello, A.; Villa, O.; Nam, K. T.; Zuckermann, R. N.; Doglia, S. M.; Vescovi, A. BMHP1-Derived Self-Assembling Peptides: Hierarchically Assembled Structures with Self-Healing Propensity and Potential for Tissue Engineering Applications. *ACS Nano* **2011**, *5* (3), 1845–1859. https://doi.org/10.1021/nn102663a.

(43) Arioz, I.; Erol, O.; Bakan, G.; Dikecoglu, F. B.; Topal, A. E.; Urel, M.; Dana, A.; Tekinay, A. B.; Guler, M. O. Biocompatible Electroactive Tetra(Aniline)-Conjugated Peptide Nanofibers for Neural Differentiation. *ACS Applied Materials & Interfaces* **2018**, *10* (1), 308–317. https://doi.org/10.1021/acsami.7b16509.

(44) Restu, W. K.; Nishida, Y.; Yamamoto, S.; Ishii, J.; Maruyama, T. Short Oligopeptides for Biocompatible and Biodegradable Supramolecular Hydrogels. *Langmuir* **2018**, *34* (27), 8065–8074. https://doi.org/10.1021/acs.langmuir.8b00362.

(45) Suga, T.; Osada, S.; Narita, T.; Oishi, Y.; Kodama, H. Promotion of Cell Adhesion by Low-Molecular-Weight Hydrogel by Lys Based Amphiphile. *Materials Science and Engineering: C* **2015**, *47*, 345–350. https://doi.org/10.1016/j.msec.2014.11.032.

(46) Liu, G.-F.; Zhang, D.; Feng, C.-L. Control of Three-Dimensional Cell Adhesion by the Chirality of Nanofibers in Hydrogels. *Angew. Chem. Int. Ed.* **2014**, *53* (30), 7789–7793. https://doi.org/10.1002/anie.201403249.

(47) Jayawarna, V.; Richardson, S. M.; Hirst, A. R.; Hodson, N. W.; Saiani, A.; Gough, J. E.; Ulijn, R. V. Introducing Chemical Functionality in Fmoc-Peptide Gels for Cell Culture. *Acta Biomaterialia* **2009**, *5* (3), 934–943. https://doi.org/10.1016/j.actbio.2009.01.006.

(48) Chronopoulou, L.; Togna, A. R.; Guarguaglini, G.; Masci, G.; Giammaruco, F.; Togna, G. I.; Palocci, C. Self-Assembling Peptide Hydrogels Promote Microglial Cells Proliferation and NGF Production. *Soft Matter* **2012**, *8* (21), 5784. https://doi.org/10.1039/c2sm25528f.

(49) Wang, Y.; Zhang, Z.; Xu, L.; Li, X.; Chen, H. Hydrogels of Halogenated Fmoc-Short Peptides for Potential Application in Tissue Engineering. *Colloids and Surfaces B: Biointerfaces* **2013**, *104*, 163–168. https://doi.org/10.1016/j.colsurfb.2012.11.038.

(50) Cheng, G.; Castelletto, V.; Jones, R. R.; Connon, C. J.; Hamley, I. W. Hydrogelation of Self-Assembling RGD-Based Peptides. *Soft Matter* **2011**, *7* (4), 1326. https://doi.org/10.1039/c0sm00408a.

(51) Rodriguez, A. L.; Wang, T. Y.; Bruggeman, K. F.; Horgan, C. C.; Li, R.; Williams, R. J.; Parish, C. L.; Nisbet, D. R. In Vivo Assessment of Grafted Cortical Neural Progenitor Cells and Host Response to Functionalized Self-Assembling Peptide Hydrogels and the Implications for Tissue Repair. *J. Mater. Chem. B* **2014**, *2* (44), 7771–7778. https://doi.org/10.1039/C4TB01391C.

(52) Rodriguez, A. L.; Bruggeman, K. F.; Wang, Y.; Wang, T. Y.; Williams, R. J.; Parish, C. L.; Nisbet, D. R. Using Minimalist Self-Assembling Peptides as Hierarchical Scaffolds to Stabilise Growth Factors and Promote Stem Cell Integration in the Injured Brain. *Journal of Tissue Engineering and Regenerative Medicine* **2018**, *12* (3), e1571–e1579. https://doi.org/10.1002/term.2582.

(53) Datta, S.; Bhattacharya, S. Multifarious Facets of Sugar-Derived Molecular Gels: Molecular Features, Mechanisms of Self-Assembly and Emerging Applications. *Chem. Soc. Rev.* **2015**, *44* (15), 5596–5637. https://doi.org/10.1039/C5CS00093A.

(54) Pfannemüller, B.; Welte, W. Amphiphilic Properties of Synthetic Glycolipids Based on Amide Linkages. I. Electron Microscopic Studies on Aqueous Gels. *Chemistry and physics of lipids* **1985**, *37* (3), 227–240.

(55) Mizrahi, S.; Rizkov, D.; Hayat, N.; Lev, O. A Low Molecular Weight Hydrogel Which Exhibits Electroosmotic Flow and Its Use as a Bioreactor and for Electrochromatography of Neutral Species. *Chemical Communications* **2008**, No. 25, 2914. https://doi.org/10.1039/b802155d.

(56) Ávalos, M.; Babiano, R.; Cintas, P.; Gómez-Carretero, A.; Jiménez, J. L.; Lozano, M.; Ortiz, A. L.; Palacios, J. C.; Pinazo, A. A Family of Hydrogels Based on Ureido-Linked Aminopolyol-Derived Amphiphiles and Bolaamphiphiles: Synthesis, Gelation under Thermal and Sonochemical Stimuli, and Mesomorphic Characterization. *Chem. Eur. J.* **2008**, *14* (18), 5656–5669. https://doi.org/10.1002/chem.200701897.

(57) Burczyk, B.; Wilk, K. A.; Sokołowski, A.; Syper, L. Synthesis and Surface Properties of N-Alkyl-N-Methylgluconamides and N-Alkyl-N-Methyllactobionamides. *Journal of Colloid and Interface Science* **2001**, *240* (2), 552–558. https://doi.org/10.1006/jcis.2001.7704.

(58) Capicciotti, C. J.; Leclère, M.; Perras, F. A.; Bryce, D. L.; Paulin, H.; Harden, J.; Liu, Y.; Ben, R. N. Potent Inhibition of Ice Recrystallization by Low Molecular Weight Carbohydrate-Based Surfactants and Hydrogelators. *Chemical Science* **2012**, *3* (5), 1408. https://doi.org/10.1039/c2sc00885h.

(59) Ohsedo, Y.; Oono, M.; Saruhashi, K.; Watanabe, H. Onset of Mixing-Induced Thixotropy in Hydrogels by Mixing Two Homologues of Low-Molecular-Weight Hydrogelators. *RSC Adv.* **2014**, *4* (82), 43560–43563. https://doi.org/10.1039/C4RA08345H.

(60) Ohsedo, Y.; Oono, M.; Saruhashi, K.; Watanabe, H. N-Alkylamido-D-Glucamine-Based Gelators for the Generation of Thixotropic Gels. *RSC Adv.* **2014**, *4* (89), 48554–48558. https://doi.org/10.1039/C4RA08346F.

(61) Minakuchi, N.; Hoe, K.; Yamaki, D.; Ten-no, S.; Nakashima, K.; Goto, M.; Mizuhata, M.; Maruyama, T. Versatile Supramolecular Gelators That Can Harden Water, Organic Solvents and Ionic Liquids. *Langmuir* **2012**, *28* (25), 9259–9266. https://doi.org/10.1021/la301442f.

(62) Cano, M. E.; Di Chenna, P. H.; Lesur, D.; Wolosiuk, A.; Kovensky, J.; Uhrig, M. L. Chirality Inversion, Supramolecular Hydrogelation and Lectin Binding of Two Thiolactose Amphiphiles Constructed on a Di-Lauroyl-l-Tartaric Acid Scaffold. *New Journal of Chemistry* **2017**, *41* (23), 14754–14765. https://doi.org/10.1039/C7NJ02941A.

(63) Clemente, M. J.; Romero, P.; Serrano, J. L.; Fitremann, J.; Oriol, L. Supramolecular Hydrogels Based on Glycoamphiphiles: Effect of the Disaccharide Polar Head. *Chemistry of Materials* **2012**, *24* (20), 3847–3858. https://doi.org/10.1021/cm301509v.

(64) Wang, W.; Wang, H.; Ren, C.; Wang, J.; Tan, M.; Shen, J.; Yang, Z.; Wang, P. G.; Wang, L. A Saccharide-Based Supramolecular Hydrogel for Cell Culture. *Carbohydrate Research* **2011**, *346* (8), 1013–1017. https://doi.org/10.1016/j.carres.2011.03.031.

(65) Xiao, X.; Hu, J.; Wang, X.; Huang, L.; Chen, Y.; Wang, W.; Li, J.; Zhang, Y. A Dual-Functional Supramolecular Hydrogel Based on a Spiropyran–Galactose Conjugate for Target-Mediated and Light-Controlled Delivery of MicroRNA into Cells. *Chemical Communications* **2016**, *52* (84), 12517–12520. https://doi.org/10.1039/C6CC07386G.

(66) Ikeda, M.; Ochi, R.; Wada, A.; Hamachi, I. Supramolecular Hydrogel Capsule Showing Prostate Specific Antigen-Responsive Function for Sensing and Targeting Prostate Cancer Cells. *Chemical Science* **2010**, *1* (4), 491. https://doi.org/10.1039/c0sc00278j.

(67) Komatsu, H.; Tsukiji, S.; Ikeda, M.; Hamachi, I. Stiff, Multistimuli-Responsive Supramolecular Hydrogels as Unique Molds for 2D/3D Microarchitectures of Live Cells. *Chemistry - An Asian Journal* **2011**, *6* (9), 2368–2375. https://doi.org/10.1002/asia.201100134.

(68) Yang, Z.; Liang, G.; Ma, M.; Abbah, A. S.; Lu, W. W.; Xu, B. D-Glucosamine-Based Supramolecular Hydrogels to Improve Wound Healing. *Chem. Commun.* **2007**, No. 8, 843–845. https://doi.org/10.1039/B616563J.

(69) Liu, J.; Sun, Z.; Yuan, Y.; Tian, X.; Liu, X.; Duan, G.; Yang, Y.; Yuan, L.; Lin, H.-C.; Li, X. Peptide Glycosylation Generates Supramolecular Assemblies from Glycopeptides as Biomimetic Scaffolds for Cell Adhesion and Proliferation. *ACS Applied Materials & Interfaces* **2016**, *8* (11), 6917–6924. https://doi.org/10.1021/acsami.6b00850.

(70) Aldaye, F. A.; Senapedis, W. T.; Silver, P. A.; Way, J. C. A Structurally Tunable DNA-Based Extracellular Matrix. *J Am Chem Soc* **2010**, *132* (42), 14727–14729. https://doi.org/10.1021/ja105431h.

(71) Buerkle, L. E.; von Recum, H. A.; Rowan, S. J. Toward Potential Supramolecular Tissue Engineering Scaffolds Based on Guanosine Derivatives. *Chem. Sci.* **2012**, *3* (2), 564–572. https://doi.org/10.1039/C1SC00729G.

(72) Rotaru, A.; Pricope, G.; Plank, T. N.; Clima, L.; Ursu, E. L.; Pinteala, M.; Davis, J. T.; Barboiu, M. G-Quartet Hydrogels for Effective Cell Growth Applications. *Chemical Communications* **2017**, *53* (94), 12668–12671. https://doi.org/10.1039/C7CC07806D.

(73) Ziane, S.; Schlaubitz, S.; Miraux, S.; Patwa, A.; Lalande, C.; Bilem, I.; Lepreux, S.; Rousseau, B.; Le Meins, J.-F.; Latxague, L.; et al. A Thermosensitive Low Molecular Weight Hydrogel as Scaffold for Tissue Engineering. *European Cells and Materials* **2012**, *23*, 147–160.

(74) Latxague, L.; Ramin, M. A.; Appavoo, A.; Berto, P.; Maisani, M.; Ehret, C.; Chassande, O.; Barthélémy, P. Control of Stem-Cell Behavior by Fine Tuning the Supramolecular Assemblies of Low-Molecular-Weight Gelators. *Angew. Chem. Int. Ed.* **2015**, *54* (15), 4517–4521. https://doi.org/10.1002/anie.201409134.

(75) Ramin, M. A.; Latxague, L.; Sindhu, K. R.; Chassande, O.; Barthélémy, P. Low Molecular Weight Hydrogels Derived from Urea Based-Bolaamphiphiles as New Injectable Biomaterials. *Biomaterials* **2017**, *145*, 72–80. https://doi.org/10.1016/j.biomaterials.2017.08.034.

(76) Li, X.; Yi Kuang; Shi, J.; Gao, Y.; Lin, H.-C.; Xu, B. Multifunctional, Biocompatible Supramolecular Hydrogelators Consist Only of Nucleobase, Amino Acid, and Glycoside.

Journal of the American Chemical Society **2011**, *133* (43), 17513–17518. https://doi.org/10.1021/ja208456k.

(77) Yuan, D.; Du, X.; Shi, J.; Zhou, N.; Baoum, A. A.; Xu, B. Synthesis of Novel Conjugates of a Saccharide, Amino Acids, Nucleobase and the Evaluation of Their Cell Compatibility. *Beilstein Journal of Organic Chemistry* **2014**, *10*, 2406–2413. https://doi.org/10.3762/bjoc.10.250.

(78) Yuan, D.; Du, X.; Shi, J.; Zhou, N.; Baoum, A. A.; Al Footy, K. O.; Badahdah, K. O.; Xu, B. Synthesis and Evaluation of the Biostability and Cell Compatibility of Novel Conjugates of Nucleobase, Peptidic Epitope, and Saccharide. *Beilstein Journal of Organic Chemistry* **2015**, *11*, 1352–1359. https://doi.org/10.3762/bjoc.11.145.

(79) Hoffmann, H.; Thunig, C.; Miller, D. Vesicle Phases from N-Methyl-N-Alkanoylglucamin and Various Co-Surfactants. *Colloids and Surfaces A: Physicochemical and Engineering Aspects* **2002**, *210* (2), 147–158.

(80) Zasloff, M. Liquid Non-Ionic Salt-Free Skin and Hair Treatment Composition That Contains n-Methyl Lauroyl Glucamide. US20140242018 A1, August 28, 2014.

(81) Liu, X. Y. Gelation with Small Molecules: From Formation Mechanism to NanostructureArchitecture. In *Low Molecular Mass Gelator*; Springer Berlin Heidelberg: Berlin, Heidelberg, 2005; Vol. 256, pp 1–37.

(82) Draper, E. R.; Adams, D. J. Low-Molecular-Weight Gels: The State of the Art. *Chem* **2017**, *3* (3), 390–410. https://doi.org/10.1016/j.chempr.2017.07.012.

(83) Yuan, B.; Liu, X.-Y.; Li, J.-L.; Xu, H.-Y. Volume Confinement Induced Microstructural Transitions and Property Enhancements of Supramolecular Soft Materials. *Soft Matter* **2011**, *7* (5), 1708–1713. https://doi.org/10.1039/C0SM00873G.

(84) Lescanne, M.; Colin, A.; Mondain-Monval, O.; Fages, F.; Pozzo, J.-L. Structural Aspects of the Gelation Process Observed with Low Molecular Mass Organogelators. *Langmuir* **2003**, *19* (6), 2013–2020. https://doi.org/10.1021/la026660u.

(85) Svenson, S.; Kirste, B.; Fuhrhop, J.-H. A CPMAS 13C NMR Study of Molecular Conformations and Disorder of N-Octylhexonamides in Microcrystals and Supramolecular Assemblies. *J. Am. Chem. Soc.* **1994**, 116 (26), 11969−11975.

(86) Fernandez, R. M.; Riske, K. A.; Amaral, L. Q.; Itri, R.; Lamy, M. T. Influence of Salt on the Structure of DMPG Studied by SAXS and Optical Microscopy. *Biochimica et Biophysica Acta (BBA) - Biomembranes* **2008**, 1778 (4), 907–916. https://doi.org/10.1016/j.bbamem.2007.12.005.

(87) Gibson, L. J.; Ashby, M. F. The Mechanics of Three-Dimensional Cellular Materials. *Proceedings of the Royal Society A: Mathematical, Physical and Engineering Sciences* **1982**, *382* (1782), 43–59. https://doi.org/10.1098/rspa.1982.0088.

(88) Budday, S.; Sommer, G.; Birkl, C.; Langkammer, C.; Haybaeck, J.; Kohnert, J.; Bauer, M.; Paulsen, F.; Steinmann, P.; Kuhl, E.; et al. Mechanical Characterization of Human Brain Tissue. *Acta Biomaterialia* **2017**, *48*, 319–340. https://doi.org/10.1016/j.actbio.2016.10.036.

II. Application as cell culture scaffolds for the growth of neurons

II.1 Neural stem cells: growth mechanisms and artificial matrices

Even though this number is still debated in the scientific world, the brain contains more than 100 billion of neurons and all our thoughts, actions, feelings are monitored through these special cells. It has now long been known that the brain is composed of a dense and complex network of distinct cells. A few decades ago, it was still thought that the number of neurons in an adult brain was fixed and that it would only decreasing with age. It is in the 80s that some works on canary birds proved that this number could actually increase, even at the adult stage.[1] Reynolds and Weiss in 1992 confirmed the observation of neurogenesis in the adult brain of rodents[2] and a few years later, this observation was also made in the adult human brain thanks to the works of Gage[3]. In 2002, this same team showed that these neural stem cells were able to integrate and become mature neurons in the adult brain[4] (Figure II-1). It is actually believed that one new neuron is added each day for every 2000 existing.[5] Even if its occurrence is still debated nowadays[6], adult neurogenesis appears to be possible and holds great promises for diseases affecting the central nervous system.

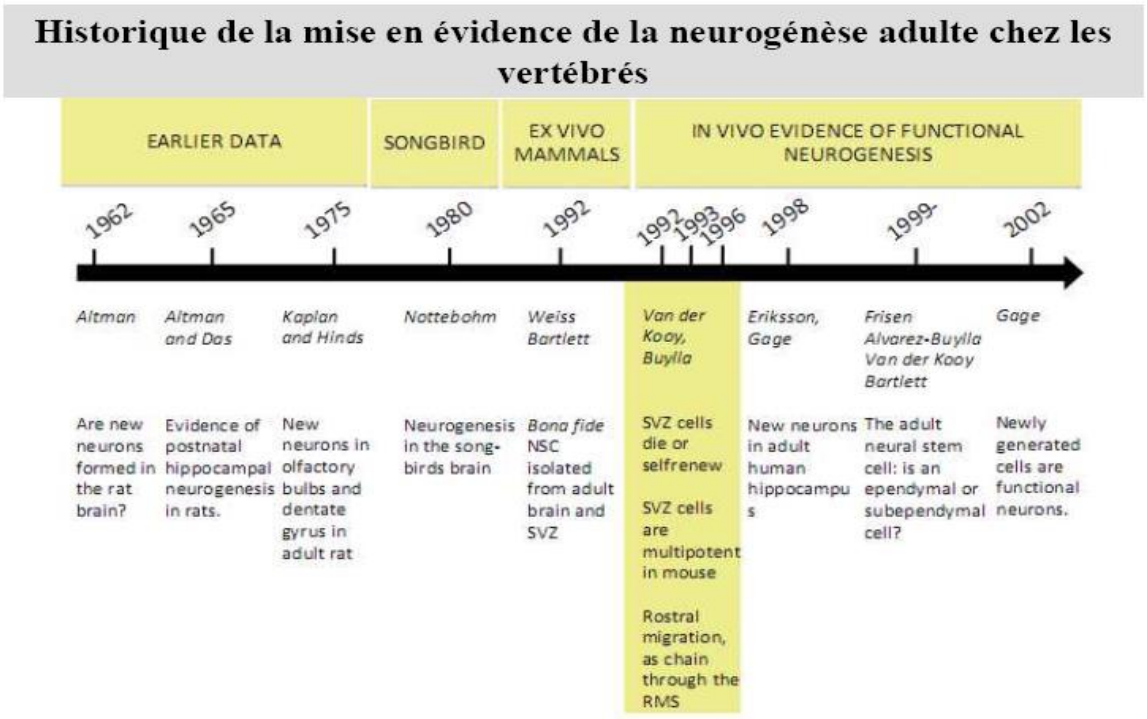

Figure II-1: Timeline of the discoveries concerning neurogenesis and neural stem cells in the adult brain.

In this part, we are going to present the specificities of neuronal cells, as well as neural stem cells (the term “neuronal cells” refers to neurons only whereas the term “neural cells” is related to the three main lineage of the brain: astrocytes, oligodendrocytes and neurons). After that, we are going to discuss the different existing biomaterials for the growth of neural stem cells.

II.1.1 Neural stem cells: definitions, structure and growth mechanisms

Before dealing with stem cells, we are going to show why neural cells are such peculiar cells compared to those of the rest of the organism, describe what their growth mechanisms are and the role of the supporting cells.

II.1.1.1 Specificities of neuronal and glial cells

Just like fibroblasts or osteoblasts, neurons are regular cells with a cytoplasmic membrane, organelles and a nucleus containing the genetic information (Figure II-2). They are the only cells in living organisms that are able to communicate and transfer information throughout a network. To do so, neurons use their own specific elements that no other cells have:

- A long elongation of the cytoplasmic membrane called “**axon**” which is used for intracellular information transfer. In the human body, some axons can extend to one meter or more.
- **Dendrites** that are also extensions of the cytoplasmic membrane but are usually shorter than the axon. This is where external information from other neurons is received.
- **Synapses** that are the contact zones between two neurons and where the information (electrical or chemical) is transferred from one cell to the other.

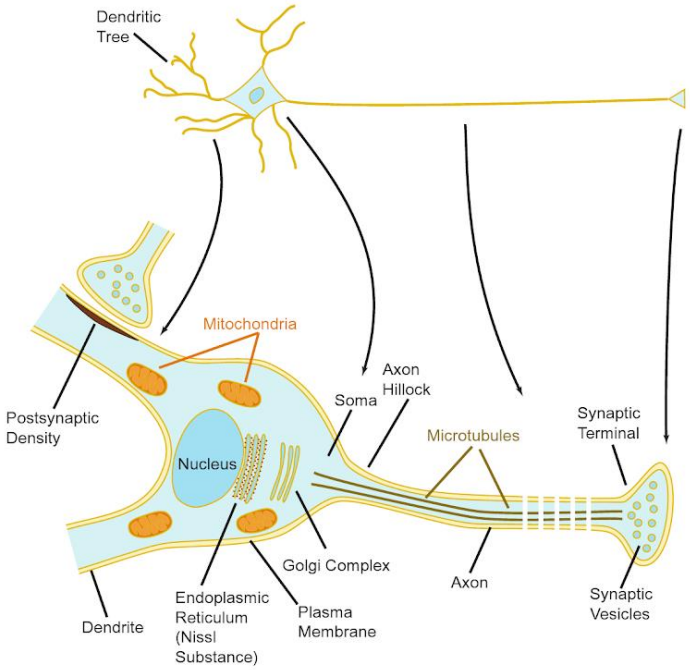

Figure II-2: Cellular structure of a neuron (from [5]).

But even if neurons are the most important cells in the brain in the sense that they are the one transmitting the information, they are neither the only ones nor the most numerous. Indeed, the supporting cells in the central nervous system (CNS) is part of what is called the neuroglia. Three types of cells compose the neuroglia: the astrocytes, the oligodendrocytes and the microglia; the three combined are more generally referred as "glial cells" (Figure II-3). Glial cells' main function is as support cells for neurons, but they have various other uses and scientists are still investigating their roles in the CNS. For instance, oligodendrocytes are very important for the functioning of neurons since they are the cells responsible for the myelination of axons in the CNS (in the peripheral nervous system, it is the role of Schwann cells). With their cytoplasm, their roll around the axons and thus form the myelin sheath that electrically insulates the axonal cytoplasm from the external environment. Astrocytes act as support cells for neurons but they also release and receive some neurotransmitters, meaning that they actively participate in intercellular signaling in the CNS. The cells forming microglia have various roles: they act as immune cells, they are responsible for the phagocytose of cell debris and they also play an important role in the development and the good functioning of synapses. Microglia cells have a hematopoietic origin whereas oligodendrocytes and astrocytes come from neural cell lineage. Without glial cells, neurons alone could not grow and function properly.[5] That is why for tissue engineering applications involving neurons, glial cells have also to be cultured along with neurons in order to ensure a good functioning of the system.

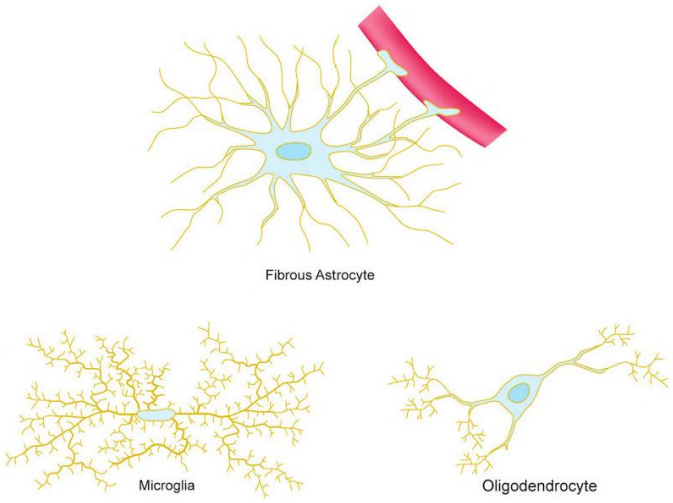

Figure II-3: Structure of the different glial cells (from [5]).

II.1.1.2 Neural stem cells

II.1.1.2.1 Formation of neurons and glial cells

In the adult brain, neurogenesis occurs thanks to special cells that are called neural stem cells (NSCs). These are immature cells that can further divide and differentiate only into neural types of cells: neurons, astrocytes or oligodendrocytes. Compared to embryonic stem cells that can develop into any kind of cell and are then referred as pluripotent cells, NSCs can only differentiate into these three types and are thus multipotent stem cells. Due to their restricted lineages and their low self-renewal capacity, human adult NSCs are sometimes considered as progenitor cells.

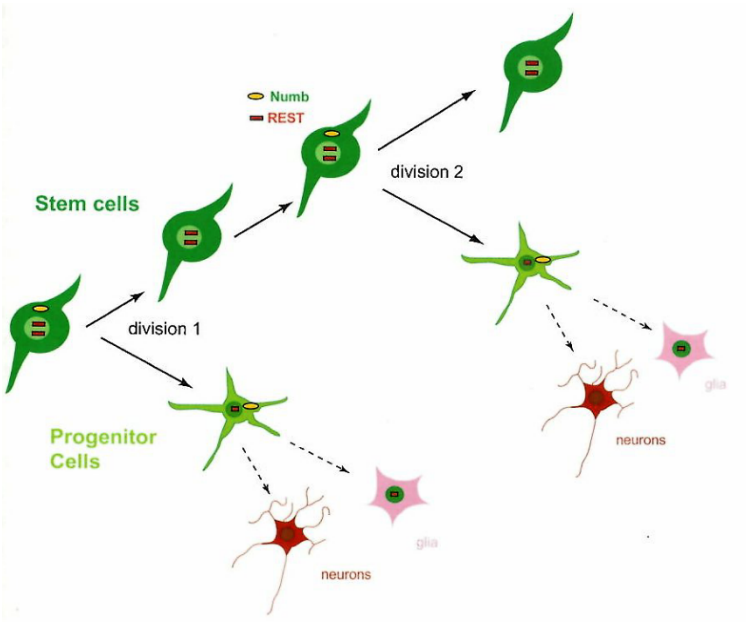

Figure II-4: The division of neural stem cells. For the generation of neurons, one NSC gives another NSC and a progenitor cell. This latter can then give either a neuronal or a glial cell. Like this, the pool of stem cells remains constant.

The functioning of NSCs is so that when they divide in the brain, they can produce another stem cell plus one neural cell that is a progenitor cell (Figure II-4). Depending on the factors to which it will be exposed, this neural cell can give either a neuron, an astrocyte or an oligodendrocyte. These differentiation factors are released by surrounding cells. When isolated *in vitro* and cultured in non-adherent conditions, the NSCs divide and have the capacity to form cellular assemblies in suspension called "neurospheres" (Figure II-5). NSCs are then easy to isolate because they are the only cells spontaneously forming these spheres. In the presence of growth factors as EGF and bFGF (see II.1.1.3.1), this self-organization is favorable to their amplification as NSCs. As it can be seen on Figure II-5, the BrdU marker (which is a marker of DNA replication) is present at the center of the neurospheres, meaning that some cells are still dividing in those structures. Cell differentiation can also be induced by using adherent conditions and appropriate mediums.

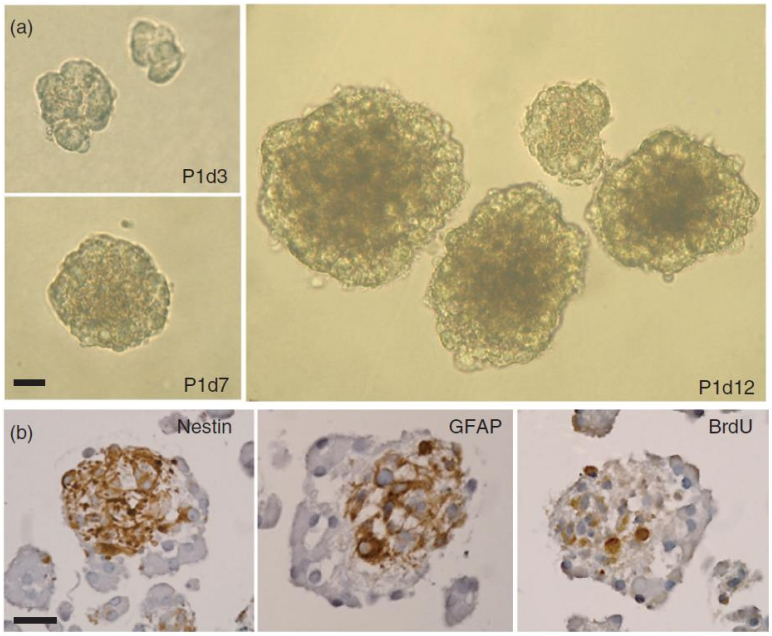

Figure II-5: Neurospheres obtained from patient biopsies in the temporal lobe. a. Secondary neurospheres after 3, 7 and 12 days of culture. b. Immunostaining of secondary neurospheres after 10 days of culture with nestin (neurons), GFAP (glial cells) and BrdU (marker of cell division). Scale bars = 50 µm. From [7].

Throughout their differentiation, NSCs are going to express different types of cell makers as it is represented on Figure II-6. These markers are specific of the different cell types: for instance, astrocytes express the glial fibrillary acidic protein (GFAP) or S100B, oligodendrocytes express O4 or A2B5 and neurons can be characterized by the presence of β3-tubulin and then NeuN or MAP2. The expression of the different markers can be evidenced by immunostaining in order to have an insight into the cells' differentiation.

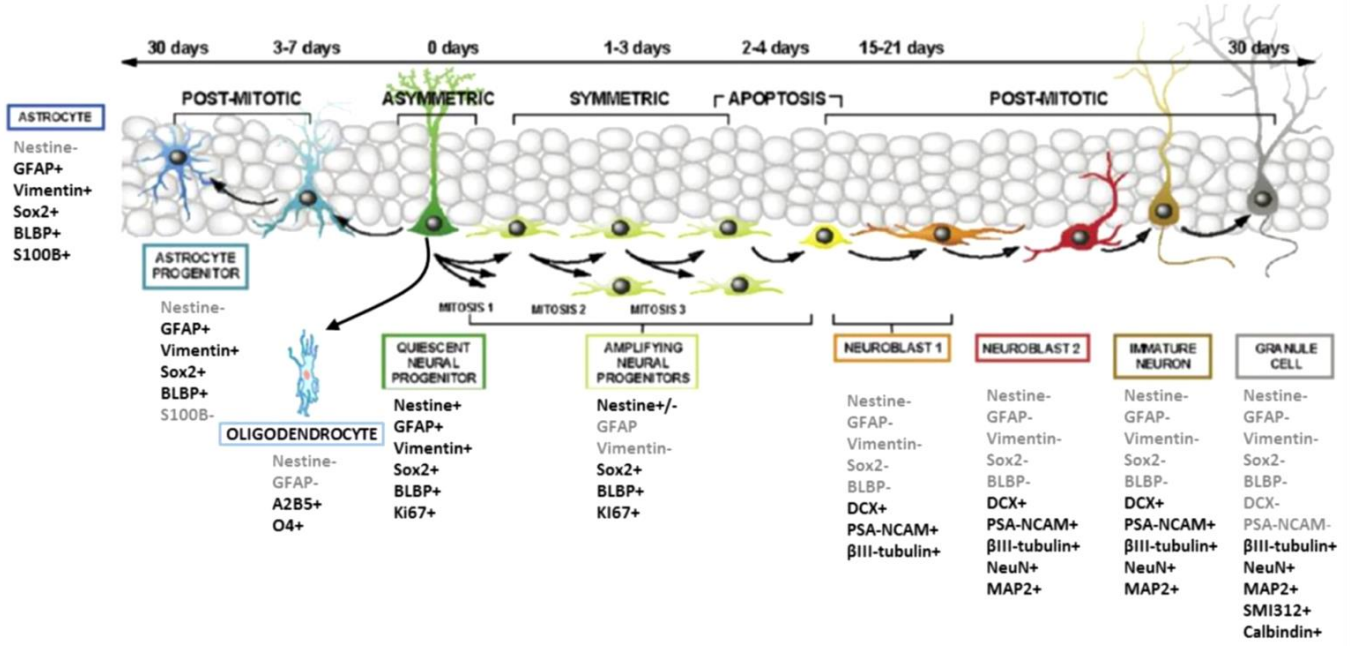

Figure II-6: Differentiation of NSCs into the three possible cell types with the corresponding markers expressed at the different stages throughout the various cellular stages. From [8].

II.1.1.2.2 Location in the adult brain and hNSCs retrieval

Neural stem cells in the adult human brain are located in some particular zones of the brain called "niches". These zones present very specific conditions favorable for the growth of neural stem cells. The two main areas where stem cells are located in the adult mammalian brain are the subventricular zone (SVZ) of the lateral ventricles and the subgranular zone (SGZ) of the dentate gyrus in the hippocampus (Figure II-7).

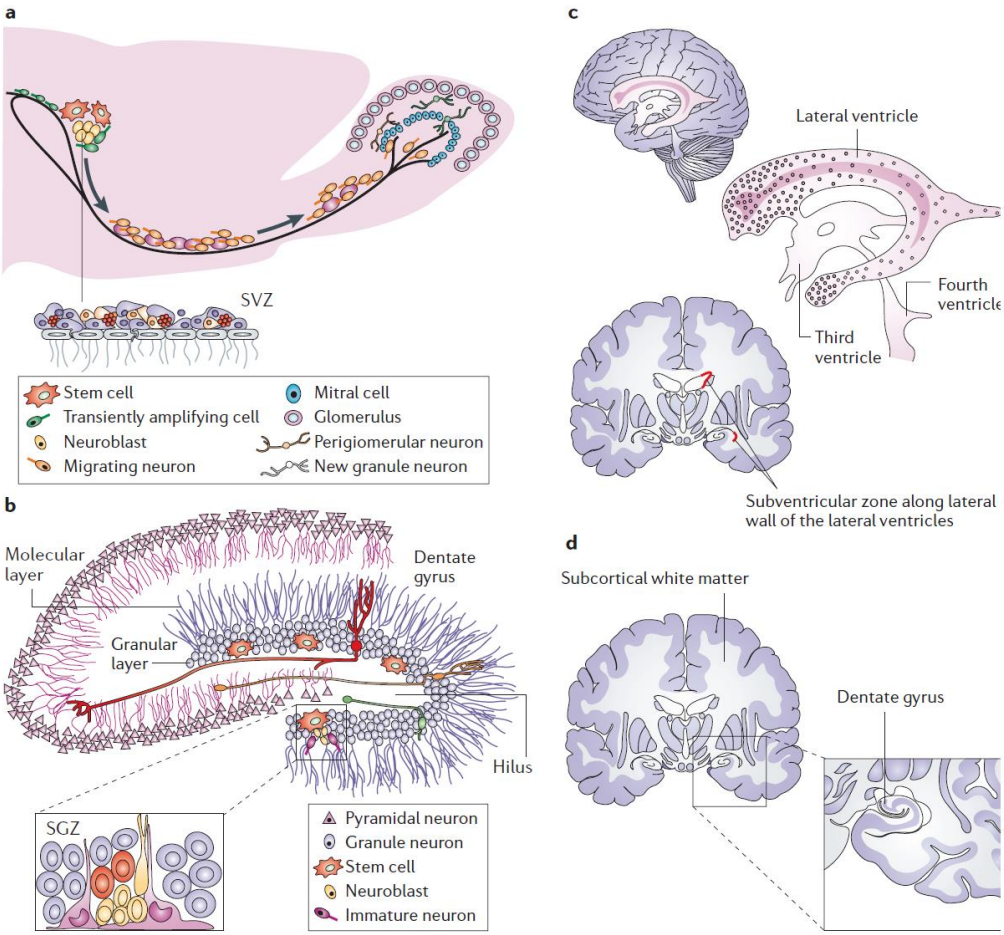

Figure II-7: "The anatomy and functioning of the subventricular zone and subgranular zone in rodents and humans. a | A sagittal section through the lateral ventricle that shows the larger area of adult neurogenesis; that is, the subventricular zone (SVZ). This region lines the lateral ventricles of the forebrain and is comprised of three main cell types. The multipotent, type B astrocytes, that have been identified as the bona fide SVZ stem cells, give rise to fast-cycling transiently proliferating precursor cells that are called type C precursors and that, in turn, generate mitotically active type A neuroblasts. The type A cells, while dividing, migrate tangentially towards the olfactory bulbs where they integrate as new interneurons. b | An additional adult neurogenetic region is found in the subgranular zone (SGZ), which is located within the dentate gyrus of the hippocampus. A cellular hierarchy, somewhat similar to that of the SVZ, is seen in the SGZ in which the true stem cell is probably the type B astrocyte, which produces the intermediate type D precursor that eventually gives rise to the type G granule neurons. These neurons integrate functionally into the granule cell layer. c | In the adult human brain, a population of SVZ astrocytes that is organized as a periventricular ribbon has been identified as comprising neural stem cells. In contrast to the rodent SVZ, no signs of tangential neuronal chain migration were detected from the corresponding human area. d | The germinal zone of the adult human hippocampus is located within the dentate gyrus. Neurogenesis in this region has been demonstrated to take place in adult humans." From [9].

In the SVZ, once the stem cells give newly born neurons, these ones migrate to the olfactory bulb through what is called the rostral migratory stream. In the SGZ, the newly born neurons settle in the dentate gyrus which is actually a region thought to be important for the acquisition of new memories.

However, it is admitted that neural progenitor cells (NPCs) also exist in other parts of the adult brain. These cells can be located in different regions other than the SVZ and the SGZ, such as the cortex[10], the amygdala[11] or even the subcortical white matter[12]. One of the zones where these cells

can also be found is the temporal lobe. Cells that are called "hNSCs" (human neural stem cells) in our study come from either this region or from the SVZ of the human brain.

II.1.1.3 The growth of neurons

The growth and differentiation of NSCs require some specific conditions in order to give the right type of cells. *In vivo*, they need to grow and migrate according to the brain organization. To do so, NSCs are helped by several biological cues and factors. We are here going to see how the growth of neurons and glial cells can thus be monitored in the brain.

II.1.1.3.1 Growth factors

Growth factors (GFs) are molecules that influence the growth, development and differentiation of cells. They will act on the cell fate and determine its future properties. These molecules have two ways of action: they either activate specific genes that later will activate different functions in the cell (instructive mechanism), or they promote the survival of cells that already express specific properties (selective mechanism). One GF can actually use both mechanisms and they intervene at very specific times in the cell development. GFs can be located on the cell membranes of adjacent cells or they can be secreted by distant non-neuronal cells. These distant emissions induce the presence of gradients of GF concentration in the environment which will guide the developing cells. Examples of neuron GFs are basic fibroblast growth factors (bFGFs) or epidermal growth factors (EGFs). Despite their names, these molecules do act on the growth of neurons. They were actually first discovered in non-neuronal cells, hence the names. Neurotrophins are also a type of soluble GF acting on neurons by preventing their apoptotic death. They ensure the survival of neurons during their development and their maintenance once adult. Nerve growth factors (NGFs) and brain-derived neurotrophic factors (BDNFs) are common GFs for neurons that belong to the neurotrophin family. NGFs do not act on the mitosis of neurons but they act on the normal development of sympathetic neurons and on their normal functioning in adult life, participating also in the neurite outgrowth. BDNFs, as their name imply, are mostly present in the brain and they induce a more prolonged survival of sensory neurons. Other types of neurotrophins exist, acting mostly in the brain for neuronal growth, survival, differentiation and other properties.

However, the development of cells in the CNS also relies on cell-cell communication. As a matter of fact, the location and the neighbors of one cell have an influence of its development in order to make it differentiate in the right kind of cell at the right position in the system. The molecules resulting from this kind of interactions are called morphogens. One well-known mechanism for the differentiation of neurons is the Notch signaling pathway for instance. Notch receptors are

present on the plasma membrane of cells and are activated by contact with other cells. This enables groups of cells to influence each other and form large structures.[13]

II.1.1.3.2 Neurite outgrowth

In order to develop its neurites (this term is used when axons and dendrites are still immature and cannot be distinguished yet), a neuron needs fairly strong adhesion to a surface (such as other cells, protein fibers or any substrate) but it also needs to know in which direction it has to grow.

First, the neurite outgrowth occurs through the growth cone, situated at the extremity of the neurites. It is composed of a central core with microtubules to set its structure and where many mitochondria and other cellular material are found. Surrounding the central core are the lamellipodia that are composed of actin fibers. Again, at the extremity of lamellipodia, processes that are called microspikes or filopodia are found (Figure II-8).

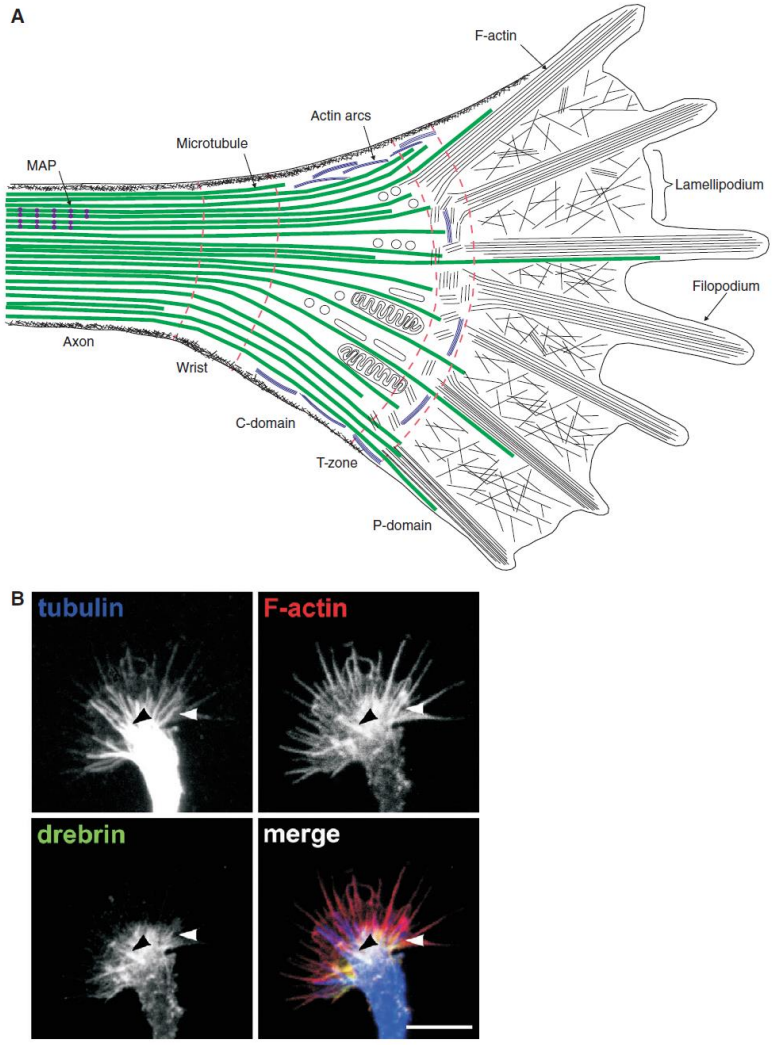

Figure II-8: A. Structure of the growth cone cytoskeleton with the microtubules and the actin forming the lamellipodia and the filopodia. B. Different fluorescent markers enable to stain the different components of the growth cone. From [14].

These filopodia are the ones exploring the substrate and guiding the growth cone by being in constant extension and retraction. Once a filopodium finds an adhesion after extension, this one then retracts again and drags the growth cone on the adhering surface (Figure II-9).

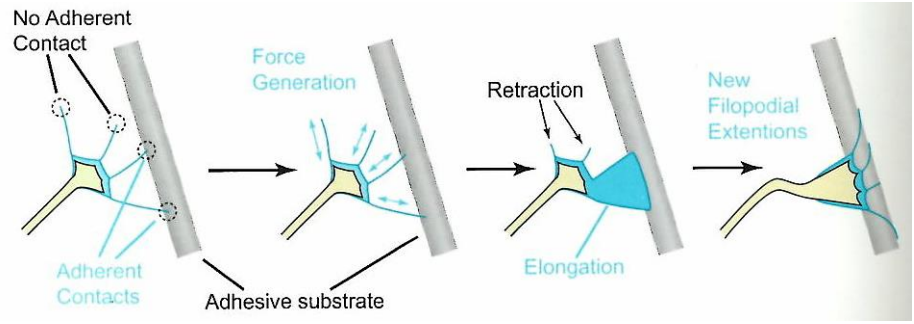

Figure II-9: Action mechanism of the filopodia for the neurite outgrowth. The microspikes are constantly elongating and retracting in order to search for adherent contacts. Once it is found, the retraction of the microspikes drags the neurite to the surface. From [5].

Actually, the movement of the growth cone is made possible by the perpetual polymerization and depolymerization of actin, helped by the protein myosin2, which is a molecular motor (Figure II-10).

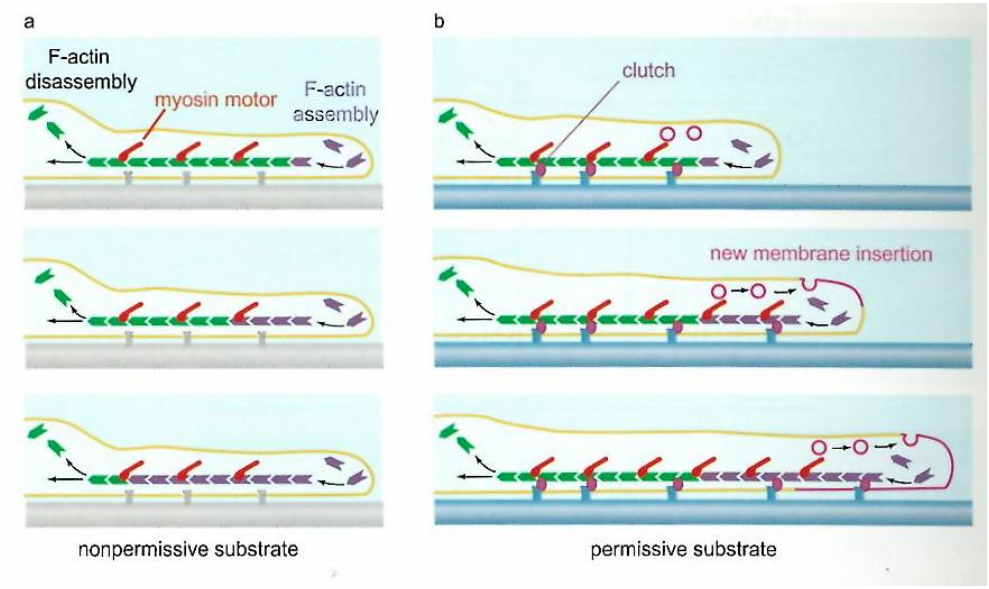

Figure II-10: "Actin assembly in the lamellipodium. a: Experiments by Paul Forscher and colleagues[15] suggest that on a surface that is nonpermissive for axon elongation, F-actin filaments are not closely linked to the surface, leading to persistent retrograde flow of newly assembled F-actin. b: When the F-actin cytoskeleton is coupled to the substrate, polymerization of F-actin at the leading edge leads to forward extension of the growth cone. This is accompanied by insertion of new plasma membrane." From [5].

If the substrate is not adherent, the actin is constantly pushed back to the core of the cell while more is supplied at the end of the growth cone, resulting in a rotatory flow of the actin without an extension of the growth cone. On the contrary, if adhesion factors are present on the substrate, the actin can bind to these molecules and its polymerization at the extremity of the growth cone

makes it extend on the surface, resulting in the growth of the axon. The stronger the adhesion is to the substrate, the faster the growth is. Moreover, the plasma membrane has also to be extended, and this is made possible by the supply of internal vesicles that integrate in the plasma membrane.[15,16]

Along their path, growth cones secrete proteases, which are digesting enzymes for proteins of the ECM such as fibronectin or laminin. This phenomenon is actually used as a cell-to-cell communication tool.

II.1.1.3.3 Guidance cues

As previously mentioned, the neurites have to know in which direction to grow. For this, molecules called guidance cues guide the growth cone, either by being attached on a surface or secreted by other cells. Molecules that will attract the growth cone of neurons are called chemoattractants and the unfavorable ones are chemorepulsives. For guidance cues that are present at the surface of a substrate, the growth cone has to touch this surface in order to "know" if it is a favorable or repulsive surface. These are referred to as contact-dependent attraction or repulsion. Their way of action is binding to receptors on the cell membrane that then activate mechanisms in the growth cone. In the case of chemoattractants, these mechanisms are the increase in the polymerization rate of actin as well as the faster addition of cell membrane. Chemorepellants on the contrary provoke the collapse of actin fibers and the shrinking of the cell membrane where it is in contact with the cue, forcing it to grow away from the repulsive surface. Concentration gradients of guidance cues can for instance force a cell to develop more on one side than the other. Moreover, according to the development time of a cell, one guidance cue can either be attractant or repellant, thus guiding the cell through more complicated pathways (Figure II-11).

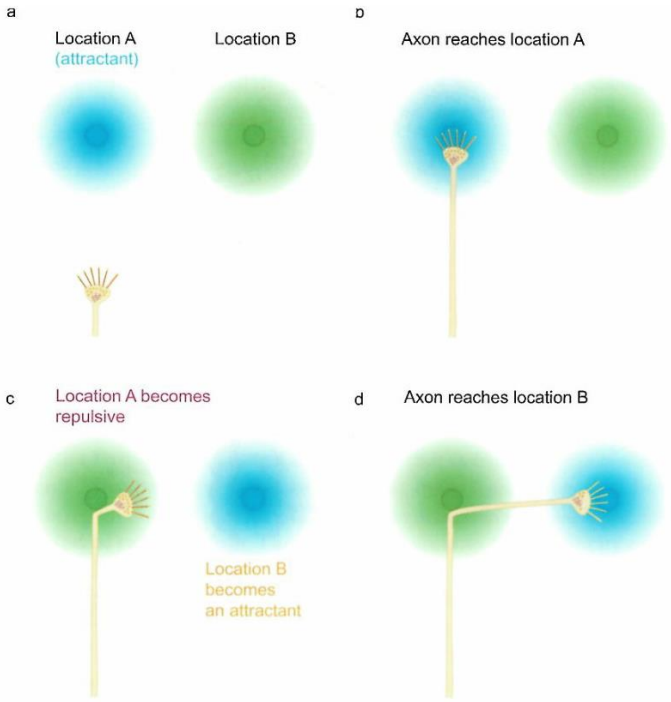

Figure II-11: Neurite outgrowth with guidance cues: at some point of neuronal development, some guidance cues can change their chemoattractat or chemorepellant property to tune the path of neurites. From [5].

It exists various types of guidance cues. The semaphorins for instance can either be found on the membrane of cells or in solution and they can be both chemoattractant or chemorepellant molecules. They can be present on axons or on non-neuronal cells but they do not cause the cells to aggregate. Netrins are also a kind of soluble guidance cues that are related to laminin and thus contain the RGD sequence. Like semaphorins, they can be attractants or repellants. Slits and ephrins are other kinds of guidance cues.

Another somehow crucial guidance cue is Nogo. As its name implies, is a repellant molecule. It actually can be found on oligodendrocytes, as well as on some neurons, and its repulsive effect is especially problematic after an injury. Indeed, it is particularly difficult to recover from brain or spinal lesions. This is due to the presence of Nogo on the myelin sheath (which results from oligodendrocytes) that forbids the growth of axons on the injured site and thus prevents the regeneration. However, these guidance cues are not present on Schwann cells in the peripheral nerve system, explaining why it is then much easier to recover from a nerve lesion in this region. Yet, the repulsive effect of Nogo can be inhibited with the use of antibodies.

II.1.1.3.4 Adhesion molecules

Along with guidance cues, adhesion molecules help for the growth and differentiation of neurons. They can be of two types: cell-to-substrate adhesion or cell-cell adhesion. The first are present on the surface of the extracellular matrix or ECM. The ECM is composed of glycoproteins and sugars

and forms a fibrillar network to which the cells can cling. It is majorly composed of collagen, laminin, fibronectin, hyaluronic acid and other glycoproteins. As already explained in the previous chapter, fibronectin and laminin are integrin-binding proteins, which means that they specifically bind to the cell membranes, especially through the RGD (Arg-Gly-Asp) sequence (chapter I.1.2.1).

Nevertheless, in the CNS, neurons mostly grow on other cells rather than on ECM. Indeed, ECM in the CNS is located around blood vessels and around cerebral ventricles that are filled with fluids. Cell adhesion molecules (CAM) are thus needed to help neurons spread and adhere on top of other cells. It is also what is happening in the peripheral nerve system for the formation of nerves: many axons grow on top of each other and end up forming bundles of axons called fascicles. CAMs make this association of cells possible by their presence on the cell membrane. The current explanation for their cell-to-cell adhesion property is that they bind to similar CAMs on the surface of other cells. Actually, those molecules are different from substrate adhesion molecules but similarly to fibronectin or laminin, they can also contain some integrin-binding sequences such as RGD.

II.1.1.3.5 Substrate mechanics

Another factor influencing neuronal growth and that has been investigated only recently is the mechanics of the substrate. It has been long thought that solely biochemical cues were critical for the development of neurons but topography and mechanics also influence a lot the way neurons grow.

Many *in vitro* studies used synthetic substrates, of which they varied the stiffness, and looked at the effects on the growth of neural cells. Saha *et al.* studied materials with stiffnesses from 0.01 to 10 kPa to culture adult neural stem cells. They showed that first, very soft substrates with a modulus < 0.1 kPa do not allow the growth of neural cells for they inhibit cell spreading, self-renewal and differentiation; and second that softer substrates (from 0.1 to 0.5 kPa) tend to favor the differentiation of neurons whereas stiffer surfaces (from 1 to 10 kPa) tend to favor glial cells.[17] In a more general manner, we can say that rigidities in the range of 1–20 kPa tend to favor the differentiation into glial cells while lower rigidities (0.1–10 kPa) tend to increase the differentiation into neurons.[18–20] Sur *et al.* observed the same behavior on their hydrogel with two different stiffnesses (Figure II-12). A lot more astrocytes are counted on stiff substrates whereas neurons tend to be more numerous of softer materials. Moreover, they observed a better development of the axons on softer substrates. They explain this phenomenon by the fact that the growth cone has a higher motility on softer substrates and thus, it increases the chances for a neurite to grow to the critical length to become an axon.[21]

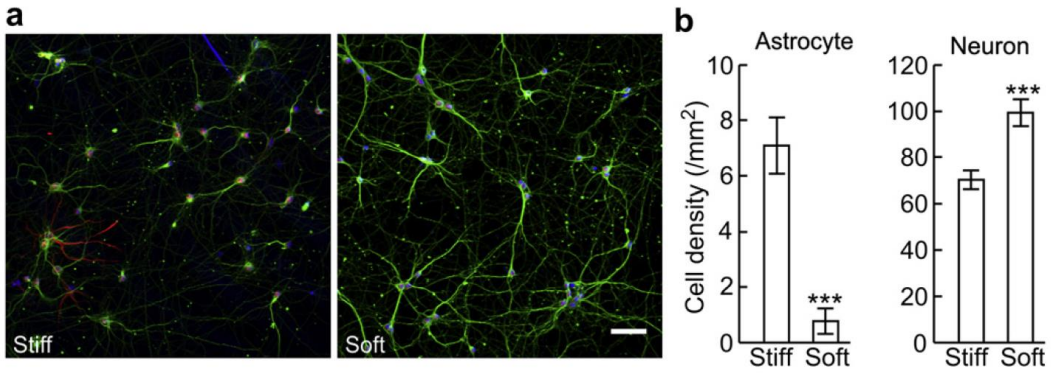

*Figure II-12: Culture of hippocampal cells on substrates of different stiffnesses. a. Microscopy observations of neurons (green) and astrocytes (red) on a soft (right) and stiff (left) substrate (scale bar: 50 µm). b. Cell densities observed for neurons and astrocytes on the two substrates (***: $p < 0.001$, triplicate). From [21].*

Koser *et al.* in 2016 observed the same behavior where the growth cone motility is increased on softer substrates. Nevertheless, they observed that neurites grew faster but also formed bundles on stiffer substrates (1 kPa) contrary to soft ones. They also proceeded to *in vivo* experiments by measuring brain stiffness with AFM, showing that there are stiffness gradients in the developing brain and that axons tend to grow towards softer tissues. This study also showed that mechanical stress applied on the brain could reshape it and reorganize the neurons. One of the conclusions of this study is also that, for the growth of neurons, harder substrates are preferred when the axons have to go through a tissue and softer substrates should be favored when new connections have to be made with surrounding cells. On top of that, neuronal cells are sensitive to the mechanics of the substrate but the reason for that might be because it induces changes in chemical signaling pathways or also because non-neuronal cells around are affected too.[22] But reciprocally, the cells also exert a mechanical strength on the substrate they grow on, sometimes even reshaping it.[23]

In summary, the growth and development of neural cells are affected by many factors such as chemical, adhesion and mechanical cues. It is the right complex combination of all these factors at the right time that ensures the correct development of the brain towards its adult stage.

II.1.2 *In vitro* growth of neural stem cells

After their discovery in the adult mammal brain, NSCs have raised a lot of interest in the fields of neurology and tissue engineering. Indeed, in the living brain, NSCs can migrate and colonize the site of a lesion after a trauma or a neurodegenerative disease. However, these new cells have trouble surviving and maturing in the lesion site.[24] The idea of curing brain lesions through the use of NSCs that will be previously amplified *in vitro* is very promising.[25] Another interesting aspect of NSCs is their use for creating *in vitro* models of brain in order to get a better understanding of its functions or to study the effects of some drugs for instance[26].

Naturally, the first *in vitro* cultures of NSCs were performed on culture plates that were generally polystyrene[2] or glass or plastic coated with proteins such as polylysine or laminin[7,27]. These adherent conditions are suitable for the growth of glial cells and neurons, as well as the development of neurites, though their maturation can be incomplete. Yet, growing neurons *in vitro* solely on flat adherent substrates is very far from the physiological conditions in which these cells have to interact with many others all around them in a well-defined organization. Substrates to grow NSCs are thus needed to better mimic the ECM and the complex environment in which the cells develop *in vivo* but also to bring them the biological and mechanical cues as discussed before. In this part, we are going to review the types of scaffolds used in the literature to reproduce the best the three-dimensional growth and organization of NSCs.

II.1.2.1 Hydrogels

The ideal scaffolds used for 3D *in vitro* cell growth will need to have structural properties consistent with their applications. First, their porosity needs to be quite high in order to let the cells penetrate and grow into the scaffold. Secondly, the rigidity of the matrix needs to be consistent with its application. As we have previously seen, substrate mechanics influence a lot the differentiation of stem cells. Rather soft materials will thus be privileged to be the closest possible from the *in vivo* conditions regarding rigidity. As a result, the study of hydrogels has thrived in the past years and they are now the most suited materials for soft tissue engineering.[28] These hydrogels can be of various natures, synthetic but also from natural sources.[29] Here, we are going to see various examples of hydrogel scaffolds used for this application.

II.1.2.1.1 ECM derived hydrogels

ECM is the natural supporting network secreted by cells *in vivo* and is composed of many proteins such as collagen, hyaluronic acid, laminin, etc. Naturally, using hydrogels derived from these compounds to grow cells *in vitro* appears to be the best strategy.

Many works use collagen as a scaffold for NSCs, but often combined to another material. Indeed, collagen alone can be perfectly adapted to cell culture since it is directly derived from the ECM, but most of the time it gives rather stiff hydrogels that are not so permissive for cells. Tang-Schomer *et al.* developed a composite matrix made out of silk protein sponges that are filled with collagen I gels, and they compared it with the silk sponge only or the collagen only. The primary cortical neurons are previously seeded on the silk porous scaffold which is further filled with the collagen hydrogel. Thanks to this technique, the neurons are able to grow and develop throughout the scaffold and very long neurites are only obtained on collagen if the silk network is present. Moreover, a nearly functional brain-like tissue can be obtained out of these scaffolds that actually

mimic some *in vivo* behaviors.[30] Sur *et al.* also tried to combine collagen I with a short self-assembling peptide amphiphile (PA) containing the IKVAV and YIGSR sequences for the growth of cerebellar neurons. They found that compared to collagen-only scaffolds, the cell penetration and the neurite outgrowth were higher in the presence of the PA. What is more, they observed that according to the concentration in PA and the number of epitopes present in it, they could tune dendrite and axon growth, thus modulating the growth of the neurons into their scaffolds (Figure II-13).[31]

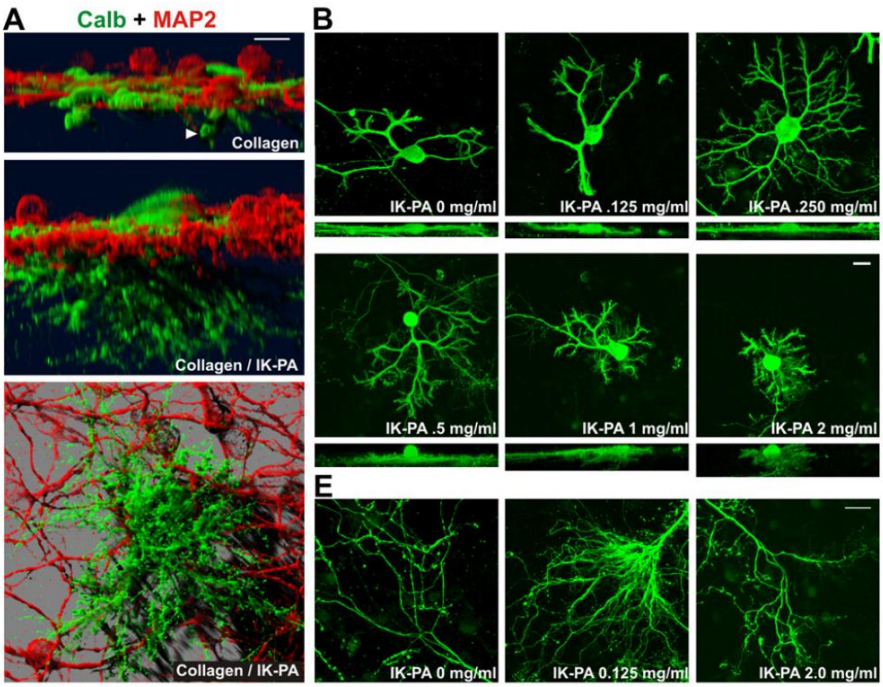

Figure II-13: A. Simulated fluorescence process volume rendered images of neuronal cells seeded on top of collagen-only and collagen coupled to a PA scaffolds after 16 days of culture (scale bar: 10 µm). B. Top and side views of neuronal cells seeded on scaffolds with different PA concentration after 16 days in vitro *(scale bar: 20 µm). E. Characteristic morphologies of neuronal cells on the scaffolds with various PA concentrations (scale bar: 20 µm). From [31].*

Hyaluronic acid (HA) is another natural component of the ECM and can also be coupled to collagen I[32,33], or even used on its own. For example, Seidlits *et al.* functionalized HA with methacrylate (MA) in order to obtain various degrees of MA cross-liking to thus tune the mechanics of the substrates. NPCs were encapsulated in the hydrogels by photoreticulation of the MA-HA: yet, after 21days of culture, very few neurite outgrowths are observed. Tarus *et al.* also used hyaluronic acid-based hydrogels with tunable stiffness and cell-adhesive peptides (containing RGD) to grow neural progenitor cells in 3D. Neurospheres are seeded on top of the scaffolds and after 21 days *in vitro*, the neurites colonize the hydrogel in depth, especially in the softest hydrogels (storage modulus of 400 Pa) and even without cell-adhesive peptides (Figure II-14).[34]

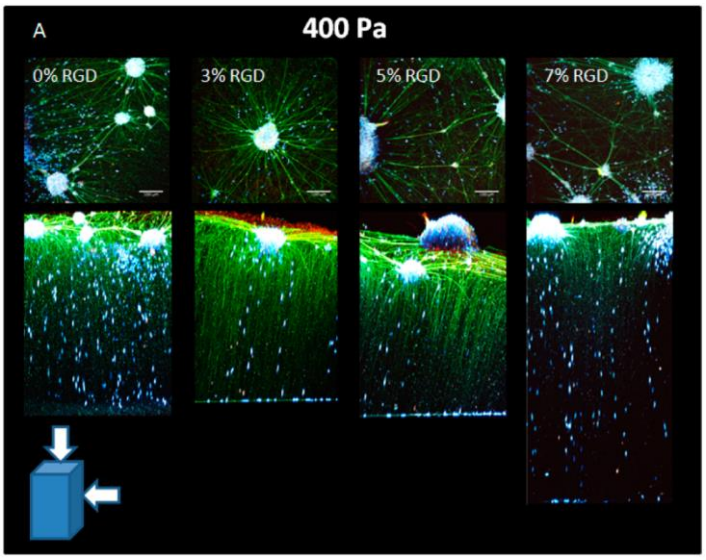

Figure II-14: Two photon microscopy 3D images (top and side views) of the neurites outgrowth of neuronal cells seeded on top of hyaluronic acid hydrogels (modulus of 400 Pa) with different concentrations of RGD-containing peptides after 17 days. β3-tubulin appears in green and GFAP in red, the nucleus were stained with Hoechst. Scale bar: 100 µm. From [34].

II.1.2.1.2 Polysaccharide-derived hydrogels

Natural polysaccharides such as cellulose, alginate or chitosan are often used for (neural) cell culture applications.[35] These polymeric hydrogels are often quite cheap raw material, generally simple to use and biocompatible. This is why these hydrogels have gained much interest in the past years.

For instance, Gonçalves-Pimentel *et al.* developed a cellulose exopolysaccharide biomaterial that can be extracted from sugar cane molasses. The neuron and astrocyte primary cells showed a good viability, growth and adhesion, as well as cell functions on these bio-sourced scaffolds.[36] Wei *et al.* synthesized self-healing hydrogels composed of a mixture of N-carboxyethyl chitosan and oxidized sodium alginate, among other components. They used this hydrogel for the growth and differentiation of NSCs: these expressed neuronal and glial markers after 9 days. The scaffolds stiffness can be tuned and range between 100 and 1000 Pa, which is said to be the ideal rigidity for the growth of neurons (see II.1.1.3.5). However, the cells cultured into those scaffolds showed a lack of adhesion for they display a rather round shape. Yet, because of their injectable property, these hydrogels could be used for stem cell therapy and direct injection into the brain of non-differentiated cells.[37]

II.1.2.1.3 Commercial hydrogels

Commercial hydrogels such as Matrigel or PuraMatrix™ have also been developed. PuraMatrix™ is a peptide hydrogel (RADA16-1, see I.1.2.1) whereas Matrigel is an ECM-derived hydrogel extracted from the Engelbreth-Holm-Swarm mouse sarcoma cells. Because it is made out of

peptides, PuraMatrix™ gives reproducible hydrogels in terms of composition. However, since Matrigel is extracted from biological tissues, its composition can vary from batch to batch, which makes its use sometimes disputed. Yet, many studies use Matrigel as cell culture scaffolds.

Ylä-Outinen *et al.* used PuraMatrix™ to grow neurons out of human embryonic stem cells. They seeded the cells either on top, encapsulated inside the gel or at the bottom of the well. Very good cell survival as well as neurite outgrowth were observed, especially with the encapsulated cells. The neurons were even able to create active electrical connections between themselves.[38] Thonhoff *et al.* compared PuraMatrix™ and Matrigel, along with another polymer hydrogel. Here again, PuraMatrix™ is the one that gave the best results for the growth and differentiation of hNSCs, with a lot of neuronal markers and long neurites. Neurospheres have also been encapsulated in PuraMatrix™ and cells were able to differentiate and to migrate out of the neurospheres in these conditions.[39]

II.1.2.2 Other types of scaffolds

A lot of other materials exist for the 3D growth of NSCs, such as electro-spun polymeric scaffolds. For instance, Carlson *et al.* developed transplantable electro-spun scaffolds made out of tyrosine-derived polycarbonate. By tuning the fibers' diameter they can thus tune the scaffold's porosity which determines the cell penetration, resulting in 2D or 3D cell culture conditions (Figure II-15).[40]

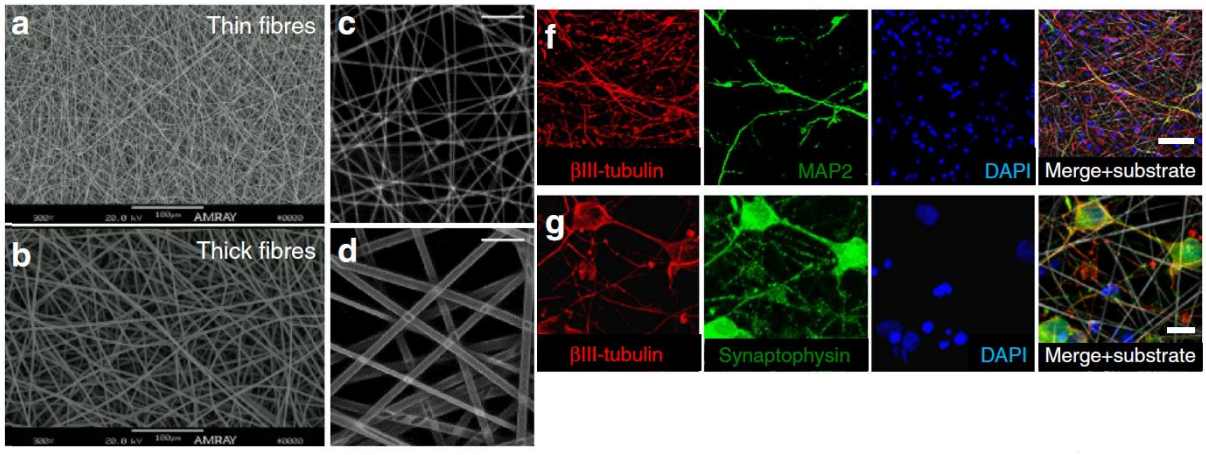

*Figure II-15: **a**-**d**: SEM (**a** and **b**, scale bar: 100 µm) and reflectance (**c** and **d**, scale bar: 50 µm) observations of the electro-spun fibers with two different diameters resulting in different porosities. **f** and **g**: Fluorescence imaging of neurons grown on 3D electro-spun structures after 12 days (scale bars: 50 µm for **f** and 10 µm for **g**). From [40].*

Omidinia-Anarkoli *et al.* used electro-spinning to integrate orientated fibers into fibrin hydrogels. The alignment of axons in the case of neuronal cell culture is particularly interesting in terms of modelling *in vivo* conditions since in the cerebral cortex the axons form well-aligned bundles. To

do so, they mixed poly(lactic-co-glycolic acid) (PLGA) with superparamagnetic iron oxide nanoparticles (SPIONs) and this mixture was electro-spun to form fibers. These fibers were then cut in small pieces, incorporated into the fibrin hydrogel and aligned in a certain direction thanks to a magnetic field. This allowed the growth of primary neurons and their neurite elongation along the aligned fibers inside these scaffolds.[41] Zhu *et al.* for instance also used electro-spun composite microfibers of collagen and silk. They managed to find a suitable composition for their fibers to have a good tensile strength, strain and elasticity and to easily tune the diameter of the fibers. The use of electrospinning allows a direct alignment of the fibers once deposited on the plate. Human decidua parietalis placental stem cells (hdpPSCs) were seeded on the scaffolds and proliferated at the same rate than on pure collagen scaffolds. They were able to differentiate into neurons with an alignment of the neurites along the composite fibers.[42]

Another way that was found to mimic the bundles that the axons form in the cerebral cortex is the use of micro-patterned substrates. For instance, micro-grooved polydimethylsiloxane (PDMS) can be used to grow neuronal cells with a very nice alignment of the growing neurites (Figure II-16).[43,44]

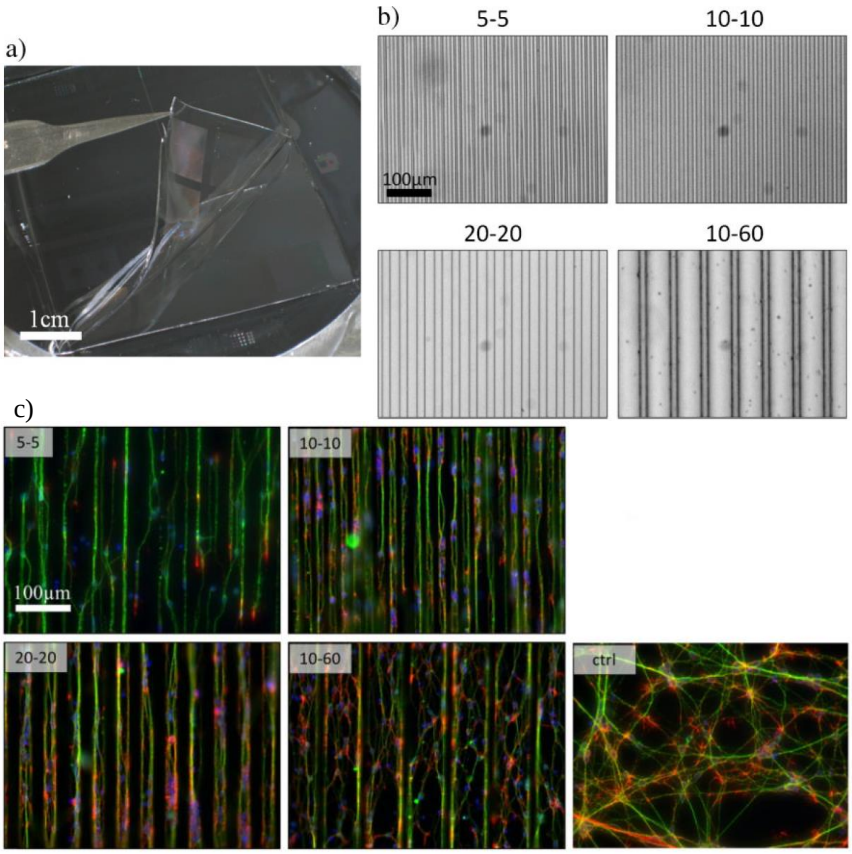

Figure II-16: a. Macroscopic view of the PDMS substrates after removal from the master. b. The different types of micro-grooves used: the first number is the length in µm of the terrace and the second of the grooves. c. Optical fluorescence images of luhmes neuronal cell line cultures on microstructured PDMS substrates. From [43].

These PDMS substrates were then implanted in the injured brain of rats. It has been shown that, after several months, the animals had an improved motor recovery when the micro-grooved PDMS substrates seeded with hNSCs were implanted in the lesion.[8,45] In the last few decades, microfluidic chips also proved to be particularly suited tools for the *in vitro* study of some biological systems as well as for cell alignment.[46]

Colloidal beads can also be used for the creation of 3D neuronal networks including glial cells. Pautot *et al.* developed the use of silica beads that they coated with poly-L-lysine in order to grow rat hippocampal cells on them. By forming colloidal assemblies, the beads allow the neurons to construct 3D functional networks, with processes making connections with other neurons very far from their somas.[47] However, here the material used is biocompatible, but not biodegradable and its use for transplantation could be problematic. This system can then be used for the study of neuronal network activity or for drug screening.

Many other 3D matrices are developed to mimic best the *in vivo* growth conditions of neural cells.[48] However, another kind of *in vitro* brain model has been intensively studied lately.

II.1.2.3 Organoids

Very recently, another type of cellular construct has been emerging as a tool for the *in vitro* modelling of brain. Those structures are called organoids for they display very close cellular organization and functions as the organs from where the cells are originated. Brain organoids have thus been developed by searchers in the past years. Muguruma *et al.* for instance reported the self-organization in 3D of cerebellar cells from human embryonic stem cells and this without any supporting scaffold. This organoid has a functional organization similar to the cerebellar one and display an electrical activity.[49] Other studies though used the help of initial scaffolds for the development of their organoids. A device that is often used for the formation of cellular superstructures is a spinning bioreactor: it helps keeping the cellular clusters in suspension to form bigger aggregates when growing without sedimentation.[50] A cellular matrix is often needed to first grow the cells before putting them into the bioreactor. Thus, collagen[51] or Matrigel[52] are often used for this purpose. Brain-like organoids are of real interest because they provide *in vitro* models of the brain and help us learn a lot on its development and structure (Figure II-17).

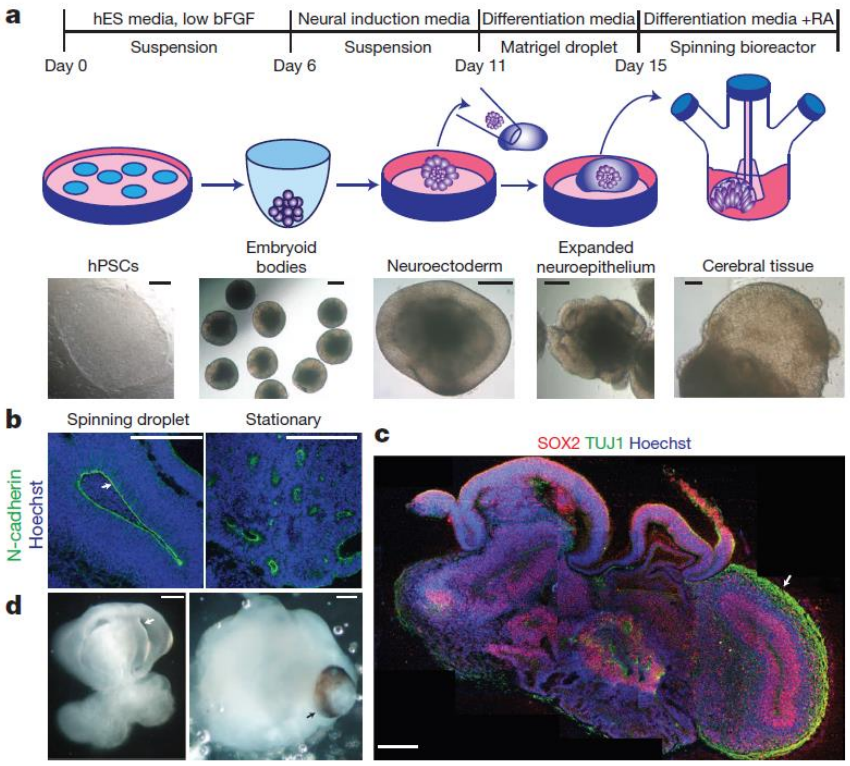

Figure II-17: "Description of cerebral organoid culture system. a, Schematic of the culture system described in detail in Methods. Example images of each stage are shown. bFGF, basic fibroblast growth factor; hES, human embryonic stem cell; hPSCs, human pluripotent stem cells; RA, retinoic acid. b, Neuroepithelial tissues generated using this approach (left) exhibited large fluid-filled cavities and typical apical localization of the neural N-cadherin (arrow). These tissues were larger and more continuous than tissues grown in stationary suspension without Matrigel (right). c, Sectioning and immunohistochemistry revealed complex morphology with heterogeneous regions containing neural progenitors (SOX2, red) and neurons (TUJ1, green) (arrow). d, Low-magnification bright-field images revealing fluid-filled cavities reminiscent of ventricles (white arrow) and retina tissue, as indicated by retinal pigmented epithelium (black arrow). Scale bars, 200 mm." From [52].

However, for stem cell therapies, they are perhaps not the best-suited structures to implant for cell integration. In the long term, there is also a high necrosis rate at the center of these organoids because of the difficulty for oxygen and nutrients to penetrate all the way. Still, organoids are a very good example of 3D cell culture and of what can be achieved with stem cells.

II.1.3 Conclusion

Since their recent discovery, neural stem cells appear as a promising tool for the repair of brain lesion or even for *in vitro* brain models. A lot of materials are being developed in order to replicate best the *in vivo* conditions which those cells normally grow and differentiate in. Hydrogels of various compositions are majorly studied because they resemble the natural ECM on which the cells grow. They can precisely be derived from ECM compounds or natural polysaccharides for instance. Other types of materials can also be used such as polymers and be shaped by different techniques like electro-spinning.

However, these matrices are often not ideal in terms of chemical synthesis, cost or even properties for neuronal cell culture. Polysaccharide hydrogels for instance have troubles providing a good adhesion to the encapsulated cells. Collagen gels are known to be a bit too stiff for the growth of neurons that requires very soft materials. That is why in this work we wanted to evaluate the growth of hNSCs on our simple carbohydrate hydrogels that are easy to synthesize, from cheap raw matter and built out of biocompatible moieties.

II.2 Study of biocompatibility and cell growth with the alkylgalactonamide hydrogels

In this part, we are going to describe the work that has been done to evaluate the biocompatibility of our native alkylgalactonamide hydrogel scaffolds for the growth of neural stem cells. First, the toxicity of the molecules has been assessed with a neuronal cell line. After conforming their innocuousness, cell growth and cell penetration on slow cooled hydrogels was studied with the same easy-to-handle neuronal cell line. Afterwards, when the conditions were optimized, we got interested into the behavior and growth of hNSCs from patient biopsies. For these experiments, the cells and hydrogels have been characterized with fluorescence optical and confocal microscopies.

II.2.1 Hydrogel preparation for biological assays

Prior to the direct characterization of cell growth and even prior to cell seeding in the scaffolds, hydrogels have to be prepared so that they become suited for cell culture. Indeed, when they are first prepared in bulk, they are full of water. The problem is that cells cannot live in water-only mediums; they need salts, nutrients and oxygen in order to develop correctly. Moreover, cells actually die in water because of osmotic pressure: water flows inside the cell so that the concentration inside decreases, but this water addition leads eventually to the explosion of the cell membrane. For this reason, prior to cell seeding, water from the hydrogel has to be replaced with cell culture medium such as Dulbecco's modified Eagle's medium (DMEM). The gels are first rinsed for a few hours and several times with several hundred microliters of DMEM so that cells can grow in favorable conditions inside the hydrogels. Actually, we also tried to avoid this long washing step, by directly dissolving the gelator into DMEM or PBS to form gels, but neither gave a hydrogel in the end. This shows that indeed, many factors such as salinity or ionic strength can affect a lot gelation mechanisms by interfering with intermolecular interactions.

The first cell culture trials were performed with gels prepared with a "0 min" cooling rate in the chamber slide wells. The final gel thickness was of 3-4 mm, so that the cells only felt the hydrogel stiffness and not that of the plate. However, we found out that when the gels were prepared with instant cooling, gels had really poor resistance notably to necessary washes before cell culture. Once the efficiency of the controlled cooling rate was validated for the improvement of their resistance, all the gels for cell culture trials were prepared with a 90 min cooling rate (see chapter I.2.2.2). For this, a lot of work was done in order to find the easiest way to prepare the gels, seed the cells and characterize them all in the same apparatus. Indeed, the regular 8-well camber slides

with removable walls cannot resist the cycles of heating and cooling during the gel preparation for the seal between the walls and the slide leaks. We thus developed an apparatus in order to prepare the gels with temperature ramp directly inside the wells of a chamber slide (Figure II-18). 8-well chamber slides with silicon seal were used along with a hand-made tool holding the walls and the slide together very tightly so that there are no leaks during the gelation process.

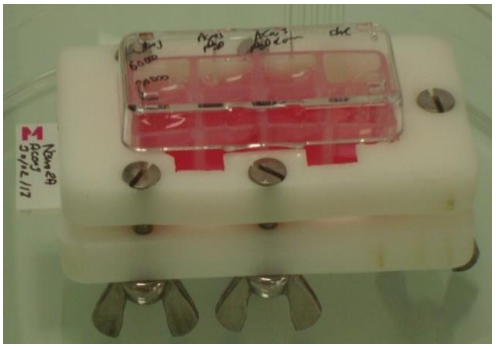

Figure II-18: 8-well chamber slide with the tool used to prepare hydrogels with controlled cooling rate conditions.

The hot gelator solutions are pipetted in the wells, which then are sealed with a foil sticker in order to prevent water evaporation. After undergoing the temperature sweep, the gels can directly be washed and seeded with the cells, still in the tightening tool. Once the desired time of cell growth reached, the tool is removed and the cell-containing hydrogels can be observed through the glass slide (Figure II-20).

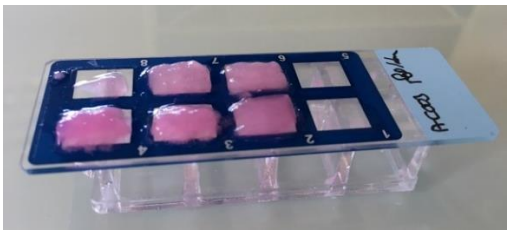

Figure II-19: Typical aspect of 90 min cooled Gal-C7 hydrogels after 7 days of cell culture on an 8-well chamber slide (after chamber removal). The two wells at the right are controls.

II.2.2 Biocompatibility assays with the alkylgalactonamide hydrogels

Naturally, the first thing to do when developing a new biomaterial is to check its biocompatibility. A lot of factors have to be taken into account and long term studies are needed to evaluate the biocompatibility of a material, but firstly we focused on two main characteristics: the material/molecule has to be non-toxic for the cells, but also the cells have to grow and duplicate on the scaffold. In order to check these criteria, two tests were performed: first, the live/dead cell assay that gives an idea of the molecule's toxicity and second the MTT test, which is a colorimetric

assay that reports the mitochondrial activity of the cells and permit to deduce cell proliferation. The cells used for these experiments were from a murine neuroblastoma cell line called Neuro2a.

II.2.2.1 Cell survival study

The live/dead cell assay measures the intracellular esterase activity and reveals the plasma membrane integrity. When observed in fluorescence microscopy, the first appears in green and accounts for live cells and the second in red reports the dead cells (Figure II-20).

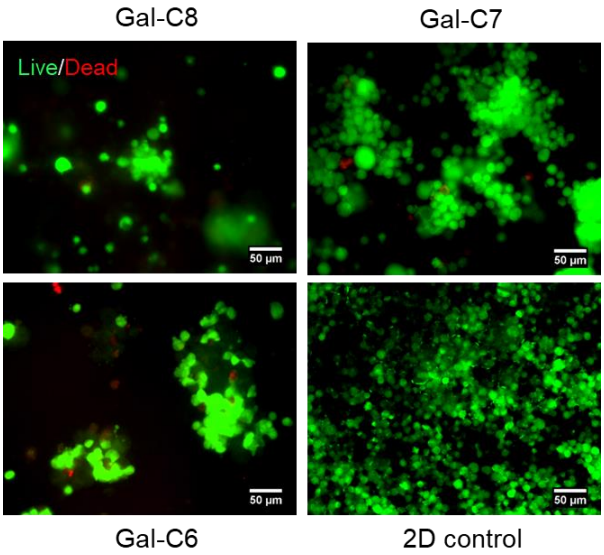

Figure II-20: Live/Dead staining of Neuro2a cells on the galactonamide gels after 7 days of culture ("0 min" cooled gels, scale bar: 50 µm).

Being the first ones to have been performed to evaluate the gels, those tests were actually done on instantly ("0 min") cooled gels. Live cells were found on all tested gels. After 7 days of culture, Gal-C7 gels always displayed a higher cell density compared with the two other gels with 98 ± 1% of cell viability. Some toxicity was detected with the Gal-C6 gel, where dead cell aggregates were sometimes observed. The percentage of viability was evaluated at 78 ± 6% for Gal-C6 gels and at 81 ± 13% for Gal-C8 gels. The cell density at the end of the experiment seemed however lower in the gels than in a 2D control without gel, even with the Gal-C7 gel.

II.2.2.2 Cell growth assessment

To confirm this last observation, the cell growth with the different gels with or without a controlled cooling was quantified using a MTT assay (Figure II-22 and Figure II-23). The MTT is a molecule – the 3-(4,5-dimethylthiazol-2-yl)-2,5-diphenyltetrazolium bromide – that once reduced by enzymes in the mitochondria forms a deep purple precipitate called formazan. Its concentration can be assessed by spectrophotometry after dissolving the formazan crystals in a

solvent. The optical activity is proportional to the number of cells present in the well and with different assays made at different time points, the cell growth rate can be calculated.

In the case of "0 min" cooled gels, collecting data was quite difficult because, unless very careful washings were made, many gels tended to break up during the experiment. Conversely, 90 min cooled gels, which are more homogeneous and resistant, did not break up (Figure II-19). For the Gal-C7 gel with a controlled cooling, cells seemed to penetrate the gels instead of only staying on the surface (Figure II-21). For this reason, two cell densities were used (35 000 and 70 000 cells/well) in order to avoid a low growth due to a too important cell dispersion.

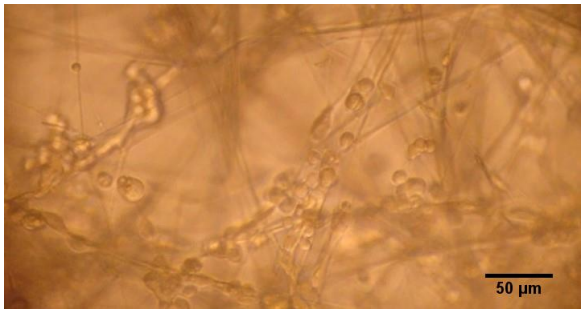

Figure II-21: Neuro2a cells were observed directly into the gel fibers by bright-field microscopy (Gal-C7 90 min cooled gel) after 7 days of culture.

The MTT assays were performed after 1 and 4 days of culture without changing the medium to avoid cell loss during culture medium renewal. The cell growth with the hydrogels was then compared to a control well corresponding to a culture reaching confluence after 4 days on a 2D plastic surface.

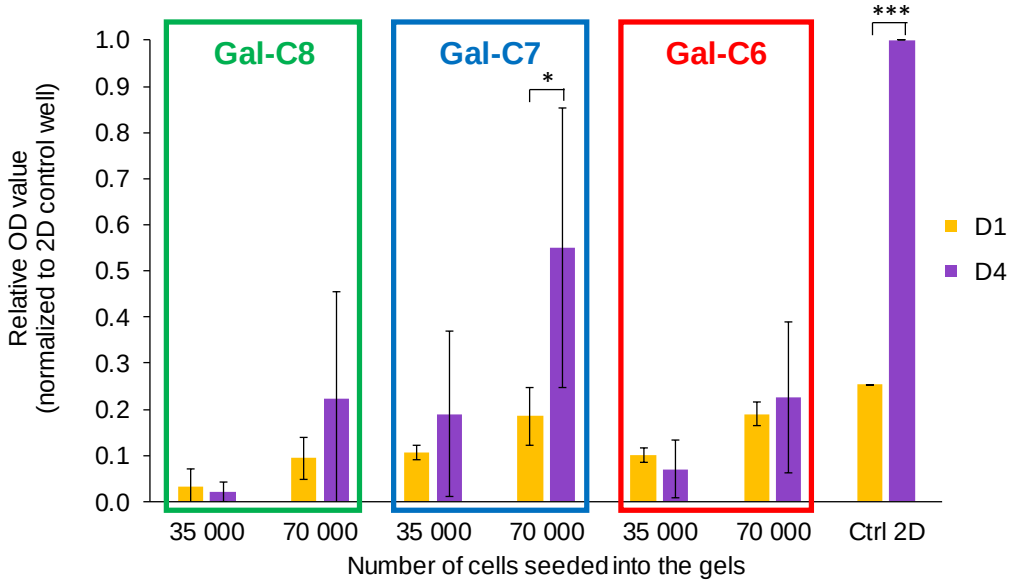

Figure II-22: MTT test after 1 and 4 days of cell culture with Neuro2a cells on the different gels. The displayed results are the blank-corrected mean OD value +/- SD. Asterisks denote statistical significance (: $p < 0.05$ and ***: $p < 0.005$).*

Concerning the impact of the cooling rate, MTT assays showed that for the three gels there was no significant difference of cell growth between gels prepared with a "0 min" cooling or a 90 min cooling (Figure II-23). The gels without controlled cooling are too fragile for a practical use in cell culture, but the morphology of the gels, that differs mainly on fiber length and the number of nucleation points, did not really affect cell growth.

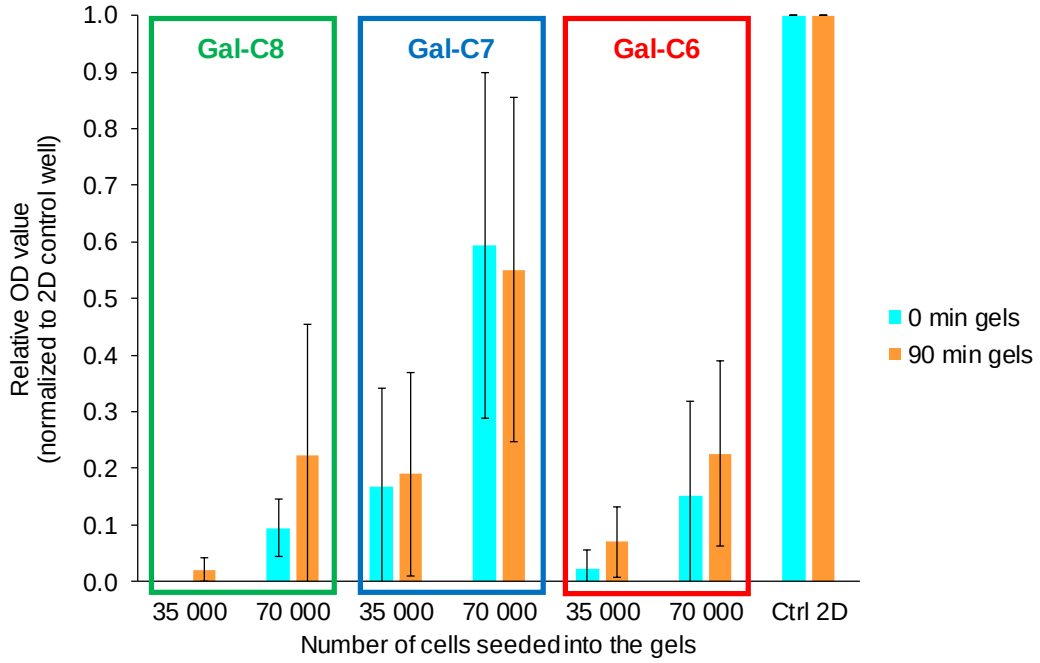

Figure II-23: Comparison of MTT tests with "0 min" and "90 min" gels after 4 days of culture and at different cell densities with Neuro2a cells. The results represent the blank-corrected mean OD value +/- SD (n=3). No significant difference is observed between "0 min" and 90 min cooled gels after 4 days of culture, and this for the three different gels.

Concerning the difference between the three gels, in all MTT experiments, the cell growth between day 1 (D1) and day 4 (D4) was found significantly higher for Gal-C7 compared with Gal-C8 and Gal-C6, as shown by the analysis of variance ($p < 0.05$ according to ANOVA statistical analysis) (Figure II-22). For Gal-C6 and Gal-C8 gels, the cell number was not statistically different between D1 and D4. Cells seemed to stay more in a "latency stage". A non-controlled variability in growth results was observed with the Gal-C8 certainly due to its high gelation point, which made it hard to manipulate. With the Gal-C7 gel, when the seeded cell density was sufficient (70 000 cells/well instead of 35 000), the cell number increased more than 2.9-fold during the culture period ($p < 0.05$). The growth was however slower than on a 2D control where a 4-fold increase was observed between D1 and D4 ($p < 0.0005$). The cell density needed on this kind of support was higher, certainly due to cell penetration within the fibers network. This phenomenon has already been pointed out in other studies. Different cell lines have already shown reduced proliferation rate in 3D cultures compared to those cultured in 2D but the behavior of cells grown in 3D seems to better reflect *in vivo* cellular response.[48,53]

Overall, these results emphasize that the Gal-C7 gel is suitable for cell growth, while Gal-C6 and Gal-C8 are less favorable. The three gels only differ by a one-carbon increment in their alkyl chain, but this tiny difference affects many physicochemical properties of the gels (microscopic and network topography, mechanics, solubility, gelator release, etc.) that also probably affects their biochemical properties (metabolic pathways) and their interactions with cells.

II.2.2.3 Determination of cell penetration inside the scaffolds: 3D cell growth

The observations by conventional optical fluorescence microscopy (Figure II-20) already highlighted a probable 3D penetration of the cells into the gels and not only a "pseudo-3D" growth at the surface of the gels. Such penetration was not observed with Gal-C7 hydrogels prepared without controlled cooling. To confirm these previous observations, a confocal study was performed with the 90 min cooled Gal-C7 hydrogel, with the cells still seeded only on the top of the hydrogels. To preserve the scaffold structure and to visualize easily the cells without extensive gel manipulations, a Neuro2A cell line expressing the green fluorescent protein (GFP) was generated.

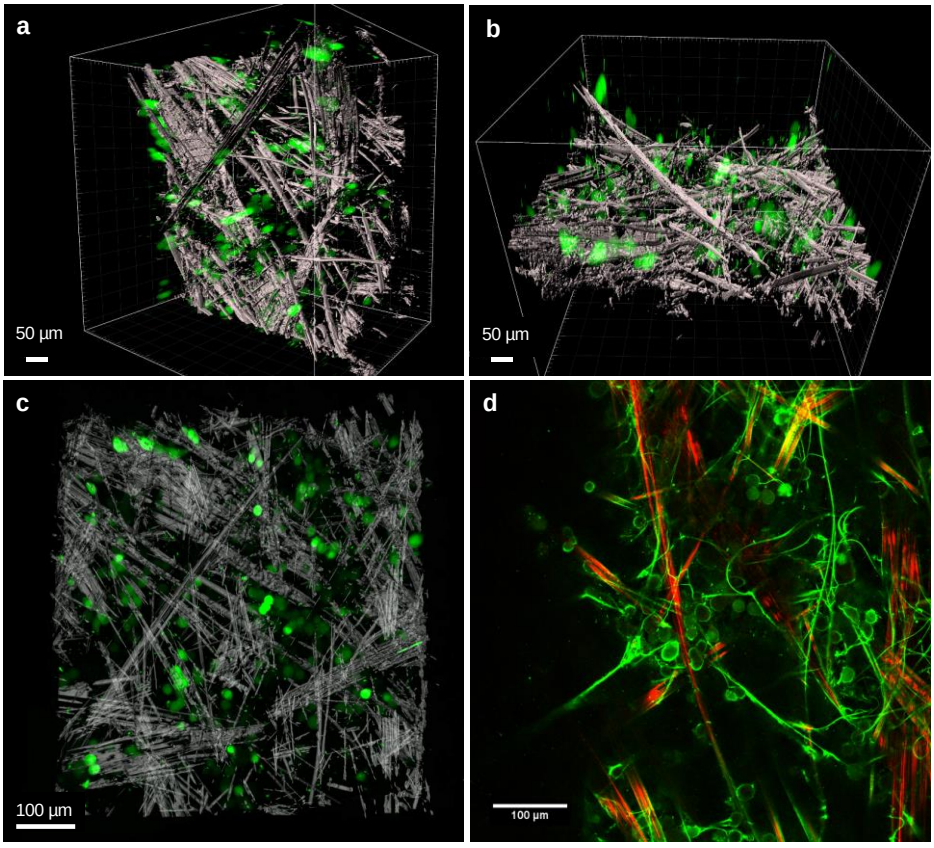

Figure II-24: 3D penetration of GFP-Neuro2A cells into a Gal-C7 gel (90 min cooling) after 5 days. Confocal microscopy observations of the gel by laser reflection technique and by fluorescence. (a,b,c): fibers in white (reflection), cells in green (fluorescence). (a,b): perspective views and (c) enlargement. (d): image after incubation of the gel with FITC-polylysine. Wide fibers in red (reflection), narrow fibers and cells in green (fluorescence). scale bar: 50 µm.

First, the gels were observed by laser reflection technique without any staining, except the green fluorescent protein from the cells. Only the large fibers can be observed with this technique (Figure II-24a–c and Figure II-25). Cells with a quite round shape were observed throughout the scaffold and showed the capacity to penetrate approximately up to 200 µm into the scaffold. Samples were also incubated with FITC-labeled polylysine. It also enabled the observation of the narrow gel fibers with fluorescent confocal microscopy (Figure II-24d). The coupling of the two techniques highlighted quite well the complex architecture of the scaffold and the interaction with the cells. It showed how a network of narrower and flexible fibers, not visible with reflection, linked the wide and straight fibers together. The cells were nested into this scaffold often in small clusters, interacting with each other and with several large or narrow fibers. These images confirm that the 90 min cooled Gal-C7 gel is suitable for neuronal cell growth, including growth in 3D.

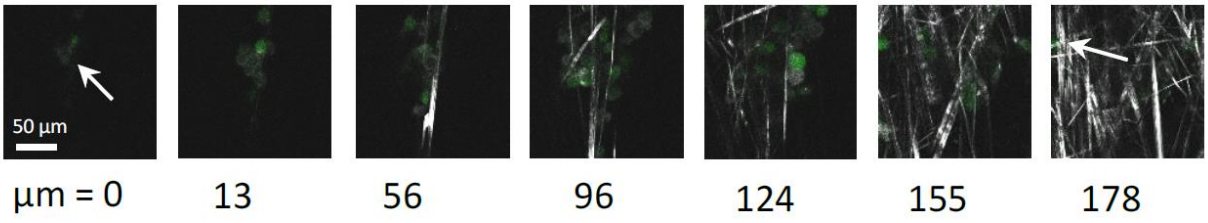

Figure II-25: Maximum depth observed for GFP-Neuro2A cells penetration within a Gal-C7 gel. On this section of the gel, first cells have been observed in the plane referred to as "0 µm", and deepest cells have been observed at a depth of 178 µm. (technique: confocal microscopy observations by laser reflection of the cells (green) within the gel fibers (white) at different planes after 5 days of culture. The stack was made from the top of the gel to the bottom) (scale bar: 50 µm). This example demonstrated that cells have settled in the gel at a depth of at least 178 µm.

II.2.3 Characterization of cell growth and differentiation of hNSCs on Gal-C7 hydrogels

Once the biocompatibility of our hydrogels confirmed with a commercial cell line, we tried to grow hNSCs on the gel we assumed to be best suited: Gal-C7. Indeed, the live/dead cell assays and the MTT tests confirmed that it was the hydrogel on which the cells grew best and in which there was a real 3D culture. Until then, only 90 min cooled Gal-C7 hydrogels had been used. What is more, in order to characterize more precisely the growth of the hNSCs and their differentiation on the hydrogels, we performed immunolabeling on the cells. For this, we had to develop a specific technique in order to keep the resulting cellular organization throughout the washes that alter a lot the hydrogel.

II.2.3.1 Development of immunolabeling techniques on hydrogels

To characterize the growth of hNSCs on the Gal-C7 hydrogels we have to determine the differentiation of cells within the scaffold. To do so, immuno-labelling is the method of choice to distinguish the different kinds of cells obtained. Indeed, once in culture, neural stem cells can grow into either astrocytes, oligodentrocytes or neurons. Each type displays specific markers that can be targeted by immunochemistry, such as β3-tubulin for neurons that can be marked with Tuj-1 or O4 for oligodendrocytes and GFAP for astrocytes (see Figure II-6).

Immunolabelling is a very common technique used in biology to characterize cells. However, it requires a lot of soakings and washes. For instance, for an 8-well chamber slide and for the staining of two different markers and DAPI for the nucleus, more than 5 ml of liquid per well can be used! The back and forth movement of the liquid with the micropipette added to that, the Gal-C7 hydrogels often disappeared by the end of the protocol and no gel but most importantly, no cells remained to be observed (Figure II-26).

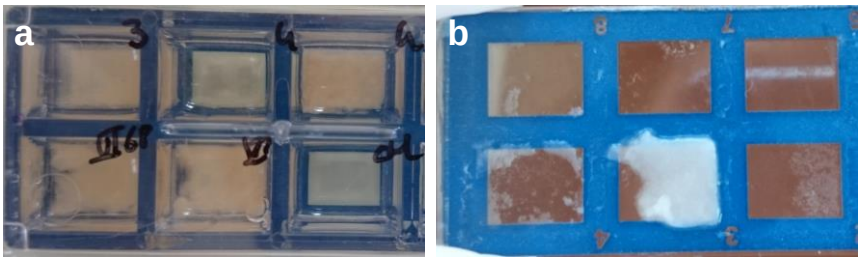

Figure II-26: (a) Alkylaldonamide hydrogels after 8 days of cell culture with Neuro2as. (b) The same wells after immunolabelling, almost all the hydrogel is gone.

To overcome this, a method had to be developed in order to at least preserve the cell structure after their growth in the hydrogels. We actually used the CLARITY method that is already employed for the mapping of brain tissues.[54] The biological tissues are embedded in a transparent polyacrylamide hydrogel that enables the lipidic tissues to be extracted from the cellular tissue and results in a transparent and standing sample to image. The CLARITY method also allows the samples to be immunostained (even though the washes duration can be of several days depending on the thickness of the samples).

Inspired by this method, after 7 days of incubation, the hNSC-seeded Gal-C7 hydrogels underwent cell membrane fixation in a 4% PFA solution and were then embedded in acrylamide hydrogel. In the process, the Gal-C7 hydrogel was actually dissolved (although sometimes a few large fibers remained) but the fragile cellular network was well preserved. What is more, it resulted in a more transparent sample that is easier to image. After polymerization and a few washes, the cells could be immunostained thanks to the classical procedure.

II.2.3.2 Growth and differentiation of human neural stem cells

Finally, the study was performed with human neural stem cells. Biopsies were performed on patients undergoing neurosurgery for the treatment of pharmacoresistant epilepsy. Once the biopsy obtained, it is dissociated with trypsin, hyaluronidase and kyruneic acid in order to separate the stem cells from the other tissues. The cells are then amplified as neurospehres in non-adherent conditions in DMEM containing growth factors and other nutrients. Once the cells are ready to be used, the neurospheres are dissociated in order to get single-cell suspensions and are seeded on the scaffolds.

The hNSCs were seeded on a 90 min cooled Gal-C7 gel (Figure II-27). After 7 days of culture, reflection microscopy (Figure 8a) or live/dead cell assay (Figure II-27b) showed live stem cells throughout the gel. As for the Neuro2a cells, hNSCs were most of the time present as small clusters or neurospheres-like structures into the hydrogels showing also a clear cell-cell interaction and one between cells and gel fibers.

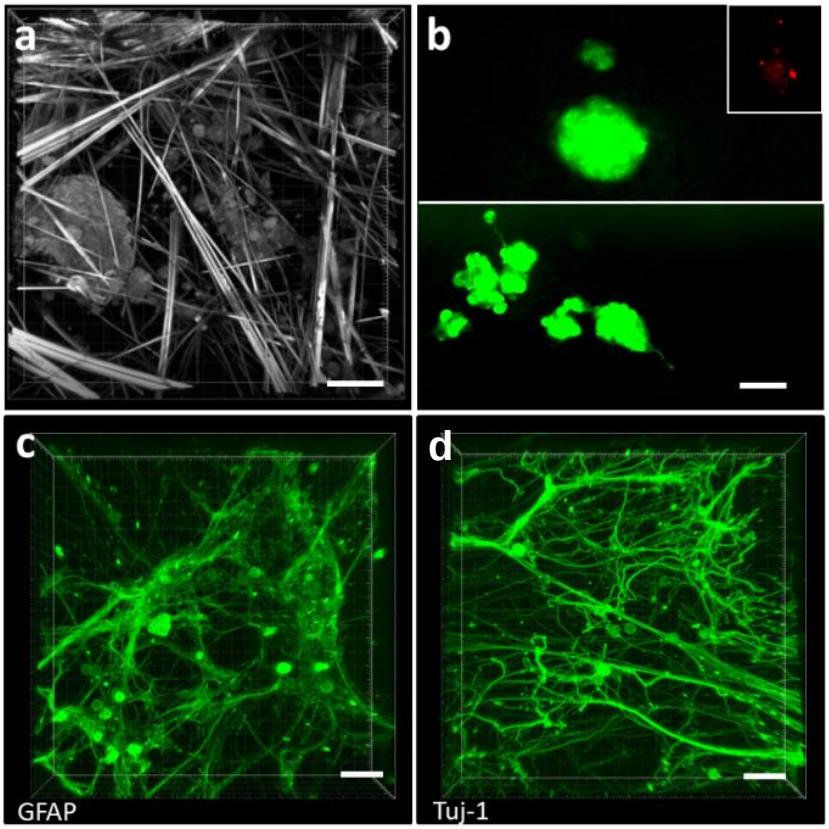

Figure II-27: Human neural stem cell differentiation on Gal-C7 aldonamide gel. Human adult neural stem cells extracted from patient brain biopsy after 7 days of culture on the Gal-C7 gel in differentiation conditions. (a) Laser reflection microscopy observation of hNSCs in the gel fibers and (b) live/dead cell staining assay. The inset represents the red channel alone where only a few dead cells were observed, as usual, in the core of the neurospheres. Immunostaining was performed to observe the cellular neural network with GFAP (glial fibrillary acidic protein), marker of glial cells (c), and Tuj-1 (β3-tubulin), marker of neuronal cells (d) (scale bar: 50 µm).

These techniques did not fully allow the visualization of neurofilaments. Nevertheless, they showed that the loose fiber meshing allowed a real self-assembling and self-organization of the cells in 3D structure between the fibers.

To visualize the differentiation potential of the hNSCs in the Gal-C7 scaffold and neuronal network formation, hNSCs were seeded at high density and immunostaining was performed after 7 days of culture (Figure II-27c and d). The CLARITY-like method for gel embedding was then used. As previously explained, the gel fibers were dissolved during the procedure, revealing only the cell network.

As previously described for hNSCs, differentiation into glial cells was observed as assessed by immunostaining for the GFAP (Figure II-27c). Likewise, numerous positive cells for the early neuronal marker tuj-1 were observed (Figure II-27d). For both markers, a robust network was observed with an important neurite outgrowth. Interestingly, the morphologies of the two networks seem rather different. Glial cells formed a diffuse network, contrasting with straight neurites projected by the neuronal cells. The latter are often organized in bundles that seem to have followed the wide and straight gel fibers. Apart from these bundles, curved neurites were also observed, both highlighting the 3D permissive nature of the hydrogel. These data clearly indicate that the Gal-C7 hydrogel can support adult hNSC differentiation and cell–cell interaction in a 3D environment even if long-term experiments are still needed to study expression of more mature neuronal markers.

II.2.4 Biocompatibility tests with other hydrogels

Other biocompatibility tests have been performed on another gelator from a different family: *N*-dodecylamido-D-glucamine (Glu-C12). As described in the previous chapter, this hydrogel is prepared by dissolution of 3 wt % of the gelator in a mixture of 7 wt % HFP in water. The solution is heated for dissolution and cooled down at room temperature, here without a controlled cooling rate. The resulting gel is then rinsed with water through a sieve in order to eliminate the remaining HFP. To perform the biological assays, the gel was then transferred into the wells of an 8-well chamber slide and Neuro2a cells were seeded on top of it. From the beginning the gel was not really cohesive, it had somehow a “yoghurt” aspect. Its cohesion was furthermore altered by the several DMEM washes.

Live/dead cell assays and MTT tests were performed with Glu-C12. After 7 days of culture, the first one revealed that the cells were majorly living in the Glu-C12 hydrogel, even though they were quite dispersed in it. Some living cells were actually attached to small gel aggregates (Figure

II-28). The MTT test after 4 days of culture was somehow less conclusive for the solvent used at the end was not able to dissolve the hydrogel, resulting in an opaque mixture that could not be read in spectrophotometry. However, with the naked eye we were able to see that the color changed in the well containing the cells compared to the one without (Figure II-28), meaning that the cells were living as well as dividing.

Nevertheless, this hydrogel was no further investigated for the growth of neural cells because of its more complex preparation. Indeed, HFP is required for its good gelation and this induces a potential source of toxicity if the hydrogels are not well rinsed. Yet, its structure and consistency are quite interesting because, contrary to alkylgalactonamides, they do not undergo synearesis and they are very soft, resembling somehow the brain consistency.

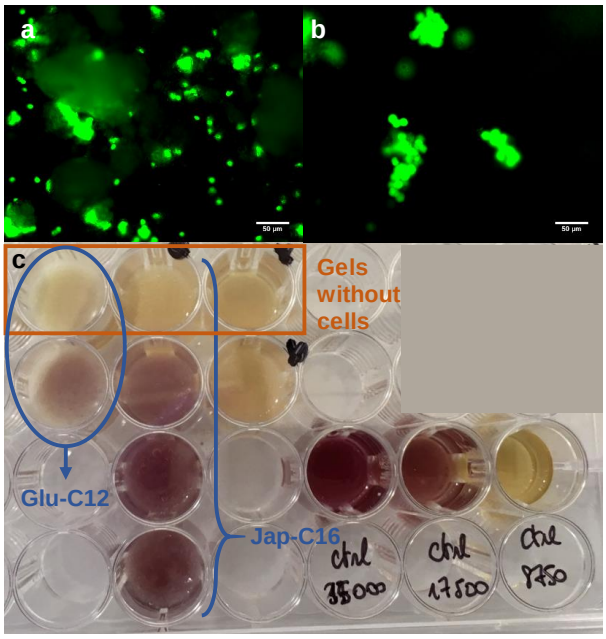

Figure II-28: Biocompatibility results of Glu-C12 and Jap-C16. a. Live/dead cell assay after 7 days of Neuro2a cells cultured in Glu-C12 hydrogel (scale bar: 50 µm). b. Live/dead cell assay after 3 days in a Jap-C16 hydrogel (scale bar: 50 µm). c. Photo of the culture plate with the MTT assay after 3 days before reading it in spectrophotometry. At the top of the column are the gels without cells and under are the gels seeded with 70000 Neuro2a cells. At the bottom right are the control wells with different cell concentrations (35000, 17500 and 8750 cells).

Another kind of gelators was assessed in cell culture. Actually, Watanabe's team in Japan first synthesized this hydrogelator[55] and we tried to investigate it as well, particularly for its thixotropic behavior. The synthesized molecule is the palmitoyl-glycine-D-glucamide, shortened as Jap-C16 (Scheme II-1), and was synthesized according to the protocol described by Watanabe.

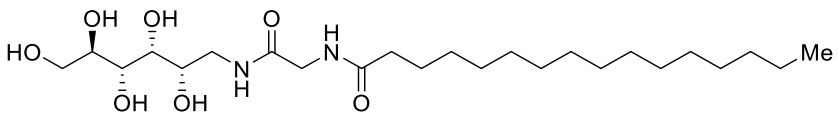

Scheme II-1: Molecular structure of palmitoyl-glycine-D-glucamide (Jap-C16).

This hydrogel was similarly tested by live/dead cell assay and with a MTT test. Even though its characterization by microscopy was difficult because of the gel opacity, come clusters of living Neuro2a cells were found in the hydrogel after 3 days in culture (Figure II-28). Concerning the MTT test, the cells showed a significant metabolic activity meaning that they developed in the hydrogel. Here again, albeit its promising results in biocompatibility, this hydrogel was no further exploited for cell culture trials because the priority was on the alkylgalactonamide family, which are new molecules that have never been described in literature yet, contrary to Jap-C16. However, it was studied for its injectable properties, which will be described in the next chapter.

II.3 Discussion on the hydrogels and the biological results

New supramolecular hydrogels suited for neural cell culture have been found in this study. The alkylgalactonamide hydrogels display fibers with original dimensions, structures, and entanglements. They form long ribbon-like fibers that can reach several hundreds of micrometers in length and several micrometers in width. The meshing also is quite loose. Nevertheless, the three gels do not have exactly the same properties. They affected cell growth to some extent. The different features we have studied that differentiate the three gels are the following: chain parity, fiber dimensions and distribution, solubility and macroscopic stiffness. Those factors are not independent, because the chemical structure of the gelator itself affects the physicochemical properties of the gel. Nevertheless, it is worth gathering and comparing here the results of the cell growth on the three gels in relation with the gel physicochemical properties investigated.

The results tend to show that the 90 min cooled Gal-C7 gel is the most suitable scaffold for cell culture, according to both dead-live, MTT assays and practical issues. This gel has the longest and widest straight fibers and the smallest population of small fibers. Its macroscopic stiffness is very low, around 15 kPa (at high compression speed); its solubility is also low (1.2 µmol/ml, see Table I-4), and it is the only one of the series with an odd number of carbons in the alkyl chain. It is also more practical to handle compared with Gal-C8. In addition, the slow cooling process conferred an advantage on this gel mostly in terms of gel self-standing, handling, homogeneity, 3D penetration, and neurite guidance.

Gal-C6 seems the least favorable even if some cells can be living during 7 days of culture. Most cell cultures stagnated between day 1 (D1) and day 4 (D4) and several clusters of dead cells being found in dead-live experiments at day 7 (D7). It might be related to several gel features. Gal-C6 gel is the stiffest (153 ± 31 kPa at high compression speed). Gal-C6 also has a 5-fold higher solubility compared with the other two gelators (5.0 µmol/ml, see Table I-4) and it has to be used in higher concentration. Since cytotoxic effects are concentration dependent, those factors have to be taken into account in future prospects on these gels, especially in the case of Gal-C6. The toxicity of shorter alkylamines is also known to be higher than the one of longer alkylamines.[56] Otherwise, this molecule gives gels with much shorter and thinner fibers. In the case of Gal-C6, thus many factors might explain the difference of cell growth compared to Gal-C7 and Gal-C8.

For Gal-C8 gels, again the cell growth appeared less favored compared with Gal-C7. The physicochemical differences between Gal-C8 and Gal-C7 gels seem to be a lot more subtle. Gal-C8 is less soluble than Gal-C7 (0.7 µmol/ml, see Table I-4). Like Gal-C7, it also has a population of long, wide and straight fibers. The mechanical properties, measured by rheology on “0 min” cooled

gels and by uniaxial compression on 90 min cooled gels are quite close for both gels. Slow cooled Gal-C8 gels are only slightly stiffer (24 ± 3 kPa at high compression speed) than Gal-C7 gels (14 ± 3 kPa). Gal-C8 is harder to manipulate because of its high gelation point. The two main differences in our observations are rather the chain parity and the difference of the fibers' length distribution. An important difference can be seen on the fiber length histogram in 90 min cooled gels (Figure I-22b): an important population of short fibers is observed for Gal-C8 compared with Gal-C7. This distribution corresponds to a higher density of fibers. It has been shown that nanofibers of poorly soluble self-assembling dipeptides[57] or peptides[58] can be detrimental for cells when penetrating through the cell membrane and tend to provoke the apoptosis of the cell. In the case of Gal–C6–C7-C8 gels, changing the cooling rate from "0 min" to "90 min" changed the fiber lengths profile and the nucleation points for a given gelator but it did not change strongly the cell growth in MTT experiments: the same difference of cell growth between Gal-C6, Gal-C7, and Gal-C8 is observed on "0 min" cooled gels and on 90 min cooled gels (Figure II-23). It tends to show that at least the micrometric fiber distribution might not be the most critical parameter explaining the difference of cell viability and growth between Gal-C6, Gal-C7, and Gal-C8. Thus, other factors not addressed here should be considered further and among others the metabolic fate of the gelators.

When it comes to chain parity, it is known that the metabolic paths of odd and even chains are different.[59] The packing of LMWGs is also known to be sensitive to the chain length, even for a one-carbon odd–even increment.[60] This difference then affects in cascade all the other properties of the gels, from the way it self-assembles up to the effect on cell growth. For example, a previous work has shown that some gel fibers induce different biological properties and cell growth according to the chirality of helixes.[61] We tried to obtain gels from the related odd-numbered alkylgalactonamides, Gal-C9 and Gal-C5 (see I.2.1.1) but as previously described, these molecules did not give cohesive enough gels. For these reasons, it was not possible to work with these related odd-numbered alkylgalactonamides.

Finally, Gal-C7 is an optimal gel within this family. It is well adapted to the growth and differentiation of neuronal cells in 3D, including human adult neural stem cells. The network organization really seems to mimic the extracellular matrix architecture. It mixes a population of very large, straight, and stiff ribbons linked by a population of narrower flexible ribbons. It is also quite easy to prepare. Concerning mechanical properties, Gal-C7 is in the convenient range of stiffness (Y = 14 ± 3 kPa at 5 mm/s; Y = 8 ± 2 kPa at 0.1 mm/s, Table I-2) for both neuronal and glial cell growth. Actually, the results of the cell culture with hNSCs demonstrate that the gel favors the differentiation into both glial cells and neurons, providing a dense interpenetrated network of neuronal cells. It is worth pointing out that the measurement of the macroscopic rigidity, as provided by rheology and compression tests, only gives the "macroscopic" mechanical properties.

In fact, the cells experience a local rigidity at microscopic scale that may be different from the rigidity measured by macroscopic measurements. The presence of different kinds of fibers, some being large, straight, and stiff and others being narrow and flexible may favor the dual differentiation which is required for neural tissue regeneration. It led to the growth of neurites with different morphologies, like in the brain. The dual network of fibers may help neurites outgrowth and both long and short distance interconnection between cells. It has also been shown that the topography and the roughness of the fibers, at the nanometric scale, can affect cell responses.[62] Actually, immunostaining revealed bundles of neurites that have followed the straight fibers (Figure II-27), probably because they follow their grooved topography. It is well observed on the widest ones (Figure II-26). This phenomenon has already been highlighted in previous studies.[44] Finally, this combination of microscopic vs macroscopic properties makes these matrixes very original in respect to many polymer scaffolds and other fibrillar supramolecular networks. Notably, the extension of such very flat and large fibers over several micrometers instead of twisted fibers and linked with thinner fibers is quite unique.[63]

The other kinds of molecular gelators already used for cell culture and based on amino acids or saccharides provide smaller fibers often twisted, and it has been shown that this topology at the microscale has an impact on cell adhesion and growth.[61] The simplicity of the chemical structure of the alkylgalactonamide gels may also be an advantage: more complex chemical functionalities may induce toxicity.[64] In addition, compared with peptide-based gelators, the fiber structure of allkylgalactonamides and also the molecules released are very different and will lead to differences in metabolizing.

Still to compare with other matrixes already described for neuronal cell culture, in 90 min cooled Gal-C7 alkylgalactonamide gels, the cells penetrated in depth in the matrix and interacted with several fibers and with other cells, forming neurosphere-like structures. They formed a dense network of cells after 7 days, and less commonly, they developed straight neurite outgrowths over long distances by following the gel fibers. Its extreme softness and its highly porous network allow the migration of the neural cells throughout the network, while providing a large carrier for the cells. With regular scaffolds made of collagen I only or hyaluronic acid neurite outgrowth is generally neither very extended nor dense.[30–32] With composite scaffolds using a combination of ECM components with silk protein11 or synthetic peptides[30,38,39,65], much denser neurons networks are observed. However, these kinds of scaffolds are more difficult to produce. In comparison, the Gal-C7 gel also provides, but with a very simple molecule, a suitable environment for 3D growth and neural network development.

II.4 Conclusion

The three alkylgalactonamide hydrogels, but most particularly Gal-C7 provided gels suitable for the 3D-culture of neuronal cells. A neuronal cell line, but also adult human neural stem cells, have been grown on these gels. The very large and long flat ribbons that form the hydrogel and which are linked by narrower ribbons, form an adequate substrate for sustaining the cells. The entanglement of the ribbons is loose, providing large and open interspaces, not cross-linked, into which the cells can migrate and grow in 3D.

On the three gels studied (hexyl, hepty, octylgalactonamide), the cells stay alive after 7 days but the Gal-C7 gels appeared to be the most suitable for the growth of the neuronal cells. Quite strikingly, a one-carbon increment in the alkyl chain length of the gelator affected significantly the biocompatibility. In fact, this tiny chain length difference induced a cascade of differences. It started from the self-assembly in different sizes and the morphologies of ribbons and finally affected the network organization, the stiffness, and the solubility. In the case of Gal-C7 and Gal-C8, the stiffness lies within a suitable range for neuronal cells differentiation and growth. As a result, experiments with human adult neural stem cells (hNSCs) from patient biopsies demonstrated that the scaffold is suitable for the differentiation into both glial cells and neuronal cells. It allowed the outgrowth of numerous neurites and the development of a full interpenetrated neuronal network, showing the potential of this hydrogel to support neural tissue regeneration.

In vivo experiments on rats have already started. The inflammatory response to the hydrogels was first assessed with subcutaneous implants of hydrogels and this gave good results: the hydrogels do not provoke any inflammation on the rats. Then, trials for the implantation of the gels alone in the brain of rats have been performed, but we realized that the hydrogels were really complicated to manipulate, especially with the all the fluids that deteriorate the gel structure. A first work on the gels' stability has thus to be done so that the hydrogel structure remains the longest inside a brain lesion.

References

(1) Goldman, S. A.; Nottebohm, F. Neuronal Production, Migration, and Differentiation in a Vocal Control Nucleus of the Adult Female Canary Brain. *Proceedings of the National Academy of Sciences* **1983**, *80* (8), 2390–2394. https://doi.org/10.1073/pnas.80.8.2390.

(2) Reynolds, B.; Weiss, S. Generation of Neurons and Astrocytes from Isolated Cells of the Adult Mammalian Central Nervous System. *Science* **1992**, *255* (5052), 1707–1710. https://doi.org/10.1126/science.1553558.

(3) Eriksson, P. S.; Perfilieva, E.; Björk-Eriksson, T.; Alborn, A.-M.; Nordborg, C.; Peterson, D. A.; Gage, F. H. Neurogenesis in the Adult Human Hippocampus. *Nature Medicine* **1998**, *4* (11), 1313–1317. https://doi.org/10.1038/3305.

(4) Song, H.; Stevens, C. F.; Gage, F. H. Neural Stem Cells from Adult Hippocampus Develop Essential Properties of Functional CNS Neurons. *Nature Neuroscience* **2002**, *5* (5), 438–445. https://doi.org/10.1038/nn844.

(5) Levitan, I. B.; Kaczmarek, L. K. *The Neuron: Cell and Molecular Biology*, Fourth edition.; Oxford University Press, 2015.

(6) Sorrells, S. F.; Paredes, M. F.; Cebrian-Silla, A.; Sandoval, K.; Qi, D.; Kelley, K. W.; James, D.; Mayer, S.; Chang, J.; Auguste, K. I.; et al. Human Hippocampal Neurogenesis Drops Sharply in Children to Undetectable Levels in Adults. *Nature* **2018**, *555* (7696), 377–381. https://doi.org/10.1038/nature25975.

(7) Vaysse, L.; Labie, C.; Canolle, B.; Jozan, S.; Béduer, A.; Arnauduc, F.; Vieu, C.; Sol, J. C.; Loubinoux, I. Adult Human Progenitor Cells from the Temporal Lobe: Another Source of Neuronal Cells. *Brain Injury* **2012**, *26* (13–14), 1636–1645. https://doi.org/10.3109/02699052.2012.700084.

(8) Davoust, C. Greffe de cellules souches neurales adultes sur bioimplants comme stratégie thérapeutique dans un modèle de lésion du cortex moteur primaire chez le petit animal. Suivi par analyses comportementales, IRM et histologie., Université Paul Sabatier-Toulouse III, 2016.

(9) Vescovi, A. L.; Galli, R.; Reynolds, B. A. Brain Tumour Stem Cells. *Nature Reviews Cancer* **2006**, *6* (6), 425–436. https://doi.org/10.1038/nrc1889.

(10) Walton, N. M. Derivation and Large-Scale Expansion of Multipotent Astroglial Neural Progenitors from Adult Human Brain. *Development* **2006**, *133* (18), 3671–3681. https://doi.org/10.1242/dev.02541.

(11) Arsenijevic, Y.; Villemure, J.-G.; Brunet, J.-F.; Bloch, J. J.; Déglon, N.; Kostic, C.; Zurn, A.; Aebischer, P. Isolation of Multipotent Neural Precursors Residing in the Cortex of the Adult Human Brain. *Experimental Neurology* **2001**, *170* (1), 48–62. https://doi.org/10.1006/exnr.2001.7691.

(12) Nunes, M. C.; Roy, N. S.; Keyoung, H. M.; Goodman, R. R.; McKhann, G.; Jiang, L.; Kang, J.; Nedergaard, M.; Goldman, S. A. Identification and Isolation of Multipotential Neural Progenitor Cells from the Subcortical White Matter of the Adult Human Brain. *Nature Medicine* **2003**, *9* (4), 439–447. https://doi.org/10.1038/nm837.

(13) Artavanis-Tsakonas, S.; Matsuno, K.; Fortini, M. E. Notch Signaling. *Science* **1995**, *268* (5208), 225–232. https://doi.org/10.1126/science.7716513.

(14) Geraldo, S.; Gordon-Weeks, P. R. Cytoskeletal Dynamics in Growth-Cone Steering. *Journal of Cell Science* **2009**, *122* (20), 3595–3604. https://doi.org/10.1242/jcs.042309.

(15) Forscher, P.; Smith, S. J. Actions of Cytochalasins on the Organization of Actin Filaments and Microtubules in a Neuronal Growth Cone. *J. Cell Biol.* **1988**, *107*, 1505–1516. https://doi.org/10.1083/jcb.107.4.1505.

(16) Itofusa, R.; Kamiguchi, H. Polarizing Membrane Dynamics and Adhesion for Growth Cone Navigation. *Molecular and Cellular Neuroscience* **2011**, *48* (4), 332–338. https://doi.org/10.1016/j.mcn.2011.03.007.

(17) Saha, K.; Keung, A. J.; Irwin, E. F.; Li, Y.; Little, L.; Schaffer, D. V.; Healy, K. E. Substrate Modulus Directs Neural Stem Cell Behavior. *Biophysical Journal* **2008**, *95* (9), 4426–4438. https://doi.org/10.1529/biophysj.108.132217.

(18) Sun, Y.; Yong, K. M. A.; Villa-Diaz, L. G.; Zhang, X.; Chen, W.; Philson, R.; Weng, S.; Xu, H.; Krebsbach, P. H.; Fu, J. Hippo/YAP-Mediated Rigidity-Dependent Motor Neuron Differentiation of Human Pluripotent Stem Cells. *Nature Materials* **2014**, *13* (6), 599–604. https://doi.org/10.1038/nmat3945.

(19) Keung, A. J.; Asuri, P.; Kumar, S.; Schaffer, D. V. Soft Microenvironments Promote the Early Neurogenic Differentiation but Not Self-Renewal of Human Pluripotent Stem Cells. *Integrative Biology* **2012**, *4* (9), 1049. https://doi.org/10.1039/c2ib20083j.

(20) Keung, A. J.; Dong, M.; Schaffer, D. V.; Kumar, S. Pan-Neuronal Maturation but Not Neuronal Subtype Differentiation of Adult Neural Stem Cells Is Mechanosensitive. *Scientific Reports* **2013**, *3* (1). https://doi.org/10.1038/srep01817.

(21) Sur, S.; Newcomb, C. J.; Webber, M. J.; Stupp, S. I. Tuning Supramolecular Mechanics to Guide Neuron Development. *Biomaterials* **2013**, *34* (20), 4749–4757. https://doi.org/10.1016/j.biomaterials.2013.03.025.

(22) Koser, D. E.; Thompson, A. J.; Foster, S. K.; Dwivedy, A.; Pillai, E. K.; Sheridan, G. K.; Svoboda, H.; Viana, M.; Costa, L. da F.; Guck, J.; et al. Mechanosensing Is Critical for Axon Growth in the Developing Brain. *Nature Neuroscience* **2016**, *19* (12), 1592–1598. https://doi.org/10.1038/nn.4394.

(23) Ahearne, M. Introduction to Cell-Hydrogel Mechanosensing. *Interface Focus* **2014**, *4* (2), 20130038–20130038. https://doi.org/10.1098/rsfs.2013.0038.

(24) Lindvall, O.; Kokaia, Z. Neurogenesis Following Stroke Affecting the Adult Brain. *Cold Spring Harb Perspect Biol* **2015**, *7* (11), a019034. https://doi.org/10.1101/cshperspect.a019034.

(25) Richardson, R. M.; Singh, A.; Sun, D.; Fillmore, H. L.; Dietrich, D. W.; Bullock, M. R. Stem Cell Biology in Traumatic Brain Injury: Effects of Injury and Strategies for Repair. *Journal of Neurosurgery* **2010**, *112* (5), 1125–1138. https://doi.org/10.3171/2009.4.JNS081087.

(26) Maoz, B. M.; Herland, A.; FitzGerald, E. A.; Grevesse, T.; Vidoudez, C.; Pacheco, A. R.; Sheehy, S. P.; Park, T.-E.; Dauth, S.; Mannix, R.; et al. A Linked Organ-on-Chip Model of the Human Neurovascular Unit Reveals the Metabolic Coupling of Endothelial and Neuronal Cells. *Nature Biotechnology* **2018**, *36* (9), 865–874. https://doi.org/10.1038/nbt.4226.

(27) Kukekov, V. G.; Laywell, E. D.; Suslov, O.; Davies, K.; Scheffler, B.; Thomas, L. B.; O'Brien, T. F.; Kusakabe, M.; Steindler, D. A. Multipotent Stem/Progenitor Cells with Similar Properties Arise from Two Neurogenic Regions of Adult Human Brain. *Experimental Neurology* **1999**, *156* (2), 333–344. https://doi.org/10.1006/exnr.1999.7028.

(28) Li, X.; Katsanevakis, E.; Liu, X.; Zhang, N.; Wen, X. Engineering Neural Stem Cell Fates with Hydrogel Design for Central Nervous System Regeneration. *Progress in Polymer Science* **2012**.

(29) Murphy, A. R.; Laslett, A.; O'Brien, C. M.; Cameron, N. R. Scaffolds for 3D in Vitro Culture of Neural Lineage Cells. *Acta Biomaterialia* **2017**. https://doi.org/10.1016/j.actbio.2017.02.046.

(30) Tang-Schomer, M. D.; White, J. D.; Tien, L. W.; Schmitt, L. I.; Valentin, T. M.; Graziano, D. J.; Hopkins, A. M.; Omenetto, F. G.; Haydon, P. G.; Kaplan, D. L. Bioengineered Functional Brain-like Cortical Tissue. *Proceedings of the National Academy of Sciences* **2014**, *111* (38), 13811–13816. https://doi.org/10.1073/pnas.1324214111.

(31) Sur, S.; Pashuck, E. T.; Guler, M. O.; Ito, M.; Stupp, S. I.; Launey, T. A Hybrid Nanofiber Matrix to Control the Survival and Maturation of Brain Neurons. *Biomaterials* **2012**, *33* (2), 545–555. https://doi.org/10.1016/j.biomaterials.2011.09.093.

(32) Farrell, K.; Joshi, J.; Kothapalli, C. R. Injectable Uncrosslinked Biomimetic Hydrogels as Candidate Scaffolds for Neural Stem Cell Delivery. *Journal of Biomedical Materials Research Part A* **2017**, *105* (3), 790–805. https://doi.org/10.1002/jbm.a.35956.

(33) Duan, H.; Li, X.; Wang, C.; Hao, P.; Song, W.; Li, M.; Zhao, W.; Gao, Y.; Yang, Z. Functional Hyaluronate Collagen Scaffolds Induce NSCs Differentiation into Functional Neurons in Repairing the Traumatic Brain Injury. *Acta Biomaterialia* **2016**, *45*, 182–195. https://doi.org/10.1016/j.actbio.2016.08.043.

(34) Tarus, D.; Hamard, L.; Caraguel, F.; Wion, D.; Szarpak-Jankowska, A.; van der Sanden, B.; Auzély-Velty, R. Design of Hyaluronic Acid Hydrogels to Promote Neurite Outgrowth in Three Dimensions. *ACS Applied Materials & Interfaces* **2016**, *8* (38), 25051–25059. https://doi.org/10.1021/acsami.6b06446.

(35) Diekjürgen, D.; Grainger, D. W. Polysaccharide Matrices Used in 3D in Vitro Cell Culture Systems. *Biomaterials* **2017**, *141*, 96–115. https://doi.org/10.1016/j.biomaterials.2017.06.020.

(36) Gonçalves-Pimentel, C.; Moreno, G. M. M.; Trindade, B. S.; Isaac, A. R.; Rodrigues, C. G.; Savariradjane, M.; de Albuquerque, A. V.; de Andrade Aguiar, J. L.; Andrade-da-Costa, B. L. da S. Cellulose Exopolysaccharide from Sugarcane Molasses as a Suitable Substrate for 2D and 3D Neuron and Astrocyte Primary Cultures. *Journal of Materials Science: Materials in Medicine* **2018**, *29* (9). https://doi.org/10.1007/s10856-018-6147-0.

(37) Wei, Z.; Zhao, J.; Chen, Y. M.; Zhang, P.; Zhang, Q. Self-Healing Polysaccharide-Based Hydrogels as Injectable Carriers for Neural Stem Cells. *Scientific Reports* **2016**, *6*, 37841. https://doi.org/10.1038/srep37841.

(38) Ylä-Outinen, L.; Joki, T.; Varjola, M.; Skottman, H.; Narkilahti, S. Three-Dimensional Growth Matrix for Human Embryonic Stem Cell-Derived Neuronal Cells. *J Tissue Eng Regen Med* **2014**, *8*, 186–194. https://doi.org/10.1002/term.1512.

(39) Thonhoff, J. R.; Lou, D. I.; Jordan, P. M.; Zhao, X.; Wu, P. Compatibility of Human Fetal Neural Stem Cells with Hydrogel Biomaterials in Vitro. *Brain Research* **2008**, *1187*, 42–51. https://doi.org/10.1016/j.brainres.2007.10.046.

(40) Carlson, A. L.; Bennett, N. K.; Francis, N. L.; Halikere, A.; Clarke, S.; Moore, J. C.; Hart, R. P.; Paradiso, K.; Wernig, M.; Kohn, J.; et al. Generation and Transplantation of Reprogrammed Human Neurons in the Brain Using 3D Microtopographic Scaffolds. *Nature Communications* **2016**, *7*, 10862. https://doi.org/10.1038/ncomms10862.

(41) Omidinia-Anarkoli, A.; Boesveld, S.; Tuvshindorj, U.; Rose, J. C.; Haraszti, T.; De Laporte, L. An Injectable Hybrid Hydrogel with Oriented Short Fibers Induces Unidirectional Growth of Functional Nerve Cells. *Small* **2017**, *13* (36), 1702207. https://doi.org/10.1002/smll.201702207.

(42) Zhu, B.; Li, W.; Lewis, R. V.; Segre, C. U.; Wang, R. E-Spun Composite Fibers of Collagen and Dragline Silk Protein: Fiber Mechanics, Biocompatibility, and Application in Stem Cell Differentiation. *Biomacromolecules* **2015**, *16* (1), 202–213. https://doi.org/10.1021/bm501403f.

(43) Béduer, A.; Gonzales-Calvo, I.; Vieu, C.; Loubinoux, I.; Vaysse, L. Investigation of the Competition Between Cell/Surface and Cell/Cell Interactions During Neuronal Cell Culture on a Micro-Engineered Surface. *Macromol. Biosci.* **2013**, *13* (11), 1546–1555. https://doi.org/10.1002/mabi.201300202.

(44) Béduer, A.; Vieu, C.; Arnauduc, F.; Sol, J.-C.; Loubinoux, I.; Vaysse, L. Engineering of Adult Human Neural Stem Cells Differentiation through Surface Micropatterning. *Biomaterials* **2012**, *33* (2), 504–514. https://doi.org/10.1016/j.biomaterials.2011.09.073.

(45) Béduer, A. Micro/Nano ingénierie pour le contrôle de la croissance de cellules neuronales et l'élaboration d'une bioprothèse cérébrale à base de cellules souches organisées, Université Paul Sabatier-Toulouse III, 2012.

(46) Yamada, A.; Vignes, M.; Bureau, C.; Mamane, A.; Venzac, B.; Descroix, S.; Viovy, J.-L.; Villard, C.; Peyrin, J.-M.; Malaquin, L. In-Mold Patterning and Actionable Axo-Somatic Compartmentalization for on-Chip Neuron Culture. *Lab on a Chip* **2016**, *16* (11), 2059–2068. https://doi.org/10.1039/C6LC00414H.

(47) Pautot, S.; Wyart, C.; Isacoff, E. Y. Colloid-Guided Assembly of Oriented 3D Neuronal Networks. *Nature Methods* **2008**, *5* (8), 735–740. https://doi.org/10.1038/nmeth.1236.

(48) Edmondson, R.; Broglie, J. J.; Adcock, A. F.; Yang, L. Three-Dimensional Cell Culture Systems and Their Applications in Drug Discovery and Cell-Based Biosensors. *Assay Drug Dev Technol* **2014**, *12* (4), 207–218. https://doi.org/10.1089/adt.2014.573.

(49) Muguruma, K.; Nishiyama, A.; Kawakami, H.; Hashimoto, K.; Sasai, Y. Self-Organization of Polarized Cerebellar Tissue in 3D Culture of Human Pluripotent Stem Cells. *Cell Reports* **2015**, *10* (4), 537–550. https://doi.org/10.1016/j.celrep.2014.12.051.

(50) Qian, X.; Jacob, F.; Song, M. M.; Nguyen, H. N.; Song, H.; Ming, G. Generation of Human Brain Region–Specific Organoids Using a Miniaturized Spinning Bioreactor. *Nature Protocols* **2018**, *13* (3), 565–580. https://doi.org/10.1038/nprot.2017.152.

(51) Ma, W.; Tavakoli, T.; Chen, S.; Maric, D.; Liu, J. L.; O'Shaughnessy, T. J.; Barker, J. L. Reconstruction of Functional Cortical-like Tissues from Neural Stem and Progenitor Cells.

Tissue Engineering Part A **2008**, *14* (10), 1673–1686. https://doi.org/10.1089/ten.tea.2007.0357.

(52) Lancaster, M. A.; Renner, M.; Martin, C.-A.; Wenzel, D.; Bicknell, L. S.; Hurles, M. E.; Homfray, T.; Penninger, J. M.; Jackson, A. P.; Knoblich, J. A. Cerebral Organoids Model Human Brain Development and Microcephaly. *Nature* **2013**, *501* (7467), 373–379. https://doi.org/10.1038/nature12517.

(53) Du, J.; Tan, E.; Kim, H. J.; Zhang, A.; Bhattacharya, R.; Yarema, K. J. Comparative Evaluation of Chitosan, Cellulose Acetate, and Polyethersulfone Nanofiber Scaffolds for Neural Differentiation. *Carbohydrate Polymers* **2014**, *99*, 483–490. https://doi.org/10.1016/j.carbpol.2013.08.050.

(54) Chung, K.; Deisseroth, K. CLARITY for Mapping the Nervous System. *Nature Methods* **2013**, *10* (6), 508–513. https://doi.org/10.1038/nmeth.2481.

(55) Ohsedo, Y.; Oono, M.; Saruhashi, K.; Watanabe, H. N-Alkylamido-D-Glucamine-Based Gelators for the Generation of Thixotropic Gels. *RSC Adv.* **2014**, *4* (89), 48554–48558. https://doi.org/10.1039/C4RA08346F.

(56) Greim, H.; Bury, D.; Klimisch, H. J.; Oeben-Negele, M.; Ziegler-Skylakakis, K. Toxicity of Aliphatic Amines: Structure-Activity Relationship. *Chemosphere* **1998**, *36* (2), 271–295.

(57) Kuang, Y.; Xu, B. Disruption of the Dynamics of Microtubules and Selective Inhibition of Glioblastoma Cells by Nanofibers of Small Hydrophobic Molecules. *Angew. Chem. Int. Ed.* **2013**, *52* (27), 6944–6948. https://doi.org/10.1002/anie.201302658.

(58) Petkova, A. T. Self-Propagating, Molecular-Level Polymorphism in Alzheimer's -Amyloid Fibrils. *Science* **2005**, *307* (5707), 262–265. https://doi.org/10.1126/science.1105850.

(59) Gotoh, N.; Moroda, K.; Watanabe, H.; Yoshinaga, K.; Tanaka, M.; Mizobe, H.; Ichioka, K.; Tokairin, S.; Wada, S. Metabolism of Odd-Numbered Fatty Acids and Even-Numbered Fatty Acids in Mouse. *Journal of Oleo Science* **2008**, *57* (5), 293–299. https://doi.org/10.5650/jos.57.293.

(60) Shimizu, T.; Masuda, M. Stereochemical Effect of Even-Odd Connecting Links on Supramolecular Assemblies Made of 1-Glucosamide Bolaamphiphiles. *Journal of the American Chemical Society* **1997**, *119* (12), 2812–2818.

(61) Liu, G.-F.; Zhang, D.; Feng, C.-L. Control of Three-Dimensional Cell Adhesion by the Chirality of Nanofibers in Hydrogels. *Angew. Chem. Int. Ed.* **2014**, *53* (30), 7789–7793. https://doi.org/10.1002/anie.201403249.

(62) Wong, J. Y.; Leach, J. B.; Brown, X. Q. Balance of Chemistry, Topography, and Mechanics at the Cell–Biomaterial Interface: Issues and Challenges for Assessing the Role of Substrate Mechanics on Cell Response. *Surface Science* **2004**, *570* (1–2), 119–133. https://doi.org/10.1016/j.susc.2004.06.186.

(63) Du, X.; Zhou, J.; Shi, J.; Xu, B. Supramolecular Hydrogelators and Hydrogels: From Soft Matter to Molecular Biomaterials. *Chemical Reviews* **2015**, *115* (24), 13165–13307. https://doi.org/10.1021/acs.chemrev.5b00299.

(64) Fitremann, J.; Lonetti, B.; Fratini, E.; Fabing, I.; Payré, B.; Boulé, C.; Loubinoux, I.; Vaysse, L.; Oriol, L. A Shear-Induced Network of Aligned Wormlike Micelles in a Sugar-Based

Molecular Gel. From Gelation to Biocompatibility Assays. *Journal of Colloid and Interface Science* **2017**, *504*, 721–730. https://doi.org/10.1016/j.jcis.2017.06.021.

(65) Kaneko, A.; Sankai, Y. Long-Term Culture of Rat Hippocampal Neurons at Low Density in Serum-Free Medium: Combination of the Sandwich Culture Technique with the Three-Dimensional Nanofibrous Hydrogel PuraMatrix. *PLoS ONE* **2014**, *9* (7), e102703. https://doi.org/10.1371/journal.pone.0102703.

III. Shaping of hydrogels

III.1 Shaping of hydrogels: towards 3D bioprinting

Over the past decades, a lot of progress and breakthroughs have been achieved concerning tissue engineering thanks to the development of 3D artificial scaffolds for cell culture, but also with the emergence of organoids. The first has the advantage of spatially and precisely distributing material with controlled properties for specific cell types and applications, whereas the latter results in biological models closer to the *in vivo* conditions thanks to the self-organization of the cells and the secretion of their own ECM. However, these two methods have drawbacks: 3D scaffolds tend to lack biological functionalities such as guidance cues and cell-cell communication that are crucial for their development; and organoids, despite their similarity with real organs, lack vascularization and thus often undergo necrosis at their center because of the deprivation of nutrients and oxygen. The next step is thus to try to combine these two approaches in order to construct artificial tissues with a determined cellular structure and organization in order to reproduce the best the *in vivo* conditions, like with organ-on-chip for instance[1]. 3D printing also constitute an interesting tool that can address this challenge because it uses the artificial scaffolds already well-known for tissue engineering, but it can also shape well-designed structures to mimic native ones.[2,3]

In this next part, we are going to quickly describe 3D printing and bioprinting tools for the fabrication of artificial tissues and then we will focus on one particular way of shaping hydrogels that could be applied to our alkylgalactonamide gelators.

III.1.1 3D printing and bioprinting

3D printing has considerably developed recently and is applied to a multitude of domains going from construction industry to micrometric electrical components. The first 3D printing of a material was described in 1986 by Charles W. Hull, who named his method “stereolithography”. It consisted in a computer-assisted deposition of layers of a UV-curable polymer to form 3D objects.[4] Since then, the process has been applied to a huge variety of materials, though with some apparatus adaptations.

Eventually, 3D printing has also started being applied to biology to construct artificial tissues. Two approaches can then be employed: either a porous cell-free scaffold is 3D-printed and then further seeded with cells, or the cells are directly printed inside a scaffold, or even without one, to

fabricate tissues. This latter is called 3D bioprinting. Compared to 3D printing of cell-free scaffolds where the cells need to colonize the structure after seeding, 3D bioprinting enables the readily and precise deposition of cells already inside the scaffold.

Several techniques can be employed for 3D bioprinting that will be presented below.

III.1.1.1 Different types of printing processes

For 3D bioprinting, three main methods can be employed that, of course, can also be used for regular 3D printing: extrusion-based, inkjet-based and laser-assisted printing, as represented on Figure III-1.

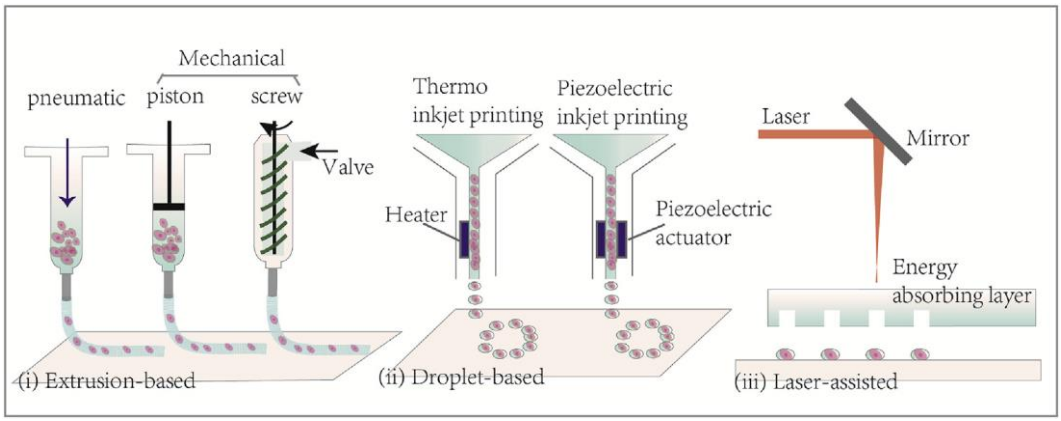

Figure III-1: The three types of processes used for 3D bioprinting. (i) Extrusion-based techniques where a bioink containing cells is continuously pushed out of the nozzle either by pneumatic or mechanical force. (ii) Droplet- or inkjet-based printing where droplets of free or encapsulated cells are deposited on a surface. (iii) Laser-assisted printing that propels individual cells on a substrate on which they can further adhere and grow. From [2].

Inkjet-based and laser-assisted printing consist in droplet deposition of cell and/or material, induced by high-pressure bubbles. These bubbles can be produced by a laser, by the use of a heater or by a piezoelectric actuator inside the dispenser. It enables the precise deposition of small droplets on a substrate, resulting in high printing speed and very good printing resolutions, especially in the case of laser-assisted printing. Besides, electrospinning has recently been developed for the fabrication of 3D scaffolds and referred as “direct-writing electrospinning”.[5] However, we are going to focus on the type of printing described here after, since it is the one we employed in our work.

Extrusion-based printing is the most common method used for 3D printing and it simply consists in the continuous supply of material by pneumatic or mechanical forces to form a fiber that is deposited on a surface. By adding the layers of fibers and by the solidification of the material, 3D structures can thus be built. The most important requirement for this kind of printing is that ink

has to flow during extrusion but once deposited, it has to set rapidly. For this, the inks and the set-ups used can be very different, as represented on Figure III-2.

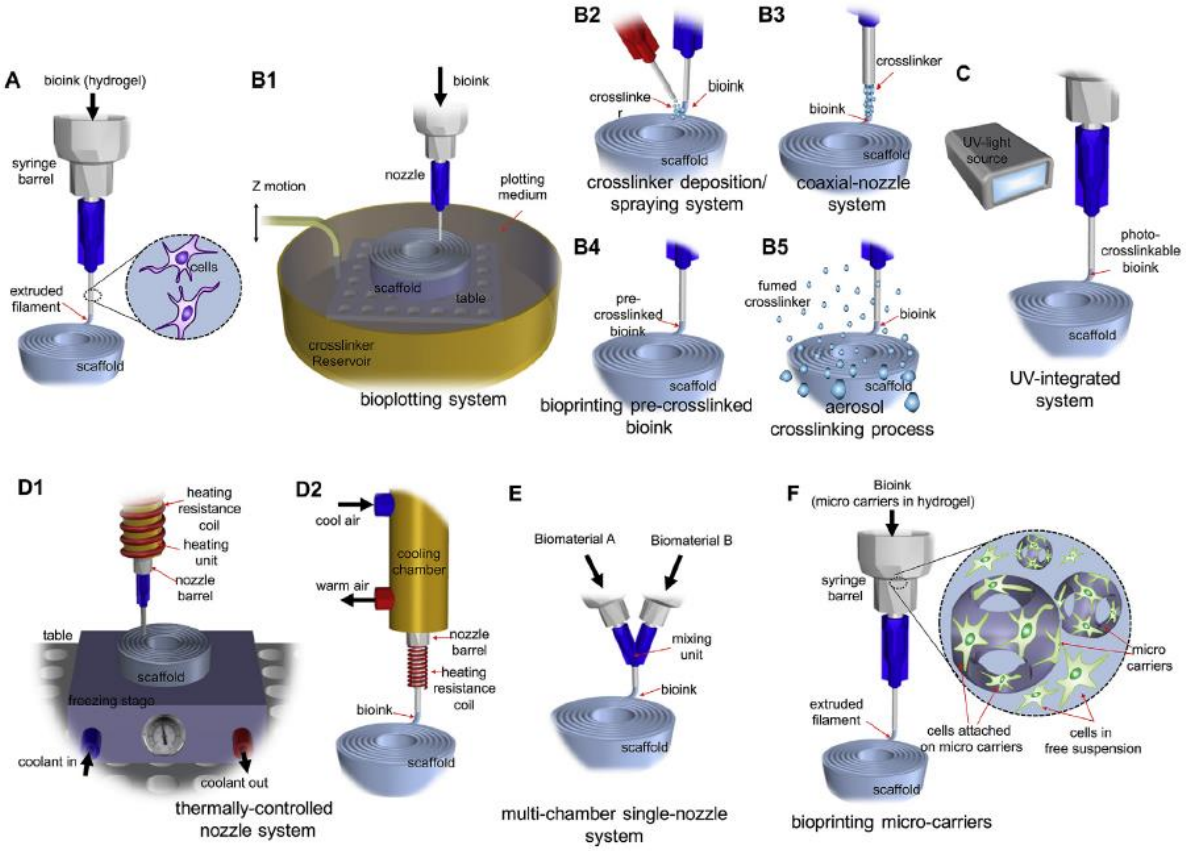

Figure III-2: Different kinds of set-up used for the extrusion-based printing. A. Direct extrusion of a hydrogel loaded with cells. B1. Extrusion in a cross-linking bath. Gelation can also be achieved by spraying (B2), co-extrusion (B3) or fumigation (B5) of the cross-linker, but also by UV curing (C). The ink can also be pre-cross-linked (B4). Heat control can also be employed for the printing of thermosensitive hydrogels (DI and D2). Several components can also be mixed into the nozzle prior to extrusion (E). Micro-carriers can also be used as supports for cells and extruded (F). From [6].

Various materials can be extruded: molten polymers, hydrogels, or even cell aggregates, etc. Next, we will briefly review the 3D printing and bioprinting of hydrogels only.

III.1.1.2 3D printing and bioprinting of hydrogels

For the extrusion of hydrogels, several methods can be employed according to how their gelation is triggered. This one can be induced either by temperature, by a cross-linker, by solvent exchange, etc. Thixotropic gels (also called “shear-thinning” gels) can be used and these ones have the advantage of not needing any gelation trigger since they flow under a strain and become highly viscous again when the strain stops. Many studies thus use this kind of hydrogels for 3D printing. Nolan *et al.* for instance developed two LMWGs based on Fmoc-dipeptides that can be extruded into superimposed layers to form 3D constructs (Figure III-3). Interestingly they used two different methods to obtain the gels (solvent- and pH-triggered approaches) and they were able

to extrude and 3D print them in each case. The extrusion also sometimes induced an alignment of the microscopic fibers composing the gels.[7]

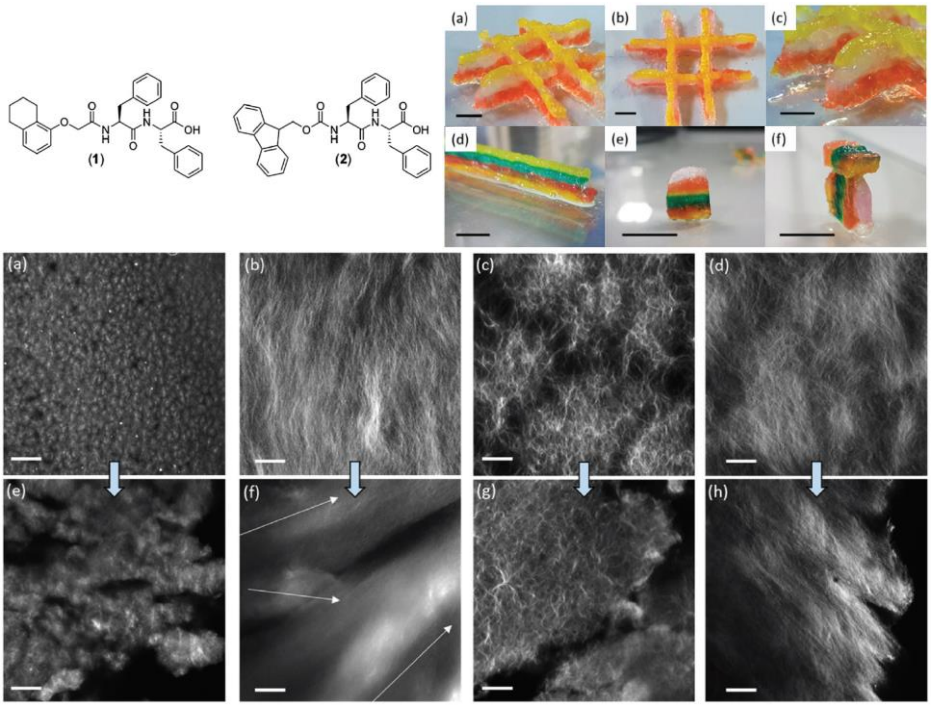

Figure III-3: Top left: Chemical representations of the two LMWG synthesized by Nolan et al. Top right: Examples of 3D printed structures obtained from the different types of hydrogel they developed. They stained the hydrogels with different dyes to show the several layers (scale bars: 1 cm). Bottom: Confocal images of the microscopic fibers composing the different hydrogels before (a-d) and after (e-h) extrusion from a syringe (scale bars: 20 µm). The white arrows in image f are a suggestion of different orientations. From [7].

Raphael *et al.* also exploited the shear-thinning property of a commercialized SAP (self-assembling peptide) hydrogel (PeptiGelDesign Ltd.), in which they incorporated mammary epithelial cells, to construct 3D bioprinted scaffolds.[8] Another way to take advantage of thixotropy was explored by Highley *et al.* who used a thixotropic hydrogel as an ink and as a printing support. They developed two molecules derived from hyaluronic acid, and one is grafted with adamantane and the other with a cyclodextrine. By mixing the two of them, they form a self-healing hydrogel thanks to the guest-host interaction between the adamantane and the cyclodextrine. This hydrogel mixture can thus be extruded but it can also self-heal when a needle goes through it, which enabled the researchers to 3D print one hydrogel into the other one, as it can be seen on Figure III-4. By modifying the hyaluronic acid with methacrylates, they can also obtain a cross-linkable material that can then be extruded in another sacrificial hydrogel and retrieved by the dissolution of the non-cross-linked gel.[9]

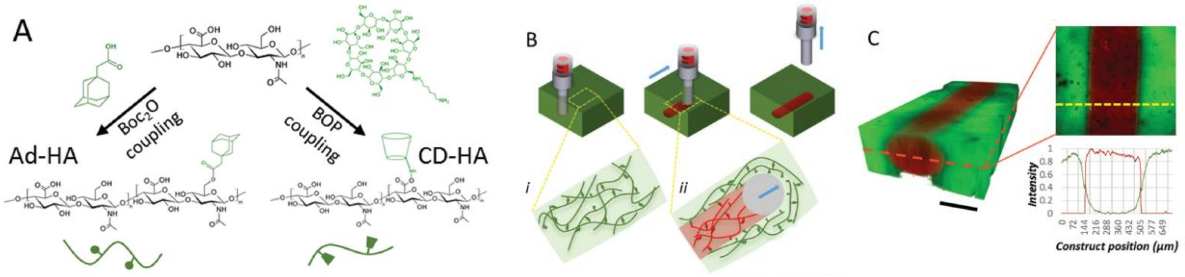

Figure III-4: "A) Conjugation of adamantane (Ad, guest) and β-cyclodextrin (CD, host) to hyaluronic acid (HA). B) Schematic illustration of the extrusion of a supramolecular ink (red) into a supramolecular support gel (green), where (i) the undisturbed network (ii) receives the printed ink. C) Left: 3D reconstruction of a confocal Z-stack of an ink filament (rhodamine- labeled, red) printed into a support gel (fluorescein-labeled, green). Right: Confocal cross-section and signal intensity profile, indicating no mixing of printed ink with support material. Scale bar: 200 µm." From [9].

In the case of non-thixotropic gelators, other strategies have to be employed since the gel is destroyed by the constraints imposed during extrusion. For instance, Yan *et al.* used a mixture of thiolated gelatin, a PA (peptide amphiphile, containing the IKVAV motif) and cells as a bioink that they could extrude to form 3D scaffolds. These ones can retain their shape after extrusion on the condition that the set-up is kept at 4 °C. In order to work with biological conditions, the scaffolds need to be cross-linked. They used a modified PEG as a cross-linker that reticulates the hydrogel network at 37 °C.[10] A type of hydrogels that is often used for 3D bioprinting applications is alginate. The method of gelation for alginate is very simple and can easily be adapted for 3D printing thanks to co-axial nozzles (see Figure III-2, B3). Aqueous alginate solutions are usually reticulated by a divalent cations such as with aqueous solutions of $CaCl_2$. A way to readily gel and print at the same time alginate is by dispensing simultaneously alginate and $CaCl_2$ solutions in a co-axial nozzle. This process can be applied to other hydrogels that can be gelled the same way. Lozano *et al.* for example used this method to 3D-bioprint a RGD-functionalized gellan gum (a microbial-derived polysaccharide) as brain-like structures (Figure III-5). Primary neuronal cells were mixed in the bioink and they used either a $CaCl_2$ solution or DMEM to cross-link the hydrogel. However, a further soaking to cross-link after printing was still necessary to ensure the good gelation of the material.[11]

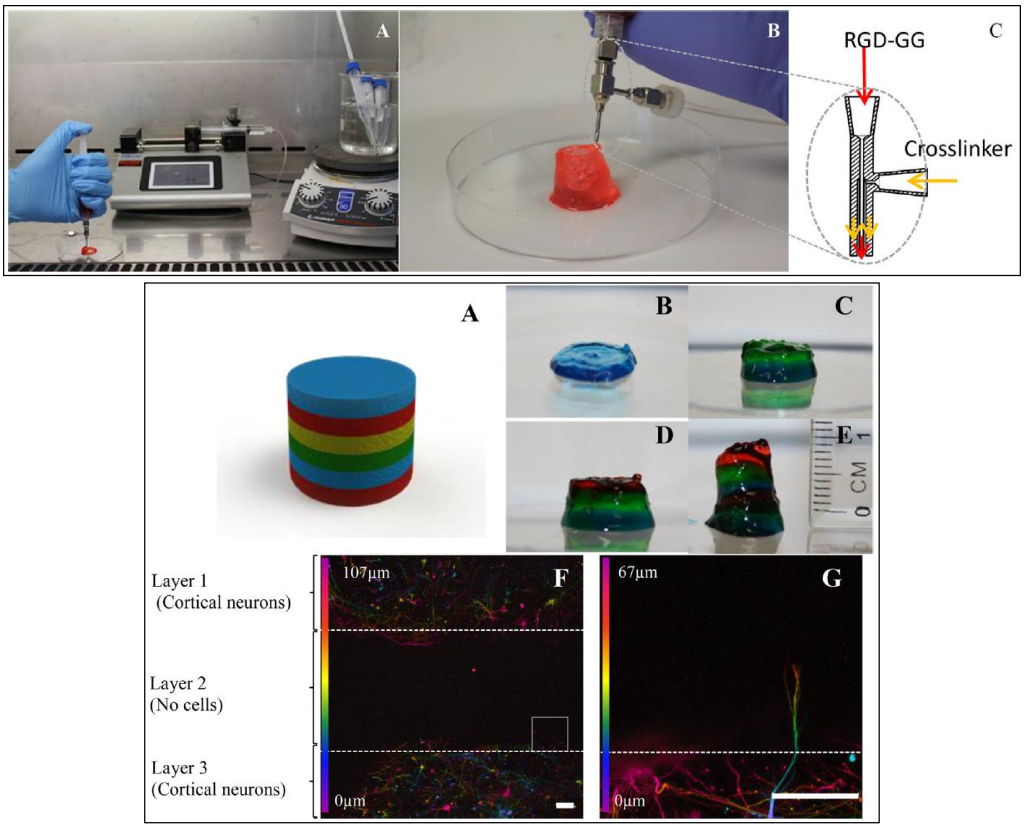

Figure III-5: Top: "Hand-held reactive bathless printing. A) Cell printing system inside a biosafety cabinet. B) 3D printed structure. B) Schematic diagram of the extrusion tip." Bottom: "Printed brain-like layered structure. A) Solidworks representation of proposed brain-like layer structure. B-E) Printing process to create a brain-like structure, each color represents a layer. F) Confocal microscope images of neurons in different layers after 5 days of culture. The image is colored for the distribution of the cells through the z-axis in the bio-ink RGD-GG gel as indicated. G) Expanded view of an area (…) showing an axon penetrating into the adjacent layer. Scale bars represent 100 µm." From [11].

This technique to shape hydrogel filaments by putting the gelator solution in contact with a cross-linker solution is actually often employed for 3D printing and bioprinting and has been recently reviewed by Constantini *et al.*[12] This type of gelation method in which a "polymer" solution is put in contact with a "coagulation" bath has been in fact well known since the beginning of the century and is called "wet spinning". In the next part, we are going to see the specificities of this process.

III.1.2 Wet spinning

III.1.2.1 Definition and principles

Wet spinning is a technic that has been known for decades and has been tremendously employed in the textile industry for the fabrication of viscose[13] or nylon[14], but also for the production of orientated DNA fibers for instance[15]. This type of process consists in dissolving a polymer into a good solvent and extruding it into a non-solvent (called "coagulation bath"), which triggers the precipitation of the polymer by counter diffusion. To obtain nice textile fibers, the resulting thread

is usually washed in various baths, stretched and dried before being retrieved on rollers, as represented on Figure III-6.

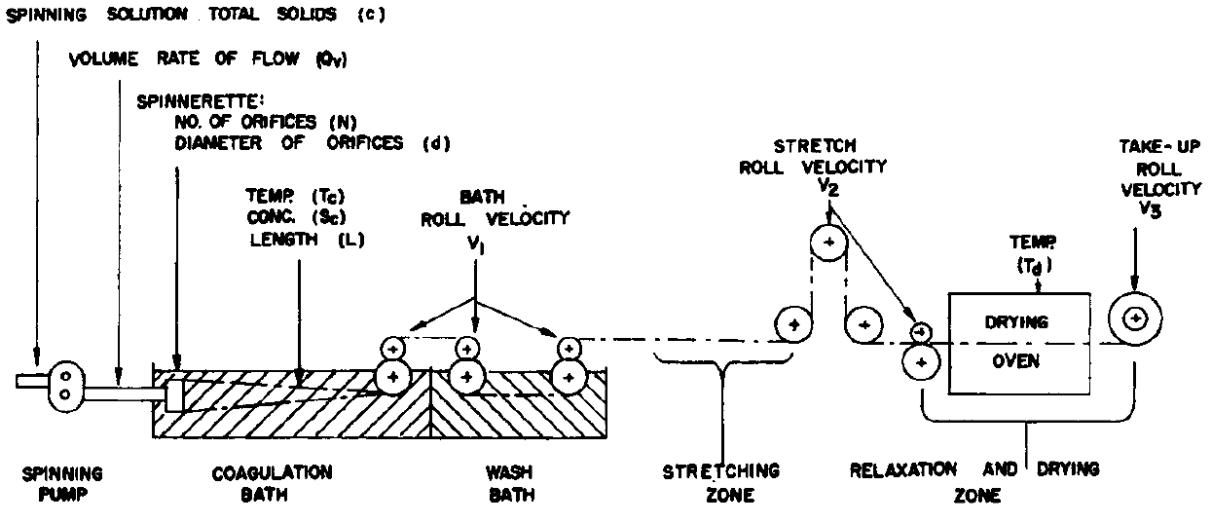

Figure III-6: Schematic of a typical wet spinning set up for the fabrication of modacrylic fibers. From [16].

This technique has mostly been employed with polymers at the beginning of its use, but within the past years, wet spinning has regained much interest because it can be applied with various new materials. It is a very good method for the shaping of fibers and many scientific fields became interested in this way of producing them, and especially in biomedical applications. As a matter of fact, a lot of biopolymers can be shaped with this method such as poly-L-lactic[17] acid or polycaprolactone derivatives[18] for instance.

As mentioned in the previous section, this method can also be applied to 3D printing. Puppi and Chiellini recently reviewed the 3D printing of biomedical polymers with the use of wet spinning.[19] Neves *et al.*, for instance, developed a process to 3D print poly-(ethylene oxide terephthalate)/poly-(butylene terephthalate) block copolymer scaffolds for culture of mesenchymal stem cells by wet spinning (Figure III-7). By varying the printing conditions, they were able to form different types of structures.[20]

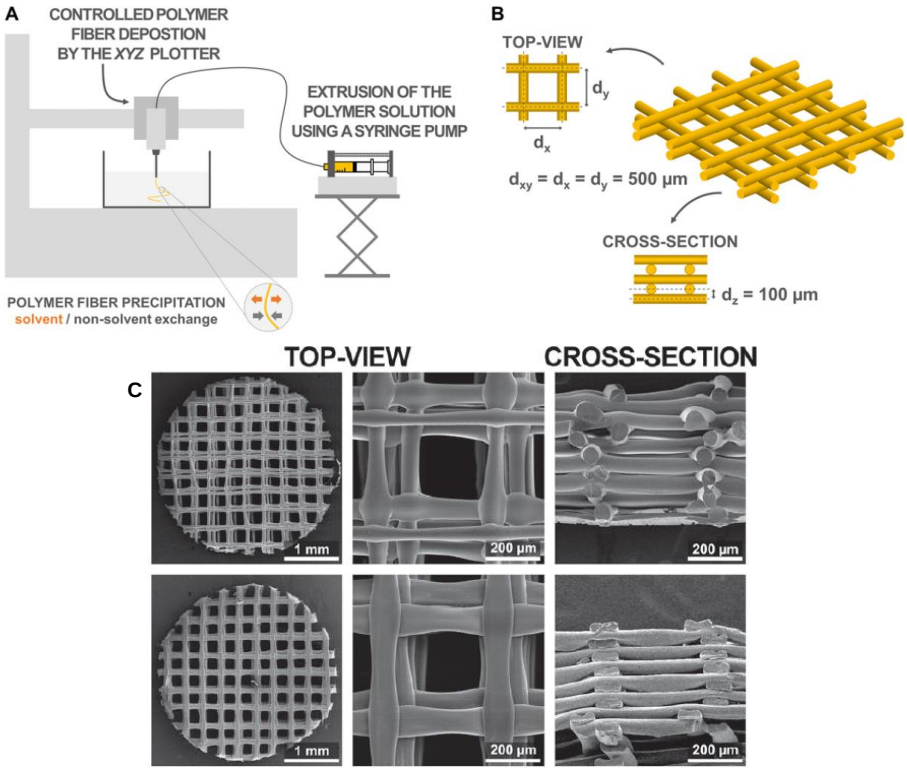

Figure III-7: A. Set-up developed by Neves et al. for the fabrication of polymeric scaffolds. B. Design used for the 3D scaffolds. C. Examples of SEM images of the printed scaffolds in different conditions. From [20].

Indeed, various parameters can influence the process:

- the dope concentration, i.e. the concentration of polymer (or gelator) in the solution that will be extruded
- the composition of the coagulation bath
- the temperature of the dope and/or of the bath
- the applied flow rate and syringe diameter for the extrusion of the dope
- the residence time into the coagulation bath
- etc.

These parameters can affect several structural characteristics of the wet spun fibers such as the porosity of the materials, its roughness, tensile strength, etc. Several studies tried to establish mathematical and physical models of the coagulation phenomena and the influence of the parameters on the wet spun materials' properties. For instance, in 1968, D. R. Paul tried to establish a model for the diffusion of solvents during the wet spinning of acrylic fibers. However, his conclusions were that none of his mathematical models were precise enough and that the counter diffusions of solvents in the case of wet spinning is an "extremely complex problem for fundamental treatment".[21] Later, A. Rende also did a theoretical study for a physicochemical model for counter-diffusion during wet spinning. A conclusion of his study is that the time of complete coagulation depends on the initial radius of the dope jet, on the temperature (which

affects the diffusion coefficients), on the bath composition and on phase equilibrium conditions. They did not include the flow of the dope in this study. The equation for the coagulation time is then:

$$t_C = \frac{1}{2}\rho_0^2 \frac{1}{D_2}\frac{\Delta c_2}{\Delta' c_2}$$

with t_c the coagulation time, ρ_0 the initial jet radius, D_2 the diffusion coefficient of the coagulant (here water) in the solvent (here DMSO or DMF, in which is dissolved polyacrylonitrile) and $\Delta c_2/\Delta' c_2$ a ratio characterizing the radial concentration gradient of water within the growing filament, related to the composition difference between the dope and the coagulation bath.[22] As a result, larger fibers and compounds with lower diffusion coefficients take more time to fully coagulate.

Other and more recent studies also tried to understand the effects of the spinning parameters on the structure and properties of wet spun polyacrylonitrile fibers. Dong *et al.* for instance took the case of a solution of polyacrylonitrile in DMSO wet spun into a DMSO/H_2O bath (the water triggers the precipitation of the polymer). [23] They tuned the bath composition, temperature and the stretching of the fibers during the process. They characterized the fibers' morphologies, their solvent contents and their crystallization. They found that the stretching of the fibers having an influence on their diameter, it also affects the diffusion rate into the fibers which then affects the solvent content into them. As expressed by Stokes-Einstein's law, the bath temperature also significantly affects the diffusion rates of the different solvents, and the hotter the bath, the faster the diffusion. What is also interesting in their study is that the addition of DMSO in the water coagulation bath help tuning the diffusion of both compounds. They also explain that because of the polymer pellicle that is formed throughout the process at the surface of the fiber, the diffusion of solvent is more and more muffled throughout the spinning. If the parameters are not controlled well enough, this can result in inhomogeneous fibers in terms of structure. Yi *et al.* studied the same system and they introduced a new variable that they called the coagulation ability, which is the product of the diffusivity of water and the one of DMSO (calculated according to Crank's equation) in the set conditions. They concluded that the lower the coagulation ability, the more homogeneous the fiber structure because the coagulation occurs slowly and uniformly. Moreover, the larger the difference of concentration in DMSO between the dope and the bath, the higher the diffusivity and the quicker the gelation.[24]

The influence of the parameters of wet spinning has thus been extensively studied for polymeric systems as in the case of fabrication of polyacrylonitrile fibers. However, these works can be

extrapolated to other systems such as hydrogels. In the next paragraph, we are going to see how wet spinning can also be applied to hydrogel systems.

III.1.2.2 Applications: wet spinning of hydrogels

Most of the hydrogels prepared by wet spinning are ones for which the gelation can be triggered by solvent exchange or ion exchange (see chapter I.1.1.2), because the process is particularly suited to this type of gelation. Several natural polysaccharides such as alginate, chitosan, gellan, etc. can be extruded this way. The preparation of alginate by wet spinning has actually been described back in 1944 by Speakman and Chamberlain.[25]

Wet spinning of polysaccharide hydrogels can be used for various applications such as drug-release[26], but mainly for biological applications since this kind of hydrogels is biocompatible. Yang *et al*. for instance managed to wet spin alginate fibers with tunable diameters with the help of a rotating collector. By tuning the rotation speed of the roller, the nascent alginate fiber is more or less extended, and its diameter can thus be tuned (from 20 µm to 600 µm). They managed to grow fibroblasts and neuronal cells on these alginate fibers.[27] In another paper, the same team succeeded in obtaining micro-grooved alginate fibers with the same set-up, and they played with the fluids' instability and shear stress to shape the surface of the fibers (Figure III-8). The osteosarcoma and neuronal cells they seeded on the hydrogels thus grew along the micro-grooves.[28]

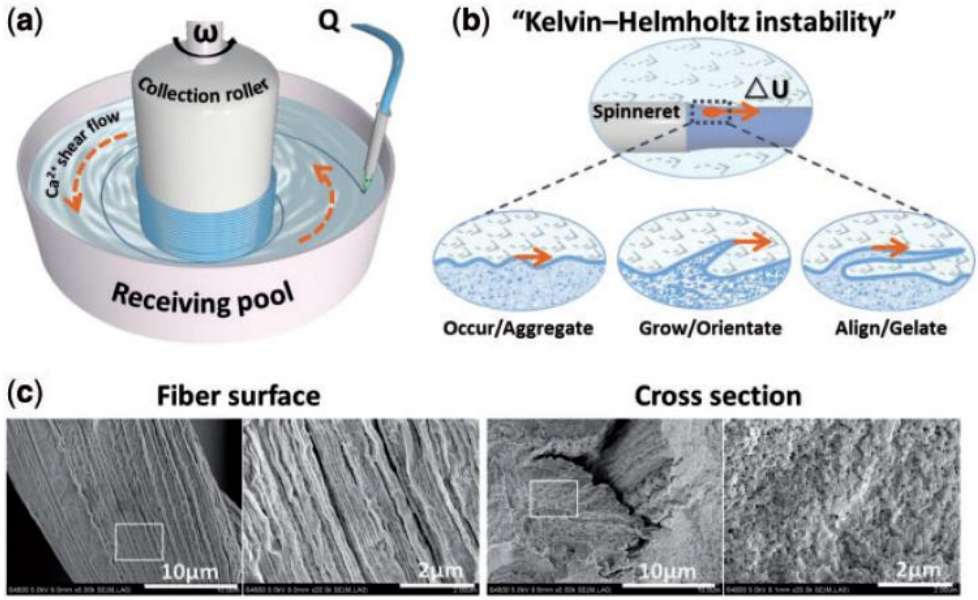

Figure III-8: a. Set-up developed by Yang et al. to wet spin alginate fibers: The alginate solution is extruded in the coagulation bath in which the collection roller is rotating. b. Schematic of the Kelvin-Helmholtz instability occurring at the surface of the alginate flow. c. SEM images of the wet spun alginate fibers with micro-grooved structures at their surface. From [28].

Cell encapsulation is also often employed with the wet spinning of polysaccharide hydrogels. Lin *et al.* for instance wet spun alginate containing gelatin particles in order to create a microporous material after dissolving the gelatin. They encapsulated primary dorsal root ganglia cells in their scaffolds by mixing them with the alginate/gelatin solution.[29]

Still in this field, another technology that is more and more developed is the use of microfluidic devices to control precisely the wet spinning conditions.[30,31] Kiriya *et al.* for instance used microfluidic channels to encapsulate supramolecular fibers of a small organic molecule into sodium alginate hydrogel.[32] Of course, with this process, living cells can be encapsulated into hydrogels as well. Ghorbanian *et al.* did it with human embryonic kidney cells into alginate thanks to their "microfluidic direct writer" set-up (Figure III-9). What is interesting with their microfluidic system is that they developed a system to prevent the clogging inside the chip by adding a channel where EDTA can flow and dissolve the clogs.[33]

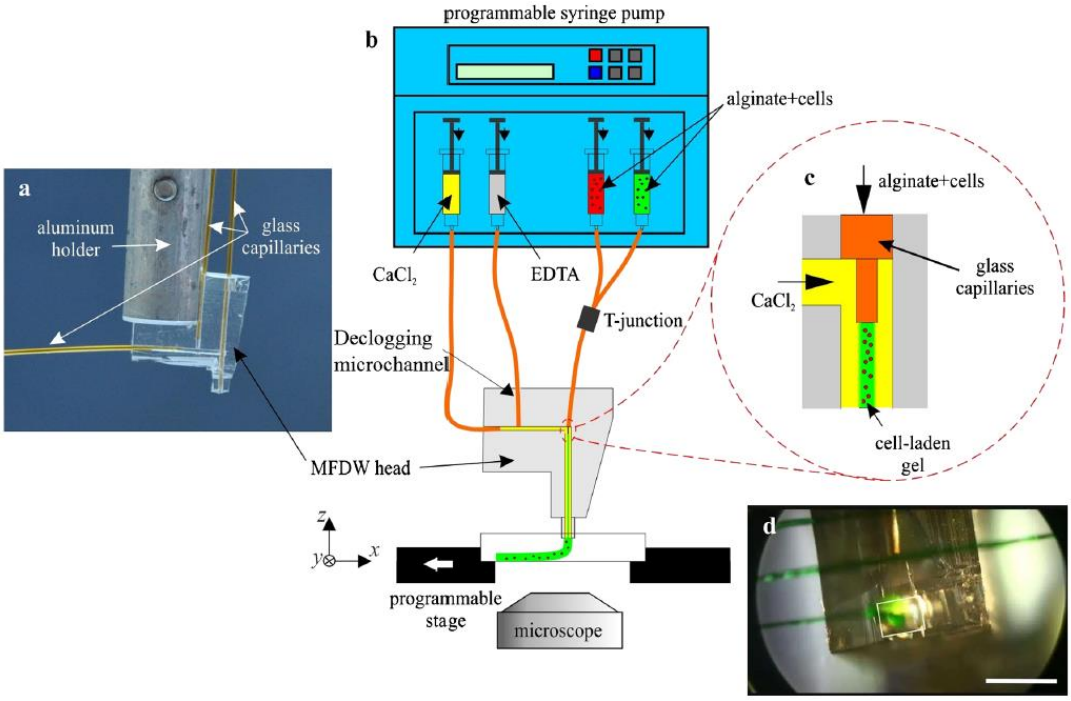

Figure III-9: The "microfluidic direct writer" developed by Ghorbanian et al. to encapsulate cells into alginate and control the deposition of the fibers. From [33].

Lee *et al.* also developed a microfluidic system to encapsulate liver cells inside a mixed hydrogel of alginate and chitosan.[34] Yamada *et al.* used microfluidic chips to create anisotropic hydrogel fibers for the encapsulation of various types of cells (Figure III-10). By adding propylene glycol alginate in the side flows, they were able to produce stiffer alginate, resulting in a "sandwich-like" structure guiding the growth of the cells encapsulated in the central gel.[35]

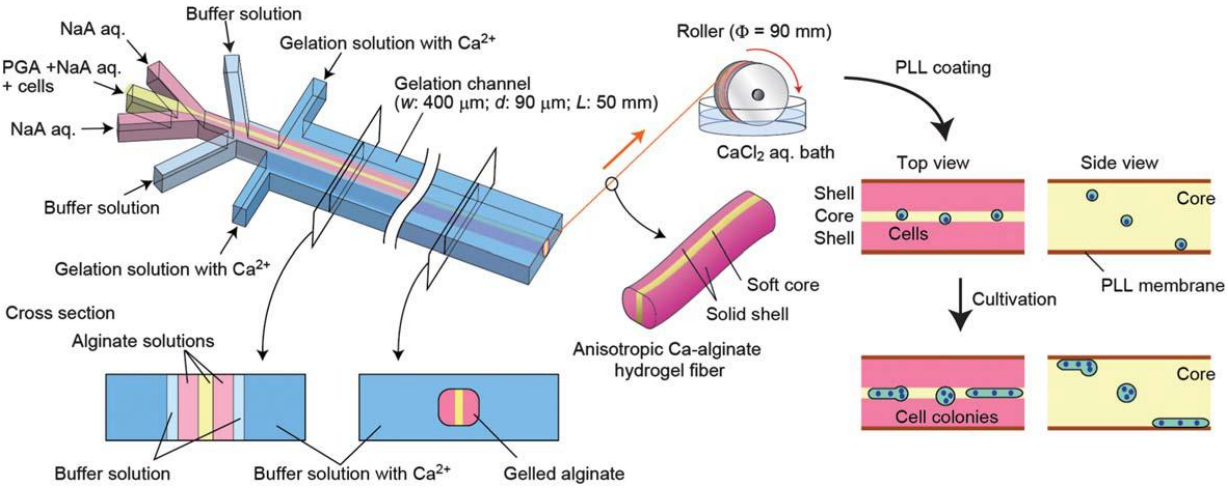

Figure III-10: Schematic of the microfluidic wet spinning process developed by Yamada et al. for the fabrication of anisotropic hydrogel fibers (NaA = sodium alginate, PGA = propylene glycol alginate). From [35].

Onoe *et al.* also used a microfluidic device for the wet spinning of alginate hydrogels, but this time to create core-shell structures with the cells inside a hollow fiber. This core-shell way of spinning hydrogels with encapsulated cells is particularly interesting for tissue engineering in the case of blood vessels.[36]

The wet spinning technique was thus very well developed with polysaccharide hydrogels. However, this type of gelators is not the most interesting for tissue engineering because, despite their good biocompatibility, cell adhesion and spreading are very limited in these scaffolds. This is why most of the cells cultured on or in alginate or chitosan remain rather round throughout their growth. This can alter their further differentiation. Yet, apart from polysaccharides, very few types of hydrogels are studied with the wet spinning process, and to our knowledge, no LMWG were wet spun yet in literature. The next step is thus to find better suited biomaterials that can be used with this shaping method.

III.1.3 Objectives – Fiber alignment in the hydrogels

Our objective in this last part of the project was thus to try to apply the wet spinning and 3D printing techniques to our LMWGs. Indeed, very few studies have used this type of hydrogels to shape and build scaffolds. Instead, most of them use polymer hydrogels such as alginate. The only LMWG described for 3D printing applications are Fmoc-diphenylalamine[7] and some peptide hydrogels[8,37]. With the wet spinning technique, to our knowledge no work has been performed on small organic molecules. However, with the use of another spinning technique, tannic acid has been shaped into fibers thanks to electro-spinning, even if this process too is mostly employed with polymers.[38] It would be very interesting to try to shape our alkylgalactonamide hydrogels with wet spinning or 3D printing to create well-defined biocompatible scaffolds out of them.

Another objective of this project was to induce the alignment of the hydrogel's fibers during gelation. As already mentioned in the previous chapter (see II.1.2.2), in the case of materials for the growth of neurons, the alignment of the axons throughout their growth in the scaffold is very interesting because it mimics the architecture of some parts of the brain like the cortex. Moreover, it may help obtaining a convenient tissue reconstruction. This is why many studies report the development of anisotropic scaffolds (hydrogels or not) for the growth of neurons.

The previous chapter (II.1.2.2) already reported the use of micro-grooved PDMS substrates[39,40], electro-spun collagen/silk composite[41] or magnet-induced aligned electro-spun scaffolds[42] for the growth and alignment of neuronal cells. Fiber alignment in hydrogels can also be achieved by mechanical techniques, such as the one described by Stupp's research team already reported in the first chapter (see I.1.2.1). In this tudy, they annealed a peptide solution and then extrude it during its gelation to obtain aligned nanofibers in the hydrogel.[43] Mechanical alignment was also achieved by Antman-Passig *et al.* who simply applied a controlled uniaxial strain on their collagen hydrogels after gelation with the neuronal cells encapsulated inside.[44] Numata *et al.* also induced the alignment of supramolecular nanofibers inside polysaccharide strands thanks to shear stress in a microfluidic device. By tuning the polysaccharide concentration and the flow rate applied in the device, they were able to obtain more or less aligned nanofibers inside (Figure III-11).[45]

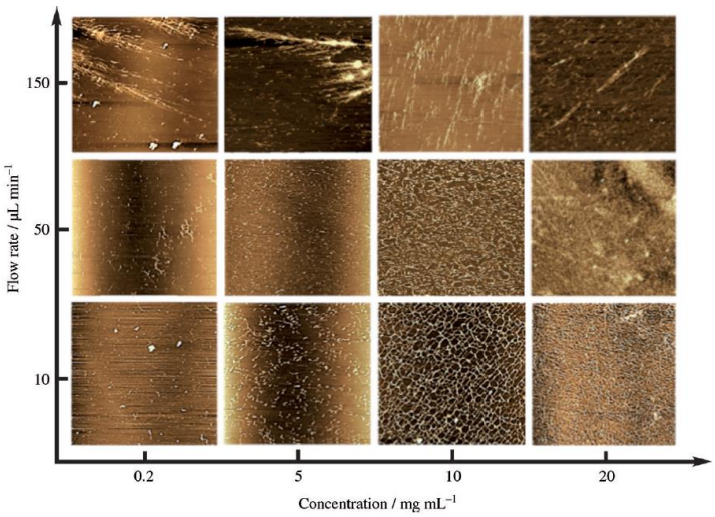

Figure III-11: AFM images of the self-assembled nanofibers inside schizophyllan strands obtained when tuning the polymer concentration and the flow rate (5 µm x 5 µm images). From [45].

Various techniques thus exist in order to align the fibers of a hydrogel, whether by shear stress, elongation, magnetic field, etc. Alignment, both at the microscopic or at the macroscopic levels, is interesting for guiding growing cells, and more especially for neurites and axons of neurons. Thus, in our work, we tested different strategies among those described above to align the fibers in our hydrogels or to shape them in order to obtain anisotropic scaffolds for the growth of neurons. Those strategies are described in the next part.

III.2 Shaping and fiber alignment of the alkylgalactonamide hydrogels and other families

In this part, we are going to describe the work that has been done in order:

1. to try to align the fibers inside the hydrogel, this with the hope to further guide the neurite outgrowth inside the scaffold,
2. to shape the hydrogel with the aim of 3D printing it to design specific scaffolds adapted to their application.

The simplest method for the first objective would be the extrusion of the hydrogel because the flow and mechanical strains applied in this case are anisotropic. This can help obtain anisotropic materials too. Unfortunately, direct extrusion of the alkylgalactonamide family was impossible because of the strong synaeresis of the hydrogels when submitted to mechanical stress (see chapter I.2.1.1), synaeresis is the irreversible separation of water from the hydrogel fibers when a strain is applied). Other compounds had to be used. For the second objective, we demonstrate a novel method based on solvent exchange to extrude and form filaments[d] out of the Gal-C7 gelator.

III.2.1 Extrusion tests

III.2.1.1 Gelation under a strain

The first trials that have been made to attempt to align the fibers inside the alkylgalactonamide hydrogels were by their gelation (induced by cooling) under a flow. The idea is that if the fibers form under a shear strain, they will grow following the direction of the flow, and this will result in their alignment in the hydrogel. For this, we used the Gal-C6 gelator for it was the one with the lowest gelation temperature (around 38 °C). The hot gelator solution was pushed inside a tube plunged into a water bath at 95 °C in order to progressively cool down the solution after exiting the hot bath, resulting into its gelation. One of the used set-ups is represented on Figure III-12.

[d] N.B.: In this whole chapter, the distinction will be made between the term “filament” (or sometimes “rope”) which refers to the gels that are obtained by the wet spinning technique, and the term “fiber” that refers to the microscopic self-assembled structures composing the hydrogels.

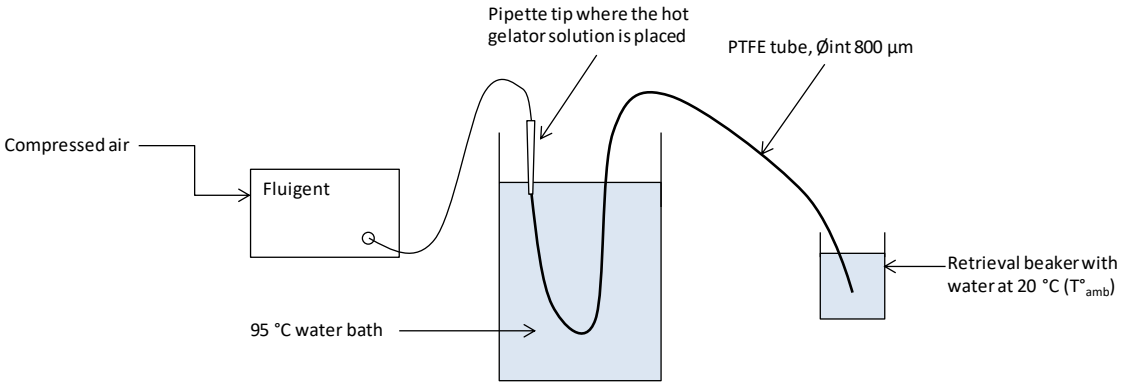

Figure III-12: Example of a set-up used for the gelation under strain of the Gal-C6 hydrogel.

Several trials were made, with different tube diameters and lengths, different pressures applied, but none of these allowed to obtain a hydrogel at the end of the tube. Actually, only synaeresis occurred: at first, some water got out of the tube but it then rapidly clogged. These poor results are likely due to contradictory constraints in order to obtain a gel: the gelling solution should be liquid enough to flow out of the tube, but it needs to be already almost gelled in order to keep its integrity while going out of the tube. Controlling both these parameters at the same time is particularly tricky.

Other trials have been made with PDMS microfluidic chips. Hot Gal-C6 and Gal-C7 solutions were injected at different flow rates in a channel through the inlet. The gelation then occurred in the chip. Compared to the previous method, no clogs were obtained with this one. This can probably be explained by the fact that the dimensions of the channels (2×0.4×50 mm) were bigger than the one of the PTFE tubes. There was also a time gap between the extrusion and the gelation. No fiber alignment was observed with this technique, only nucleation points (Figure III-13). This result might be explained by the fact that the channels in those chips were rather wide (2 mm), with a low height (400 µm). Perhaps there was an alignment of the fibers observable in the height of the channel, but this one could not be observed by simple microscopic observation. Chips with thinner channels could have been used to observe a potential fiber alignment in the width.

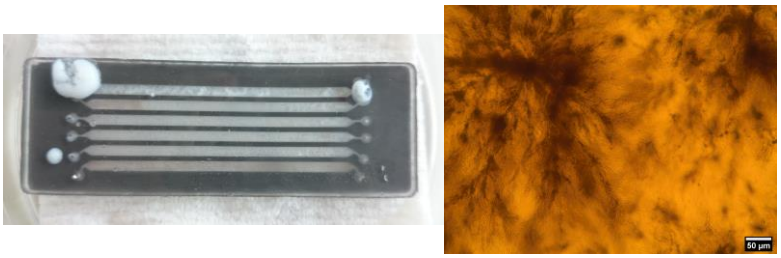

Figure III-13: Left: PDMS chip used for the gelation under extrusion of Gal-C6 and Gal-C7 hydrogels. The six channels are identical and their dimensions are 50×2×0,4 mm (length × width × height). Right: microscopic observation of a 1 wt % Gal-C6 hydrogel gelled in one of the channels at a flow rate of 30 µl/s (scale bar: 50 µm).

Because of the poor results obtained with this method, these experiments were no longer investigated and other techniques had to be found.

III.2.1.2 Gel extrusions

To circumvent the synaeresis effect and be able to extrude hydrogels, other gelators from other families were used: Gluca-C12 from the glucamine family (see I.2.1.2) and the Jap-C16 molecule, synthesized according to Watanabe's protocol and already mentioned in the previous chapter (see II.2.4).

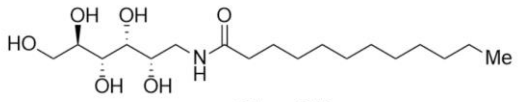

Gluca-C12

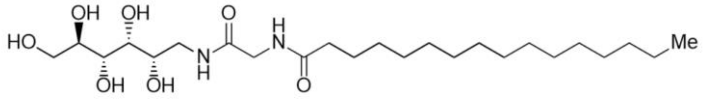

Jap-C16

Scheme III-1: Chemical structures of Gluca-C12 and Jap-C16 that were studied for extrusion tests.

The hydrogels resulting from these molecules have the property to not undergo synaeresis when submitted to a strain. On the contrary, they have been described as to be able to recover their initial organization once the strain stops. This phenomenon is called "thixotropy".

To proceed to their extrusion, the gelator solutions (2 wt % for Gluca-C12 and 1 wt % for Jap-C16) were prepared by heating the solid at high temperature in water and the hot solution was drawn in a syringe. The latter with the solution was let to cool down to room temperature, resulting in the formation of the hydrogel directly into the syringe. It must be noted that, contrary to what was described in the first chapter (see I.2.1.2), Gluca-C12 was prepared without the use of HFP (used to obtain a more stable and homogeneous hydrogel) since here the hydrogel's homogeneity would anyway be broken through extrusion.

The hydrogels were then extruded thanks to a syringe pump, at various flow rates and with various needle sizes. During extrusion, a certain quantity of water was expelled from the fibers constituting the gels: synaeresis still occurred. For comparison, Gal-C7 and Gal-C6 hydrogels have been prepared in the same conditions and extruded too: only water came out of the syringe, all of the gel fibers concentrated before the needle constriction without coming out of it. On the contrary, with Gluca-C12 and Jap-C16, a hydrogel came out of the needle, even though it was surrounded by a significant amount of water (Figure III-14). The diameters of the resulting hydrogel deposits were very heterogeneous along their length. This is due to the fact that

extrusion is rather irregular: sometimes the gel seems to accumulate in the needle and then everything comes out of it at once.

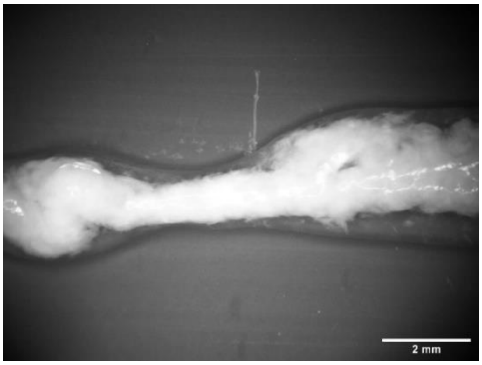

Figure III-14: Example of the extrusion of a Jap-C16 hydrogel with a 18G needle and at a flow rate of 6000 µl/min.

At the microscopic scale, the hydrogels' fibers could be observed by optical microscopy, especially for Jap-C16. The strain during the extrusion seemed to have an influence on the fibers' orientation, but not along the fiber's direction, as it can be seen on Figure III-15. As a matter of fact, the fibers look more like they have been (at least partially) packed perpendicularly to the extrusion. They were formed before extrusion and if the gel flows as one block, this one compresses them in this direction. However, if the gel flowed with a liquid-like behavior, the center of the fluid would go faster and induce an alignment in the flow direction because of the shear stress. With the resulting observations, it is not very clear how the gel behaves and how the fibers align in it under the stain.

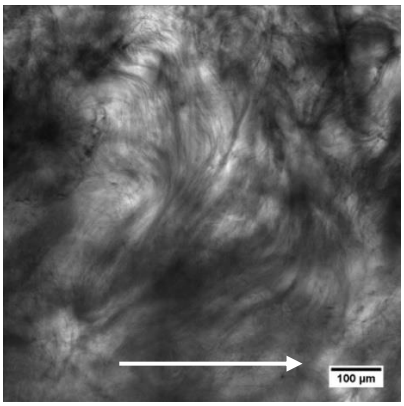

Figure III-15: Optical microscopy observation of a Jap-C16 hydrogel extruded at 6000 µl/min with a 18G needle. The direction of the extrusion is represented by the arrow.

Several conditions of extrusion have been explored with the different hydrogels: different flow rates, gel concentrations, extrusion techniques (needle, capillaries, pipette cones, syringe pump or pressure controller), etc. Yet, no ideal condition was found to align the fibers in the desired direction (along the extrusion direction), and the gel extrusion was still imperfect: the deposits were very heterogeneous, did not form a continuous well-shaped gel and a lot of water was still expelled.

We also found out that depending on the initial heating of the gel in the case of Jap-C16, different hydrogel morphologies could be obtained. To liquefy the gel in order to suck up the solution, the gel had to be heated, but the solution displayed two different stages: first, the hydrogel became liquid but the solution remained white, then, when the solution was further heated, it became transparent. According to the state of the solution when this one was drawn in the syringe, two different states of hydrogel could be distinguished. For better observation, the fibers of the extruded gels were stained with FITC-labelled poly-L-lysine. If the white solution was gelled in the syringe and extruded, a lot of fibers could be observed. However, in the case of the colorless solution, a rather granular and fiber-less hydrogel was obtained (Figure III-16). It was compared to a gel coming from a colorless solution that did not undergo aspiration or extrusion: fibers could also be observed in this one.

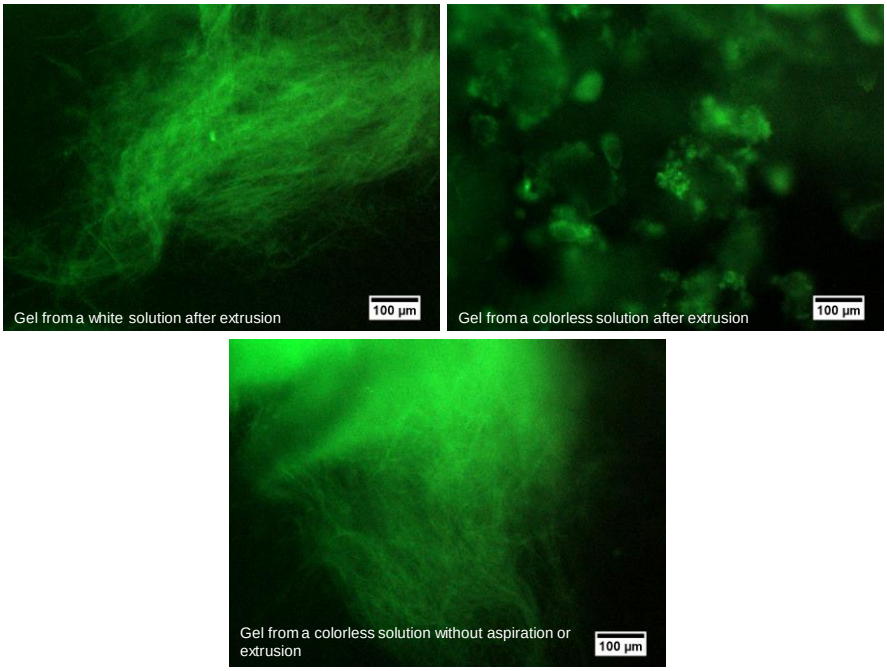

Figure III-16: Fluorescence microscopy observations of 1 wt % Jap-C16 hydrogels obtained from different states of the gelator solution, before or after extrusion. The gel fibers have been stained with FITC-PLL.

This is probably explained by the fact that, if the gelator solution is not heated enough, some fibers remain intact in it. These remnants can then constitute starting points for the self-assembly of the gelator molecules once the temperature decreases, resulting in long fibers. On the contrary, if the solution is heated enough, all the fibers are dissolved. When this solution is drawn in the syringe, the gelation has already started (because of the difference of temperature between the solution and the syringe) and this first extrusion might alter the self-assembly of the gelator molecules. One way to verify this hypothesis would be to use a heated syringe to sample the hot gelator solution and see if a different self-assembly occurs too.

However, no further results were obtained with this extrusion technique for the gelation conditions (temperature, self-assembly) are rather complicated to control. The fiber alignment in the hydrogels was not very efficient either. Moreover, the main purpose of this work was to shape the alkylgalactonamide hydrogels, which is not possible with this method. Yet, the results with the Gluca-C12 and Jap-C16 hydrogels were somehow promising, and if an improvement of the extrusion conditions is done, it can result in an interesting procedure. In addition, as previously seen in part II.2.4, these gels showed promising biocompatibility results. We then chose to develop a technique suited for the case of alkylgalactonamide hydrogels.

III.2.2 Wet spinning of Gal-C7 hydrogels

As previously seen, the direct extrusion of alkylgalactonamide hydrogels is impossible because of synaeresis. Another method has thus been developed in order to extrude and form a hydrogel at the same time, and this at room temperature without any heating of the gelator solution. This technique – wet spinning – was described in part III.1.2, and it relies on solvent exchange and counter diffusion of two miscible solvents. Instead of being dissolved in water at high temperature, the gelator is now dissolved in an organic solvent and this solution is then extruded into a coagulation bath (constituted of another solvent), which induces the gelation. When in a "good solvent", the gelator molecules are dissolved and in a stable state, but when they encounter a "bad solvent", these ones self-assemble (almost precipitate) and form a gel. When this happens under a flow, it results in the formation of a hydrogel filament (Figure III-17).

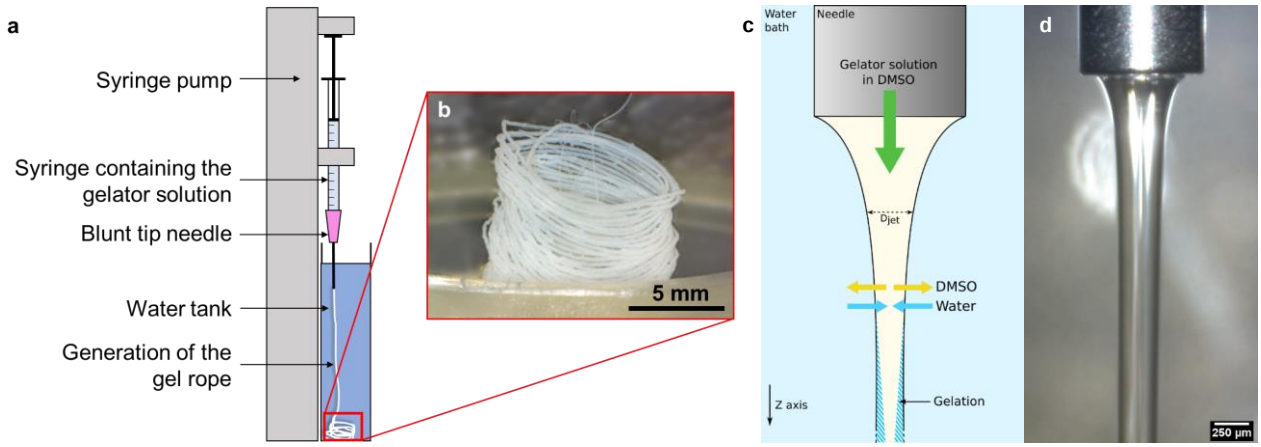

Figure III-17: Hydrogel wet spinning. a. Scheme describing the experimental setup used for the generation of a continuous gel rope. b. Coiled rope obtained after the extrusion of a 4 wt % Gal-C7 solution in DMSO at 50 µl/min with a 20G needle (ID 600 µm). c. Principle of the wet-spinning technique: the gelator solution in DMSO is extruded through the syringe and a counter-diffusion between DMSO and water occurs, resulting in the progressive gelation of the jet. d. Observation of the DMSO jet after the needle with a 30 µl/min flow.

In our case, we chose only to work with the Gal-C7 gelator because of its good results in cell culture trials. For the coagulation bath, distilled water at room temperature was used. The solvent chosen

to dissolve the gelator was DMSO because it is one of the scarce good solvents for the molecule. It is also denser than water and thus forms a jet falling down into the bath, resulting in the gel shaped as a filament. Moreover, in the case of cell culture trials, it could be the most tolerable solvent for the cells since at low concentrations (below 10 % in volume) it is considered as non-toxic. In addition, since this solvent is miscible with water, it can be easily rinsed from the filaments with several washes.

As previously mentioned, this wet spinning technique relies on solvent exchange and counter-diffusion. When water diffuses inside the DMSO jet, the gelator molecules self-assemble because of the change in solubility and thus form supramolecular fibers, themselves forming the hydrogel. At the same time, DMSO diffuses out of the jet (Figure III-17c). A dedicated set-up has been built and used throughout this study. It consisted of a syringe containing the gelator solution in DMSO adapted on a syringe pump. The needles used were blunt-tip needles of different gauges (controlling the inner diameter of the initial jet) and the tip was immersed in the coagulation bath, resulting in a fall of approximately 8 cm for the jet (Figure III-17a). Figure III-17b shows a hydrogel rope obtained by this technique.

III.2.2.1 Determination of the conditions leading to the formation of a filament: establishment of the phase diagrams

In order to determine the most suited conditions to obtain Gal-C7 filaments, but also to check the robustness of the process, phase diagrams were established by setting different chosen parameters: the applied flow rate, the solution concentration of Gal-C7 and the needle gauge. The bath temperature was kept constant at 22 °C (room temperature). The flow rates applied by the syringe pump varied from 0.5 to 200 µl/min, the solution concentrations from 1.25 to 5 wt % and the needle inner diameters (ID) from 160 to 600 µm (30G to 20G). The phase diagrams were then based on simple visual observations and five regimes were identified (the colors correspond to the ones on Figure III-18):

i) the gel forms a clog directly after exiting the needle (red)
ii) a filament is formed but the needle is clogged after a few seconds (pink)
iii) a stable filament is obtained (violet)
iv) the gelation occurs but rather low in the bath (blue)
v) the gelation does not occur before reaching the bottom of the bath and no filament is formed (cyan)

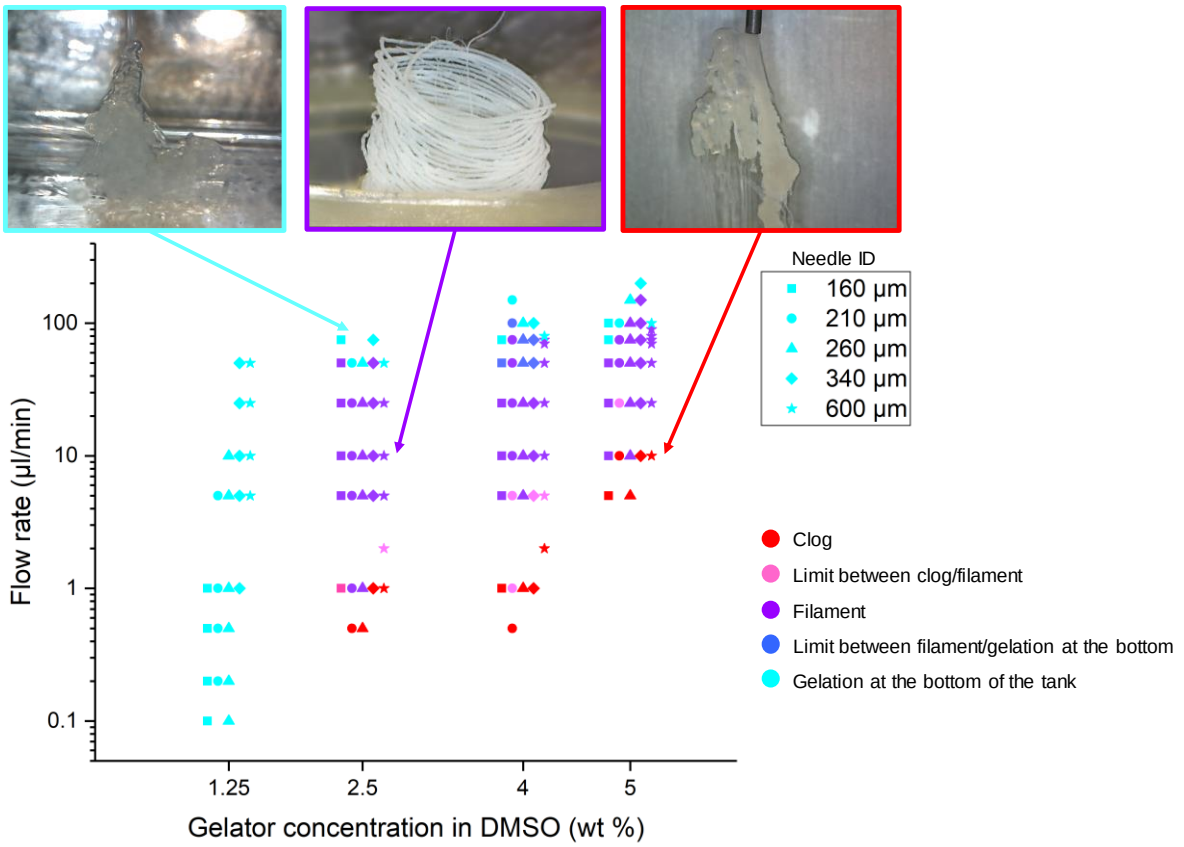

Figure III-18: Phase diagrams for the generation of a gel rope with different needle inner diameters (ID). On the X-axis is represented the different concentrations of the gelator solution in DMSO and on the Y-axis is the applied flow rates (logarithmic scale). The general aspect of these diagrams remains similar whichever the needle ID. On top are displayed photos of the different states of the gel: (from left to right) either the gelation occurs at the bottom of the tank, or the gel forms a filament, or a clog is formed at the exit of the needle.

The obtained phase diagrams are represented on Figure III-18 (the points for the gelator concentrations have been shifted for more clarity). What can be understood from these diagrams is that, for a given concentration, a clog tends to form at the exit of the needle at low flow rates. On the contrary, when the flow rate is too high the solution does not have time to gel before reaching the bottom of the bath. The formation of a filament of gel thus occurs in-between those two states. Indeed, the diffusion of water into the DMSO jet triggers the gelation, and diffusion is here in competition with the speed of the jet. To form a nice filament there needs to be an equilibrium between the diffusion rates and the velocity of the DMSO in the bath.

Now, concerning the influence of the solution concentration, if this one is too diluted, no cohesive network can be formed to obtain a homogeneous filament throughout the fall. As a matter of fact, a condition in which the solution at 1.25 wt % would form a filament could not be found. When the gelator solution gets more concentrated, the range of flow rates in which a filament can be obtained is reduced. The gelation occurs more rapidly, and higher flow rates are needed to avoid the formation of a clog.

Concerning the needle diameter, surprisingly, this parameter does seem to influence much the limits' position of the diagram.

III.2.2.2 Physical characterization of the spinning process

We then wanted to better understand the influence of the parameters on the gelation during the spinning of Gal-C7 hydrogels, but also to predict the dimensions of the hydrogel structures. For this purpose, we have characterized the fluid velocity in the jet and we have driven systematic measurements of the diameters of the DMSO jet and of the resulting filaments.

III.2.2.2.1 Jet velocity

First, we wanted to measure the speed of the DMSO jet after exiting the needle. From a pragmatic point of view, this piece of information is crucial for the potential application to 3D printing, since the printing speed has to be in accordance with the extrusion velocity. However, this data cannot be simply calculated with the needle section and the flow rate because of the composition of the jet that is changing along the fall in the bath, due to solvent exchange. To measure the jet velocity, 15 µm fluorescent polystyrene beads were incorporated in the gelator solution and the extrusion was observed with a microscope camera suited for fluorescence observations. The beads were big enough to be easily observed with the camera, and diluted enough so that they did not disrupt the flow. Only low flow rates were analyzed in order to be able to clearly see the beads while flowing. 5 and 10 µl/min have been tested with a 20G needle and a 2.5 wt % gelator solution containing the beads. The jet diameter along the Z axis has been measured thanks to superimposed images of the fluorescent beads, such as the one represented on Figure III-19f.

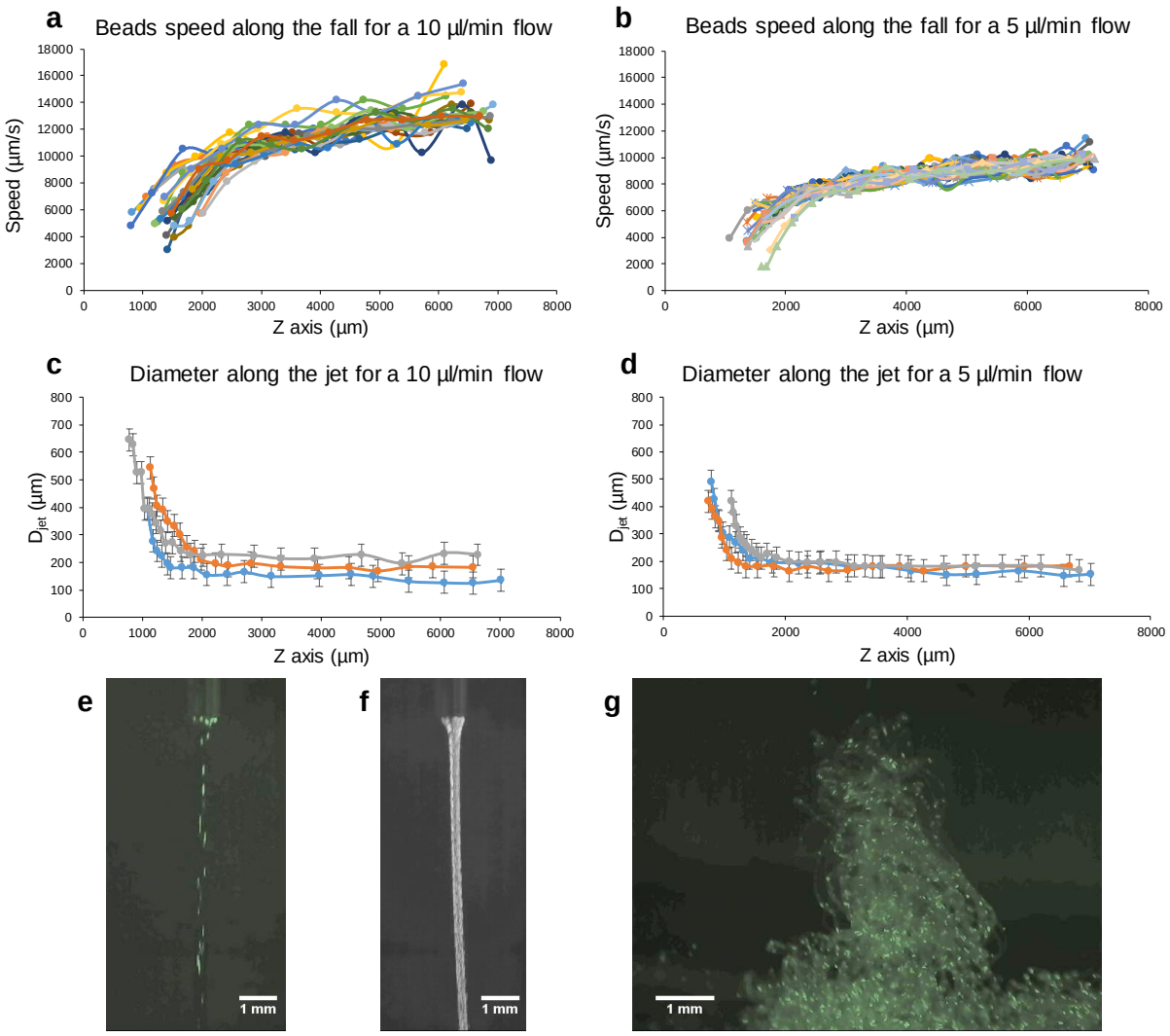

Figure III-19: Speed analysis of the flow during the extrusion of the 2.5 wt % gelator solution. a and b. Speed of the fluorescent beads along their fall at 10 and 5 µl/min (the origin of the Z axis is the end of the needle). The speed was analyzed manually for different beads throughout the acquisition (typical image shown on e.), the several curves represent the beads analyzed. c and d. Measurement of the diameters along the jet for flow rates of 10 and 5 µl/min. The diameters were measured on the same acquisitions than for the speed, the different frames were superimposed, resulting in the fluorescent beads forming a homogeneous jet (f). Three different superimpositions at different times were used, hence the three curves. The error on the diameters was estimated to 40 µm (the size of two pixels on the pictures). g. Gel rope containing the fluorescent beads obtained after these experiments, here with a 10 µl/min flow rate.

What can be seen on Figure III-19 is that the velocity of the beads is consistent with the shape of the DMSO jet since it increases as the diameter of the jet decreases in both cases. This thinning of the jet is actually due to gravity that pulls on the DMSO jet, making it have this hyperbolic shape at the exit of the needle. After a few millimeters, jet velocity is quasi constant as well as jet diameter, probably due to a balance between gravity forces and viscous friction that establishes between the jet and the resting solution surrounding it.

A first approximation of the theoretical velocity of the jet has been calculated without considering the change in its composition through the fall, thanks to the formula $v = \frac{Q}{S}$ (with v the speed, Q the flow rate and S the jet section). For this, the diameters used in the calculation to get the section

of the jet were the ones measured on the plateaus of the graphs from Figure III-19c and d. These results are reported in Table III-1.

Table III-1: Measured velocities and diameters of the DMSO jet compared to the corresponding predicted velocities calculated. The measured jet velocity is the mean of the mean velocities of all the analyzed beads ± the associated standard deviation. The error on the predicted jet velocity was calculated with the errors on the flow rate and on the measured jet diameters (estimated to 40 µm).

Flow rate	**5 µl/min**			**10 µl/min**		
Replicate n°	**1**	**2**	**3**	**1**	**2**	**3**
Measured jet diameter (mm)	0.168	0.176	0.185	0.146	0.184	0.222
Measured jet velocity (mm/s)	8.6 ± 0.5	8.3 ± 0.5	8.1 ± 0.4	10.5 ± 0.4	10.4 ± 0.5	11.1 ± 0.8
Predicted jet velocity (mm/s)	3.8 ± 0.9	3.4 ± 0.8	3.1 ± 0.7	10 ± 3	6 ± 1	4.3 ± 0.8

These computed velocities are rather different from the ones measured. There are big discrepancies between the two speeds since most of the time, the measured velocities are more than twice the value of the predicted ones. It can come from the fact that the counter-diffusions of water and DMSO cannot be neglected in the calculation. But this can also be explained by some measurement bias: the jet diameter can be overestimated because of the fluorescent beads for instance. Despite the difference between the measured and predicted velocities, they are in the same order of magnitude.

III.2.2.2.2 Analyses of the jet and filament diameters

Still to characterize the wet spinning of Gal-C7 hydrogels, we became interested in the relationship between the set conditions and the resulting diameters of the DMSO jet and of the final filament. To do so, the diameter of the DMSO jet and the one of the obtained filament were measured under various conditions. The main influence we wanted to evaluate was the one of the flow rate. Two needle gauges were also used: 20G (ID of 600 µm) and 27G (ID of 210 µm). Two solution concentrations were used as well, but this was more related to the shape of the phase diagram (Figure III-18). Indeed, at low flow rates, only the less concentrated solution forms a filament and at higher flow rates, a more concentrated one is needed. For each condition, the filament diameter was measured by optical microscopy, as well as the jet diameter at 2.3 mm after the needle (maximum distance on the acquired images) thanks to a microscope camera. The results are reported on Figure III-20.

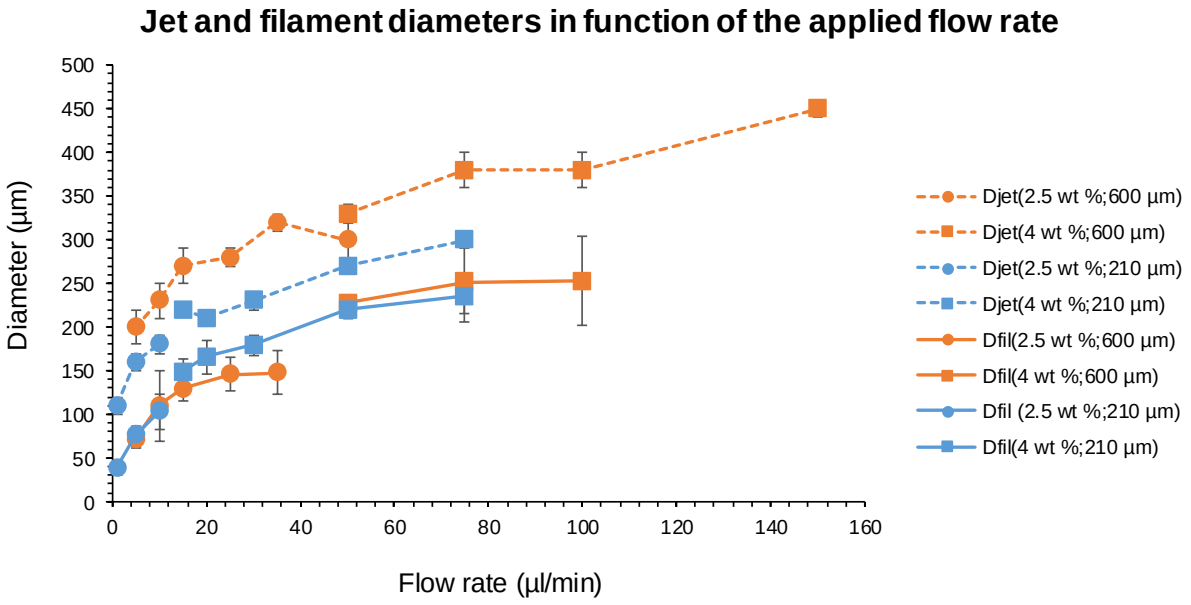

Figure III-20: Jet and filament diameters measurements. The jet (2.3 mm after the needle) and the resulting filament diameters were measured for different flow rates and for different needle ID. For lower flow rates, a 2.5 wt % gelator solution had to be employed and for higher flow rates, a 4 wt % one.

The first thing to notice is that, the higher the flow rate, the wider the diameters. Moreover, the resulting filament diameter is much smaller than the one of the jet after the needle. The needle gauge does not seem to have a significant influence on the filament diameter, even if it influences the one of the jet. Actually, the jet diameter is measured very close to the needle exit (2.3 mm after, whereas the total fall height is of 80 mm) and at this distance, it is mainly set by the needle size. With the jet thinning along its fall in the bath, it is normal to obtain a filament diameter much reduced. However, the fact that their sizes are very similar for both needles is less obvious. What is also noticeable is that the solution concentration does not seem to influence much the diameter of the jet since the curves are almost superimposed. The filament and jet diameters thus seem to be mainly set by the flow rate and by gravity. In addition, the concentration in gelator has a slight influence on filament diameter and almost none on the jet diameter, whereas the needle diameter influences only the jet and not the filament. These last observations could mean that it is at the ulterior steps of jet evolution that the quantity of gelator plays a role.

These characterizations gave us some insight into the wet spinning process and in the conditions to obtain filaments of gel. They are also useful for applying the wet spinning method to 3D printing, or at least to a controlled deposition.

III.2.2.3 Microscopic characterization and composition of the filaments

Once the filaments formed, it is interesting to characterize their microscopic structure as well as their composition. For this, several methods have been employed such as optical and electronic microscopies, as well as thermogravimetric analysis.

III.2.2.3.1 Optical and electronic microscopy observations

The resulting filaments can be easily observed with transmission optical microscopy because their size is of several hundreds of micrometers and they are translucent enough to see through (Figure III-21). The composing fibers of the gel can even sometimes be outlined, especially on the edges of the filaments, and a radial fiber organization is suspected (Figure III-21b). The diameters of the filaments were measured by this technique. For example, on Figure III-21a, the resulting diameter of the filaments is of 205 µm and of 180 µm on Figure III-21b.

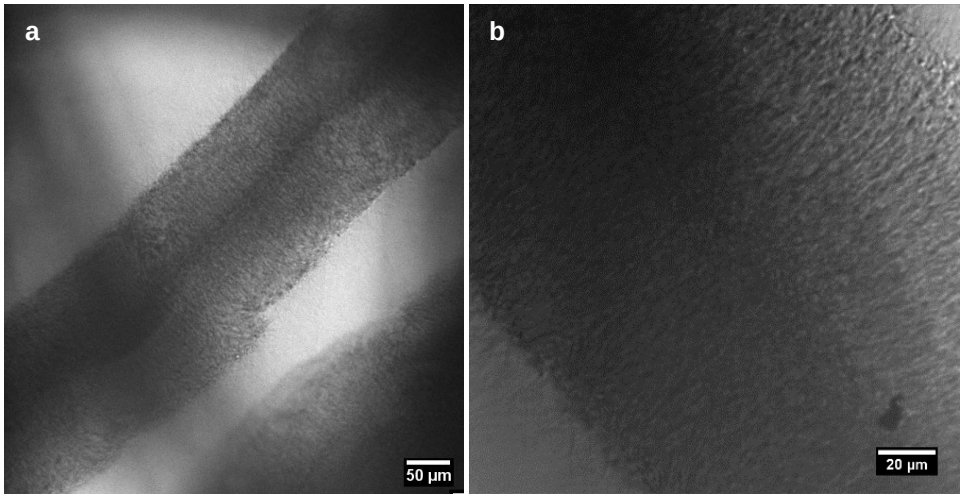

Figure III-21: Optical microscopy observations of filaments resulting from the extrusion of a 4 wt % Gal-C7 solution in DMSO at 50 µl/min with a needle ID of 600 µm, scale bars of 50 µm (a) and 20 µm (b).

To observe these structural fibers that constitute the gel rope with a higher resolution, cryo-SEM characterization was performed (Figure III-22). The most robust filaments, corresponding to the following conditions, have been studied: a 4 wt % solution extruded at 50 µl/min (Figure III-22a) and a 5 wt % solution extruded at 50 µl/min (Figure III-22b).

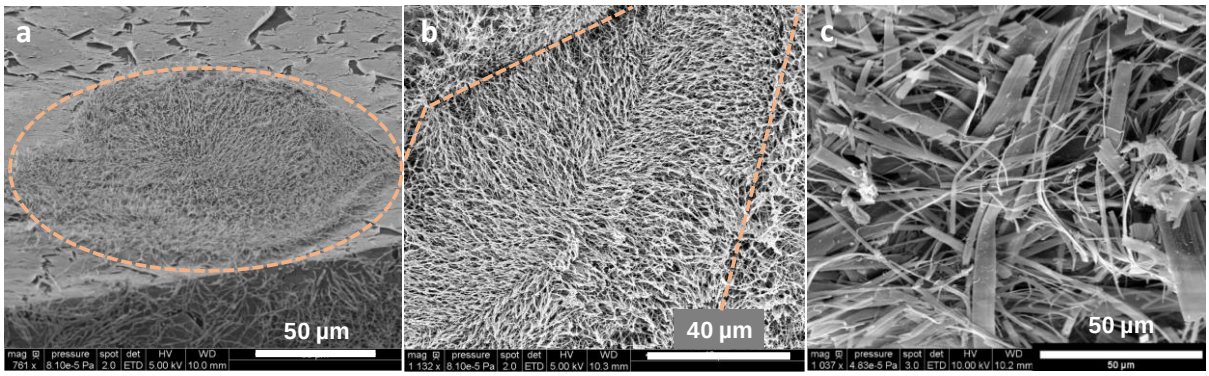

Figure III-22: Cryo-SEM observations of gel ropes: a: Section of a rope from a 4 wt % solution extruded at 50 µl/min with a 20G needle. The dotted circle shows the section of the rope. The resulting diameter is around 120 µm. b. Observation of the fibers in a filament of a 5 wt % solution extruded at 50 µl/min. The dotted lines show the edges of the filament. c. Cryo-SEM observation of a Gal-C7 gel prepared by cooling down a hot gelator solution in water (0.45 wt %) and not by wet spinning. Here the maximum width a fiber can reach is around 15 µm.

What is most striking here is that the microscopic structure of wet spun Gal-C7 hydrogels is very different from the bulk ones as prepared in the previous chapters. The sizes of the composing fibers and their distribution are much reduced in the case of wet spun gels compared to the bulk ones (Figure III-22c): the mean fiber width is around 140 nm for wet spun hydrogels whereas the median width for bulk Gal-C7 hydrogels is of 1.1 µm (see chapter I.2.2.2.3).

The filaments' diameters could sometimes be measured on cryo-SEM clichés as on the one of Figure III-22a: the diameter on this picture is around 120 µm, which is in the same range as the filaments on Figure III-21. What can be observed as well is the general orientation of the fibers within the filament. As on Figure III-21a, the fibers seem to form radially in the gel, actually following the diffusion of water inside the rope. This can be observed on Figure III-22b too, where the edges of a filament can be outlined. On this photo, we can make out that the fibers grew perpendicularly to the edge of the filament and go towards its center. These observations thus let us think that there is a certain alignment of the gel fibers in the same direction than the water diffuses inside the rope.

III.2.2.3.2 Thermogravimetric analysis

Thermogravimetric analyses (TGA) were also performed on samples of wet spun Gal-C7 gels in order to get the ratio of water, DMSO and gelator content in the gel rope (Figure III-23). The experiment was performed on filaments obtained with the most suited conditions, which are with a 4 wt % solution, 50 µl/min and a 20G needle. TGA was also performed with the Gal-C7 solid alone and with a solution of 1 wt % DMSO in pure water as references. The results show that the final composition of the filament is of 3 wt % of Gal-C7 and 97 wt % of water. There seems to be no remaining DMSO (less than 1 wt %) in the filament since nothing was detected by TGA around 130 °C.

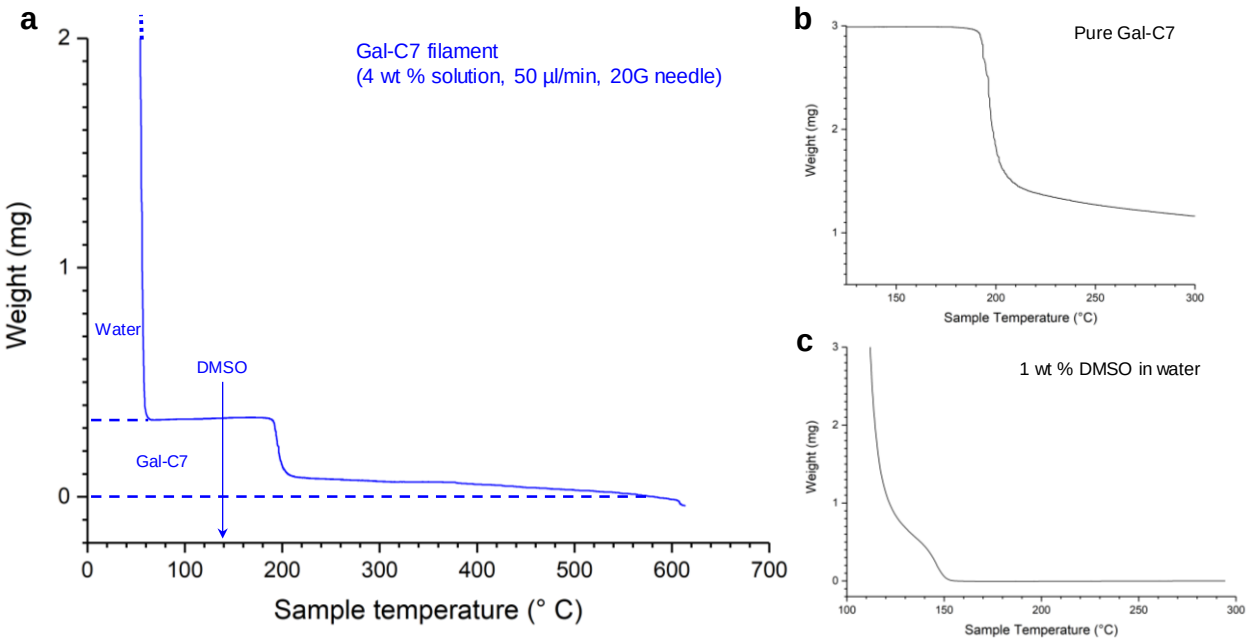

Figure III-23: Thermo-gravimetric analyses. a. Magnification on the TGA graph of a wet-spun Gal-C7 filament. Its analysis gives a 97 wt % of water and 3 wt % of Gal-C7. No DMSO appears to be remaining in the gel. b. Magnification on the TGA graph of pure Gal-C7. c. Magnification on the TGA graph of water containing 1 wt % of DMSO which shows that DMSO is evaporated along with water at a temperature of approximately 130 °C. Since there is no such a variation on the TGA of the filament, it indicates that no DMSO was remaining in it.

This result is promising for cell culture applications because the diffusion in the bath during the wet spinning process already significantly decreases the amount of residual DMSO into the filament. Cells can withstand up to 10 % of DMSO in a solution. Thus, the resulting wet spun gel should be biocompatible, and could even probably be extruded along with cells in certain conditions (with cells in the coagulation bath for instance). What is also interesting is that the amount of gelator in the final material is quite low but still more concentrated than in the bulk gels where the maximal amount of Gal-C7 is of 0.45 wt %. Hydrogels with higher gelator content can thus be obtained by wet spinning.

III.2.2.4 Lifetime of the wet spun filaments

I.3.1.1.1 Morphological transformation of the filaments into crystals

Because of the potential use of these wet spun filaments for cell culture applications, their lifetimes and dissolution into liquids have been studied. For this, the wet spun Gal-C7 filaments have been kept in different solutions under different conditions. Pure water, DMEM (supplemented with 10 % FBS) or PBS have been used. For DMEM, the filaments have been kept either at room temperature or at 37 °C. 30 µl of the gelator solution were extruded. Once formed, the filaments were transferred into wells and 1 mL of the various solutions was added. However, the gel ropes actually float on top of the liquid. To avoid this contact with air (which would change

the dissolution rate), a cover slip was placed on top of the liquid. These two different immersion conditions were thus assessed: one with and one without a cover slip on top. Two different spinning conditions were also studied: 25 µl/min and 50 µl/min, with a 4 wt % Gal-C7 solution in DMSO and a 20G needle. The results are displayed in Table III-2.

Table III-2: Lifetime study of the wet spun Gal-C7 gel filaments from a 4 wt % gelator solution in DMSO in different conservation conditions. Throughout the time, the filaments dissolve in the solution and then recrystallize (except for the condition with DMEM at $T°_{amb}$ where no crystals have yet been observed).

Flow rate	**25 µl/min**		**50 µl/min**	
Conditions	**Lifetime exposed to air (days)**	**Lifetime under cover slip (days)**	**Lifetime exposed to air (days)**	**Lifetime under cover slip (days)**
Water ($T°_{amb}$)	3	> 4	3	[e]
DMEM ($T°_{amb}$)	> 31	> 31	> 34	> 34
DMEM (37 °C)	7	4	< 1	4
PBS ($T°_{amb}$)	< 1	3	<1	2

Throughout the days, the filaments progressively dissolved in the liquid (Figure III-24). But, instead of remaining in solution, the gelator molecules then recrystallized to form parallelepipedal translucent crystals as displayed on Figure III-24b. This occurred whatever the solution used, except for the DMEM at room temperature where crystals have not yet been observed after more than a month.

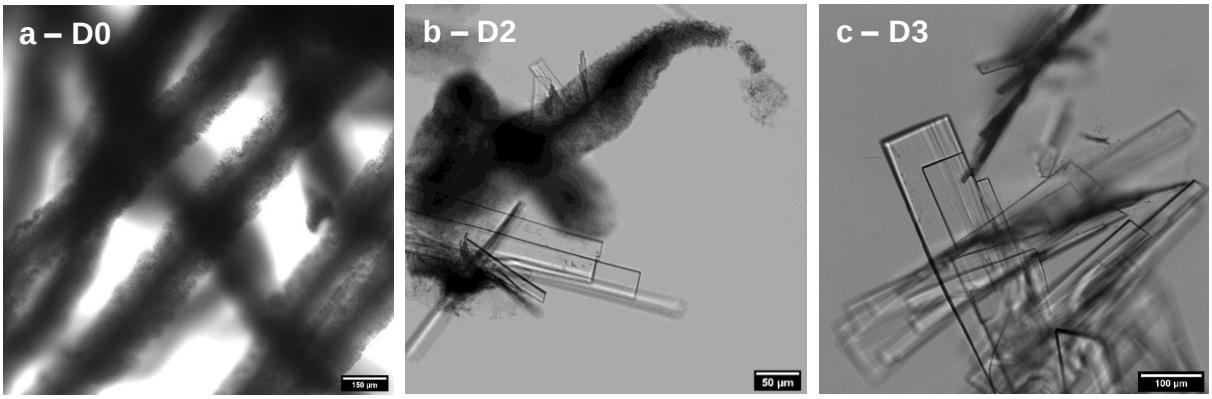

Figure III-24: Evolution of the gal-C7 filaments' morphology throughout the days in water: a. right after their extrusion, b. 2 days after and c. 3 days after. The conditions used here were of filaments wet spun with a 4 wt % solution at 50 µl/min with a 20G needle and that were kept in pure water at room temperature without a cover slip on top. Scale bars: 100 µm (a and c), 50 µm (b).

Between these two states, spikes on the edges of the filaments can also be observed after some time, as seen on Figure III-25.

[e] These experiments are still in progress, which is why some data is missing.

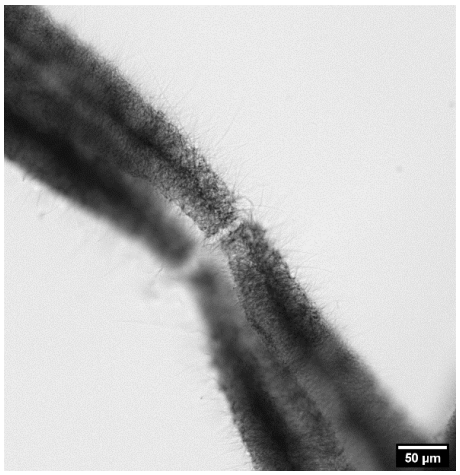

Figure III-25: Optical microscopy observation of a wet spun Gal-C7 filament kept in water after 2 days showing spikes on its edges (scale bar: 50 µm).

These observations show the polymorphism of the gelator molecules that can either form self-assembled fibers resulting in the formation of a hydrogel, or regular and translucent crystals. Actually, the self-assembly of Gal-C7 molecules into fibers, by decreasing temperature or by solvent exchange, is somehow a kind of crystallization phenomenon. In the case where the filaments of gel are kept in a solution, the most stable state for the gelator molecules are the crystals instead of nanometric fibers, thus leading to their formation. This morphological transformation was sometimes (but scarcely) also observed with bulk alkylgalactonamide hydrogels that had been kept in a big amount of water for a few days. This phenomenon has actually been described in literature for alkylaldonamides derived from other aldoses, notably octylgluconamide.[46]

What is also important to notice on Table III-2 is that the hydrogel filaments have a much longer lifetime in DMEM than in solutions containing less dissolved compounds like water or PBS. As a matter of fact, the filaments can be kept for more than a month in DMEM at room temperature, compared to solely 3 days in water or PBS. However, once the DMEM is left at 37 °C, as in cell culture conditions, the lifetime is much reduced to only a few days. Actually, when the temperature is increased, the solubility of the molecules is as well increased. To explain the reduced solubility of Gal-C7 in DMEM compared to water or PBS, several explanations can be hypothesized. First, the DMEM, and especially when supplemented with FBS, contains many ions, amino acids, proteins, enzymes, glucose, etc. These solutes already make the solution highly concentrated and reduce a lot the solubility of other compounds. Another explanation could be the fact that some proteins get adsorbed at the surface of the filaments, thus preventing their dissolution. However, in any case, once placed at 37 °C, the solubility is much more increased. This last point will have to be improved for the use of wet spun filaments for cell culture applications.

Work should be made in order to reduce their degradation, by trying to cross-link the gel for instance or by working on composite systems.

I.3.1.1.2 X-Ray analysis of the morphological transformation

The organization of the Gal-C7 molecules in the two morphological states has been studied by Small Angle X-Ray scattering (filament of gel and crystals) and X-Ray diffraction (crystals). The SAXS curve for the wet-spun gel is reported on Figure III-26 (a and b) and is indicative of a well-defined lamellar organization.

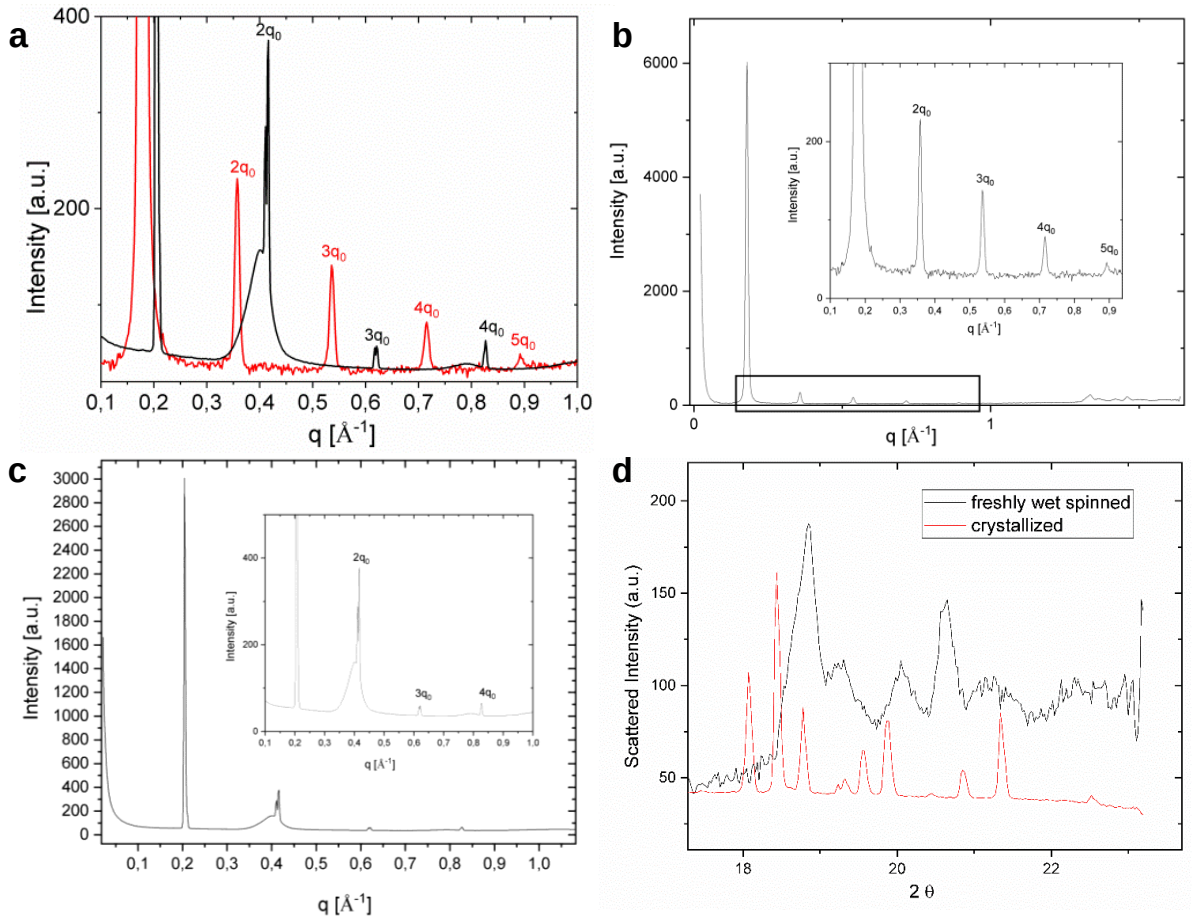

Figure III-26: a. SAXS spectra of a fresh Gal-C7 wet-spun gel (red curve) and Gal-C7 crystals (black curve). b. SAXS intensity as a function of the scattering vector of the fresh wet-spun Gal-C7 gel. c. SAXS intensity as a function of the scattering vector of the Gal-C7 crystals. d. WAXS intensity as a function of the scattering vector of the crystallized and freshly wet-spun Gal-C7.

The long period spacing of the lamellar structure is d=35.1 Å and a fiber thickness of 60 nm can be estimated. In the "bulk gel" produced by cooling hot aqueous solutions of the gelator, we described in a preceding paper that the dominant molecular organization of the gelator is also lamellar with a spacing of 35 Å, but a second, less abundant, molecular arrangement with an interaction distance of about 38 Å was also observed (see I.2.2.3). Thus, these results show that the mode of self-assembly of Gal-C7 is mainly the same for the bulk gels and the wet-spun gels,

but the wet spinning leads to a better control of the self-assembly since it produces only one kind of spacing.

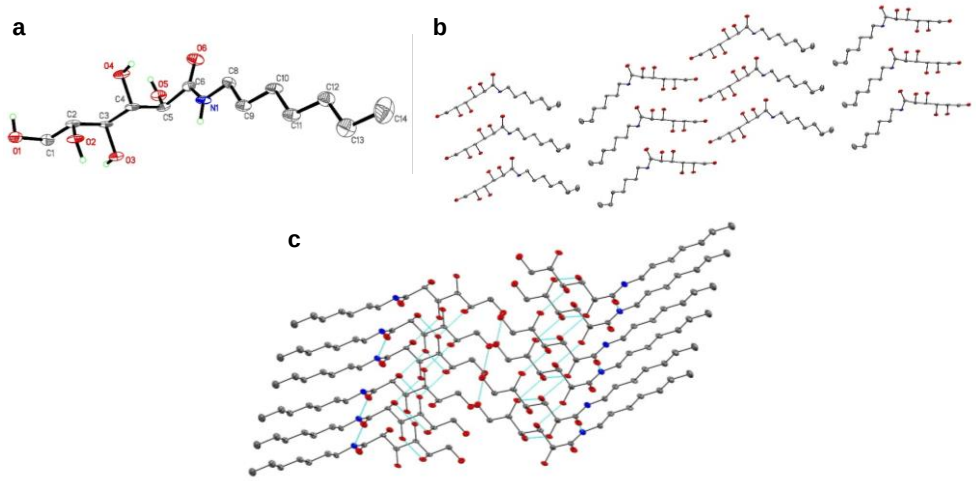

Figure III-27: a. Molecular view of Gal-C7 in the crystal. Thermal ellipsoids represent 50% probability level. H atoms (except for that on O and N atoms) are omitted for clarity. b. Molecular packing of Gal-C7 in the crystals (H atoms have been omitted for clarity). c. Representative O-H---O and N-H---O bonds are drawn as dotted lines (H atoms are omitted for clarity).

The crystals issued from the morphological transformation were also analyzed by SAXS, WAXS and X-Ray diffraction. The SAXS highlights a lamellar order with a smaller spacing of 30.5 Å (peak position, 0.204 Å-1) (Figure III-26a and c). The crystallographic structure was determined from X-ray diffraction of bigger crystals (Figure III-27). The *N*-heptyl-D-galactonamide (Gal-C7) crystallizes in monoclinic system (space group P21). The molecular packing is a symmetric tail-to-tail bilayer sheet comparable to that of the gulonamide[47] and talonamide[48] analogues (Figure III-27b) but is in contrast with the head-to-tail packing observed in the gluconamide analogue[49]. All fatty chains run parallel to each other but quite intriguingly an angle of ~120° is observed between the packed chains at the junction of the tail-to-tail arrangement. An angle of 90°C has been also described previously in the case of *N*-octyl-D-talonamide[48]. In the crystal, intermolecular O-H---O and N-H---O hydrogen bonds link the molecules into a three-dimensional network (Figure III-27c and Table III-3).

Table III-3: Hydrogen bonds for Gal-C7 in the crystal [Å and °].

D-H...A	d(D-H)	d(H...A)	d(D...A)	<(DHA)
O(1)-H(1)...O(1)#1	0.85(8)	2.05(8)	2.894(5)	170(8)
O(2)-H(2)...O(4)#2	0.89(9)	2.00(8)	2.738(7)	139(7)
O(3)-H(3)...O(2)#3	0.83(9)	1.90(9)	2.722(7)	167(9)
O(4)-H(4)...O(5)#4	0.86(8)	1.85(8)	2.700(7)	171(8)
O(5)-H(5)...O(3)#5	0.78(8)	2.07(8)	2.760(7)	147(8)
N(1)-H(1N)...O(6)#2	0.89(7)	2.06(7)	2.943(7)	172(6)

Symmetry transformations used to generate equivalent atoms:

#1 -x+2,y-1/2,-z+1 #2 x,y+1,z #3 x+1,y,z

#4 x-1,y,z #5 x,y-1,z

The stereochemistry of the galactonamide polar head enables the development of a strong hydrogen-bond pattern between hydroxyl groups of adjacent crystal sheets that drives the tail-to-tail molecular packing. In the case of gluconamide, the stereochemistry of the hydroxyl groups is different and led to a head-to-tail packing. Still for crystals, the WAXS region looks like a powder diffraction spectrum with well-defined peaks, while in the case of gel filament, the same region of the spectrum shows much larger peaks with peak positions different compared with crystals (Figure III-26d). This observation indicates a probable difference in the molecular conformation of the Gal-C7 molecule between the supramolecular fibers and the crystals. Together with the difference in water content, it may explain the spacing difference between the two kinds of assembly.

III.2.2.5 Conclusion

The wet spinning technique offers a very interesting way to shape the alkylgalactonamide hydrogels other than by cooling down hot solutions. This process, based on solvent exchange, allows us to readily obtain hydrogel filaments at room temperature, without heating to dissolve the gelator. Different conditions of flow rates, concentrations and needle sizes have been determined to obtain filaments. Their diameter can be tuned by playing on the applied flow rate. Moreover, the microscopic structural network is very different from the one of the bulk gels. In the case of wet spun gels, the self-assembled fibers are very thin and with a narrow width dispersion. Yet, these hydrogel ropes degrade rapidly in liquids at room temperature such as water or PBS. They proved to be much more resistant when kept in DMEM supplemented with FBS, except when incubated at 37 °C. This last point is problematic for the further use of these gels

as cell culture scaffolds, but other applications could be envisioned such as biocompatible sacrificial hydrogels for instance.

Some parameters of the wet spinning process can be further investigated. For instance, the coagulation bath composition or its temperature can be tuned. Some first trials in baths of DMEM allowed the formation of filaments. A method to improve the gels stability in liquids, and particularly in cell culture conditions should be developed as well.

III.3 Application of wet spinning to 3D printing of hydrogels

As previously seen, wet spinning is a very efficient method to shape the alkylgalactonamide hydrogels. The process can be done at room temperature, with an easy preparation step. The gelation occurs throughout the fall of the gelator solution into the coagulation bath. However, if the fall height is reduced, the hydrogel can be deposited on a surface before its gelation as a rope. By doing several depositions, a process of additive manufacturing for hydrogels could be developed. In this part, we will describe how we proceeded to apply the wet spinning method to 3D printing. The results presented here are preliminary since most of the study (which was conducted by Morgane Mauduit as part of her internship) has been performed on a single layer of gel.

III.3.1 Printing set-up and phase diagrams

In order to precisely control the deposition of the hydrogels on a surface, the wet spinning set-up had to be adapted (Figure III-28). The same solutions, syringes, needles and syringe pump were used. However, the needle had to be deported on a programmable XY-moving stage to spatially control the deposition. It was also placed on a support, itself placed on a Z-moving stage in order to set the distance between the needle and the deposition surface. The XY-moving stage was controlled by a computer.

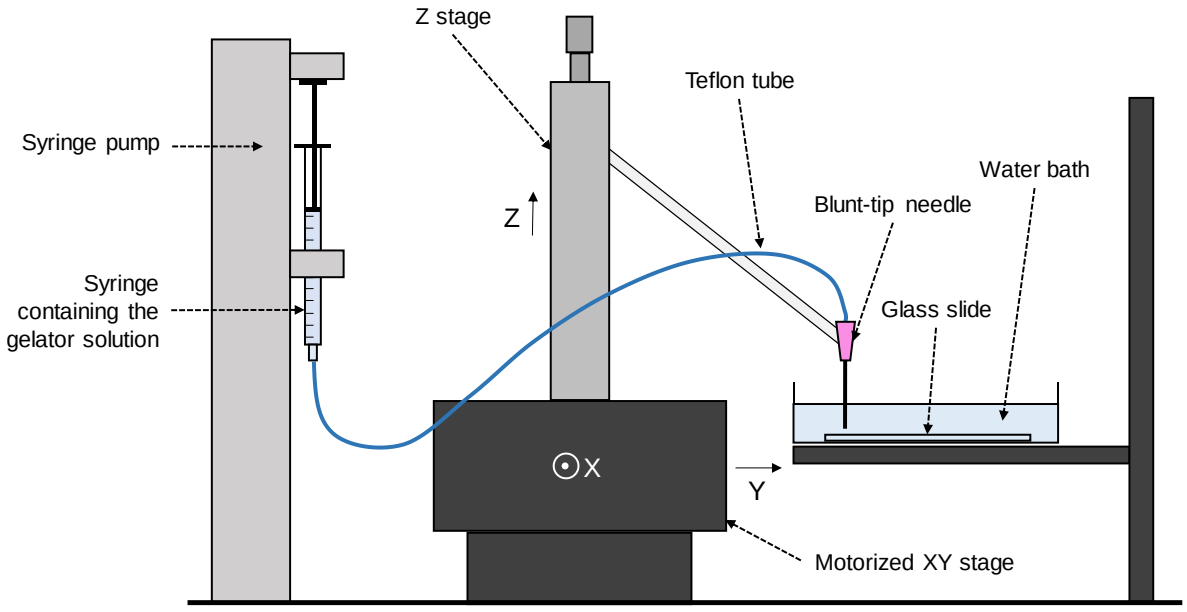

Figure III-28: Scheme of the set-up used for the 3D printing of Gal-C7 hydrogels.

By adjusting the speed of the stage, the flow rate and the distance between the needle and the substrate, it was possible to deposit the gelator solution before full gelation so that it adheres to the surface without spreading too much. However, concerning the deposition surface, some adaptations had to be made too. As a matter of fact, it has been found that the hydrogel did not adhere well on some substrates. For instance, the simple deposition on glass was impossible because the hydrogel very poorly adhered on it: with the slightest water movement from the bath, almost all the deposition was removed. Various methods were tried to improve the adhesion: charged glass slides, plasma treatment, coating with a solution of the gelator, etc., but none of them worked. Porous polymer membranes were then tried and polycarbonate (PC) membranes were the ones that showed the best adhesion results. They were therefore used throughout this study. The same motif was always printed as represented on Figure III-29.

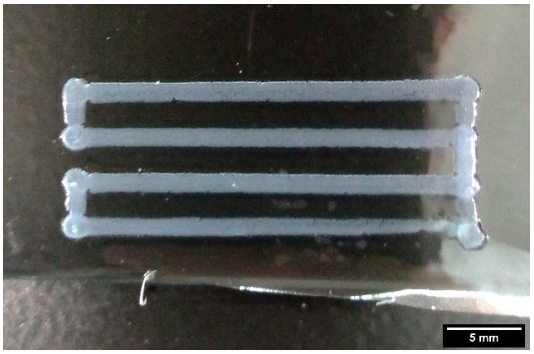

Figure III-29: Example of a printed Gal-C7 hydrogel (2.5 wt % solution, 10 µl/min, 2 mm/s printing speed, 2 mm between the needle and the membrane). Scale bar: 5 mm.

Yet, the hydrogel's adhesion was still not perfect and in addition, the range of parameters that induce the gel deposition differed a bit from the ones determined for the wet spinning of filaments. Consequently, other phase diagrams had to be established to determine the best printing conditions. In this case, the tuned parameters were the printing speed versus the distance between the needle and the membrane. Two flow rates were investigated: 5 and 10 µl/min because for this process, thin and slow DMSO jets are needed so that the deposit is not too large, and the gelation occurs quickly enough. Flow rates lower than 5 µl/min often resulted in the clogging of the needle, and so did the use of a 4 wt % gelator solution. As a consequence, a 2.5 wt % gelator solution in DMSO has been used. Moreover, two needle sizes were tested: 22G (ID of 410 µm) and 23G (ID of 340 µm). Here, the adhesion to the membrane has been visually assessed for each condition by removing the glass slide from the bath and looking if water washed out poorly attached stripes or not. The results are displayed on Figure III-30.

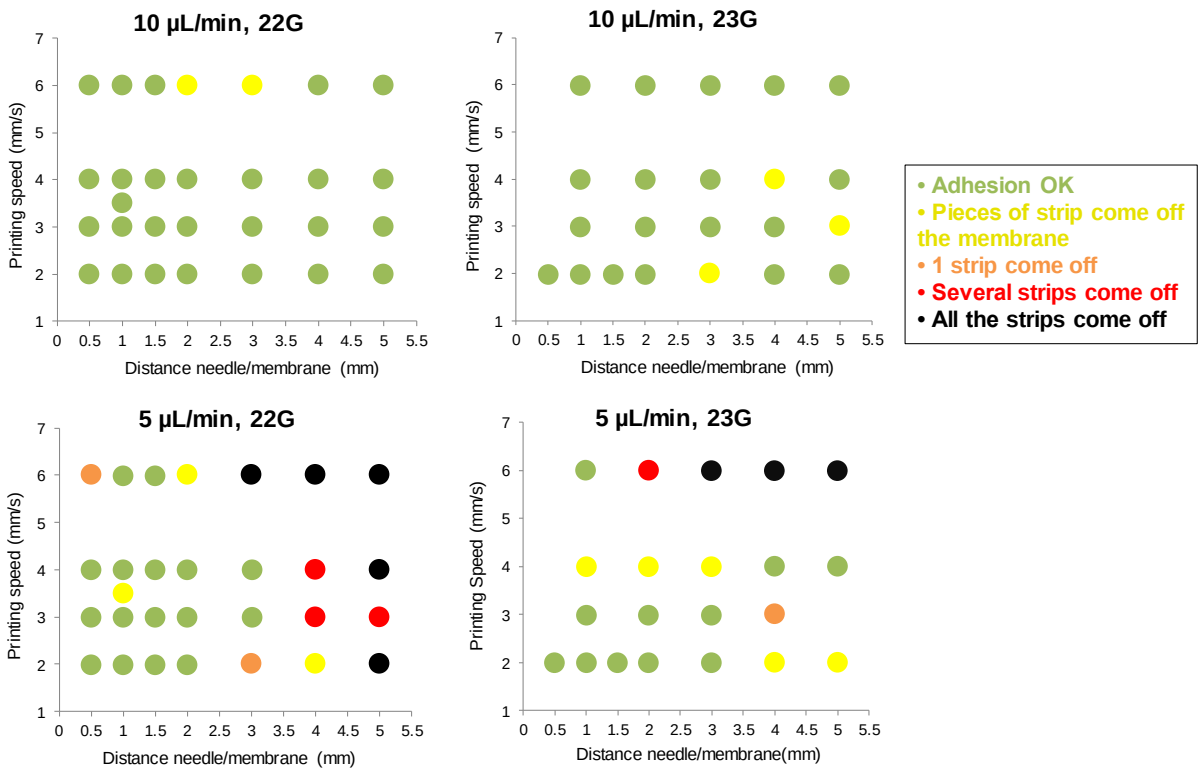

Figure III-30: Phase diagrams for the 3D printing technique in different conditions of flow rates and needle size. The printing speed and the distance between the needle and the deposition membrane have been varied to study the adhesion of the hydrogel on the substrate. Two flow rates (5 and 10 µl/min) and two needle diameters (22G and 23G) have been used. The adhesion was assessed by removing the glass slide with the membrane from the bath and checking if the printed strips were remaining on the membrane or not.

These results show that with a 10 µl/min flow rate and for each needle size, the deposits have a good adhesion for almost every conditions of printing speed and needle/membrane distance. However, for 5 µl/min rates, the residence time of the filament in the bath is increased and some conditions give very poor adhesion. Indeed, since the residence time increases compared to 10 µl/min, the gelation is more engaged when the DMSO jet reaches the substrate. Because of that, the adhesion to the membrane is reduced. This is particularly true when the distance between the needle and the membrane increases because here again the residence time is increased (graph "5 µl/min, 22G" from Figure III-30). This is also true when the printing speed is too high, not because of the residence time in this case but because if the displacement is too rapid, the adhesion of the deposit might not be optimal.

Other trials have been made with thinner needles (25G, ID of 260 µm). However, even when the flow rate was increased to supply more material, no deposit adhered on the membrane. Similarly, trials have been also done with a more concentrated gelator solution (4 wt %) but no conditions were found to obtain adherent deposits. These results might be explained by the faster gelation in those conditions, resulting in a poor adherence to the substrate. The thinner the needle, the faster the water diffusion and the faster the gelation. The more concentrated the solution, the

faster the gelation as well. This was indeed predicted by the relationship established by Rende[22] (see III.1.2.1). As a consequence, for the rest of the study, only 2.5 wt % gelator solutions in DMSO were used with 22G and 23G needles and flow rates of 5 and 10 µl/min.

III.3.2 Width of the deposits

A characterization of the deposits was made by measuring their final width on the substrate. These measurements were done by optical microscopy for the conditions corresponding to the phase diagrams and are represented on Figure III-31. These graphs show that globally, the faster the needle goes above the substrate, the narrower the deposit is. An increased printing speed has the effect of thinning the DMSO jet, whereas a slow deposition leaves time for the liquid to spread on the membrane and increases the width of the deposited hydrogel. However, this parameter seems to depend less on the needle/membrane distance since all the curves are more or less superimposed considering the error bars, except for the conditions at 5 µl/min. Maybe in this last case the stretching of the jet is stronger and results in thinner deposits.

Concerning the size of the needle, it does not either seem to have an influence on the width of the deposit. However, for 5 µl/min flow rates, the widths are decreased compared to 10 µl/min. For similar conditions, a lower flow rate implies less material supplied and thus a smaller quantity of fluid per unit length, resulting in a narrower deposit.

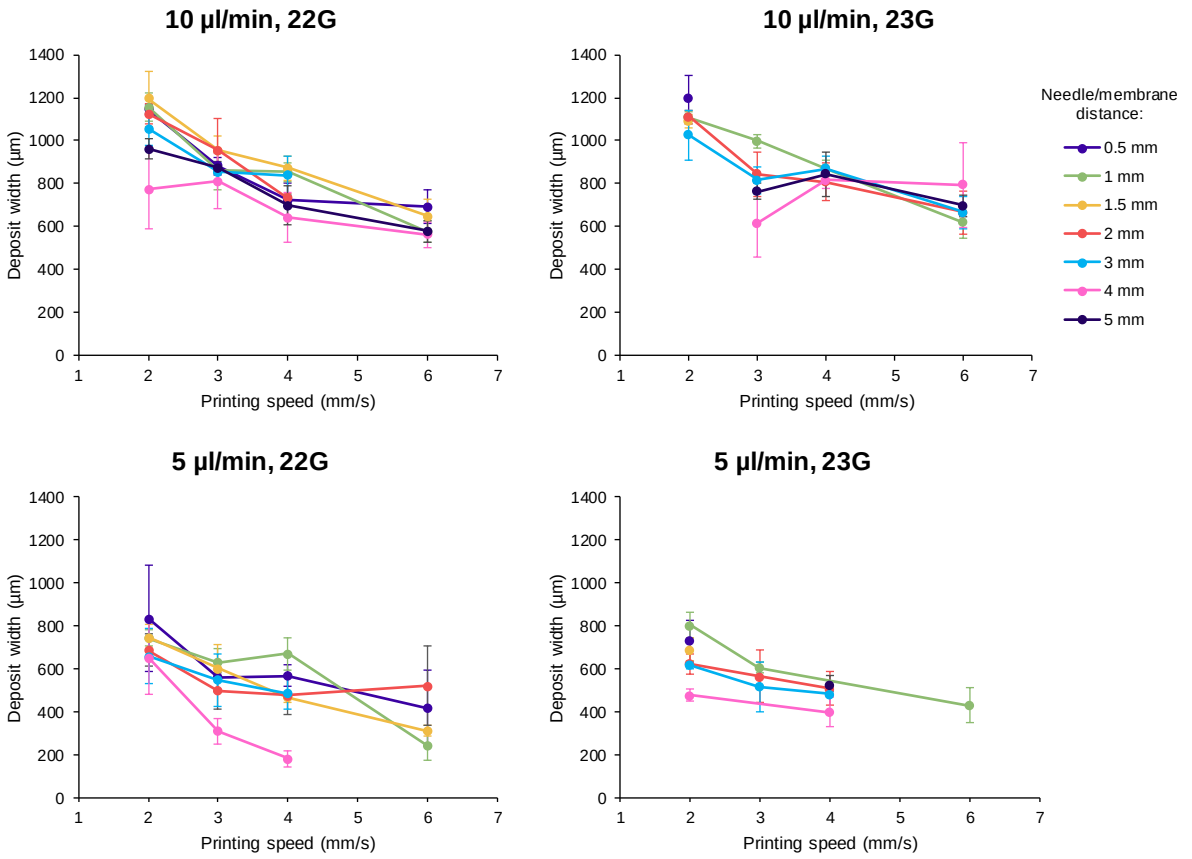

Figure III-31: Widths of the deposits (measured by optical microscopy) in function of the printing speed for different distances between the needle and the membrane, different flow rates and needle diameters.

Another remark is the fact that the membranes had to be taken out of the bath in order to proceed to the microscope observations. During this process, the deposited hydrogels might have dried a little bit, which might have resulted in bias in the measurements because when the gel dries, it tends to shrink. However, everything was done in order to proceed to the observations the quickest possible.

III.3.3 Thickness of the deposits

Another characterization that has been made was the measurement of the thickness of the deposits by profilometry. This parameter is somehow crucial for 3D printing since we want to create a 3D scaffold with a certain height. Several depositions will have to be made in order to achieve this and it is important to know the thickness of one layer.

For this, a first numerical microscope (Hirox microscope) was used as an optical profilometer by determining the height of best focus (thanks to an electronic Z stage). It enabled us to observe the deposits and measure their thicknesses. At first, only one layer was deposited on the membrane in various conditions of flow rate, needle gauge and printing speed. The samples were then

observed with the microscope and their profile was established manually by measuring the change of focus along the width of the gel strips. Here, only one distance between the needle and the membrane was used (2 mm), because the measurements from Figure III-31 showed that this parameter had little influence on the dimensions of the deposits. The results are represented on Figure III-32.

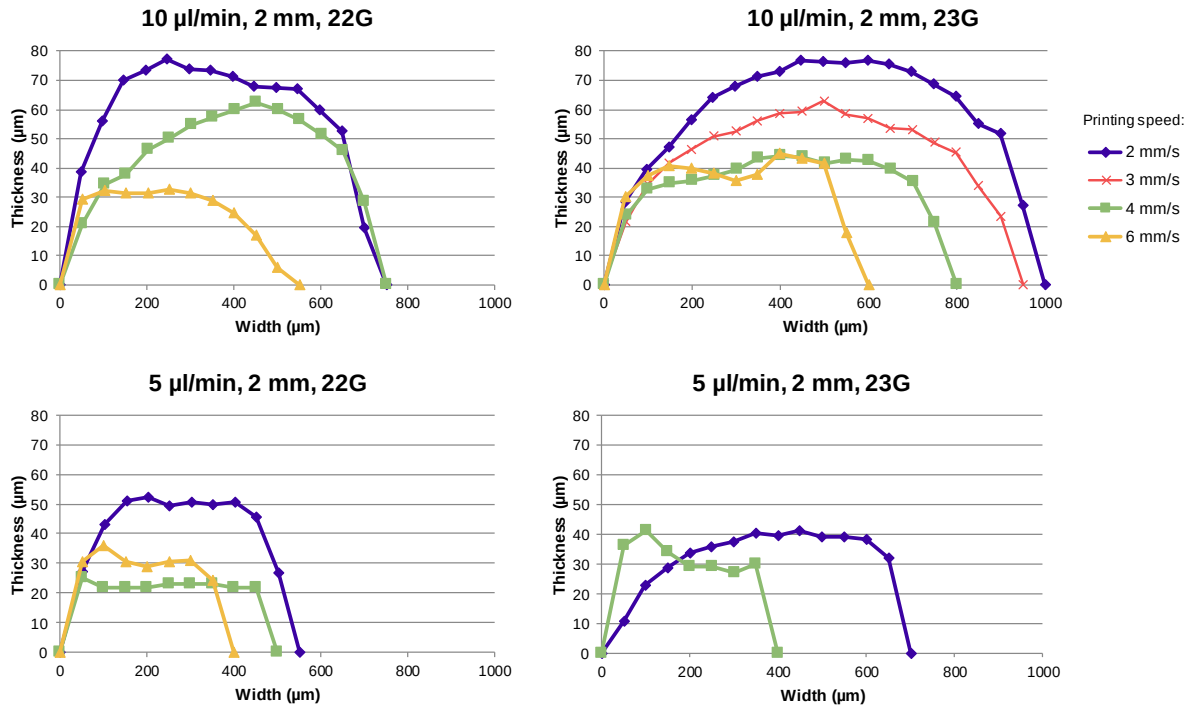

Figure III-32: Comparison of the deposits' profiles for different printing conditions. The profiles were obtained by profilometry with a numerical microscope equipped with a motorized Z stage to measure the focus displacement along the width of a strip.

These graphs show that when the flow rate is reduced, the thickness and the width of the deposits are reduced as well. In this case also, the needle diameter seems to have little influence on the resulting dimensions. However, printing speed seems to control the sizes of the gel strips. The faster the needle goes, the smaller the deposits are, both in thickness and in width. It can also be noticed that the widths measured by profilometry are consistent with the ones measured by optical microscopy from Figure III-31.

Here again there might have been some bias coming from the drying of the hydrogels. It was not possible to observe the deposits if the hydrogels stayed in the bath, the edges of the gel strips could then not be outlined. The glass slides with the membranes rested on top of a soaked paper during observation in order to limit the drying of the hydrogels. Yet, considering the time of measurement (several minutes for one profile), the hydrogels still dried a little bit. This can explain why the widths measured by profilometry (Figure III-32) are usually smaller than the

ones from optical microscopy (Figure III-31) where the measurements were more straightforward, even though these results are in the same range of values.

To overcome the drying of the samples, a second numeric microscope was used (Keyence microscope from the CIRIMAT laboratory), with an automatic focus and profile measurement. The observation time was therefore much reduced. This time, the height of two hydrogel layers was also measured.

In this case, with one layer of hydrogel, the width/thickness ratio is around 20 for both conditions, whereas for the same conditions with the Hirox, this ratio was about twice less. This means that in these printing conditions, the deposited hydrogel strips are very thin compared to their width. Actually, even if the analysis time was decreased with the Keyence, the transportation time to access the facilities was much longer, even if all the care was taken to prevent most gel drying. It is thus delicate here to discuss the influence of the drying on the gels' thickness. An *in situ* preparation of the sample before analysis with the Keyence would help us give an answer to this question.

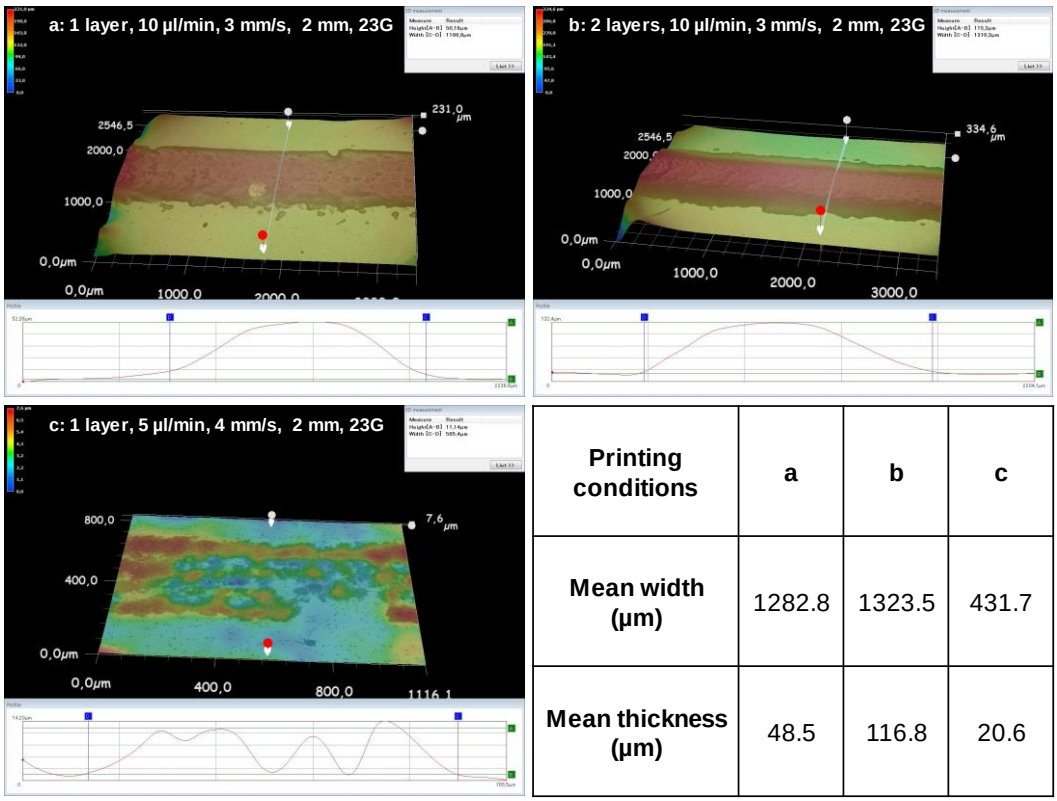

Printing conditions	a	b	c
Mean width (µm)	1282.8	1323.5	431.7
Mean thickness (µm)	48.5	116.8	20.6

Figure III-33: Profilometry analysis of the deposits for different printing conditions. a,b,c: Images obtained from the Keyence microscope for three conditions: a) 1 layer, flow rate of 10µl/min, 3 mm/s as printing speed, 2 mm of distance between the needle and the membrane, 23G needle; b) 2 layers, 10 µl/min, 3 mm/s, 2 mm, 23G and c) 1 layer, 5 µl/min, 4 mm/s, 2 mm, 23G. The table gives the mean widths and thicknesses of the deposit for the different conditions.

The superimposition of several layers enabled to increase the thickness of the deposit. However, it would be interesting to find conditions for which the width/thickness ratio is reduced in order

to print more resolved structures. As previously described, the use of smaller needles or reduced flow rates does not help for it gives non-adherent gel strips or even clogging. Working on the adhesion issues, on the ink formulation or on the bath composition for instance might improve the spreading of the gelator solution on the substrate.

III.3.4 Microscopic structure of the hydrogel

The microscopic structure of the Gal-C7 deposits was also investigated by cryo-SEM. The analyzed sample was printed with the following conditions: 2.5 wt % gelator solution in DMSO, 23G needle, flow rate of 10 µl/min, membrane-needle distance of 1 mm and printing speed of 3 mm/s (Figure III-34).

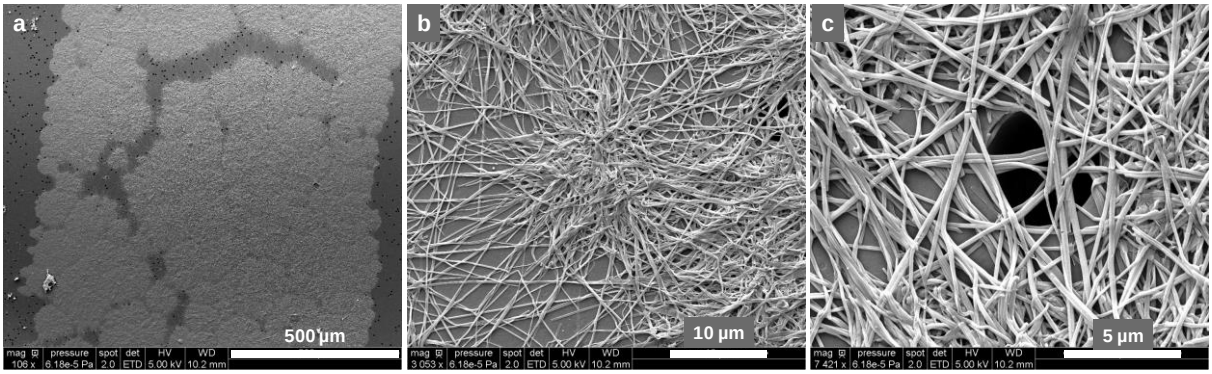

Figure III-34: Cryo-SEM observations of a printed Gal-C7 hydrogel (2.5 wt % gelator solution in DMSO, 23G needle, flow rate of 10 µl/min, distance of 1 mm between the membrane and the needle and printing speed of 3 mm/s).

Figure III-34a shows that the deposited hydrogel was somehow irregular since the fibers are not evenly widespread throughout the deposit. This phenomenon was also seen on some optical microscopy observations. The fibers seem to grow from nucleation points like in bulk hydrogels (see chapter I.2.2.1), as it can be seen on Figure III-34b. In addition, even if porous membranes are used, Figure III-34c confirms that the fibers do not penetrate the pores of the membrane but rather go over them.

Concerning the fibers' morphology, it is very similar as the one obtained by wet spinning (Figure III-22), with also a very narrow size distribution. However, in the case of printed gels, the fibers' width is a little bit increased compared to the gel filaments obtained by wet spinning (see III.2.2.3.1). Here the mean fiber width is around 235 nm, compared to 140 nm for wet spun filaments.

III.3.4.1 Conclusion

A set-up was thus developed in order to apply the wet spinning process to 3D printing of Gal-C7 hydrogels. The gel deposits were characterized in terms of adhesion, width, thickness and fiber morphology. The adhesion was made possible thanks to polycarbonate porous membranes and the deposits are very wide with a low thickness. However, superimposing layers of hydrogel is efficient to increase the thickness, as with an additive process. The fibers composing the hydrogels have widths with the same order of magnitude as the ones of wet spun Gal-C7 filaments and with a homogeneous size distribution.

In order to improve the process, many parameters could be investigated in order to obtain a better ink for printing. It could help obtaining thicker and narrower deposits, which would be more suited to develop a process similar as additive manufacturing. In the end, suspended 3D structures (as the ones from Figure III-7 for example) could even be obtained. Trials have been already performed with baths of DMEM, like for wet spinning, in order to tune the gelation. However, these tests revealed that the hydrogel could not adhere to the membrane in this case. One parameter that has also been overlooked here was the bath temperature. Varying this one could also be a way to improve the printing.

III.4 Conclusion

To conclude this last part of the project, a novel method for the shaping of the alkylgalactonamide hydrogels has been developed, based on the wet spinning process. This technique allowed us to directly extrude the Gal-C7 hydrogel while forming thanks to the exchange of two solvents, DMSO and water, at room temperature and with a very simple set-up. The extrusion of alkylgalactonamide hydrogels after gelation was indeed impossible because of the synaeresis phenomenon that destroys the gel structure. However, other gelator families provided self-healing materials such as Gluca-C12 or Jap-C16, which can be extruded after their gelation.

The wet spinning of Gal-C7 gave nice hydrogel filaments in various conditions, but it was also possible to apply it to 3D printing by precisely and spatially controlling the deposition of the gelator solution. By adding several layers of hydrogel on top of each other, a process comparable to additive manufacturing could be developed in order to design scaffolds out of these biocompatible hydrogels.

However, the wet spinning and 3D printing processes could be upgraded to obtain very thin filaments while controlling at the same time their gelation and their deposition. Improvements are also needed concerning the adhesion of the hydrogels but also on their lifetime in liquids since they degrade in a matter of days. Hollow gel filaments, where the gelation starts from the inside, could bring a solution concerning the adhesion of the gel on the substrate. Moreover, the biocompatibility of these shaped hydrogels should be investigated. The bulk hydrogels proved to be suited for the growth of hNSCs, but in the case of wet spinning, DMSO is used to obtain these gels. Their fibrillar structure is also very different. These specificities could induce different cell behaviors within these new scaffolds. Preliminary cell culture tests with Neuro2a cells on wet spun hydrogels have actually been performed by collaborators of the project. The wet spun gels seemed to be biocompatible at first sight, but they were very fragile and unstable as they rapidly degraded after 3 days. These tests must be pursued to find suitable conditions for cell culture.

Resolving all of these issues concerning the wet spinning of Gal-C7 hydrogels could end up in the development of a novel LMWG bioink for 3D bioprinting, which, in the end, would be a great innovation in this field.

References

(1) Bhatia, S. N.; Ingber, D. E. Microfluidic Organs-on-Chips. *Nature Biotechnology* **2014**, *32* (8), 760–772. https://doi.org/10.1038/nbt.2989.

(2) Zhuang, P.; Sun, A. X.; An, J.; Chua, C. K.; Chew, S. Y. 3D Neural Tissue Models: From Spheroids to Bioprinting. *Biomaterials* **2018**, *154*, 113–133. https://doi.org/10.1016/j.biomaterials.2017.10.002.

(3) Murphy, S. V.; Atala, A. 3D Bioprinting of Tissues and Organs. *Nature Biotechnology* **2014**, *32* (8), 773–785. https://doi.org/10.1038/nbt.2958.

(4) Hull, C. W. Apparatus for Production of Three-Dimensional Objects by Stereolithography. US4575330A, March 11, 1986.

(5) Bourdon, L.; Maurin, J.-C.; Gritsch, K.; Brioude, A.; Salles, V. Improvements in Resolution of Additive Manufacturing: Advances in Two-Photon Polymerization and Direct-Writing Electrospinning Techniques. *ACS Biomaterials Science & Engineering* **2018**, *4* (12), 3927–3938. https://doi.org/10.1021/acsbiomaterials.8b00810.

(6) Ozbolat, I. T.; Hospodiuk, M. Current Advances and Future Perspectives in Extrusion-Based Bioprinting. *Biomaterials* **2016**, *76*, 321–343. https://doi.org/10.1016/j.biomaterials.2015.10.076.

(7) Nolan, M. C.; Fuentes Caparrós, A. M.; Dietrich, B.; Barrow, M.; Cross, E. R.; Bleuel, M.; King, S. M.; Adams, D. J. Optimising Low Molecular Weight Hydrogels for Automated 3D Printing. *Soft Matter* **2017**, *13* (45), 8426–8432. https://doi.org/10.1039/C7SM01694H.

(8) Raphael, B.; Khalil, T.; Workman, V. L.; Smith, A.; Brown, C. P.; Streuli, C.; Saiani, A.; Domingos, M. 3D Cell Bioprinting of Self-Assembling Peptide-Based Hydrogels. *Materials Letters* **2017**, *190*, 103–106. https://doi.org/10.1016/j.matlet.2016.12.127.

(9) Highley, C. B.; Rodell, C. B.; Burdick, J. A. Direct 3D Printing of Shear-Thinning Hydrogels into Self-Healing Hydrogels. *Adv. Mater.* **2015**, *27* (34), 5075–5079. https://doi.org/10.1002/adma.201501234.

(10) Yan, M.; Lewis, P. L.; Shah, R. N. Tailoring Nanostructure and Bioactivity of 3D-Printable Hydrogels with Self-Assemble Peptides Amphiphile (PA) for Promoting Bile Duct Formation. *Biofabrication* **2018**, *10* (3), 035010. https://doi.org/10.1088/1758-5090/aac902.

(11) Lozano, R.; Stevens, L.; Thompson, B. C.; Gilmore, K. J.; Gorkin III, R.; Stewart, E. M.; in het Panhuis, M.; Romero-Ortega, M.; Wallace, G. G. 3D Printing of Layered Brain-like Structures Using Peptide Modified Gellan Gum Substrates. *Biomaterials* **2015**, *67*, 264–273. https://doi.org/10.1016/j.biomaterials.2015.07.022.

(12) Costantini, M.; Colosi, C.; Święszkowski, W.; Barbetta, A. Co-Axial Wet-Spinning in 3D Bioprinting: State of the Art and Future Perspective of Microfluidic Integration. *Biofabrication* **2018**, *11* (1), 012001. https://doi.org/10.1088/1758-5090/aae605.

(13) Luciano, J. Thread Stretching Device for Wet Spinning More Particularly of Viscose Rayon. US2920346A, January 12, 1960.

(14) White, J. L.; Hancock, T. A. Fundamental Analysis of the Dynamics, Mass Transfer, and Coagulation in Wet Spinning of Fibers. *J. Appl. Polym. Sci.* **1981**, *26* (9), 3157–3170. https://doi.org/10.1002/app.1981.070260928.

(15) Rupprecht, A. Preparation of Oriented DNA by Wet Spinning. *Acta Chem. Scand.* **1966**, *20* (2), 494–504.

(16) Hersh, S. P.; Higgins, T. D.; Krause, H. W. The Influence of Processing Variables on the Physical Properties of a Wet-Spun Modacrylic Fiber. *J. Appl. Polym. Sci.* **1963**, *7* (2), 411–442. https://doi.org/10.1002/app.1963.070070202.

(17) Nelson, K. D.; Romero, A.; Waggoner, P.; Crow, B.; Borneman, A.; Smith, G. M. Technique Paper for Wet-Spinning Poly (L-Lactic Acid) and Poly (DL-Lactide-Co-Glycolide) Monofilament Fibers. *Tissue engineering* **2003**, *9* (6), 1323–1330.

(18) Tuzlakoglu, K.; Pashkuleva, I.; Rodrigues, M. T.; Gomes, M. E.; van Lenthe, G. H.; MÃ¼ller, R.; Reis, R. L. A New Route to Produce Starch-Based Fiber Mesh Scaffolds by Wet Spinning and Subsequent Surface Modification as a Way to Improve Cell Attachment and Proliferation. *Journal of Biomedical Materials Research Part A* **2010**, *92A* (1), 369–377. https://doi.org/10.1002/jbm.a.32358.

(19) Puppi, D.; Chiellini, F. Wet-Spinning of Biomedical Polymers: From Single-Fibre Production to Additive Manufacturing of Three-Dimensional Scaffolds: Wet-Spinning of Biomedical Polymers. *Polymer International* **2017**. https://doi.org/10.1002/pi.5332.

(20) Neves, S. C.; Mota, C.; Longoni, A.; Barrias, C. C.; Granja, P. L.; Moroni, L. Additive Manufactured Polymeric 3D Scaffolds with Tailored Surface Topography Influence Mesenchymal Stromal Cells Activity. *Biofabrication* **2016**, *8* (2), 025012. https://doi.org/10.1088/1758-5090/8/2/025012.

(21) Paul, D. R. Diffusion during the Coagulation Step of Wet-Spinning. *J. Appl. Polym. Sci.* **1968**, *12* (3), 383–402. https://doi.org/10.1002/app.1968.070120301.

(22) Rende, A. A New Approach to Coagulation Phenomena in Wet-Spinning. *J. Appl. Polym. Sci.* **1972**, *16* (3), 585–594. https://doi.org/10.1002/app.1972.070160305.

(23) Dong, X.-G.; Wang, C.-G.; Bai, Y.-J.; Cao, W.-W. Effect of DMSO/H2O Coagulation Bath on the Structure and Property of Polyacrylonitrile Fibers during Wet-spinning. *Journal of Applied Polymer Science* **2007**, *105* (3), 1221–1227. https://doi.org/10.1002/app.25665.

(24) Yi, K.; Li, Q. F.; Zhang, L.; Li, N.; Zhou, Y.; Ryu, S. K.; Jin, R. G. Diffusion Coefficients of Dimethyl Sulphoxide (DMSO) and H2O in PAN Wet Spinning and Its Influence on Morphology of Nascent Polyacrylonitrile (PAN) Fiber. *J. Eng. Fib. Fabr.* **2013**, *8*, 107–113.

(25) Speakman, J. B.; Chamberlain, N. H. The Production of Rayon from Alginic Acid. *Journal of the Society of Dyers and Colourists* **1944**, *60*, 264–272. https://doi.org/10.1111/j.1478-4408.1944.tb02258.x.

(26) Denkbaş, E. B.; Seyyal, M.; Pişkin, E. Implantable 5-Fluorouracil Loaded Chitosan Scaffolds Prepared by Wet Spinning. *Journal of membrane Science* **2000**, *172* (1–2), 33–38.

(27) Yang, Y.; Liu, X.; Wei, D.; Zhong, M.; Sun, J.; Guo, L.; Fan, H.; Zhang, X. Automated Fabrication of Hydrogel Microfibers with Tunable Diameters for Controlled Cell Alignment. *Biofabrication* **2017**, *9* (4), 045009. https://doi.org/10.1088/1758-5090/aa90e4.

(28) Yang, Y.; Sun, J.; Liu, X.; Guo, Z.; He, Y.; Wei, D.; Zhong, M.; Guo, L.; Fan, H.; Zhang, X. Wet-Spinning Fabrication of Shear-Patterned Alginate Hydrogel Microfibers and the Guidance of Cell Alignment. *Regenerative Biomaterials* **2017**, *4* (5), 299–307. https://doi.org/10.1093/rb/rbx017.

(29) Lin, S. C.-Y.; Wang, Y.; Wertheim, D. F.; Coombes, A. G. A. Production and in Vitro Evaluation of Macroporous, Cell-Encapsulating Alginate Fibres for Nerve Repair. *Materials Science and Engineering: C* **2017**, *73*, 653–664. https://doi.org/10.1016/j.msec.2016.12.016.

(30) Cheng, J.; Jun, Y.; Qin, J.; Lee, S.-H. Electrospinning versus Microfluidic Spinning of Functional Fibers for Biomedical Applications. *Biomaterials* **2017**, *114*, 121–143. https://doi.org/10.1016/j.biomaterials.2016.10.040.

(31) Bonhomme, O. Étude de la formation de fibres en microfluidique : compétition entre mise en forme et gélification de fluides complexes sous écoulement, Université Bordeaux I, 2011.

(32) Kiriya, D.; Ikeda, M.; Onoe, H.; Takinoue, M.; Komatsu, H.; Shimoyama, Y.; Hamachi, I.; Takeuchi, S. Meter-Long and Robust Supramolecular Strands Encapsulated in Hydrogel Jackets. *Angewandte Chemie International Edition* **2012**, *51* (7), 1553–1557. https://doi.org/10.1002/anie.201104043.

(33) Ghorbanian, S.; Qasaimeh, M. A.; Akbari, M.; Tamayol, A.; Juncker, D. Microfluidic Direct Writer with Integrated Declogging Mechanism for Fabricating Cell-Laden Hydrogel Constructs. *Biomedical Microdevices* **2014**, *16* (3), 387–395. https://doi.org/10.1007/s10544-014-9842-8.

(34) Lee, B. R.; Lee, K. H.; Kang, E.; Kim, D.-S.; Lee, S.-H. Microfluidic Wet Spinning of Chitosan-Alginate Microfibers and Encapsulation of HepG2 Cells in Fibers. *Biomicrofluidics* **2011**, *5* (2), 022208. https://doi.org/10.1063/1.3576903.

(35) Yamada, M.; Sugaya, S.; Naganuma, Y.; Seki, M. Microfluidic Synthesis of Chemically and Physically Anisotropic Hydrogel Microfibers for Guided Cell Growth and Networking. *Soft Matter* **2012**, *8* (11), 3122. https://doi.org/10.1039/c2sm07263g.

(36) Onoe, H.; Okitsu, T.; Itou, A.; Kato-Negishi, M.; Gojo, R.; Kiriya, D.; Sato, K.; Miura, S.; Iwanaga, S.; Kuribayashi-Shigetomi, K.; et al. Metre-Long Cell-Laden Microfibres Exhibit Tissue Morphologies and Functions. *Nature Materials* **2013**, *12* (6), 584–590. https://doi.org/10.1038/nmat3606.

(37) Xia, Y.; Xue, B.; Qin, M.; Cao, Y.; Li, Y.; Wang, W. Printable Fluorescent Hydrogels Based on Self-Assembling Peptides. *Scientific Reports* **2017**, *7* (1). https://doi.org/10.1038/s41598-017-10162-y.

(38) Allais, M.; Mailley, D.; Hébraud, P.; Ihiawakrim, D.; Ball, V.; Meyer, F.; Hébraud, A.; Schlatter, G. Polymer-Free Electrospinning of Tannic Acid and Cross-Linking in Water for Hybrid Supramolecular Nanofibres. *Nanoscale* **2018**, *10* (19), 9164–9173. https://doi.org/10.1039/C8NR01067F.

(39) Béduer, A.; Vieu, C.; Arnauduc, F.; Sol, J.-C.; Loubinoux, I.; Vaysse, L. Engineering of Adult Human Neural Stem Cells Differentiation through Surface Micropatterning. *Biomaterials* **2012**, *33* (2), 504–514. https://doi.org/10.1016/j.biomaterials.2011.09.073.

(40) Davoust, C.; Plas, B.; Béduer, A.; Demain, B.; Salabert, A.-S.; Sol, J. C.; Vieu, C.; Vaysse, L.; Loubinoux, I. Regenerative Potential of Primary Adult Human Neural Stem Cells on

Micropatterned Bio-Implants Boosts Motor Recovery. *Stem Cell Research & Therapy* **2017**, *8* (1). https://doi.org/10.1186/s13287-017-0702-3.

(41) Zhu, B.; Li, W.; Lewis, R. V.; Segre, C. U.; Wang, R. E-Spun Composite Fibers of Collagen and Dragline Silk Protein: Fiber Mechanics, Biocompatibility, and Application in Stem Cell Differentiation. *Biomacromolecules* **2015**, *16* (1), 202–213. https://doi.org/10.1021/bm501403f.

(42) Omidinia-Anarkoli, A.; Boesveld, S.; Tuvshindorj, U.; Rose, J. C.; Haraszti, T.; De Laporte, L. An Injectable Hybrid Hydrogel with Oriented Short Fibers Induces Unidirectional Growth of Functional Nerve Cells. *Small* **2017**, *13* (36), 1702207. https://doi.org/10.1002/smll.201702207.

(43) Zhang, S.; Greenfield, M. A.; Mata, A.; Palmer, L. C.; Bitton, R.; Mantei, J. R.; Aparicio, C.; de la Cruz, M. O.; Stupp, S. I. A Self-Assembly Pathway to Aligned Monodomain Gels. *Nat Mater* **2010**, *9* (7), 594–601. https://doi.org/10.1038/nmat2778.

(44) Antman-Passig, M.; Levy, S.; Gartenberg, C.; Schori, H.; Shefi, O. Mechanically Oriented 3D Collagen Hydrogel for Directing Neurite Growth. *Tissue Engineering Part A* **2017**, *23* (9–10), 403–414. https://doi.org/10.1089/ten.tea.2016.0185.

(45) Numata, M.; Takigami, Y.; Takayama, M.; Kozawa, T.; Hirose, N. Hierarchical Supramolecular Spinning of Nanofibers in a Microfluidic Channel: Tuning Nanostructures at a Dynamic Interface. *Chem. Eur. J.* **2012**, *18* (41), 13008–13017. https://doi.org/10.1002/chem.201201300.

(46) Fuhrhop, J. H.; Schnieder, P.; Boekema, E.; Wolfgang, H. Lipid Bilayer Fibers from Diastereomeric and Enantiomeric N-Octylaldonamides. *J. Am. Chem. Soc.* **1988**, *110* (9), 2861–2867.

(47) André, C.; Luger, P.; Svenson, S. The Crystal Packing of N-(n-Octyl)-d-Gulonamide Containing Tail-to-Tail Sheets Compared to Its Gluconamide Diastereomer Showing Head-to-Tail Arrangement. *Carbohydr. Res.* **1992**, *230* (1), 31–40. https://doi.org/10.1016/S0008-6215(00)90511-1.

(48) André, C.; Luger, P.; Svenson, S.; Fuhrhop, J.-H. The X-Ray Crystal Structure of N-(1-Octyl)-d-Talonamide and a Consideration of Its Hydrogen-Bonding Scheme. *Carbohydr. Res.* **1993**, *240*, 47–56. https://doi.org/10.1016/0008-6215(93)84170-B.

(49) Zabel, V.; Müller-Fahrnow, A.; Hilgenfeld, R.; Saenger, W.; Pfannemüller, B.; Enkelmann, V.; Welte, W. Amphiphilic Properties of Synthetic Glycolipids Based on Amide Linkages. II. Crystal and Molecular Structure of N-(n-Octyl)-D-Gluconamide, an Amphiphilic Molecule in Head-to-Tail Packing Mode. *Chem. Phys. Lipids* **1986**, *39* (4), 313–327. https://doi.org/10.1016/0009-3084(86)90113-1.

General conclusion and prospects

During the course of this PhD, we have been able to find a novel class of low molecular weight gelators suited for the growth and differentiation of human neural stem cells. These gelators are simple carbohydrate-derived molecules, relatively easy to synthesize at the gram-scale as well as to purify. Out of several molecules from different families, the alkylgalactonamides were found biocompatible. Surprisingly, a one carbon increment in the alkyl chain of the gelators significantly changed the properties of the hydrogels and their resulting biocompatibilities. In particular, the *N*-heptyl-ɒgalactonamide (Gal-C7), gave hydrogels with a structure and properties consistent with its final application. This one was thus chosen to be tested for the culture of human neural stem cells and proved to be a very good support for their growth and differentiation into neurons as well as glial cells after 7 days *in vitro*. Unfortunately, it is difficult to study the hydrogels for more than a week since they rapidly degrade in cell culture conditions. In a second time, we managed to find a technique to inject, extrude and shape the Gal-C7 hydrogels that are normally rather difficult to handle due to synaeresis. This method is based on gelation by solvent exchange and is called wet spinning. Thanks to it, hydrogel filaments composed of 97 wt % of water and 3 wt % of gelator can be obtained with a rather different microscopic structure than when they are in bulk. The composing fibers are much thinner, nearly monodisperse in width and they organize radially inside the filament. Moreover, we were able to adapt the wet spinning process to 3D printing. The hydrogels can thus be deposited on a substrate in a controlled way and several layers can be superimposed to increase the height of the deposits. The adhesion of the gels on the surface is not optimal yet, but this process is very promising for the application of low molecular weight gelators to 3D printing.

The alkylgalactonamide low molecular weight gelators constitute very interesting molecules for the creation of cell culture scaffolds thanks to their peculiar microscopic structure and mechanical properties. Further work should be done to improve their stability in cell culture conditions, especially for their use as *in vivo* implants. Cross-linking could be a solution, but the biggest part of the work here would be to find the right cross-linker which would not impair the native mechanical properties of the hydrogel that are essential for cell growth and differentiation. Another strategy would be to couple the alkylgalactonamide hydrogels to another more permanent material such as a polymer scaffold. Besides, the wet spun filaments should be further tested in cell culture conditions and for this, their stability must first be improved, which can also be achieved with cross-linking. In addition, both bulk and wet-spun gels were studied pure. However, it is possible to play on various parameters. For instance, incorporating additives to the bulk or the wet-spun gels can change their properties. The anisotropic organization of the

hydrogels needs to be further developed to obtain an alignment of the neurons inside the scaffolds. Simply laying the macroscopic wet spun filaments next to one another could represent a potential solution to this matter.

To conclude, this project has been fruitful and very promising in terms of scientific innovations. I learnt a lot during this PhD thanks to its pluridisciplinarity, especially in the biology and technology fields. These past three years have been fascinating in terms of scientific knowledge and they have given me the envy to pursue my career in the field of tissue engineering. As a matter of fact, a lot of work has still to be done to help people live a healthier life and working towards this has been and would be deeply rewarding for me.

Materials and methods

Synthesis of the gelator molecules

The products were used as received without purification. HPLC grade solvents were used for the syntheses and purification. NMR spectra has been recorded on a Brücker 300 MHz spectrometer for routine analysis and a Brücker 500 MHz spectrometer for correlation experiments (2D NMR). The numbering of atoms of the polyol starts at the carbonyl function.

N-heptyl-D-gluconamide (Glu-C7)

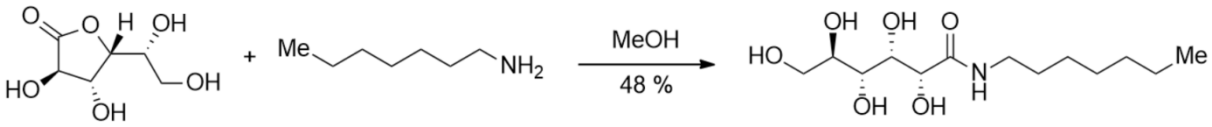

1,4-D-gluconolactone (2 g, 11.2 mmol) and *N*-heptylamine (1.66 mL, 11.2 mmol) were stirred and heated under reflux in MeOH (43 mL) at 70 °C for 3 h. After cooling, the resulting mixture formed a white precipitate that was filtered on a sintered-glass filter (pore n°4) and washed with EtOH. The white solid was then recrystallized in MeOH (21 mL), filtered, washed with MeOH and dried (1.60 g, 48 % yield). ^{1}H NMR (500 MHz, DMSO) δ 7.58 (t, *J* = 5.9 Hz, 1H, NH), 5.33 (d, *J* = 5.1 Hz, 1H, OH), 4.52 (d, *J* = 5.1 Hz, 1H, OH), 4.45 (d, *J* = 5.5 Hz, 1H, OH), 4.37 (d, *J* = 7.2 Hz, 1H, OH), 4.32 (t, *J* = 5.7 Hz, 1H, OH), 3.96 (dd, *J* = 5.0, 3.9 Hz, 1H, CH-O), 3.89 (ddd, *J* = 7.1, 3.8, 2.2 Hz, 1H, CH-O), 3.57 (ddd, *J* = 11.0, 5.8, 2.9 Hz, 1H, CH_2-O), 3.47 (td, *J* = 5.7, 2.8 Hz, 2H, CH-O), 3.36 (dt, *J* = 11.2, 5.7 Hz, 1H, CH_2-O), 3.06 (ddd, *J* = 13.1, 11.0, 7.0 Hz, 2H, CH_2-N), 1.46 – 1.33 (m, 2H, CH_2-C-N), 1.32 – 1.16 (m, 8H, CH_2 alkyl), 0.86 (t, *J* = 7.0 Hz, 3H, CH_3-C).

N-pentyl-D-galactonamide (Gal-C5)

N-pentyl-D-galactonamide has been synthetised by Delphine Bordignon at IMRCP laboratory from pentylamine and D-galactonolactone and purified according to the same protocol as Gal-C6, Gal-C7 and Gal-C8. NMR: same spectrum, except integration = 4H for signal at 1.26 ppm. Yield: 73%. Gelation: A 1%wt solution gels after 48h at 4°C. A 1.5 wt% solution gels after 12h at room temperature. A 2 wt% or a 1.75 wt% solution gels within few minutes at room temperature. Sol-gel transition (DSC): onset: 63°C, peak: 59°C.

N-hexyl-D-galactonamide (Gal-C6)

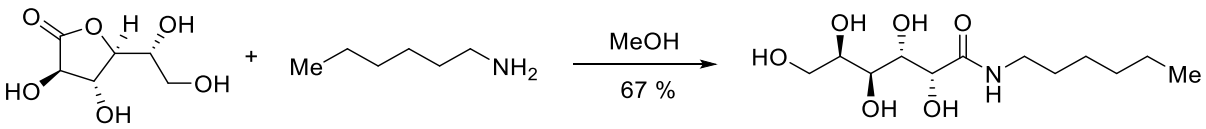

D-galactonic acid, γ-lactone (1 g, 5.6 mmol, Sigma) and hexylamine (0.74 mL, 5.6 mmol, Aldrich) were poured in MeOH (21 mL), stirred and heated under reflux at 70 °C for 3 h. A white precipitate is formed throughout the reaction. After cooling, the solid is filtered through a sintered-glass filter (pore n°4) and washed with MeOH. The solid is washed with EtOH (70 mL) at reflux during 30 min, filtered after cooling. This step is performed twice and the resulting solid is dried under vacuum (1.05 g, 67 % yield). ^{1}H NMR (500 MHz, DMSO): δ(ppm) / J(Hz): 7.52 (t, J=5.5, 1H, NH), 5.05 (d, J=7.2, 1H, OH2), 4.42 (t, J=5.4, 1H, OH6), 4.27 (d, J=8.0, 1H, OH4), 4.15 (d, J=5.5, 1H, OH5), 4.12 (d, J=6.5, 1H, H2), 4.07 (d, J=8.0, 1H, OH3), 3.78 (t, J=8.5, 1H, H4), 3.69 (q, J=5.5, 1H, H5), 3.50-3.25 (m, 3H, H3, H6, H6'), 3.08 (m, 2H, CH_2-NHCO), 1.41 (m, 2H, CH_2-CH_2-NHCO), 1.27 (m, 6H, CH_2 alkyl chain), 0.86 (t, J = 6.8, 3H, CH_3). 13C NMR (125 MHz, DMSO): δ(ppm): 173.3 (CO), 71.0 (C2), 70.8 (C4), 69.8 (C5), 69.2 (C3), 63.2 (C6), 38.3 (CH_2-NHCO), 31.1 (CH_2 chain), 29.3 (CH_2-CH_2-NHCO), 26.1, 22.1 (CH_2 chain), 14.0 (CH3). Elemental analysis: meas. C: 51.85; H: 9.01; N: 4.99. calc. C: 51.60; H: 9.02; N: 5.01. HRMS ($M+H^+$): meas. 280.1748; calc. 280.1760.

N-heptyl-D-galactonamide (Gal-C7)

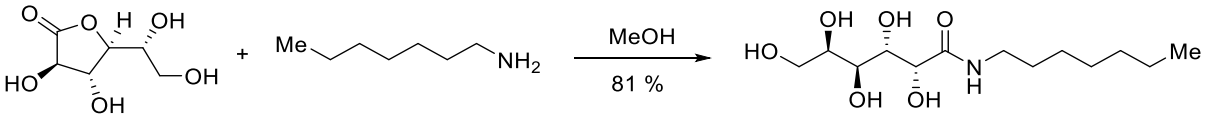

D-galactonic acid, γ-lactone (1 g, 5.6 mmol, Sigma) and heptylamine (0.83 mL, 5.6 mmol, Alfa Aesar) were poured in MeOH (21 mL), stirred and heated under reflux at 70 °C for 3 h. A white precipitate is formed throughout the reaction. After cooling, the solid is filtered through a sintered-glass filter (pore n°4) and washed with EtOH (around 20 mL). The solid is washed with EtOH or MeOH (50 to 70 mL) at reflux during 30 min and filtered after cooling. This step is performed twice and the resulting solid is dried under vacuum (1.33 g, 81 % yield). ^{1}H NMR (300 MHz, DMSO): δ(ppm) / J(Hz): 7.52 (t, J = 5.9, 1H, NH), 5.05 (d, J = 7.2, 1H, OH2), 4.42 (t, J = 5.6, 1H, OH6), 4.27 (d, J = 8.1, 1H, OH4), 4.16 (d, J = 6.5, 1H, OH5), 4.12 (dd, J = 7.3, 1.1, 1H, H2), 4.07 (d, J = 8.1, 1H, OH3), 3.78 (td, J = 8.9, 1.1, 1H, H4), 3.69 (qd, J = 1.1, 6.5, 6.4, 1H, H5), 3.5 – 3.3 (m, 3H, H3, H6, H6'), 3.07 (m, 2H, CH_2-NHCO), 1.41 (m, 2H, CH_2-CH_2-NHCO), 1.25 (m, 8H, CH_2 alkyl chain), 0.86 (t, J = 6.7, 3H, CH_3). Elemental analysis: meas. C: 53.10; H: 9.31; N: 4.81. calc. C: 53.21; H: 9.28; N: 4.78. HRMS ($M+H^+$): meas. 294.1904; calc. 294.1917.

N-octyl-D-galactonamide (Gal-C8)

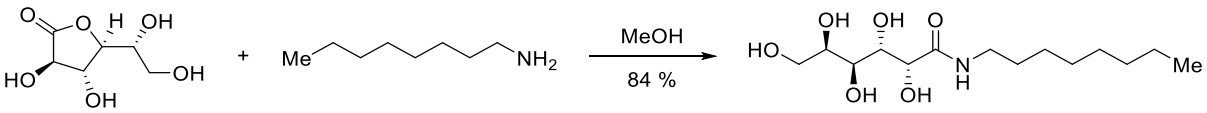

D-galactonic acid, γ-lactone (1,4 g, 7.9 mmol, Sigma) and octylamine (1.3 mL, 7.9 mmol, Fluka) were poured in MeOH (30 mL), stirred and heated under reflux at 70 °C for 2 h. A white precipitate is formed throughout the reaction. After cooling, the solid is filtered through a sintered-glass filter (pore n°4) and washed with EtOH. The solid is washed twice with EtOH (70 mL) and twice with water at reflux. After cooling the suspension is filtered and the resulting solid is dried under vacuum (2.02 g, 84 % yield). ^{1}H NMR (300 MHz, DMSO): δ (ppm) / J (Hz): 7.53 (t, J=5.8, 1H, NH), 5.07 (d, J=7.2, 1H, OH), 4.44 (t, 1H, J=5.4, OH), 4.28 (d, J=8.1, 1H, OH), 4.17 (d, J=6.3, 1H, OH), 4.11 (dd, J=0.9, 7.2 Hz, 1H, H2), 4.05 (d, J=8.4, 1H, OH); 3.78 (td, J=8.7, 0.9, 1H, H4), 3.69 (qd, J = 6.5, 0.6, 1H, H5), 3.5-3.3 (m, 3H, H3, H6, H6'), 3.07 (m, 2H, CH_2-NHCO), 1.40 (m, 2H, CH_2-CH_2-NHCO), 1.24 (m, 10H, CH_2 alkyl chain), 0.86 (t, J = 6.3, 3H, CH_3). Elemental analysis: meas. C: 55.02; H: 9.63; N: 4.58. calc. C: 54.69; H: 9.51; N: 4.56. HRMS ($M+H^+$): meas. 308.2062; calc. 308.2073.

N-nonyl-D-galactonamide (Gal-C9)

N-nonyl-D-galactonamide has been synthetised by Delphine Bordignon at IMRCP laboratory from nonylamine and D-galactonolactone and purified according to the same protocol as Gal-C6, Gal-C7 and Gal-C8. NMR: same spectrum, except integration = 12H for signal at 1.26 ppm. Yield: 84%. Gelation: Upon cooling, a hot solution at 0.5%wt forms fragments of gels floating at the surface of the solution.

N-dodecanoyl-D-glucamine (Gluca-C12)

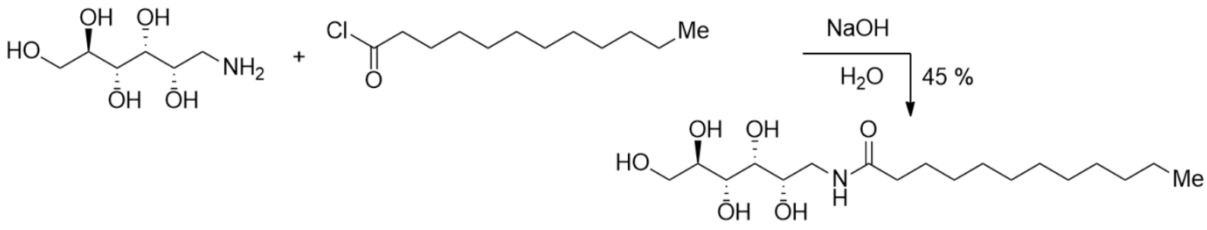

D-glucamine (2 g, 11 mmol) was dissolved in water (13 mL) and stirred mechanically. Lauroyl chloride (1.95 mL, 8.2 mmol) and NaOH solution (0.44 g in approximately 1 mL H_2O) were carefully added in turn to the reactants under stirring. A white solid was formed throughout the reaction and the reaction mixture was kept stirred for 5 min. The resulting solid was then filtered

through a sintered-glass filter (pore n°4) and washed with water (approximately 150 mL). The product was recrystallized in EtOH (15 mL), some of the solvent was removed under vacuum and the rest of the filtrate was placed in the fridge overnight. The white solid obtained was then filtered, washed with some EtOH and dried under vacuum (1.35 g, 45 % yield).

Alternative synthesis: D-glucamine (1 eq.), lauric acid (1 eq.), NHS (1 eq.) and EDC (1 eq.) were stirred together in 8.5 mL of DMF in an ice bath for 1h and then at room temperature for 12h. After evaporation of the DMF, the product was recrystallized twice in methanol. ^{1}H NMR (500 MHz, DMSO) δ 7.73 – 7.61 (m, *J* = 11.3 Hz, 1H, NH), 3.60 – 3.55 (m, 2H, H2, H6b), 3.55 – 3.53 (m, 1H, H3), 3.46 (ddd, *J* = 7.9, 6.0, 3.4 Hz, 1H, H4), 3.40 (dd, *J* = 8.1, 2.2 Hz, 1H, H5), 3.36 (dd, *J* = 12.7, 6.8 Hz, 1H, H6a), 3.25 (ddd, *J* = 13.5, 6.0, 4.8 Hz, 1H, H1a), 3.05 – 2.96 (m, 1H, H1b), 2.06 (dd, *J* = 14.0, 6.7 Hz, 2H, H8), 1.47 (dd, *J* = 14.2, 7.1 Hz, 2H, H9), 1.33 – 1.15 (m, 16H, H10 to 17), 0.90 – 0.80 (m, 3H, H18).

N-methyl-*N*-dodecanoyl-D-glucamine (Me-Gluca-C12)

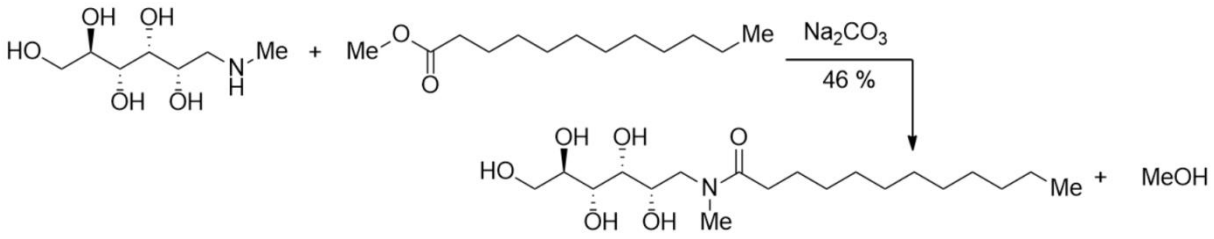

N-methyl-D-glucamine (3 g, 15.4 mmol) and methyl laurate (3.8 mL, 15.4 mmol) were stirred and heated at 145 °C under argon flow. When the reaction mixture reached 145 °C, Na_2CO_3 (0.16 g, 1.54 mmol) was added and vacuum was turned on. The mixture was kept under stirring and under vacuum for 30 min. After cooling, an orange solid was obtained which was first recrystallized with EtOH (35 mL). The resulting mixture was placed at 4 °C overnight and a white precipitate was formed. The white solid was filtrated, washed with cold EtOH and dried under vacuum (2.68 g, 46 % yield). On the ^{1}H NMR spectrum, two rotamers of the molecule are present (noted a and b). ^{1}H NMR (500 MHz, MeOD) δ 3.96 (m, J = 4.1 Hz, 1H), 3.82 – 3.55 (m, 6H, CH_2a-NH and others), 3.46 – 3.34 (m, 1H, CH_2b-NH), 3.14 (d, J = 1.3 Hz, 1.5H, N-CH_3a), 2.96 (d, J = 1.2 Hz, 1.4H, N-CH_3b), 2.47 (t, J = 7.5 Hz, 1H, CO-CH_2a), 2.39 (t, J = 7.6 Hz, 1H, CO-CH_2b), 1.59 (d, J = 6.2 Hz, 2H, CO-C-CH_2), 1.29 (s, 17H, CH_2 alkyl chain), 0.90 (dd, J = 6.9, 5.7 Hz, 3H, CH_3).

N-methyl-*N*-tetradecanoyl-D-glucamine (Me-Gluca-C14)

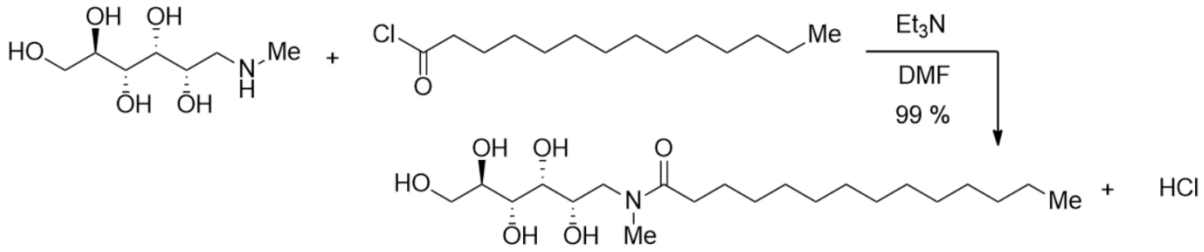

N-methyl-D-glucamine (2 g, 10.2 mmol), mirystoyl chloride (2.77 mL, 10.2 mmol) and Et_3N (1.65 mL, 12.24 mmol) are dissolved in dry DMF (20 mL) and kept stirred at room temperature for 1 day. DMF and Et_3N are removed under vacuum. The resulting solid is first recrystallized with a mixture of EtOAc and EtOH (respectively 25 mL and 6 mL), filtered and washed. A second recrystallization in carried out this time in water (210 mL). A white precipitate is obtained that is then filtered, washed and dried under vacuum (4.10 g, 99 % yield). On the ^1H NMR spectrum, two rotamers of the molecule are present. ^1H NMR (300 MHz, DMSO) δ 4.87 (d, *J* = 5.1 Hz, 1H), 4.72 (d, *J* = 5.1 Hz, 1H), 4.49 (dd, *J* = 11.3, 5.1 Hz, 1H), 4.44 – 4.25 (m, 3H), 3.82 – 3.67 (m, 1H), 3.54 (d, *J* = 5.2 Hz, 2H), 2.99 (s, ⅖H, CH_3-N), 2.80 (s, ⅗H, CH_3-N), 2.29 (dt, *J* = 14.3, 7.4 Hz, 2H, CH_2-N), 1.45 (s, 2H, CH_2-C-CO), 1.20 (d, *J* = 19.2 Hz, 20H, CH_2 alkyl chain), 0.85 (t, *J* = 6.6 Hz, 3H, CH_3).

Palmitoyl-glycine-D-glucamide (Jap-C16)

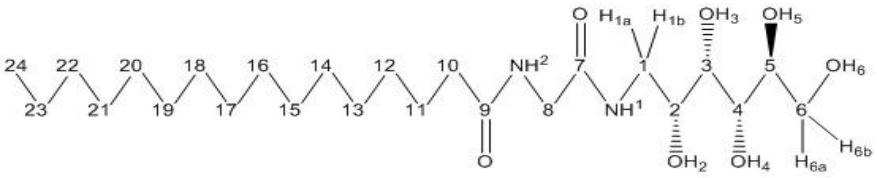

This molecule has been synthesized by Delphine Bordignon at IMRCP laboratory, following the protocol described by Ohsedo *et al.*[f]

D-glucamine (1.75 mmol), palmitoyl-glycine (1.60 mmol), NHS (1.75 mmol) and EDC (1.75 mmol) were stirred together in 8.5 ml of DMF in an ice bath for 1h and then at room temperature for 12h. After evaporation of the DMF, the product was recrystallized twice in MeOH.

Gelation: A white gel is obtained from a 1 wt % solution in water.

DSC: No noticeable transition from 10 to 90°C with a 1 wt % gel. By visual assessment, the gel seems to form above 90°C.

[f] Ohsedo, Y.; Oono, M.; Saruhashi, K.; Watanabe, H. N-Alkylamido-D-Glucamine-Based Gelators for the Generation of Thixotropic Gels. *RSC Adv.* **2014**, *4* (89), 48554–48558.

^{1}H NMR (500 MHz, DMSO) δ 7.98 (t, *J* = 5.8 Hz, 1H, NH^{2}), 7.66 (t, *J* = 5.6 Hz, 1H, NH^{1}), 4.74 (d, *J* = 4.7 Hz, 1H, OH_2), 4.45 (d, *J* = 5.7 Hz, 1H, OH_5), 4.36 (d, *J* = 6.2 Hz, 1H, OH_4), 4.32 (t, *J* = 5.7 Hz, 1H, OH_6), 4.28 (d, *J* = 6.4 Hz, 1H, OH_3), 3.65 (d, *J* = 6.6 Hz, 2H, H_8), 3.63 – 3.52 (m, 3H, H_2, H_{6a}, H_3), 3.47 (dtd, *J* = 9.2, 5.8, 3.4 Hz, 1H, H_5), 3.42 – 3.34 (m, 2H, H_4, H_{6b}), 3.31 – 3.25 (m, 1H, H_{1a}), 3.02 (ddd, J = 13.1, 7.7, 5.2 Hz, 1H, H_{1b}), 2.10 (dd, J = 13.1, 5.4 Hz, 2H, H_{10}), 1.53 – 1.41 (m, 2H, H_{11}), 1.33 – 1.15 (m, 24H, $H_{12 à 23}$), 0.85 (t, J = 7.0 Hz, 3H, H_{24}).

^{1}H NMR (500 MHz, DMSO+ D_2O) δ 3.65 (s, 1H, H_8), 3.63 – 3.52 (m, 3H, H_2, H_{6a}, H_3), 3.47 (ddd, J = 7.9, 6.0, 3.5 Hz, 1H, H_5), 3.38 (ddd, J = 14.4, 8.1, 4.0 Hz, 2H, H_4, H_{6b}), 3.28 (dd, J = 13.5, 4.5 Hz, 1H, H_{1a}), 3.03 (dd, J = 13.5, 7.7 Hz, 1H, H_{1b}), 2.10 (dd, J = 14.3, 6.6 Hz, 2H, H_{10}), 1.54 – 1.42 (m, 2H, H_{11}), 1.23 (s, 24H, $H_{12 à 23}$), 0.84 (t, J = 7.0 Hz, 3H, H_{24}).

^{13}C NMR (126 MHz, DMSO) δ 172.99 (s, C_9), 169.64 (s, C_7), 72.32 (s, C_4), 72.05 (s, C_2), 71.97 (s, C_5), 70.21 (s,C_3), 63.79 (s,C_6), 42.47 (s,C_8), 42.40 (s, C_1), 35.66 (s, C_{10}), 31.76 (s, C chain), 29.52 (s, C chain), 29.48 (s, C chain), 29.42 (s, C chain), 29.30 (s, C chain), 29.18 (s, C chain), 29.17 (s, C chain), 25.61 (s, C_{11}), 22.56 (s, C chain), 14.43 (s, C_{24}).

Hydrogel preparation

For all the gelator molecules, their corresponding hydrogels were obtained simply by dissolving the solid in pure water at high temperature (between 100 and 120 °C) and by cooling down the solution to room temperature. For Gluca-C12 however, 7 wt % of hexafluoropropanol was first added to a volume of water and the gelator was then dissolved in this water-HFP mix at 100 °C.

Controlled cooling rate of the alkylgalactonamide gels

A suspension of the Gal-Cn powder in pure water was prepared in a sealed vial (1 wt% for Gal-C6; 0.45 wt% for Gal-C7 and 0,5 wt% for Gal-C8. Caution! Take a 10 mL vial for a maximum of 2 mL solution). It was heated at resp. 100°C, 110°C or 120 °C using heating blocks, until complete dissolution. The resulting hot solution was dispensed in the wells of a cell culture plate heated at 100 °C: 400 µL/well for 48-well plates (0.95 cm^2) or 300 µL for an 8-well chamber slide (0.70 cm^2), providing a gel of ≈3 mm height (caution! Pressure must be released with a needle before opening the sealed hot vials). The wells were sealed with a sealing foil to avoid evaporation. The culture plate was introduced in a programmable oven (Vötsch VT 4004). The temperature of the sample was set following a three-step workflow: 5 min at 100 °C, a temperature linear ramp from

100 °C to 25 °C in either 15, 30, 60 or 90 min and finally 10 min at 25 °C. For culture chamber slides, a clamp was used to ensure a good sealing of the chambers.

Gels prepared without controlled cooling ("0-min" cooled gels):

The gel solution was prepared as described above, and the hot solution was dispensed directly in the wells of a culture plate at room temperature and allowed to stand for 1 hour before characterization.

Differential Scanning Calorimetry

DSC has been performed on the "0 min"-cooled gels, in a Mettler Toledo HSS8 calorimeter. The hot solution of gelator (≈ 80 mg) is introduced in a sealed stainless-steel pan and allowed to cool at room temperature. Three cycles from 10°C to 120°C at 10°C/min or 3°C/min under nitrogen were recorded.

Solubility of the alkylgalactonamides

Solubility has been measured by thermogravimetric analysis. The gels were prepared as described in the experimental part. After 21h, the aqueous phase was expelled by compressing the gel and filtrated (0.22 µm filter). Thermogravimetric analysis was performed on aliquots of around 50 mg. The temperature program was the following: switch the gas to nitrogen at 100.0 ml/min, heat from 35.00 °C to 300.00 °C at 10.00 °C/min. The water/gelator ratio was then calculated according to the results.

Surface tension measurements of the alkylgalactonamides

Hydrogels of the different alkylgalactonamides were prepared at their respective concentrations and later crushed to expel the water they contained. This resulting water was then retrieved in a syringe and filtered thanks to a 0.2 µm CHROMAFIL syringe filter. Pendant-drop surface tension measurements were then performed with these residual waters (Krüss DSA10 drop shape analyzer) with a 20G blunt-tip needle on a 1 ml Terumo syringe at room temperature. At least four measurements were performed for each sample and the surface activity was automatically calculated by the DSA10 software. Pure water was used as a control measurement.

Morphological characterization of the gels

Optical transmission microscopy

The gels prepared in the 48-well plates, in triplicate for each cooling condition, were observed directly by optical microscopy (inverted, bright field, ×10), at the end of the cooling program on undisturbed gels. Two pictures were taken per well and per gel at two places remote from each other. It resulted in 6 pictures per gel and per rate.

The nucleation points were counted manually using ImageJ counter on each photo. The mean of the nucleation sites per mm^2 was calculated for the 6 pictures and reported as a function of the cooling time.

The fiber lengths analysis was done on the same six pictures over a fixed area of 0.166 mm^2. The total number of counted fibers is different for each gel since it depends on the gelation but was around 25-90 fibers on each field. All the fiber segments visible on the images were traced semi-manually using the ImageJ plugin NeuronJ and their lengths were measured. It provided the apparent lengths of fibers exceeding the threshold of 4 µm in length, and below 550 µm (max of the observation field) and large enough to be visible. The results are represented as a box chart, giving the full extent of the fibers measured.

Transmission Electronic Microscopy (TEM)

In two different wells prepared with or without a controlled cooling, a grid (carbon film on copper, 200 mesh) is inserted within the gel for 10 minutes and removed. This sampling may have taken off mainly the unbound and broken fibers of the gels and for this reason, may not be completely representative of the whole gel. The grids are observed without any staining using a Hitachi HT7700 transmission electron microscope operating at 80kV. The widths of all the visible fibers on the images were measured manually using ImageJ. The total number of counted fibers was also different for each gel and was counted up to 450-1700 fibers per gel. The results are represented as a box chart.

Scanning electron microscopy (Cryo-SEM)

One drop of gel was deposited on the cryo-SEM cane and frozen at -220°C in liquid nitrogen. The frozen sample was fractured at -145°C under vacuum in the cryo-transfer system chamber (Quorum PP3000T). The sublimation was performed at -95°C for 30 min. The sample was metalized with Pd for 60s and introduced in the microscope chamber. The temperature was kept at -145°C. Images were recorded with a FEG FEI Quanta 250 microscope, at 5kV for the acceleration voltage. Some of them with a suitable orientation (around 10 to 20 measures/gel) provided a rough estimation of the fibers thickness. The statistical analysis on these few measures provided: Gal-C8: 136 ± 81 nm; Gal-C7: 157 ± 97 nm; Gal-C6: 105 ± 43 nm, giving the following ranges of thickness: Gal-C8 and Gal-C7: 150 ± 100 nm and Gal-C6: 100 ± 50 nm.

Small Angle X-ray Scattering (SAXS)

Scattering measurements have been performed on 1 wt % Gal-C6; 0.45 wt % Gal-C7 and 0.5 wt % Gal-C8 90 min cooled gels with a XEUSS 2.0 SAXS/WAXS laboratory beamline equipped with a Cu source (E = 8 keV) and a pixel detector PILATUS3 1 M from Detrics. Two sample-to-detector distances have been used: 0.387 m (beam size 0.8 mm × 0.8 mm) and 2.5 m (beam size 0.5 mm × 0.5 mm) allowing a q range between 0.0037 $Å^{-1}$ and 1.5 $Å^{-1}$. Samples have been mounted on a sample holder for gels. Measurements have been carried out at 25 °C.

Rheology

Rheograms were recorded with a rheometer AR1000 (TA Instruments), equipped with rough plates (2 cm diameter, Rheonova). The gap was set at 1.5mm and the temperature was 37°C. The gel was prepared in situ within the geometry: the hot solution was injected between the plates and the measurement started after 15 minutes of setting. By preparing the gels directly within the rheometer gap, the gels kept a good contact with the plates and did not undergo synaeresis during the measurement at low sinusoidal strain. The gels were fast-cooled: slow cooling was not possible because of the water evaporation in the open rheometer geometry. To avoid the drying of the gel during the setting time and measurement, a ring of water droplets and a cover were placed around the geometry. After opening the geometry, the gels were homogeneous and white throughout the surfaces, but denser points corresponding to nucleation points were however visible. The elastic modulus G' and viscous modulus G'' were recorded as a function of the frequency from 10 to 0.01 Hz, with a sinusoidal strain amplitude of 0,2%. The linear viscoelastic region was determined by a strain sweep from 0.5 to 10%.

Uniaxial compression tests

Cylinders of gels were prepared in plastic molds (half cylinders, diameter 14 mm, height 20 mm, sealed with wax and metal rings). The hot solutions (1wt% for Gal-C6; 0.45wt% for Gal-C7; 0.5wt% for Gal-C8) were dispensed in pre-heated molds. They were closed with a sealing foil and then cooled from 100°C to 25°C within 90 minutes. After cooling, the gels were gently removed from the molds, measured with a vernier calliper. All samples underwent uniaxial compression tests with Bose Electroforce 3100 mechanical testing machine equipped with a 20N loading cell. Two compressive rates were applied: 5mm/s and 0.1 mm/s, up to 10% strain. During compression, droplets of water are expelled from the gel cylinder that go back into the gel upon unloading. All tests have been made in triplicate. The curves from the first loading were fitted with polynomes. The first order terms of the polynomes were extracted and the mean of the three triplicates provided the initial modulus "Y_0" (first regime). The second regime modulus was determined from the tangent to the curves at higher strain (typically from 0.05 to 0.09).

Cell culture, cell viability assay and MTT based cell growth determination

The neuronal cell line (Neuro2A, ATCC) was cultured in Dulbecco's modified Eagle medium (DMEM) supplemented with 10% fetal bovine serum (FBS), and 1% penicillin-streptomycin at 37°C in a humidified atmosphere containing 5% CO2.

For the cell viability assay, 300 µl of the different gel compounds were prepared in an 8-well chamber slide (Lab-Tek, Nunc). After complete gelation, two extensive washes of several hours (4-5h and overnight) with 400 µl of supplemented medium were performed. 30000 cells per well were seeded and cultured for 7 days. Fluorescent live–dead staining assay (Molecular probe) was used, according to the manufacturer instructions, to visualize the proportion of viable cells in green (calcein AM) and non-viable cells in red (ethidium homodimer-1). The samples were observed using a Zeiss Axioskop microscope equipped with a Cool SNAPfx camera (Photometrics). Each experiment was done at least in triplicate. Cell viability was evaluated by cell counting (live cells in green and dead cells in red). Three different fields for three independent experiments were analyzed for each gel condition using Image J Cell Counter. The percentage of cell viability was evaluated in each condition and results were expressed as the average +/- SD).

For cell growth determination, 400 µl of the different compounds were allowed to gel in each well of a 48 well plates (CellStar, Greiner Bio-One). After complete gelation with or without controlled

cooling rate, two extensive washes of several hours (4-5h and overnight) with 600 µl of supplemented medium were performed. Neuro2A cells were then seeded at a density of 35 000 or 70 000 per well, in 350 µl of DMEM, and cultured for 1 or 4 days without changing medium to avoid cell lost. As controls, 35 000 cells were directly seeded on the plastic well (2D control) corresponding to a culture which reaches confluence after 4 days. MTT based colorimetric test quantification (Sigma-Aldrich, France) were adapted for cell culture on gel. Briefly, after the determined culture period (1 or 4 days), 75 µl of "MTT SOLUTION" (10 % of the total volume corresponding at the gel with the culture medium) were added to each well and allowed to react for 4 hours at 37 °C. The culture medium was then carefully removed and 400 µl of "MTT SOLVENT" were added in the wells, which enabled the gels to dissolve as well, to ensure a confident reading of the optical density. The absorbance was then measured spectrophotometrically at 570 nm. The background absorbance was measured at 690 nm. The absorbance of the gel alone was then subtracted to the obtained optical densities. Values were normalized to the 2D control. Three independent experiments were at least performed for each gel sample tested.

Neuro2A-GFP and 3D confocal study

Neuro2A cell line stably expressing the GFP protein were generated by transduction of the pLVB-CpGfree-hCMV/hFerL-GFP lentiviral vector (generous gift from InvivoGen) using 1.0 × 106 infective units/ml with polybrene (4µg/ml) for 1.0 × 105 Neuro2A cell seeded in a 24 well plate. Positive clones were selected by subculture using a fluorescent microscope. This part of the work has been done by Laurence Vaysse at ToNIC laboratory (INSERM UMR1214).

For 3D confocal microscopy observations, Neuro2A-GFP cells were seeded on a gel prepared in an 8-well chamber slide with controlled cooling rate as describe above (90 minutes). In some experiments, a solution of laminin (10µg/mL) was added during the last washing step for gel coating. However, no clear difference was observed between gels with (Figure 6) or without laminin (SI-8). After 5 days of culture, samples were fixed by addition of 4% paraformaldehyde solution for 30 min, washed with PBS, and then observed with a Leica SP8 confocal microscope. Gel fibers were imaged in parallel by confocal reflection microscopy. Images were captured using a x25 lens. 3D images were then reconstructed using Imaris Software.

Human neural stem cell culture

The following experiments: hNSC culture, hNSC immunostaining and statistical analysis have been done by Laurence Vaysse at ToNIC laboratory (INSERM UMR1214).

Biopsies from the temporal lobe and SVZ were obtained from individuals undergoing neurosurgery for epilepsy treatment (CHU Purpan, Service de Neurochirurgie, Prof. J.-C. Sol; n =3). All procedures were performed with informed patient consent, in accordance with our local human ethics committee (Comité de Protection des Personnes Sud-Ouest Outre Mer Toulouse I) and with institutional guidelines on human tissue handling and use. To isolate potential neural progenitor/stem cells, cell suspensions were rapidly obtained by tissue enzymatic digestion with trypsin (65 µg/ml, Sigma-Aldrich), hyaluronidase (1.4 mg/ml, Sigma Aldrich) and kyruneic acid (0.2 mg/ml, Sigma-Aldrich) in DMEM/F12 with 5% glucose as already described 51. Cells were then amplified as neurospheres in non-adherent conditions in DMEM/F12 medium containing B27 supplements (Gibco, Life technology), EGF (20ng/ml, Gibco, Life technology), bFGF (20ng/ml, Gibco, Life technology) and 1% penicillin-streptomycin. At the end of the amplification phase, the neurospheres were dissociated to obtain single-cell suspensions 51 and seeded on Gal-C7 hydrogel in a 8 well chamber slide (Millipore) at a cell density of 75000 cells/well in DMEM/F12 medium with B27 supplements and NGF (20ng/ml, Peprotech). Cell viability assay was realized after 7 days of culture as described above. Alternatively, immunostaining experiment was performed to study stem cell differentiation. Gels were pre-coated or not with laminin (10µg/ml) but in this case also, laminin does not seem also to impact cell behavior on the gel.

hNSC immunostaining

After 7 days of culture, samples were fixed by addition of 4% paraformaldehyde solution. To preserve the structure during the immunostaining procedure, samples (Gal-C7 gel with hNSCs) were embedded in acrylamide gel with a protocol adapted from "CLARITY". A fresh solution containing: 0.6 mL of PBS x10, 4.65 mL of pure water, 0.6 mL of a 40% acrylamide solution and 0.15 mL of a 2% bis-acrylamide solution and 15 mg VA-044 (2,2'-Azobis[2-(2-imidazolin-2-yl)propane] dihydrochloride) was prepared in a sealed vial at 0°C and flushed with argon for 30 min. After removing the supernatant, 300 µL of the acrylamide solution was added in each well and kept for 45 min at 4°C. This step was performed three times. The supernatant was again removed and the chamber slide was flushed with argon for 30 min at room temperature, then heated under argon at 43°C for 2 hours. After polymerization, PBS was added in each well and samples kept at 4°C. For immunostaining procedure, the samples were washed 3 times for 45 min

with 300 µl of PB per well. The samples were then permeabilized with 0.1% Triton X-100 (Sigma-Aldrich) in PB for 30 min at room temperature, washed twice for 45 min with PB, and incubated with a blocking solution (3% goat serum, DAKO) for 1h at room temperature under shacking. Samples were then allowed to react with primary antibodies using the appropriate dilution of mouse anti-Tuj1 (1:500, Sigma-Aldrich) or rabbit anti-GFAP (1:1000, DAKO), for 24 hours at room temperature under shacking. After PB washes (twice, 45 min), the appropriate secondary antibody (Alexa Fluor 488 anti-Mouse or –Rabbit, Molecular Probes), was incubated for 5h under shaking. After 3 additional extensive PB washes, the samples were observed by confocal microscopy as described above.

Statistical analyses

MTT data and Nucleation point data are presented as means ± standard deviations. Statistical analyses were performed, with GraphPad Prism v7.0 software, using a two-way ANOVA corrected for multiple comparisons by Bonferroni's test. For length and width fibers, data are represented as the median with interquartile ranges [first quartile: Q1; third quartile: Q3] for each group. Data were analyzed using the nonparametric Kruskal Wallis test followed by the Dunn's multiple comparisons test as post hoc analyses. Results were considered significant for corrected p values below 0.05 and are indicated by asterisks.

Direct extrusion of the hydrogels

Gelation of the alkylgalactonamides under a strain

PTFE tube

A hot 1 wt % Gal-C6 solution in water was put in a plastic cone, linked to a PTFE tube of various internal diameters (800, 560 or 300 µm) and various lengths (160 or 80 cm) and pneumatic pressure was applied to make the liquid flow (Fluigent MFCS-EZ 1bar, 30 or 100 mbar applied). The PTFE tube as well as the cone were plunged into a 95 °C water bath and the tube also went sometimes in a water bath at room temperature.

PDMS microfluidic chip

Hot solutions of 1 wt % Gal-C6 or 0.45 wt % Gal-C7 were dispensed at room temperature inside the channels of a PDMS chip thanks to a peristatic pump with controllable flow rate. The used chip is detachable: iron powder allows it to be held by magnets on a glass slide. The six channels on it are of the same dimensions: 50 mm in length, 2 mm in width and 400 µm in height. Several flow rates were applied to flow the gelator solutions inside the channels (from 5 to 50 µl/s).

Extrusion of Gluca-C12 and Jap-C16

1 ml of hot solutions of the gelators in water (1 wt % for gal-C6, 0.45 wt % for Gal-C7, 2 wt % for Gluca-C12 and 1 wt % for Jap-C16, no hexafluoropropanol used here for Gluca-C12) were sucked up in a syringe without a needle and the gelation occurred in the syringes after being rested at room temperature for 2 hours. Passed this delay, a needle was adapted on the syringe (18G or 20G), itself adapted on a syringe pump (CETONI neMESYS 290N). The extrusion conditions were controlled by the neMESYS UserInterface software and the resulting gels were manually retrieved on glass slides. The applied flow rates varied between 100 and 6000 µl/min.

Study of the influence of the heating conditions on Jap-C16 hydrogels

An already formed 1 wt % Jap-C16 hydrogel was melted at 110 °C until obtaining a limpid solution. This one was sucked up in a needle-less syringe and rested until full gelation. Another syringe was prepared following the same protocol, but this time after the hot gelator solution started to cloud again while remaining liquid. After full gelation into the syringes, the hydrogels were manually extruded (without a needle) on glass slides. The hydrogels were then soaked in a 10 µg/ml fluorescent poly-L-lysine (FITC poly-L-lysine, Sigma-Aldrich) solution in water for 15 min and then rinsed with phosphate buffer. The resulting hydrogels were then observed by fluorescence microscopy (Zeiss inverted microscope, AxioObserver A1, ×10).

Wet spinning of N-heptyl-D-galactonamide

Extrusion of the hydrogel filaments

To prepare the dope solutions of *N*-heptyl-D-galactonamide, the molecule was dissolved at room temperature under sonication at different mass concentrations (2.5, 4 or 5 wt %) into dimethyl sulfoxide (purchased from Fisher, 99 %, non-anhydrous).

The solutions were then directly extruded in a bath of ultrapure water (200 mL, resulting into a bath height of approximately 8 cm) at room temperature (between 21 and 23 °C) with a syringe pump (CETONI neMESYS 290N), controlled by the neMESYS UserInterface software. Different gauges of blunt-tip needles, flow rates and concentrations of the solution were used. The videos acquired during these experiments were acquired with a DinoLite digital microscope (model AM4013MTL-FVW) under white light.

Estimation of the jet velocity

For the speed analyses, 15 µm diameter fluorescent beads (Thermo Scientific, cat. n° 35-4) were used. The beads were directly diluted in DMSO to reach a concentration suitable for speed analysis (rather low to be able to distinguish the beads with the naked eye on the videos). This resulting solution was then mixed in an already-prepared solution of Gal-C7 in DMSO at 2.5 wt %. The resulting Gal-C7 concentration thus fell to 2.3 wt %. This last solution was then extruded at 5 or 10 µl/min and the DMSO jet was filmed with a DinoLite digital microscope suited for fluorescence acquisitions (model AM4115T-GFBW, excitation at 480 nm and emission filter at 510 nm). Three experiments have been performed three times for each flow rate. The velocity was analyzed thanks to the ManualTracking plugin from ImageJ. For 10 µl/min, a total of 23 beads have been tracked throughout the three videos and 30 beads for 5 µl/min. To obtain the jet diameter in these conditions, several frames of the acquired videos were superimposed, while being careful of taking ones on which the jet was stable. Three different superimpositions at different times were done. The resulting pictures then allowed the measurement of diameters, which were then plotted along the Z axis. The error bars are an estimation of the error made when measuring the diameters (the value of two pixels on the picture, namely 40 µm). The error on the predicted velocitiy was calculated with the formula: $\Delta v = v(\Delta Q/Q + \Delta d/d)$, with v the calculated velocity, Q the applied flow rate, ΔQ the error on the flow rate (=0.00002 mm^3/s because the minimal flow that can be applied by the syringe pump is of 1 nl/min with a 1 ml syringe), d the jet diameter and Δd the error on the measured diameter (40 µm).

Measurements of the jet and filament diameters

The diameters of the wet spun filaments were measured by transmission optical microscopy (see protocol below). At least three pictures we taken for each condition and the mean and standard error of the diameters (measured with ImageJ) were calculated.

Concerning the jet diameters, these ones were measured on several snapshots from videos of the extrusion. These videos were acquired with a DinoLite digital microscope (model AM4013MTL-FVW) under white light and with maximum magnification. The extrusions were recorded during approximately 2 min, and snapshots of the videos were further taken around every 30 s. The jet diameters were then measured on these snapshots with ImageJ, at a distance of 2.3 mm after the extremity of the needle (maximum distance considering the picture size). The mean and standard deviation of the measured diameters were then calculated for each condition.

Characterization of the scaffolds

Optical transmission microscopy

For microscopic observations, the resulting gel filaments were retrieved thanks to a sieve in which a round microscope slide was placed and plunged into the bath. The wet spun filaments were then analyzed by optical transmission microscopy on an Olympus inverted microscope (bright field, ×10). For diameters measurements, at least three pictures at different points of the filament were taken and analyzed with ImageJ. The resulting mean and the standard deviation of the diameters were calculated.

Cryo-SEM observations

Gel filaments were prepared according to the wet sinning previously described and retrieved thanks to a sieve placed in the coagulation bath. A piece of gel filament was then deposited on the cryo-SEM cane and frozen at −220 °C in liquid nitrogen. The frozen sample was fractured at −145 °C under vacuum in the cryo-transfer system chamber (Quorum PP3000T). The sublimation was performed at −95 °C for 30 min. The sample was metalized with Pd for 60 s and introduced in the microscope chamber. The temperature was kept at −145 °C. Images were recorded with a FEG FEI Quanta 250 microscope, at 5 kV for the acceleration voltage. Some of them with a suitable magnification and orientation (around 10 to 20 measures/ gel) provided a rough estimation of the fibers thickness.

Thermo-gravimetric analysis

Gal-C7 gel filaments were prepared by wet spinning: they were extruded at 50 µl/min with a 4 wt % solution of Gal-C7 in DMSO and a 20G blunt-tip needle. A sieve was placed at the bottom of the water tank to retrieve the formed filaments. During transportation, the filaments were kept in the sieve in a very small volume of water. A few milligrams of filaments were then placed in a crucible

and inserted into the oven for the analysis. The temperature program was the following: switch the gas to nitrogen at 100.0 ml/min, heat from 30.00°C to 300.00°C at 1.00°C/min, then heat from 300.00°C to 600.00°C at 10.00°C/min and hold for 10.0 min at 600.00°C.

Study of the lifetime of the filaments in solutions

30 µl of Gal-C7 in DMSO (2.5 or 4 wt % solutions) were extruded in approximately 200 ml of ultrapure water (~ 8 cm of fall) and the resulting filaments were retrieved thanks to a glass slide placed in a sieve at the bottom of the water tank. After spinning, the glass slide was rapidly put in a well of a 12-well cell culture plate and 1 ml of the different solutions (ultrapure water, PBS or DMEM supplemented with 10% FBS, and 1% penicillin-streptomycin) was added inside the well. In certain cases, another glass slide was put on top of the liquid while being careful to not let it sink in the liquid (an air bubble keeps the slide from sinking). The plate was then kept either at room temperature or at 37 °C in a stove in the case of trials with DMEM. The filaments were then observed every day by optical microscopy (upright Olympus microscope, bright field, ×5 or ×10). At least five different pictures were taken for each well. The resulting fibers' diameters were then manually measured with ImageJ software and the mean and standard deviation were calculated for each day.

Small Angle X-ray Scattering (SAXS) on the filaments and crystals

Scattering measurements have been performed on freshly wet-spun gels of Gal-C7 obtained from a 5 wt % DMSO solution extruded at 25 µl/min. Crystals were obtained from wet spun filaments obtained from a 2.5 wt % DMSO solution extruded at 25 µl/min aged for two weeks. XEUSS 2.0 SAXS/WAXS laboratory beamline equipped with a Cu source (E = 8 keV) and a pixel detector PILATUS3 1 M from Detrics has been used. The sample-to-detector distance was 0.387 m (beam size 0.8 mm × 0.8 mm) allowing a q range between 0.022 $Å^{-1}$ and 1.6 $Å^{-1}$. Samples have been mounted on a sample holder for gels with a kapton window. Measurements have been carried out at 25 °C.

Crystallographic data collection and structure determination for Gal-C7

The data was collected at low temperature (193K) on a Bruker-AXS APEX II QUAZAR diffractometer equipped with a 30W air-cooled microfocus source, using MoKα radiation (λ = 0.71073Å). Phi- and omega- scans were used. The data were integrated with SAINT, and an

empirical absorption correction with SADABS was applied[g]. The structure was solved by direct methods (ShelXT)[h] and refined using the least-squares method on F^2 (ShelXL)[i]. All non-H atoms were refined with anisotropic displacement parameters. The H atoms were refined isotropically at calculated positions using a riding model, excepted on oxygen and nitrogen atoms. These H atoms were located by difference Fourier map. Selected data for Gal-C7 **:** $C_{13}H_{27}NO_6$, M = 293.35, Monoclinic, space group $P2_1$, a = 4.957(3) Å, b = 5.007(4) Å, c = 30.60(2) Å, □= 92.980(8)°, V = 758.4(9) Å^3, Z = 2, crystal size 0.40 x 0.20 x 0.01 mm^3, 14967 reflections collected (3063 independent, R*int* = 0.1024), 204 parameters, 1 restraint, $R1$ [I>2σ(I)] = 0.0784, $wR2$ [all data] = 0.1680, largest diff. peak and hole: 0.345 and –0.294 eÅ^{-3}.

3D printing of Gal-C7 hydrogels

For 3D printing experiments, the same setup as wet spinning was used with the exception that the blunt-tip needle was positioned on a holder attached to a manually Z-adjustable platform, itself positioned on a programmable XY-moving stage (Newport Universal Motion Controller / Driver, model ESP300). This one was programmed to run over specified trajectories at different velocities (from 2 to 6 mm/s). The syringe and the needle were connected with a flexible tube. The needle extremity was plunged into a small water bath with a glass slide at the bottom, the distance between the glass and the needle was set between 0.5 and 5 mm. The slide was covered with a hydrophobic polycarbonate membrane (it4ip ipPORE track etched membrane, 21 µm thick, pore diameter of 5 µm, pore density of 1.00 x10^5 cm^{-2}).

Characterization of the deposits

Optical microscopy

The widths of the deposits were measured out of optical microscopy observations. After printing, the glass slides with the membrane and the gels were taken out of the water bath and rapidly observed with an inverted optical microscope (Olympus, bright field, ×4 or ×10). The widths were then manually measured with ImageJ software at different places of the deposit and the mean width as well as the standard deviation were calculated.

[g] SADABS, Program for Data Correction, Bruker–AXS.
[h] Sheldrick, G. M. SHELXT – Integrated Space-Group and Crystal-Structure Determination. *Acta Crystallogr. Sect. Found. Adv.* **2015**, *71* (1), 3–8. https://doi.org/10.1107/S2053273314026370.
[i] Sheldrick, G. M. Crystal Structure Refinement with SHELXL. *Acta Crystallogr. Sect. C Struct. Chem.* **2015**, *71* (1), 3–8. https://doi.org/10.1107/S2053229614024218.

Cryo-SEM microscopy

Hydrogel was deposited on the polycarbonate membrane following the protocol previously described. The glass slide on which rested the membrane was then taken out of the bath and kept in a humid sealed Petri dish for transportation to the facilities. A sample of the membrane with hydrogel was cut and was then deposited on the cryo-SEM cane and frozen at −220 °C in liquid nitrogen. The frozen sample was put at −145 °C under vacuum in the cryo-transfer system chamber (Quorum PP3000T) without fracturing for the PC membrane was not rigid enough. The sublimation was performed at −95 °C for 30 min. The sample was metalized with Pd for 60 s and introduced in the microscope chamber. The temperature was kept at −145 °C. Images were recorded with a FEG FEI Quanta 250 microscope, at 5 kV for the acceleration voltage.

Determination of the thickness of the deposits

Two methods were used here. For both, hydrogels were deposited on polycarbonate membranes placed on a glass slide as described in the previous protocol. After printing, the glass slide was placed on a water-soaked paper inside a Petri dish and observed with microscope.

The first microscope used was a Hirox (Hirox HI-SCOPE advanced KH-3000, CT-7 motor controller) with an electronic Z stage that enables knowing the displacement of focus. The glass slide with the membrane and the gel was kept on the soaked paper throughout the whole observation. To get the profiles of the deposits, the focus was first made on the membrane and the sample was moved perpendicularly to the direction of the deposit. The focus was adjusted every 50 µm and the displacement in Z was thus measured along the section, giving us the thickness of the gel. The Z displacement was thus plotted against the X displacement which gave a representation of the profiles of the gel deposits.

The second method used was with a Keyence optical numeric microscope (model VHX-1000), kindly provided by the CIRIMAT laboratory. This microscope has an integrated software that automatically focuses and detects the profile of the gel deposits. Here again, the glass slide was kept on soaked paper throughout the whole observation, which was much quicker than with the Hirox. Screen captures of the results were then saved.

Scientific contributions

Published articles

- Chalard, A.; Vaysse, L.; Joseph, P.; Malaquin, L.; Souleille, S.; Lonetti, B.; Sol, J.-C.; Loubinoux, I.; Fitremann, J. Simple Synthetic Molecular Hydrogels from Self-Assembling Alkylgalactonamides as Scaffold for 3D Neuronal Cell Growth. *ACS Applied Materials & Interfaces* **2018**, *10* (20), 17004–17017. https://doi.org/10.1021/acsami.8b01365.

Submitted article

- Chalard, A.; Joseph, P.; Souleille, S.; Lonetti, B.; Saffon-Merceron, N.; Loubinoux, I.; Vaysse, L.; Malaquin, L.; Fitremann, J. Controlled self-assembly and spinning of a supramolecular low molecular weight gelator into well-organized hydrogel fibers

Drafted article

- "Application of wet spinning to 3D printing of low molecular weight gelators"

Oral communications

- Anaïs Chalard, Laurence Vaysse, Pierre Joseph, Laurent Malaquin, Isabelle Loubinoux, Juliette Fitremann ; « Sugar-based supramolecular gelators as scaffolds for neuronal cell growth »; *16th European Student Colloid conference (ESC 2017)*, June 19th to 22nd **2017**, Florence, Italy; ECIS best oral communication award

- Anaïs Chalard, Laurence Vaysse, Pierre Joseph, Laurent Malaquin, Isabelle Loubinoux, Juliette Fitremann ; « Sugar-based supramolecular gelators as scaffolds for neuronal cell growth »; *31st ACSSS conference*, Warrnambool, Australia, January 29th to February 1st **2018**

- Anaïs Chalard, Laurence Vaysse, Pierre Joseph, Laurent Malaquin, Isabelle Loubinoux, Juliette Fitremann ; « Sugar-based supramolecular gelators as scaffolds for neuronal cell growth » ; *Xe journées de l'Ecole Doctorale Sciences de la Matière*, May 18th and 19th **2017**, Toulouse, France ; Best oral communication award

Poster communications

- Anaïs Chalard, Laurence Vaysse, Pierre Joseph, Laurent Malaquin, Isabelle Loubinoux, Juliette Fitremann ; « Sugar-based supramolecular gelators as scaffolds for 3D-neuronal cell growth »; *28th annual conference of the European Society for Biomaterials (ESB 2017)*, September 4th to 8th **2017**, Athens, Greece

- Anaïs Chalard, Delphine Bordignon, Laurence Vaysse, Isabelle Loubinoux, Laurent Malaquin, Sandrine Souleille, Fabien Mesnilgrente, Pierre Joseph, Juliette Fitremann ; « Supramolecular gelators for neuronal cell-growth: biocompatibility, 3D-cell growth, fibre alignment and injectability with microfluidics »; *Ecole thématique MICROFLUIDICS2017*, June 26th to 30th **2017**, Carcans-Maubuisson, France

Appendixes

N° 1: Glu-C7

N° 2: Gal-C5

N° 3: Gal-C6

N° 4: Gal-C7

N° 5: Gal-C8

N° 6: Gal-C9

N° 7: Gluca-C12

N° 8: Me-Gluca-C12

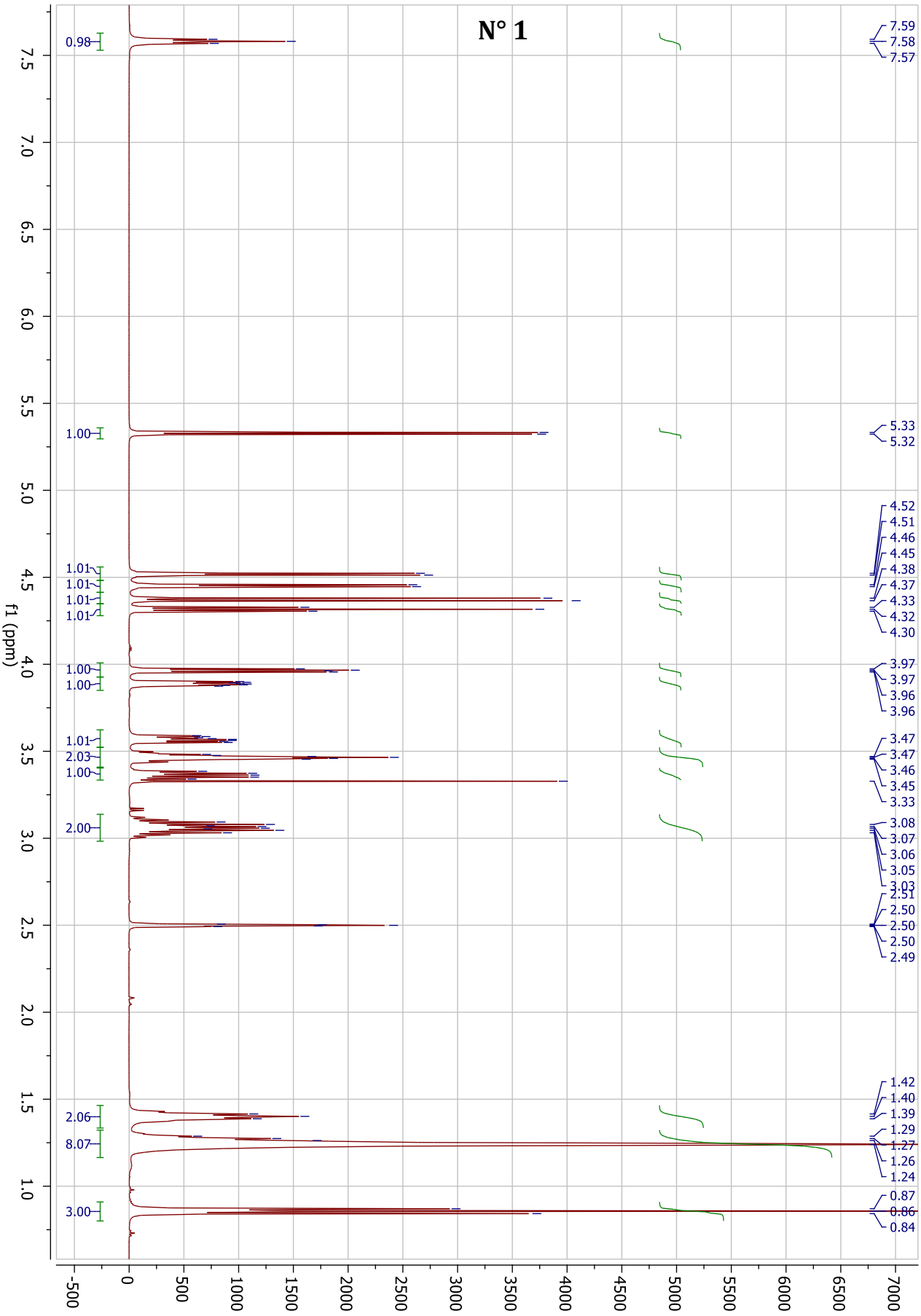
N° 1
f1 (ppm)
0.98
1.00
1.01
1.01
1.01
1.01
1.00
1.00
1.01
2.03
1.00
2.00
2.06
8.07
3.00
7.59
7.58
7.57
5.33
5.32
4.52
4.51
4.46
4.45
4.38
4.37
4.33
4.32
4.30
3.97
3.97
3.96
3.96
3.47
3.47
3.46
3.45
3.33
3.08
3.07
3.06
3.05
3.03
2.51
2.50
2.50
2.50
2.49
1.42
1.40
1.39
1.29
1.27
1.26
1.24
0.87
0.86
0.84

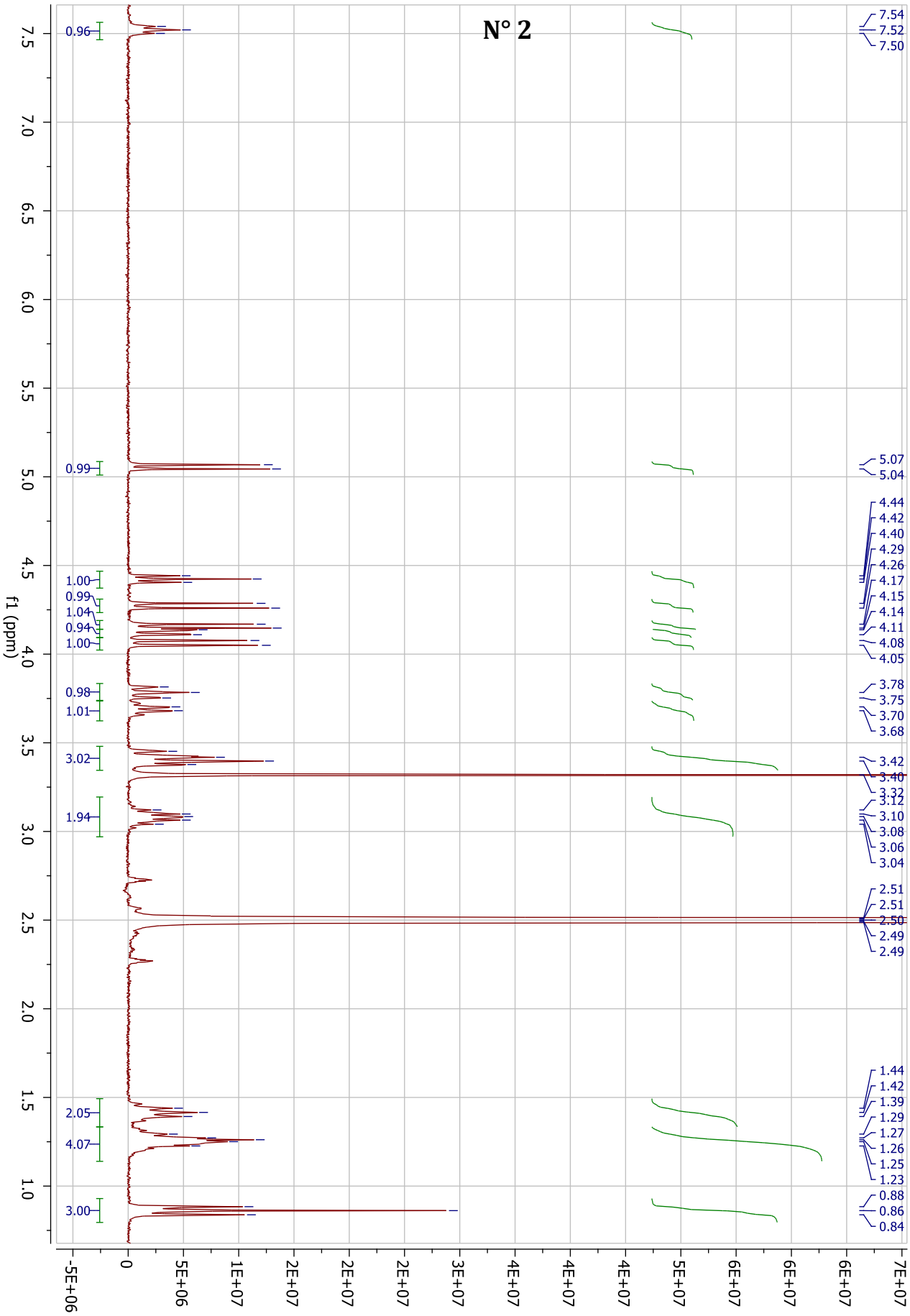
N° 2
f1 (ppm)
0.96
0.99
1.00
0.99
1.04
0.94
1.00
0.98
1.01
3.02
1.94
2.05
4.07
3.00
7.54
7.52
7.50
5.07
5.04
4.44
4.42
4.40
4.29
4.26
4.17
4.15
4.14
4.11
4.08
4.05
3.78
3.75
3.70
3.68
3.42
3.40
3.32
3.12
3.10
3.08
3.06
3.04
2.51
2.51
2.50
2.49
2.49
1.44
1.42
1.39
1.29
1.27
1.26
1.25
1.23
0.88
0.86
0.84

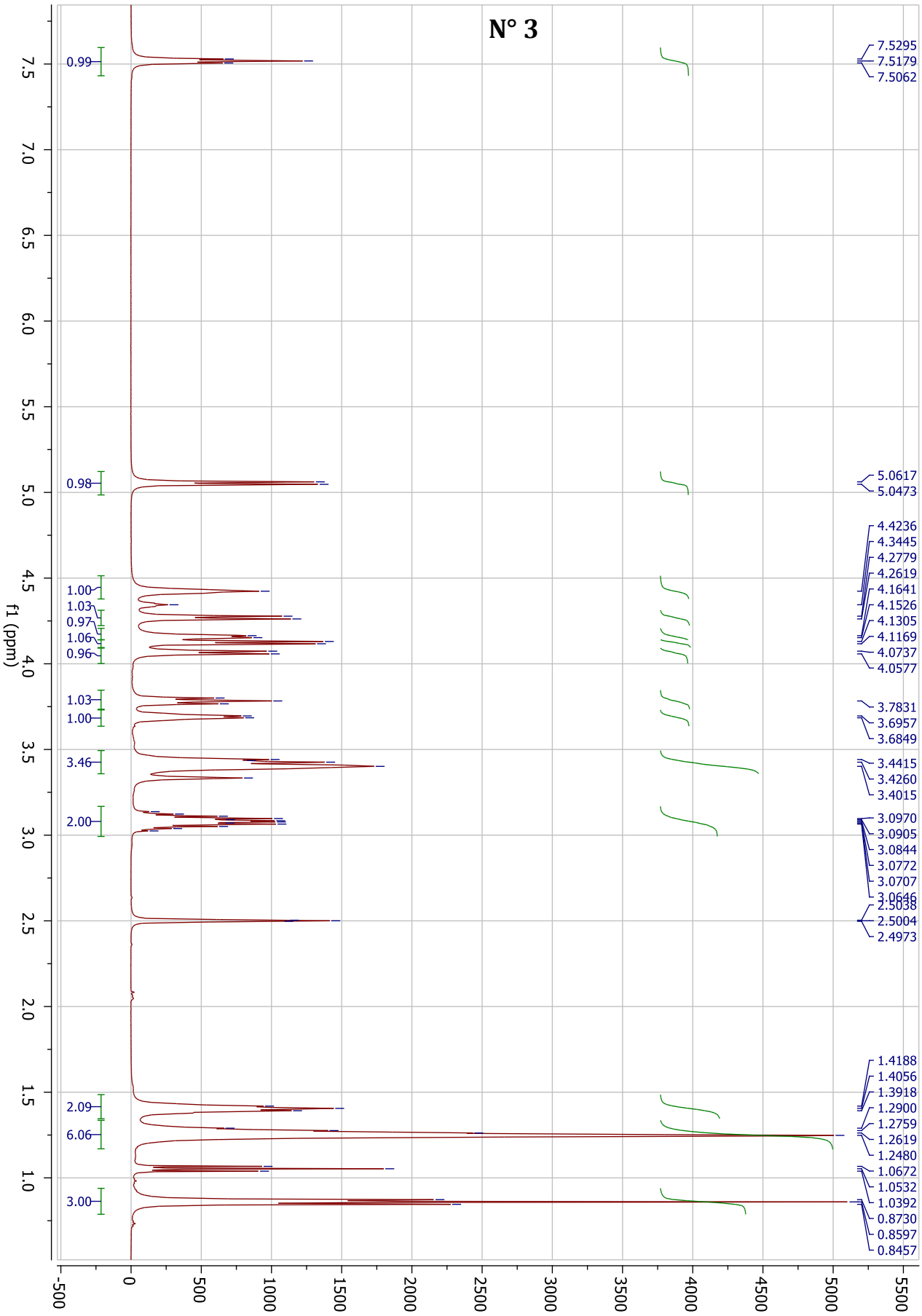
N° 3
f1 (ppm)
0.99
0.98
1.00
1.03
0.97
1.06
0.96
1.03
1.00
3.46
2.00
2.09
6.06
3.00
7.5295
7.5179
7.5062
5.0617
5.0473
4.4236
4.3445
4.2779
4.2619
4.1641
4.1526
4.1305
4.1169
4.0737
4.0577
3.7831
3.6957
3.6849
3.4415
3.4260
3.4015
3.0970
3.0905
3.0844
3.0772
3.0707
3.0646
2.5038
2.5004
2.4973
1.4188
1.4056
1.3918
1.2900
1.2759
1.2619
1.2480
1.0672
1.0532
1.0392
0.8730
0.8597
0.8457

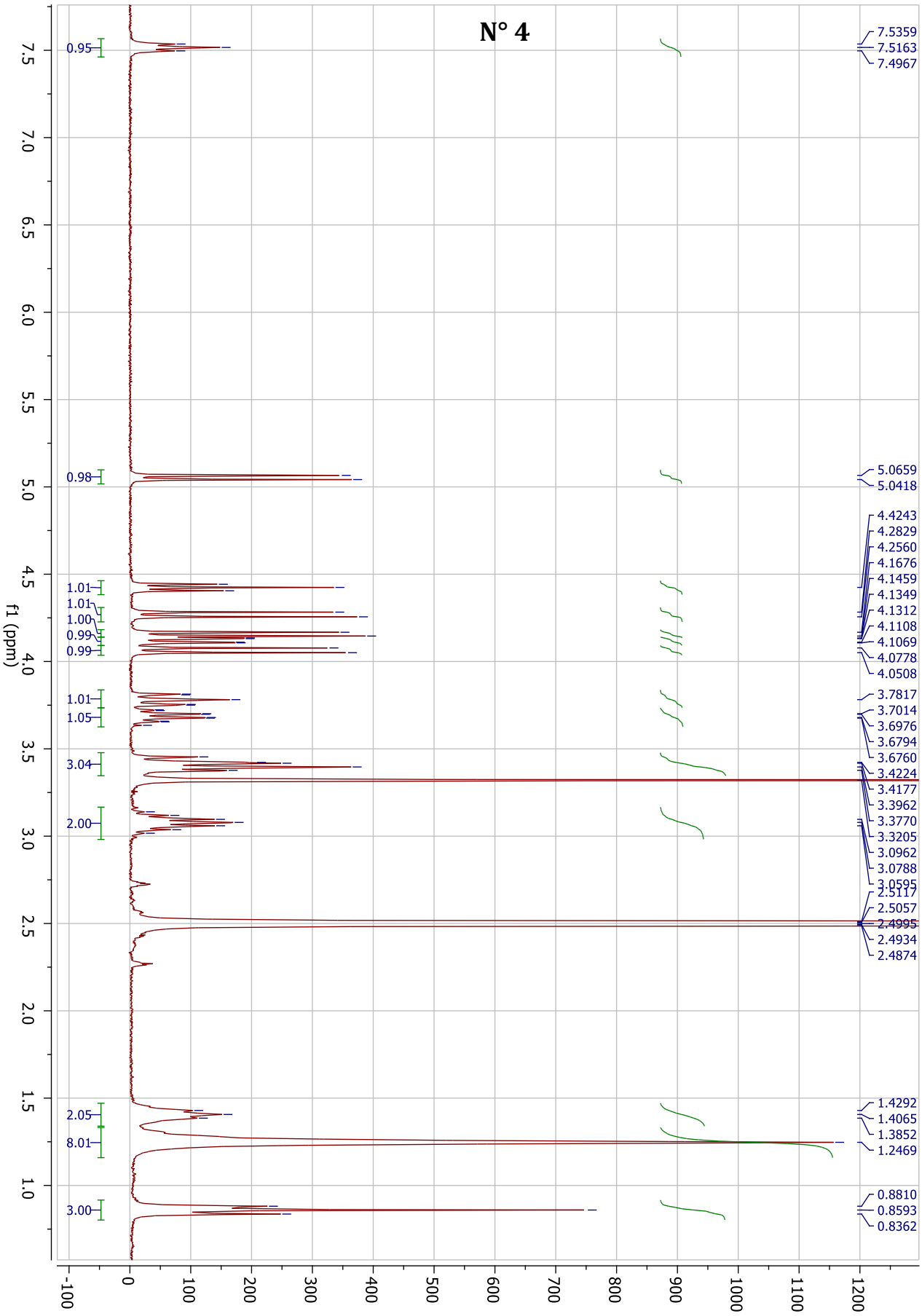
N° 4
f1 (ppm)
0.95
0.98
1.01
1.01
1.00
0.99
0.99
1.01
1.05
3.04
2.00
2.05
8.01
3.00
7.5359
7.5163
7.4967
5.0659
5.0418
4.4243
4.2829
4.2560
4.1676
4.1459
4.1349
4.1312
4.1108
4.1069
4.0778
4.0508
3.7817
3.7014
3.6976
3.6794
3.6760
3.4224
3.4177
3.3962
3.3770
3.3205
3.0962
3.0788
3.0595
2.5117
2.5057
2.4995
2.4934
2.4874
1.4292
1.4065
1.3852
1.2469
0.8810
0.8593
0.8362

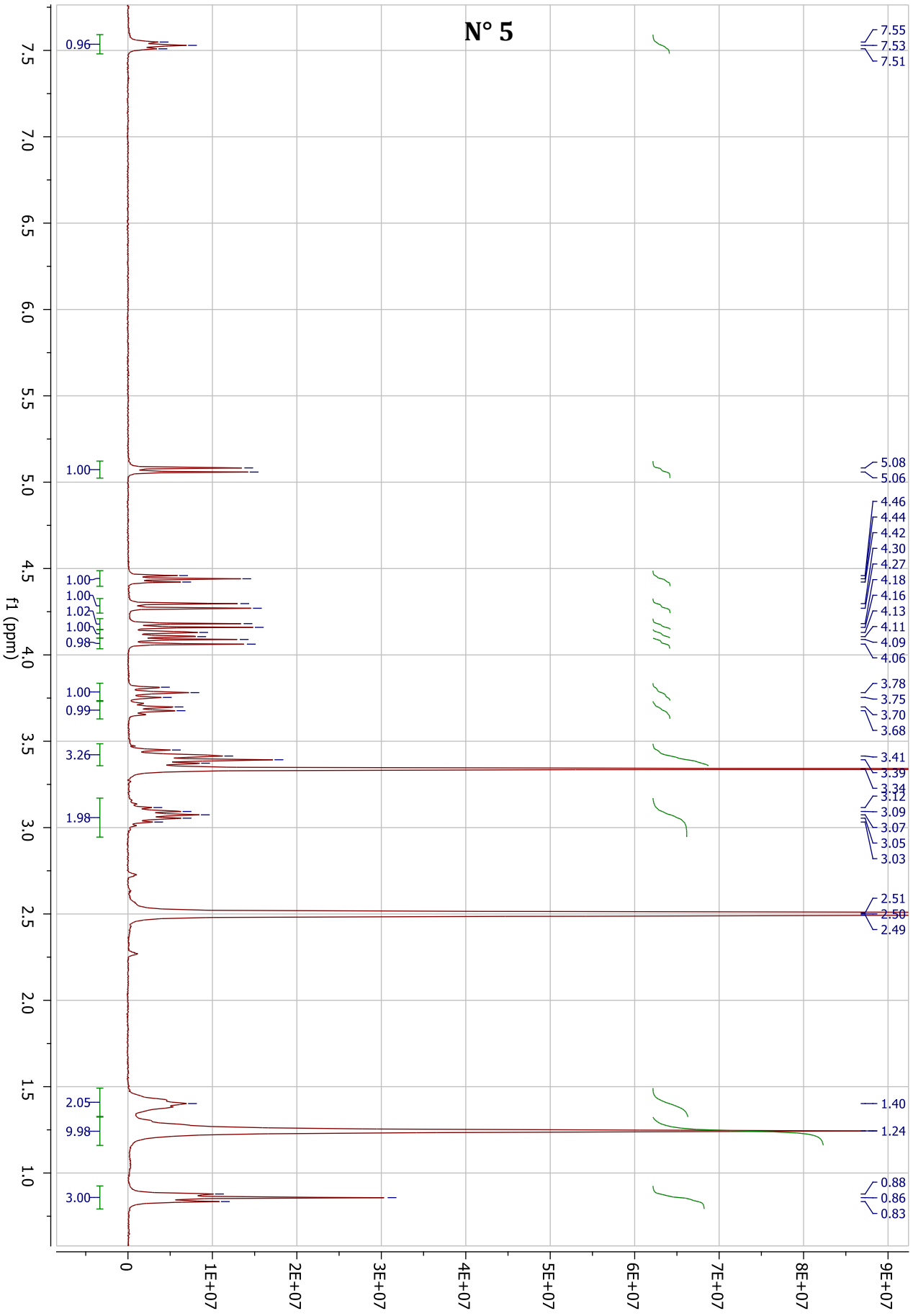
N° 5
f1 (ppm)
0.96
1.00
1.00
1.00
1.02
1.00
0.98
1.00
0.99
3.26
1.98
2.05
9.98
3.00
7.55
7.53
7.51
5.08
5.06
4.46
4.44
4.42
4.30
4.27
4.18
4.16
4.13
4.11
4.09
4.06
3.78
3.75
3.70
3.68
3.41
3.39
3.34
3.12
3.09
3.07
3.05
3.03
2.51
2.50
2.49
1.40
1.24
0.88
0.86
0.83

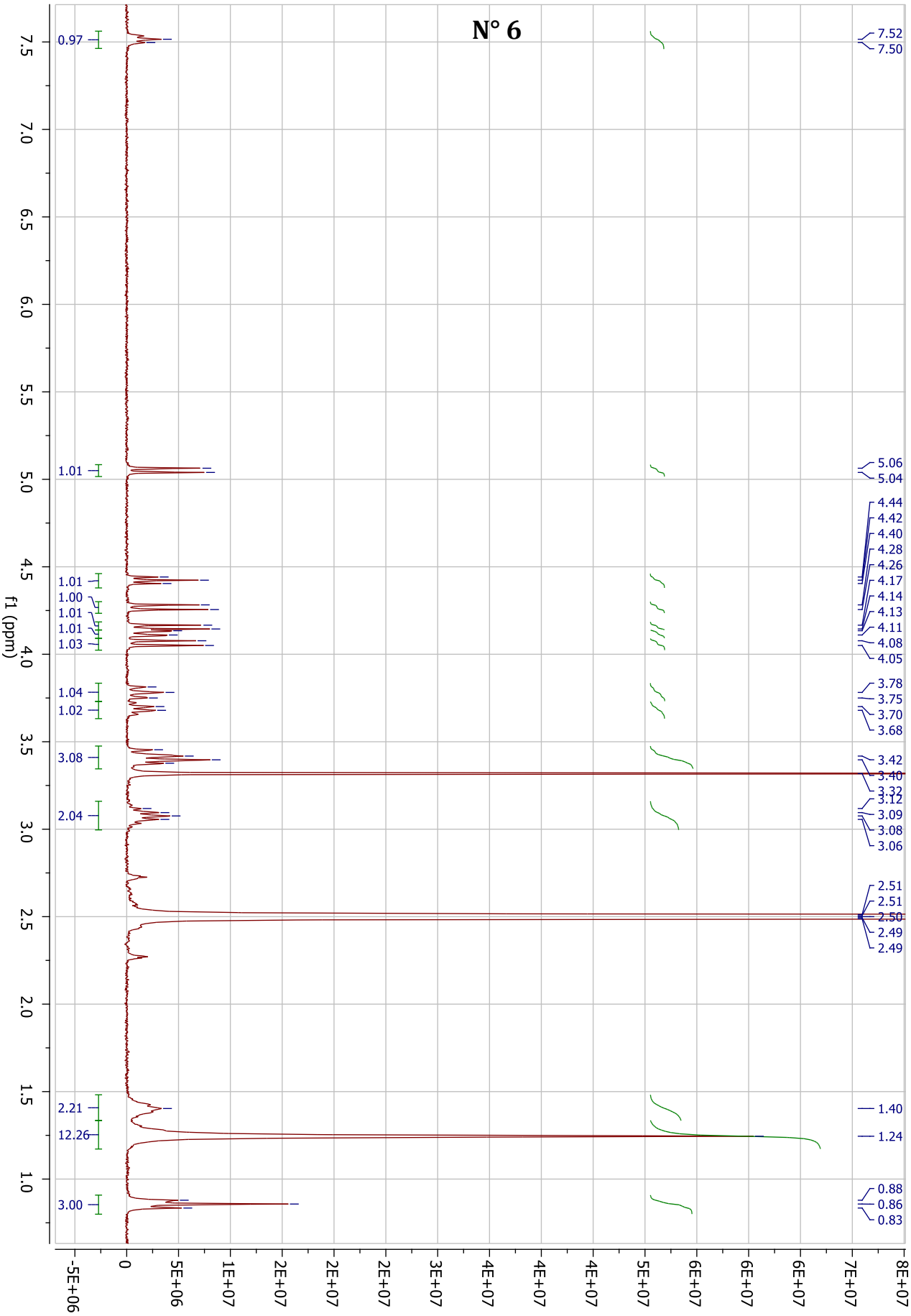
N° 6
f1 (ppm)
0.97
1.01
1.01
1.00
1.01
1.01
1.03
1.04
1.02
3.08
2.04
2.21
12.26
3.00
7.52
7.50
5.06
5.04
4.44
4.42
4.40
4.28
4.26
4.17
4.14
4.13
4.11
4.08
4.05
3.78
3.75
3.70
3.68
3.42
3.40
3.32
3.12
3.09
3.08
3.06
2.51
2.51
2.50
2.49
2.49
1.40
1.24
0.88
0.86
0.83

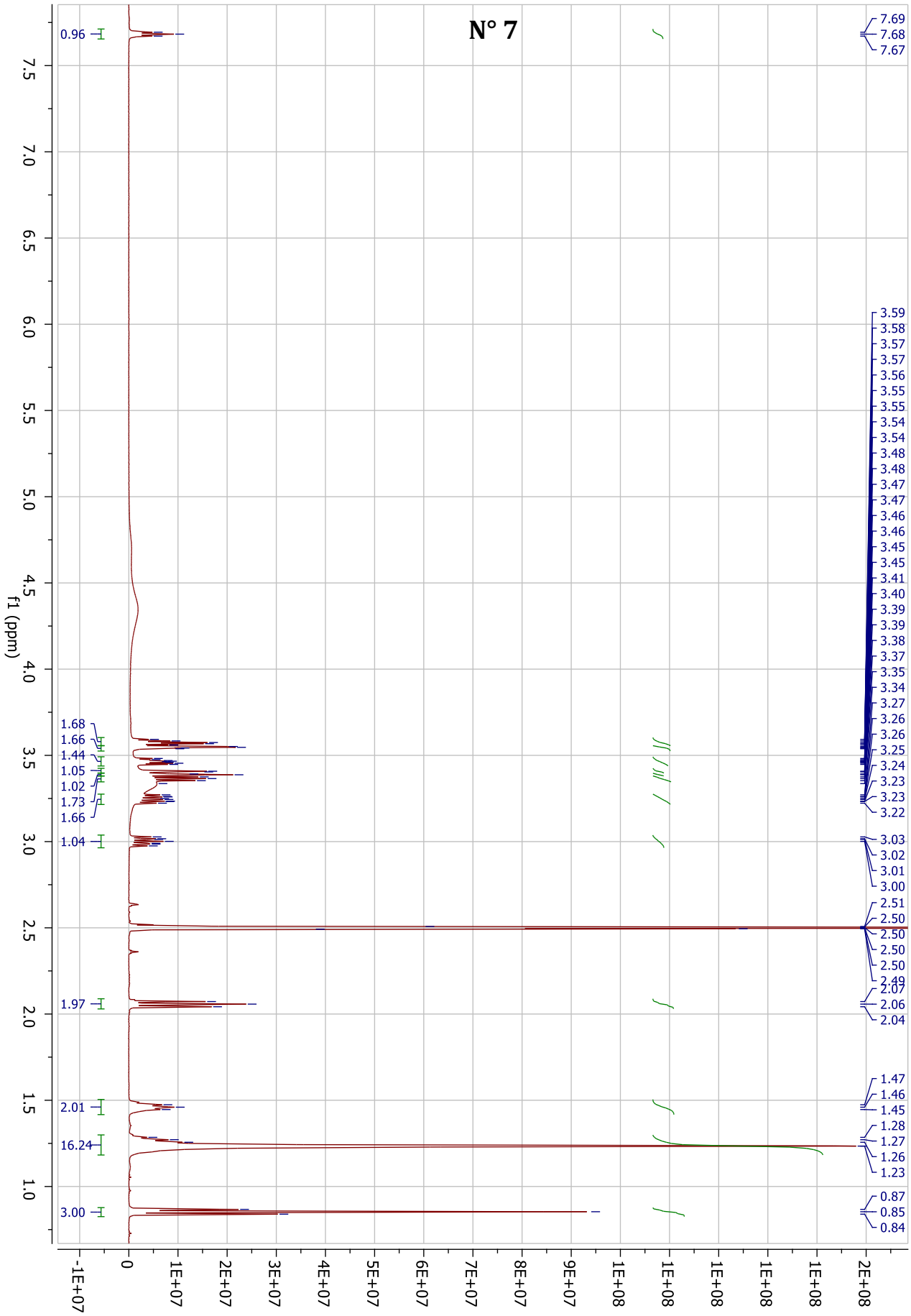
N° 7
f1 (ppm)
0.96
1.68
1.66
1.44
1.05
1.02
1.73
1.66
1.04
1.97
2.01
16.24
3.00
7.69
7.68
7.67
3.59
3.58
3.57
3.57
3.56
3.55
3.55
3.54
3.54
3.48
3.48
3.47
3.47
3.46
3.46
3.45
3.45
3.41
3.40
3.39
3.39
3.38
3.37
3.35
3.34
3.27
3.26
3.26
3.25
3.24
3.23
3.23
3.22
3.03
3.02
3.01
3.00
2.51
2.50
2.50
2.50
2.50
2.49
2.07
2.06
2.04
1.47
1.46
1.45
1.28
1.27
1.26
1.23
0.87
0.85
0.84

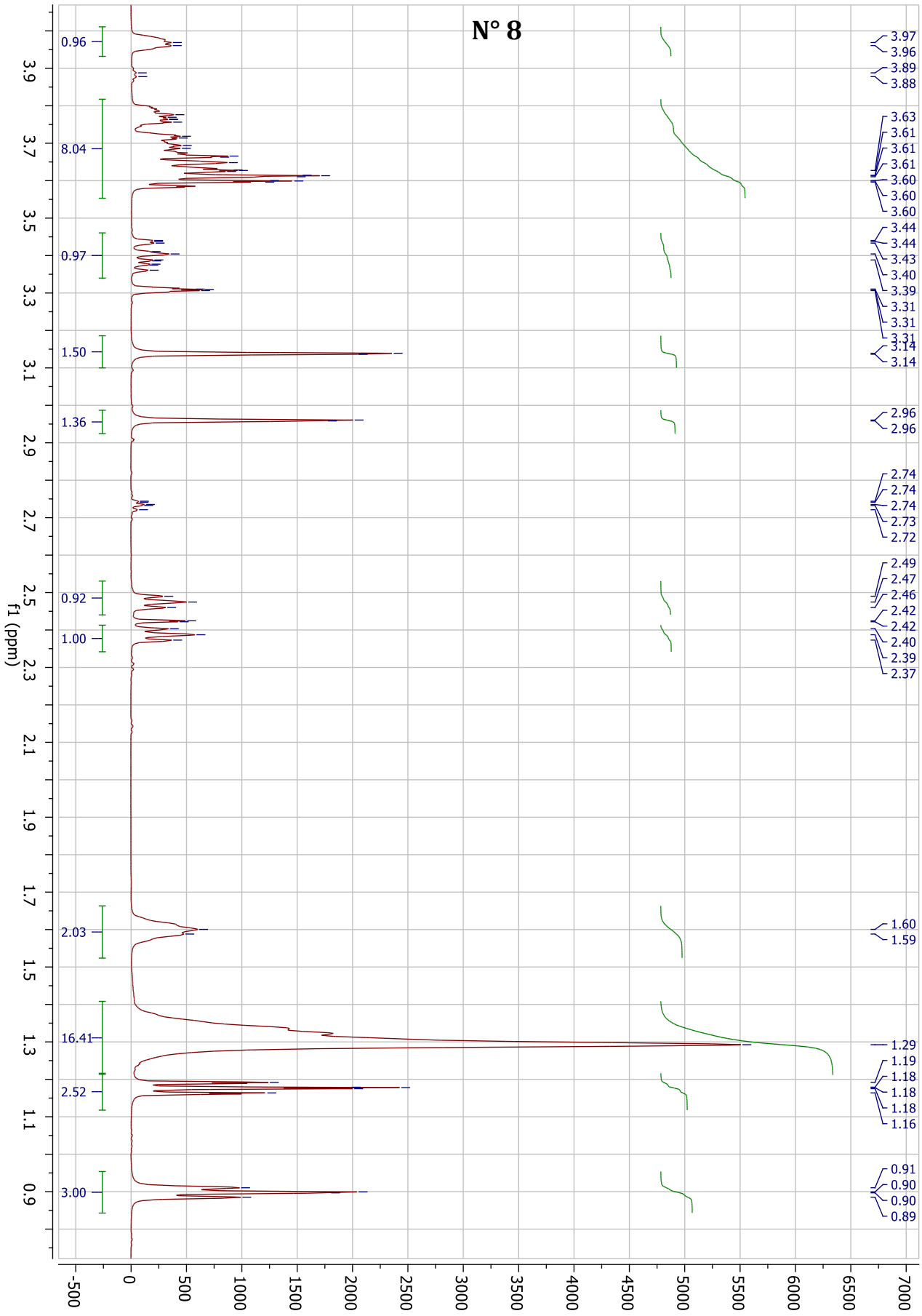
N° 8
f1 (ppm)
0.96
8.04
0.97
1.50
1.36
0.92
1.00
2.03
16.41
2.52
3.00
3.97
3.96
3.89
3.88
3.63
3.61
3.61
3.61
3.60
3.60
3.60
3.44
3.44
3.43
3.40
3.39
3.31
3.31
3.31
3.14
3.14
2.96
2.96
2.74
2.74
2.74
2.73
2.72
2.49
2.47
2.46
2.42
2.42
2.40
2.39
2.37
1.60
1.59
1.29
1.19
1.18
1.18
1.18
1.16
0.91
0.90
0.90
0.89

Résumé de la thèse

Introduction

Le cerveau est probablement l'organe le plus complexe en biologie en termes de compréhension, d'architecture et de structure. C'est pourquoi, lorsqu'une lésion se produit, telle qu'un accident vasculaire cérébral ou un traumatisme cérébral, il est particulièrement difficile de récupérer complètement toutes les fonctions motrices et cognitives, ce qui peut entraîner des handicaps lourds. Pour réparer les connexions endommagées qu'engendrent ces lésions, des cellules qui ont la capacité de produire à la fois des neurones et des cellules gliales, appelées cellules souches neurales, colonisent la zone lésée. En effet, les scientifiques ont longtemps pensé que le cerveau, à la fin de son développement, possédaient un nombre fini de neurones et que ce nombre ne faisait que décroître au cours du temps. Depuis quelques années cependant, cette croyance a été remise en question après la découverte de neurones « nouveau-nés » dans le cerveau de canaris adultes en 1980 par Goldman et Nottebohm. S'en est suivi d'autres découvertes et confirmations que de nouveaux neurones étaient en effet capables d'apparaître chez le cerveau des mammifères adultes, incluant les humains (Figure 1). Le cerveau adulte semble donc bel et bien capable de pouvoir se régénérer à l'aide de ces cellules souches, bien que cela soit encore parfois débattu à l'heure actuelle.

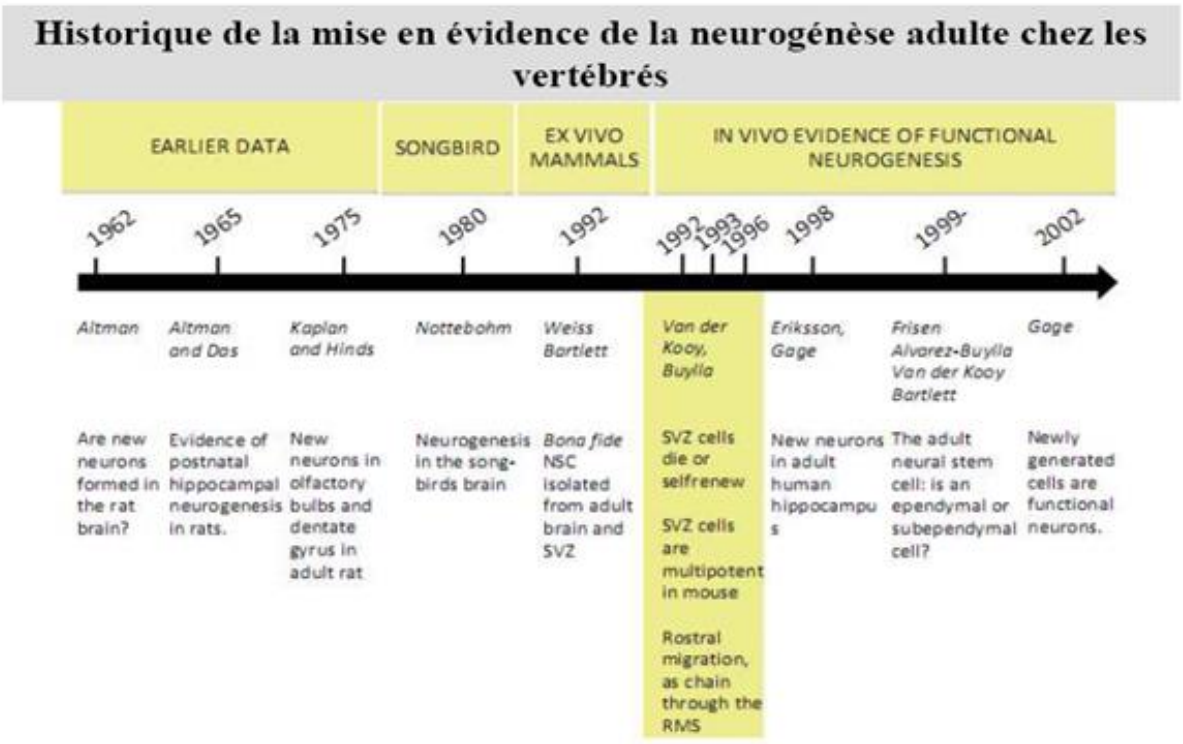

Figure 1 : Chronologie de la découverte des cellules souches neuronales.

Cependant, le processus de réparation des lésions cérébrales par les cellules souches neurales est très long car il faut du temps pour que celles-ci migrent, se divisent et se différencient. La plupart du temps, cela ne suffit pas non plus pour régénérer un tissu fonctionnel. De plus, l'environnement biologique induit par une lésion est très défavorable aux cellules souches car il inhibe leur croissance et leur différenciation, entraînant la plupart du temps la mort cellulaire. C'est pourquoi la régénération des lésions cérébrales est particulièrement compliquée. Une solution à ce problème pourrait être la transplantation directe post-traumatique de cellules souches neurales pré-différenciées dans le cerveau du patient pour fournir directement des neurones fonctionnels à l'intérieur de la lésion et accélérer la récupération. Les cellules souches pourraient même provenir du patient lui-même, qui auraient été collectées avant la lésion à titre préventif, pour procéder à des greffes autologues causant moins de réponse immunitaire et moins de complications.

Avec la réparation des lésions cérébrales, un autre grand progrès en biologie serait la possibilité de recréer des modèles cérébraux *in vitro*. Cela pourrait être utile pour étudier certaines des fonctions et pathologies du cerveau, mais également pour étudier l'administration de médicaments ou les effets de certains médicaments sur les cellules, etc. Ces modèles cérébraux pourraient ensuite être couplés à d'autres modèles d'organes et ces systèmes biologiques *in vitro* pourrait même un jour remplacer l'utilisation d'animaux pour des essais biologiques *in vivo*.

L'ingénierie tissulaire apporte des réponses à ces défis. Cette discipline scientifique se développe depuis environ 30 ans et peut être décrite comme « un champ interdisciplinaire qui applique les principes de l'ingénierie et des sciences de la vie au développement de substituts biologiques qui restaurent, maintiennent ou améliorent la fonction tissulaire » par Langer et Vacanti[j] en 1998. Des cellules vivantes, seules ou associées à des supports artificiels (souvent appelés « scaffolds »), sont développés pour recréer des tissus biologiques aussi proches que possible des conditions *in vivo*. L'un des principaux objectifs de l'ingénierie tissulaire est de pouvoir ultérieurement développer des tissus *in vitro* afin de réduire le besoin d'organes pour une greffe. Cette discipline est donc particulièrement adaptée aux problèmes décrits ci-dessus.

Pour soigner les lésions cérébrales, une stratégie possible consisterait à cultiver des cellules souches neurales *in vitro* sur un support en hydrogel de manière à ce qu'elles commencent à se différencier et à s'organiser en cellules fonctionnelles, puis à implanter ledit support directement dans le cerveau du patient (Figure 2).

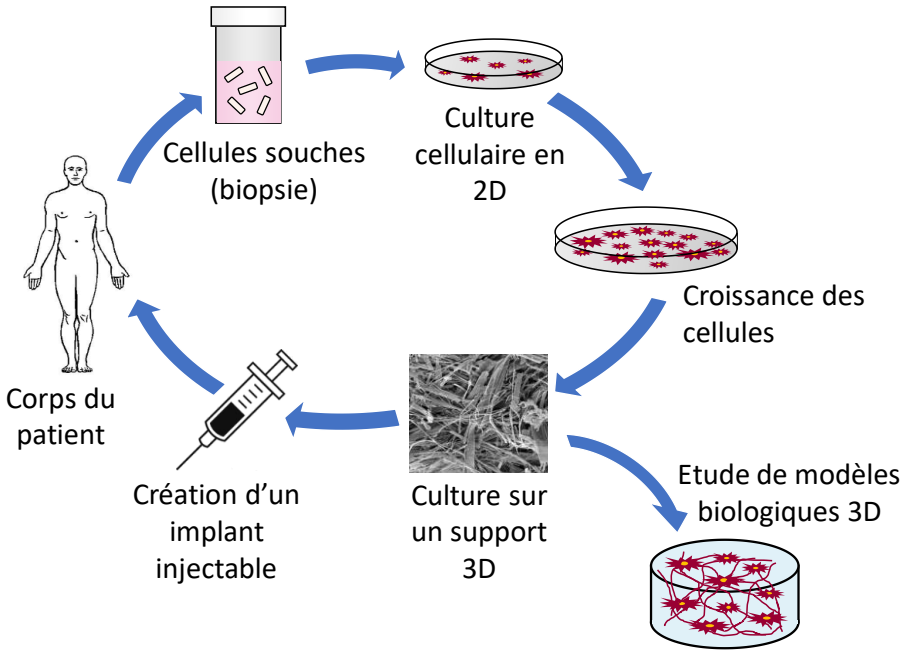

Figure 2 : Approche en ingénierie tissulaire pour la génération de greffes injectables à partir de cellules souches ou pour la production de modèles 3D in vitro.

Pour obtenir un matériau biocompatible, de préférence injectable, les recherches doivent porter leur attention principalement sur les propriétés du scaffold afin que les cellules neurales puissent se développer à l'intérieur. Une telle structure pourrait également être utilisée pour l'étude de modèles biologiques *in vitro* tridimensionnels.

[j] Langer, R.; Vacanti, J. P. Tissue Engineering. *Science* **1993**, *260* (5110), 920–926. https://doi.org/10.1126/science.8493529.

De plus, l'ingénierie tissulaire pourrait aider à imiter l'organisation *in vivo* des neurones. En effet, ceux-ci forment des faisceaux alignés à l'intérieur du cortex, avec leurs corps cellulaires à la surface et leurs axones plongeant dans la profondeur du tissu. Le biomatériau développé pourrait reproduire cette structure anisotrope du cortex afin d'obtenir des axones alignés à l'intérieur du scaffold. Recréer artificiellement cette organisation pourrait nous permettre d'obtenir un modèle plus précis, mais également, s'il était implanté *in vivo*, d'améliorer l'efficacité des connexions entre les tissus hôtes et le greffon. Cette organisation du matériel pourrait être obtenue par diverses stratégies. De plus, des structures au design très précis et même personnalisées pourraient être construites grâce à l'impression en trois dimensions.

Le premier objectif de ce travail est alors de développer un nouveau biomatériau pour la croissance et la différenciation des cellules souches neurales dans le but de reproduire au mieux les conditions *in vivo* pour les cellules afin de développer un tissu cérébral artificiel. Plus important encore, il est nécessaire de trouver un biomatériau ayant des propriétés mécaniques adaptées à la croissance des neurones. Il est maintenant bien connu que, pour se différencier, les cellules souches neurales ont besoin de matériaux très mous, avec une rigidité proche de celle du tissu cérébral. Dans l'état de l'art, une grande majorité des matériaux étudiés est à base de polymères, naturels ou synthétiques. Or la plupart de ces matrices sont souvent trop rigides pour les neurones et peu perméables aux cellules. Notre projet s'est donc plutôt intéressé à développer un support synthétique original de type hydrogel supramoléculaire. Contrairement à un gel de polymère, où ce sont de très longues molécules qui s'assemblent pour former un maillage tridimensionnel, un gel supramoléculaire est constitué de petites molécules de faible masse molaire qui s'auto-assemblent grâce à des liaisons faibles pour former un réseau de fibres. Ce réseau tridimensionnel va alors pouvoir retenir de l'eau et ainsi former un hydrogel (Figure 3). Peu d'études ont à ce jour proposé de tels matériaux en culture cellulaire. Pourtant ceux-ci présentent en général une meilleure perméabilité, une rigidité plus faible et aussi une meilleure biodégradabilité que des polymères, et sont donc de bons candidats pour la culture de cellules neuronales.

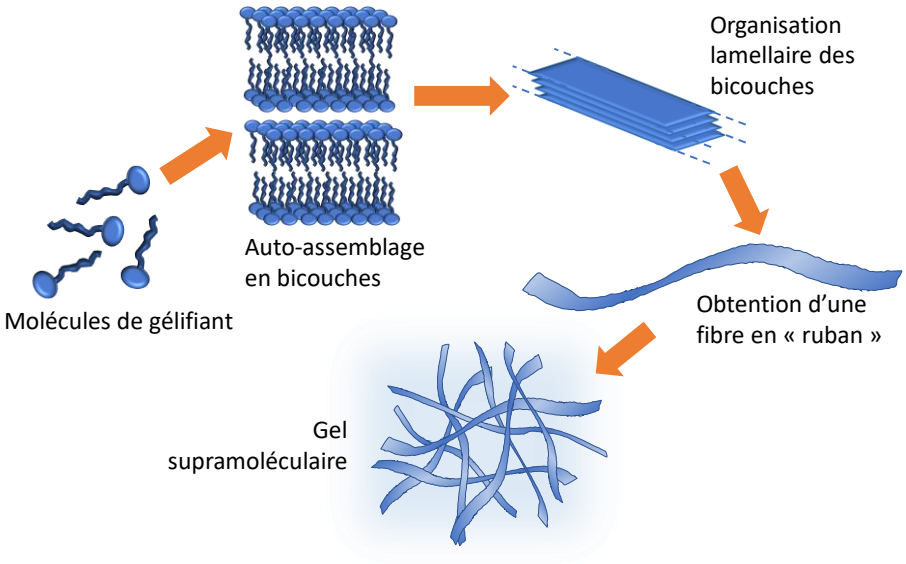

Figure 3 : Schéma illustrant l'auto-assemblage de petites molécules de gélifiant pour former un gel supramoléculaire.

La plupart des hydrogels supramoléculaires développés pour des applications en culture cellulaire sont dérivés de peptides qui, grâce à leurs fonctions aromatiques, forment aisément des hydrogels une fois en solution et qui sont intrinsèquement biocompatibles. D'autres hydrogels peuvent être obtenus à partir de nucléosides par exemple ou encore à partir de dérivés de sucres. C'est ce dernier type d'hydrogel que nous avons développé au cours de cette thèse.

Le second objectif est lui d'explorer différentes stratégies de mise en forme du gel afin de créer des motifs alignés et/ou d'être imprimé en 3D. Pour cela, une technique basée sur la gélification par échange de solvant a été développé avec nos hydrogels. Cette technique appelée « wet spinning » (filage en voie humide en français) est en fait connue depuis le début du siècle et a été beaucoup utilisé par l'industrie textile pour la production de nylon ou de polyacrylonitrile par exemple. Depuis quelques années ce procédé a été remis au goût du jour pour la production de matériaux pour des applications biomédicales notamment. Également, cette méthode de mise en forme d'un matériau peut tout à fait s'appliquer pour la construction de structures 3D. La mise en forme des hydrogels pourrait également aboutir à la production d'un matériau anisotrope qui permettrait la croissance des neurones de façon orientée.

L'objectif final de cette recherche est quant à lui d'implanter des greffes à base de ce matériau et des cellules souches pour la réparation de lésions cérébrales.

I. Synthèse et caractérisation de gélifiants dérivés de composés saccharidiques

Le premier travail au cours de cette thèse a donc consisté en la synthèse des gélifiants. Nous nous sommes intéressés à des composés dérivés de sucre et nous nous sommes alors basés sur les travaux de Pfannemülleret Welte[k] et de Fuhrhop[l] qui ont décrit par le passé des petites molécules à tête saccharidique formant des hydrogels à faible concentration. Diverses familles de molécules ont alors été synthétisées, avec la même structure de tête polaire à base saccharidique (dérivée du glucose ou galactose) reliée par une liaison amide à une chaîne alkyle plus ou moins longue. Les molécules synthétisées sont résumées dans le Tableau 1. Pour obtenir des hydrogels à partir de celles-ci, le gélifiant sous forme de solide est dissout à haute température dans de l'eau (chauffage aux alentours de 100-120 °C), puis cette solution est refroidie à température ambiante, formant ainsi l'hydrogel.

Du point de vue de la gélification et de la stabilité des hydrogels, la famille des alkylgalactonamides a été étudiée plus en détails par la suite. Ces molécules sont synthétisées selon la réaction du Schéma 1.

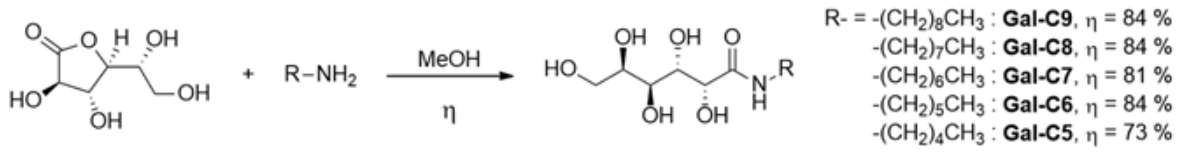

Schéma 1 : Réaction pour la synthèse des cinq molécules d'alkylgalactonamides.

Cependant, seules trois molécules parmi cette famille permettent l'obtention d'hydrogels stables et homogènes : le Gal-C8, Gal-C7 et le Gal-C6. C'est donc aux propriétés de ces molécules que nous nous sommes plus particulièrement intéressés. Bien que stables, ces hydrogels subissent cependant le phénomène de synérèse, qui consiste en l'expulsion irréversible de l'eau du gel et l'affaissement du réseau de fibres sous l'effet d'une contrainte mécanique.

[k] Pfannemüller, B.; Welte, W. Amphiphilic Properties of Synthetic Glycolipids Based on Amide Linkages. I. Electron Microscopic Studies on Aqueous Gels. *Chemistry and Physics of Lipids* **1985**, *37* (3), 227–240.

[l] Fuhrhop, J. H.; Schnieder, P.; Boekema, E.; Wolfgang, H. Lipid Bilayer Fibers from Diastereomeric and Enantiomeric N-Octylaldonamides. *J. Am. Chem. Soc.* **1988**, *110* (9), 2861–2867.

Tableau 1 : Liste des gélifiants synthétisés et de leurs propriétés

Abrévia-tion	Nom de la molécule	Structure	Concentration du gel	Aspect du gel	Références
Alkylgluconamides					
Glu-C7	*N*-heptyl-D-gluconamide	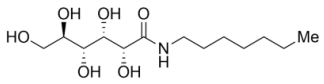	2 %m.	Gel blanc instable après quelques heures	b,c,m
Alkylgalactonamides					
Gal-C9	*N*-nonyl-D-galactonamide	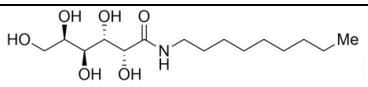	0,5 %m.	Gel blanc hétérogène	Cette étude
Gal-C8	*N*-octyl-D-galactonamide	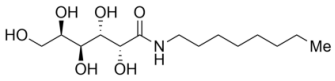	0,5 %m.	Gel blanc grossier	c
Gal-C7	*N*-heptyl-D-galactonamide	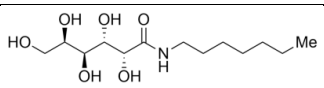	0,45 %m.	Gel blanc grossier	Cette étude
Gal-C6	*N*-hexyl-D-galactonamide	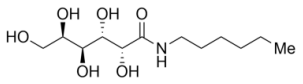	1 %m.	Gel blanc grossier	n
Gal-C5	*N*-pentyl-D-galactonamide	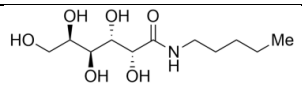	1,75-2 %m.	Gel blanc très fragile	Cette étude
Alkanoylglucamines					
Gluca-C12	*N*-dodecanoyl-D-glucamine	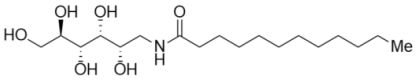	2-3 %m.	Gel blanc opaque, stable si de l'HFP est utilisé	Cette étude
N-alkanoyl-N-methyl-glucamines					
Me-Gluca-C12	*N*-methyl-*N*-dodecanoyl-D-glucamine	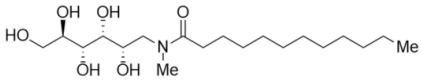	3-5 %m.	Gel transparent thixotrope	o, p
Me-Gluca-C14	*N*-methyl-*N*-tetradecanoyl-D-glucamine	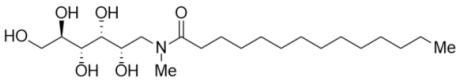	No gel	–	Cette étude

[m] Ohsedo, Y.; Oono, M.; Saruhashi, K.; Watanabe, H. Onset of Mixing-Induced Thixotropy in Hydrogels by Mixing Two Homologues of Low-Molecular-Weight Hydrogelators. *RSC Adv.* **2014**, *4* (82), 43560–43563.

[n] Mizrahi, S.; Rizkov, D.; Hayat, N.; Lev, O. A Low Molecular Weight Hydrogel Which Exhibits Electroosmotic Flow and Its Use as a Bioreactor and for Electrochromatography of Neutral Species. *Chemical Communications* **2008**, No. 25, 2914.

[o] Hoffmann, H.; Thunig, C.; Miller, D. Vesicle Phases from N-Methyl-N-Alkanoylglucamin and Various Co-Surfactants. *Colloids and Surfaces A: Physicochemical and Engineering Aspects* **2002**, *210* (2), 147–158.

[p] Zasloff, M. Liquid Non-Ionic Salt-Free Skin and Hair Treatment Composition That Contains n-Methyl Lauroyl Glucamide. US20140242018 A1, August 28,

Nous avons constaté que selon la manière dont les hydrogels d'alkylgalactonamides étaient formés, nous obtenions des gels plus ou moins homogènes. L'influence du refroidissement de la solution de gélifiant a alors été étudié : des rampes de température plus ou moins longues pour passer de 100 °C à 25 °C (0 min ou refroidissement instantané, 15 min, 30 min, 60 min ou 90 min) ont été appliquées et plusieurs mesures ont alors été effectuées. Les longueurs des fibres constituant les hydrogels (observées par microscopie optique, Figure 4) ont été mesurées, ainsi que la densité de points de nucléation (points concentrant de grandes quantités de gélifiants et à partir desquels les fibres croissent, provoquant ainsi les inhomogénéités du gel).

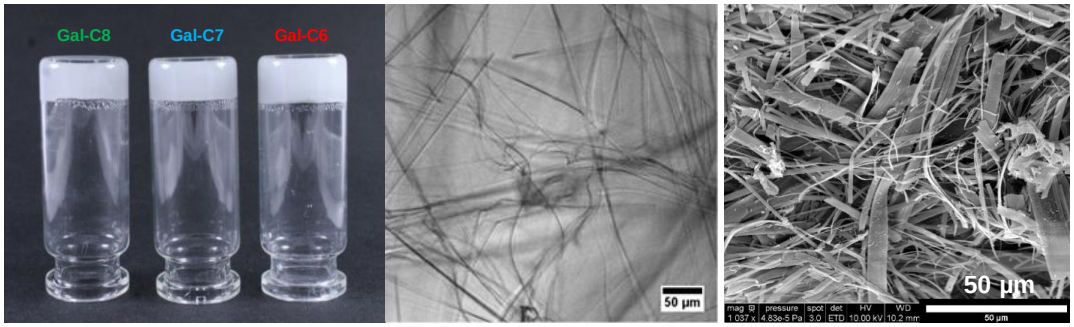

Figure 4 : Gauche : hydrogels obtenus à partir des trois molécules d'alkylgalactonamides : Gal-C8, Gal-C7 et Gal-C6. Milieu : observation en microscopie optique des fibres d'un hydrogel de Gal-C7 à 0,45 %m. Droite : observation d'un hydrogel de Gal-C7 en cryo-microscopie électronique à balayage (cryo-MEB).

Il a alors été établi que plus le refroidissement de la solution est lent, plus la densité de points de nucléation est faible (Figure 5a) et plus les fibres obtenues sont longues (Figure 5b), donnant ainsi des hydrogels plus homogènes et plus résistants, en particulier pour le Gal-C7 qui donne des gels avec des fibres particulièrement longues, pouvant même atteindre le millimètre.

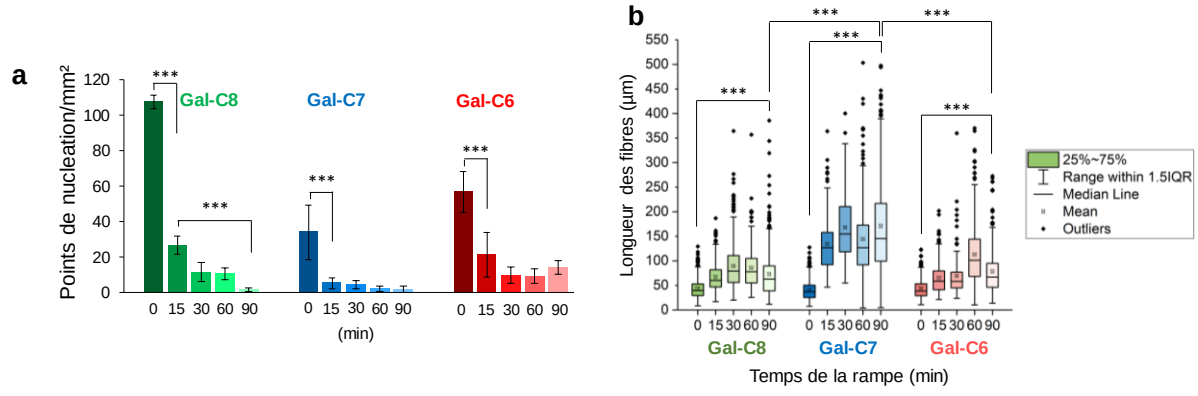

Figure 5 : a. Densité de points de nucléation en fonction du temps de la rampe de température pour les trois hydrogels. b. Longueurs des fibres des hydrogels en fonction des rampes de température pour les différents hydrogels.

Les propriétés mécaniques et rhéologiques de ces gels ont également été étudiées. Des mesures de contraintes en cisaillement et en compression ont été effectuées pour déterminer la rigidité de ces structures (Figure 6). Les modules élastiques des gels de Gal-C6, Gal-C7 et Gal-C8 à leurs

concentrations optimales sont respectivement de 50 ; 7 et 3 kPa. Ces valeurs indiquent donc des gels relativement mous, mais plus la chaîne carbonée est courte, plus le gel est rigide. En réalité cela vient probablement du fait que le gel de Gal-C6 est celui qui a la plus forte concentration (1 %m. comparé à 0,45 et 0,5 %m. pour Gal-C7 et Gal-C8).

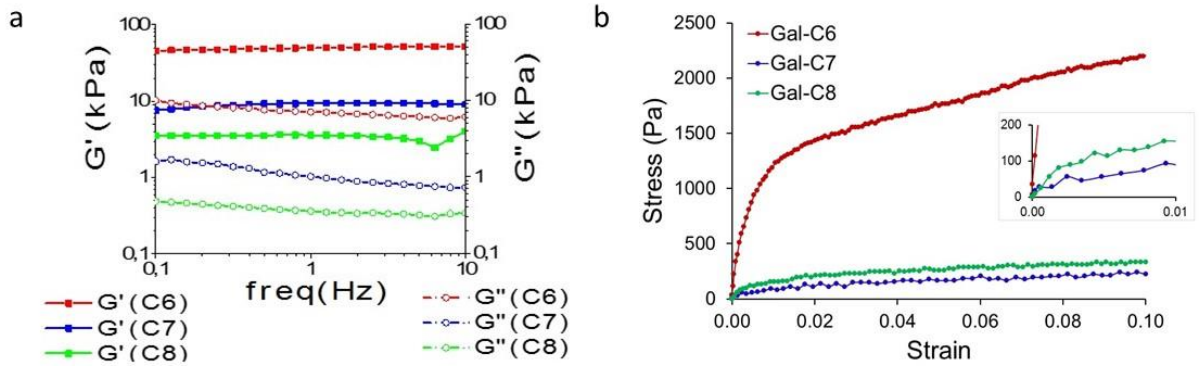

Figure 6 : a. Analyse en rhéologie des trois hydrogels (rampe de 0 min) : variation du module élastique (G') et visqueux (G") avec la fréquence (déformation = 2.10^{-3} (0,2 %), T° = 37 °C). (b) Compression uniaxiale des cylindres de gels (refroidissement à 90 min ; vitesse de compression rapide : 5 m/s, T° = 20 °C). Concentrations de gel pour les essais de rhéologie et de compression : Gal-C6 : 1 %m.; Gal-C7: 0,45 %m .; Gal- C 8: 0,5 %m.

Une fois les propriétés de ces hydrogels bien définies, l'étape suivant a été de tester leur biocompatibilité pour pouvoir les utiliser en tant que supports pour la culture de neurones.

II. Etude de la biocompatibilité et de la croissance de cellules neurales avec les gels d'alkylgalactonamides

Pour déterminer la biocompatibilité des trois hydrogels d'alklgalactonamides, de premiers tests ont été réalisés à l'aide d'une lignée cellulaire immortelle de neurones appelée Neuro2a. Les hydrogels ont été préparés avec des rampes de température de 90 min afin d'obtenir des gels les plus homogènes et résistants possibles, en particulier résistants aux nombreux lavages occasionnés par les conditions de culture cellulaire. Les hydrogels ont tous été utilisés tels quels, aucun additif n'a été ajouté.

La première caractérisation pour évaluer la biocompatibilité des hydrogels a été réalisé à l'aide d'un test visuel appelé « live/dead » qui permet le comptage des cellules vivantes et des cellules mortes en fluorescence. Après marquage et observation en microscopie de fluorescence, les premières apparaissent vertes et les dernières en rouge (Figure 7c).

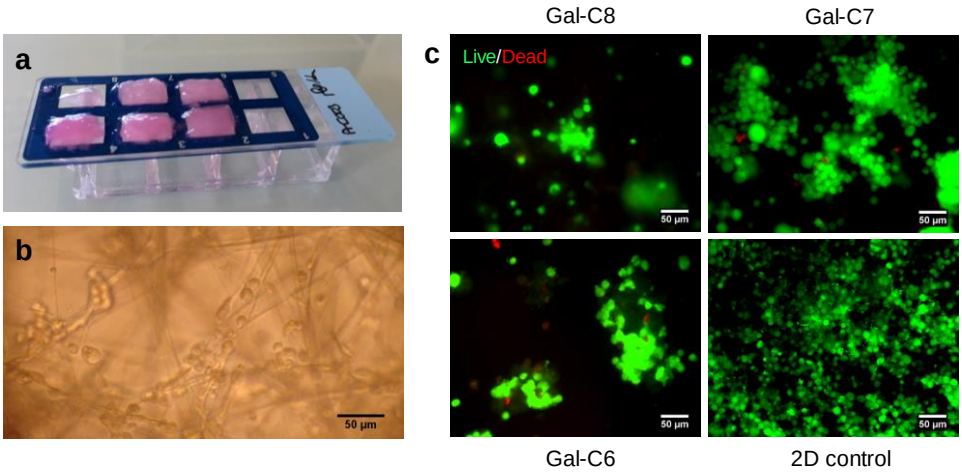

Figure 7 : a. Aspect des hydrogels après 7 jours de culture cellulaire dans une plaque 8 puits de type labtek. b. Neuro2as observées en microscopie en lumière blanche dans les fibres d'un hydrogel de Gal-C7 après 7 jours de culture cellulaire. c. Résultats des tests « live/dead » avec des Neuro2as ensemencées sur les hydrogels d'alkylgalactonamides après 7 jours de culture cellulaire, ainsi que le puits de contrôle sans gel.

La viabilité des cellules sur les hydrogels s'est donc révélée être assez élevée : environ 78 % de viabilité pour le Gal-C6 après 7 jours de culture, 98 % pour le Gal-C7 (proche de la valeur du contrôle) et 81 % pour le Gal-C8. Des cellules neuronales sont donc bien capables de survivre sur les hydrogels pendant près d'une semaine. Cependant, les gels de Gal-C6 et Gal-C8 présente une légère toxicité étant donné que leur taux de survie est un peu plus faible que celui du contrôle. Le Gal-C7 en revanche présente une très bonne survie des cellules en son sein. La prochaine étape était alors de caractériser la croissance des cellules dans les hydrogels d'alkylgalactonamides. Pour cela un autre test colorimétrique a été utilisé, appelé MTT. Ce test, réalisé à 1 et 4 jours de culture, nous a permis de quantifier la croissance des cellules dans les gels (Figure 8).

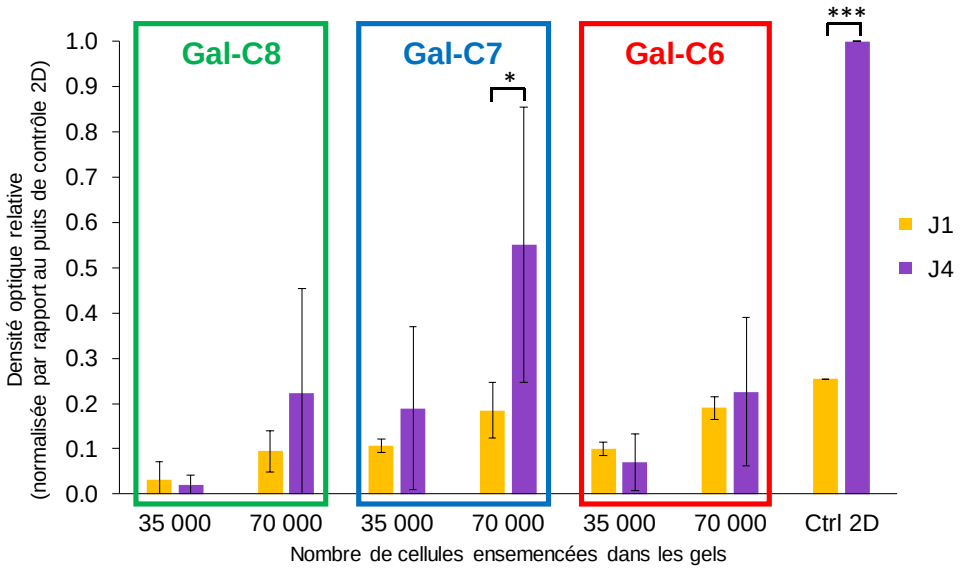

Figure 8 : Résultats du test MTT après 1 et 4 jours de culture cellulaire avec les différents hydrogels préparés en rampe de 90 min et selon deux densités de Neuro2as ensemencées. Le graphe représente les valeurs de la densité optique obtenue par le test colorimétrique après soustraction du blanc ± l'écart-type des valeurs. Les astérisques représentent la signification statistique (: $p < 0.05$ et ***: $p < 0.005$).*

Les résultats montrent donc que la croissance des cellules est plus faible dans les hydrogels que sur un simple support en deux dimensions. Cependant il ressort assez clairement que les Neuro2as prolifèrent plus sur les gels de Gal-C7 que sur les autres, en particulier pour une densité de cellules ensemencées plus importante. En effet, la pénétration des cellules dans l'hydrogel a été observée (Figure 7b) et pour garantir une meilleure croissance des cellules, une plus forte densité ensemencée est nécessaire car si les cellules sont trop éloignées les unes des autres, elles ont tendance à mourir faute de communication inter-cellulaire. Ce test confirme donc de nouveau la meilleure biocompatibilité des gels de Gal-C7 que ceux de Gal-C6 ou Gal-C8. Une simple différence d'un carbone dans la chaîne alkyle de ces gélifiants induit donc des biocompatibilités très différentes pour leurs hydrogels.

Cette différence de biocompatibilité entre les trois hydrogels peut s'expliquer par différentes choses. Premièrement par la préparation des hydrogels en elle-même. Les hydrogels de Gal-C6 par exemple nécessite une plus forte concentration de gélifiant (2 fois plus) que ceux de Gal-C7 ou Gal-C8. Une légère toxicité de la molécule pourrait donc se remarquer plus facilement dans ce gel que les autres. Aussi, les gels de Gal-C8 sont assez difficile à préparer et manipuler dû à leur très haut point de gélification, ce qui peut expliquer la grande variabilité obtenue pour le test MTT avec ces gels. Également, les hydrogels de Gal-C7 présentent différentes caractéristiques qui peuvent expliquer ces résultats. D'abord ce gel, lorsqu'il est préparé par une rampe de température de 90 minutes, est celui qui présente les fibres les plus longues, peu de petites fibres y sont observées comparé à des gels de Gal-C8 ou Gal-C6 (Figure 5b). Or il a parfois été établi que

de petites fibres nanométriques peuvent se révéler toxiques pour des cellules[q]. Aussi, concernant leurs propriétés mécaniques, les gels de Gal-C7 sont les plus mous (avec ceux du Gal-C8) et donc plus propices à la croissance des neurones qui nécessitent des substrats très mous pour croître et se différencier. De plus, le Gal-C7 est la seule molécule testée en culture cellulaire avec un nombre impair de carbone dans la chaîne alkyle. Il a parfois été observé que les molécules avec une parité différente de chaîne carbonée ne sont pas métabolisées de la même façon par les cellules[r]. Tous ces phénomènes peuvent donc expliquer la très bonne biocompatibilité des hydrogels de Gal-C7.

Pour la suite de l'étude, nous nous sommes intéressés plus précisément à la pénétration des cellules dans les hydrogels de Gal-C7, puisque les tests précédents ont montré que ceux-ci étaient les plus adaptés pour la culture de neurones. Pour cela, des cellules de Neuro2as ont été modifiées pour exprimer la protéine fluorescente GFP (« green fluorescent protein ») et les hydrogels ensemencés ont été observés par microscopie confocale.

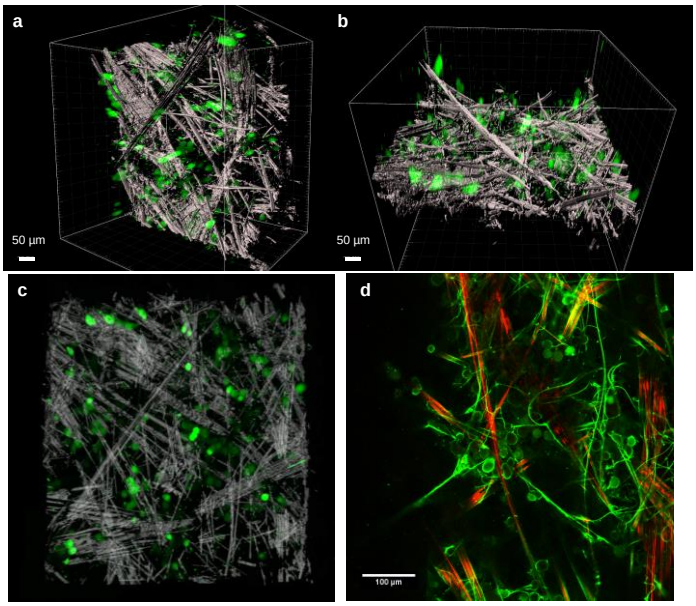

Figure 9 : a,b,c : Différentes plans d'observations en microscopie confocale d'un gel de Gal-C7 (rampe de 90 min) ensemencé avec des Neuro2as-GFP. Les fibres sont observées par réflexion et les cellules par fluorescence. d : Observation en microscopie confocale des cellules Neuro2a-GFP et des fibres du gel par réflexion laser (rouge) et par marquage par polylysine fluorescente (vert) (échelle : 100 µm).

[q] Kuang, Y.; Xu, B. Disruption of the Dynamics of Microtubules and Selective Inhibition of Glioblastoma Cells by Nanofibers of Small Hydrophobic Molecules. *Angew. Chem. Int. Ed.* **2013**, *52* (27), 6944–6948.

[r] Gotoh, N.; Moroda, K.; Watanabe, H.; Yoshinaga, K.; Tanaka, M.; Mizobe, H.; Ichioka, K.; Tokairin, S.; Wada, S. Metabolism of Odd-Numbered Fatty Acids and Even-Numbered Fatty Acids in Mouse. *Journal of Oleo Science* **2008**, *57* (5), 293–299.

On a alors pu constater que les cellules pénétraient le gel jusqu'à une profondeur d'environ 200 µm, ce qui révèle en effet une croissance des cellules en trois dimensions dans ces scaffolds d'hydrogel. Également, cette expérience a pu mettre en évidence, par le biais d'une double observation des fibres par réflexion et par marquage fluorescent, un réseau dual de fibres très fines et sinueuses (révélées par la polylysine fluorescente) et de très grandes et larges fibres rectilignes (observée par réflexion laser). Ce double réseau de fibres permet à la fois l'imbrication des cellules en leur sein mais aussi la croissance des axones le long des très grandes fibres rectilignes.

La dernière étape de cette partie de la thèse était alors de tester les hydrogels de gal-C7 pour la croissance des cellules souches neurales humaines. Ces cellules sont extraites de biopsies de patients et mises en culture dans des conditions bien spécifiques. Une fois en suspension, ces cellules souches s'assemblent en général sous formes d'agrégats appelés « neurosphères » où elles se divisent. Ces cellules ont alors été ensemencées dans des hydrogels de Gal-C7 préparés par rampe de température de 90 min et observées en microscopie confocale (Figure 10).

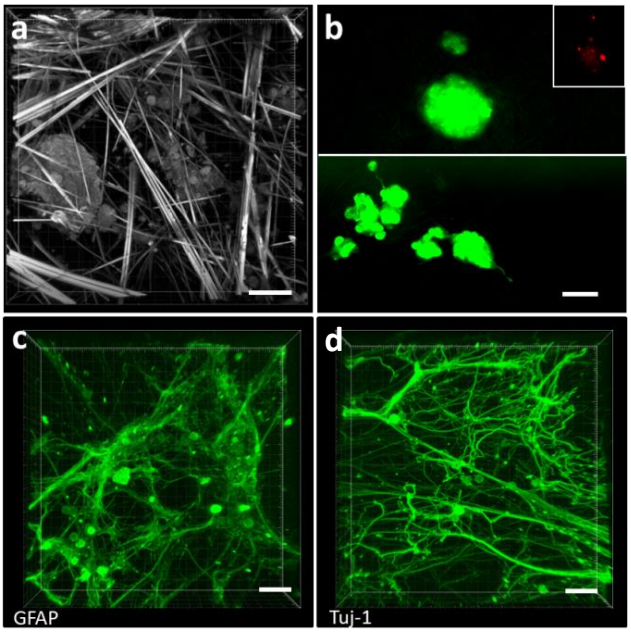

Figure 10 : Observations en microscopie confocale des cellules souches neurales humaines ensemencées dans des hydrogels de Gal-C7 préparés en rampe de 90 min après 7 jours de culture cellulaire. a. Observation en réflexion laser des fibres du gel ainsi que des neurosphères. b. Test live/dead sur les cellules souches neurales humaines rassemblées en neurosphères, révélant une bonne viabilité des cellules dans le gel (cellules vivantes en vertes et mortes en rouge, dans l'insert). L'immunomarquage révèle la présence de marqueurs des cellules gliales (c) et des cellules neuronales (d) dans le réseau de cellules en différentiation (échelles : 50 µm).

Ces observations ont donc montré que les cellules s'assemblent sous forme de neurosphères dans le gel, ce qui indique que celles-ci y survivent et se divisent. Beaucoup de cellules développent également des neurites (extensions qui plus tard deviennent des axones ou des dendrites) qui semblent s'étendre le long des fibres du gel, sur de grandes distances. La différenciation des

cellules souches est même observée dans le gel par immunomarquage, où l'on retrouve des marqueurs de cellules gliales (GFAP) ainsi que des marqueurs neuronaux (Tuj-1). Ce dernier résultat est particulièrement prometteur car non seulement les cellules survivent et croissent dans l'hydrogel, mais celles-ci sont également capables de s'y différencier et cela en deux types de cellules, neurones ou gliales.

Cependant, le principal défaut de nos supports hydrogels est leur dégradabilité en conditions de culture cellulaire. En effet, il est très difficile de faire de la culture cellulaire sur ces gels pendant plus de 7 jours car ceux-ci se dégradent rapidement. Un moyen de rendre le gel plus résistant (par réticulation par exemple, ou bien par création d'un réseau secondaire) devra être trouvé pour pouvoir poursuivre plus longuement ces essais de culture de cellules souches neurales humaines avec ce type d'hydrogel.

III. Mise en forme des hydrogels de *N*-heptyl-D-galactonamide

La dernière étape de ce projet a donc été la mise en forme des hydrogels de Gal-C7. L'idée était ici premièrement de trouver un moyen pour essayer d'aligner les fibres d'hydrogel, pour ensuite orienter la croissance des neurones dans le gel, mais deuxièmement d'essayer d'imprimer en 3D le gel pour ensuite fabriquer des structures avec un design précis.

Concernant le premier objectif, les premiers essais ont d'abord consisté en la gélification sous contrainte des alkylgalactonamides. En effet, l'extrusion directe de l'hydrogel est impossible à cause du phénomène de synérèse qui détruit complètement l'intégrité du gel. Cependant nous avons essayé de faire prendre le gel sous écoulement dans des tubes. Malheureusement cela s'est révélé infructueux puisque les tubes se bouchaient systématiquement. L'étude s'est alors portée sur une autre famille d'hydrogels – les glucamines – qui eux peuvent être extrudés directement grâce à leur propriété de thixotropie, qui est définie comme la variation réversible de la viscosité du gel sous l'effet d'une contrainte. Ce phénomène permet donc l'extrusion directe de l'hydrogel sans détruire son réseau tridimensionnel. Deux molécules, dont la Glu-C12 (Tableau 1) et une molécule déjà décrite dans la littérature[s] (appelée Jap-C16), ont donc été extrudées sous diverses conditions. L'alignement des fibres du gel a parfois été constaté dans le cas de Jap-C16. Cependant l'influence des conditions d'extrusion de ces gels étant difficiles à maitriser, nous nous sommes intéressés à une autre technique qui elle peut être appliqué aux gels d'alkylgalactonamides.

Cette technique de mise en forme d'hydrogel ne se base non pas sur la prise du gel en descente de température, mais par échange de solvant. Elle est connue depuis longtemps dans l'industrie textile et peut également s'appliquer à des gels. En effet, le gélifiant est dissout dans un solvant organique avec qui il a beaucoup d'affinité et cette solution est ensuite extrudée dans un bain de « non-solvant » où le gélifiant est peu soluble, provoquant ainsi la formation des fibres constituant le gel lorsque le non-solvant diffuse dans l'autre. Dans notre cas, la molécule de Gal-C7 est dissoute dans du diméthylsulfoxyde (DMSO) et la solution est extrudée dans un bain d'eau ultra pure. L'eau et le DMSO sont des solvants miscibles mais le DMSO étant légèrement plus dense que l'eau, par gravité, celui-ci forme un flux continu lorsqu'il est extrudé à la verticale dans le bain. Le gel prend alors la forme d'un filament et le DMSO peut être éliminé de l'hydrogel par diffusion dans le bain (Figure 11).

[s] Ohsedo, Y.; Oono, M.; Saruhashi, K.; Watanabe, H. N-Alkylamido-D-Glucamine-Based Gelators for the Generation of Thixotropic Gels. *RSC Adv.* **2014**, *4* (89), 48554–48558.

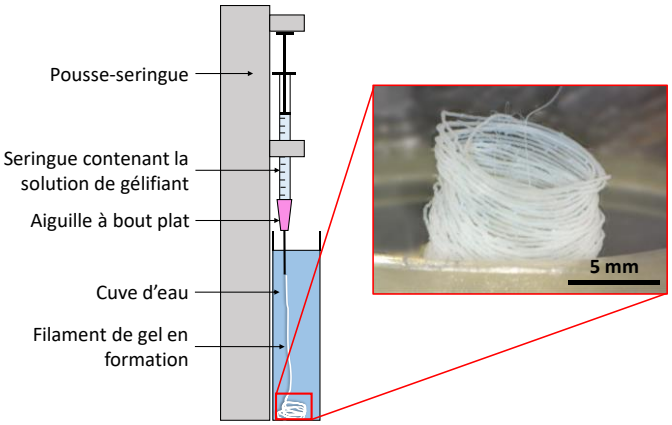

Figure 11 : Schéma du dispositif expérimental utilisé pour le wet spinning du Gal-C7 avec une photo du filament de gel formé par cette technique. Celui-ci s'est enroulé sur lui-même lors de l'extrusion.

Nous avons alors cherché les conditions d'extrusion propices à la formation d'un filament de gel, cela en faisant varier différents paramètres : la concentration en gélifiant dans la solution de DMSO, le débit auquel la solution est extrudée et la taille de l'aiguille employée. Un diagramme de phases a alors été établi visuellement pour déterminer si les conditions employées permettaient l'obtention d'un filament, induisaient le bouchage de l'aiguille, ou bien entrainaient la gélification trop tardive (Figure 12).

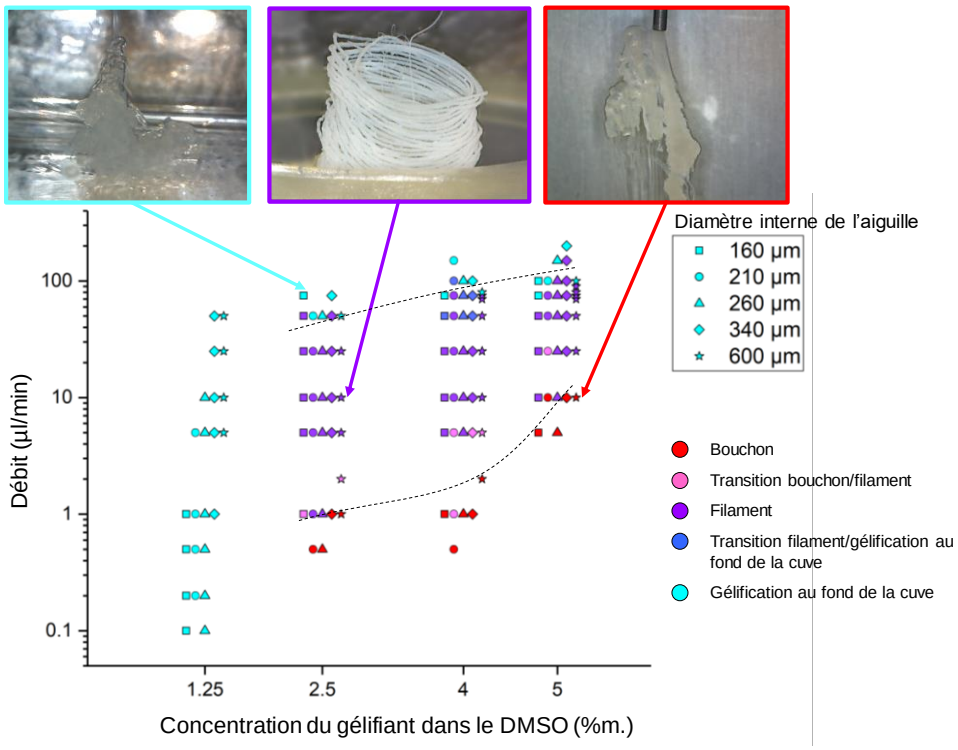

Figure 12 : Diagramme de phase sur les conditions d'obtention d'un filament de gel de Gal-C7 en wet spinning. En abscisse sont représentées les différentes concentrations en gélifiant dans le DMSO (les points sont légèrement décalés sur le graphe pour plus de clarté de lecture) et en ordonnée les débits appliqués (échelle logarithmique). Différents symboles sont utilisés pour les différentes tailles d'aiguille. Au-dessus du graphe sont disposées des photos du gel dans les différents régimes observés, de gauche à droite : gélification au fond de la cuve, obtention d'un filament et bouchage de l'aiguille.

Dans les conditions favorables à l'obtention d'un filament de gel, divers paramètres ont été caractérisés tels que la vitesse du jet de DMSO ou encore la relation entre le diamètre du jet de DMSO et celui du filament final. La composition finale en eau, DMSO et gélifiant a aussi été déterminée par analyse thermogravimétrique et a révélé qu'aucune trace de DMSO n'avait été détectée après extrusion dans le gel et que celui-ci est au final composé à 3 %m. en Gal-C7 et 97 %m. en eau (alors que la solution de départ était à 4 %m. en gélifiant dans le DMSO).

Les filaments d'hydrogel obtenus par wet spinning ont également été observés par diverses techniques de microscopie (Figure 13).

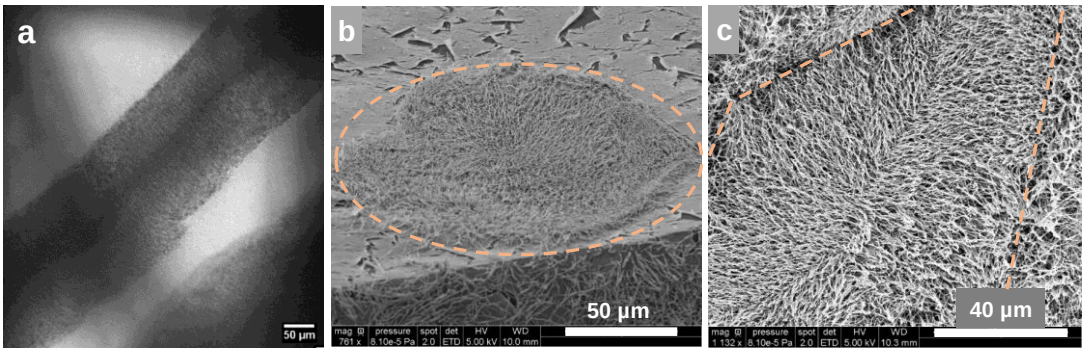

Figure 13 : Observation des filaments de gal-C7 obtenus par wet spinning. a. Observation en microscopie optique en transmission d'un filament de gel de gal-C7 extrudé à 50 µl/min à partir d'une solution à 4 %m. (échelle : 50 µm). b,c : Observations en cryo-MEB d'une coupe transversale (b) et longitudinale (c) d'un filament de gel.

En cryo-microscopie électronique à balayage, la chose la plus remarquable est la taille des fibres composant le gel qui est bien plus petite et plus monodisperse (136 ± 37 nm en moyenne) que celle des fibres des gels préparés en rampe de température (1,4 ± 2.0 µm en moyenne). Également, un certain alignement radial des fibres à l'intérieur du gel semble apparaître sur les clichés de cryo-MEB. En effet, cet alignement est certainement induit par la contre-diffusion de l'eau et du DMSO lors de l'extrusion du filament étant donné que c'est la diffusion de l'eau dans le jet de DMSO qui provoque la formation des fibres.

Le temps de vie des filaments dans diverses solutions a également été étudié. Dans des milieux tels que de l'eau pure ou du milieu physiologique conservés à température ambiante, la durée de vie des filaments d'hydrogels ne dépasse pas quelques jours. En se dégradant, les molécules de gélifiants se solubilisent dans le milieu et finissent par recristalliser, formant de grands cristaux translucides. Cependant, lorsque l'on utilise du milieu de culture cellulaire complété par du sérum de veau, à température ambiante, cette durée de vie dépasse le mois. En revanche, si le milieu est gardé à 37 °C (conditions de culture cellulaire), les filaments ne reste stables pas plus de quelques jours également, ce qui peut s'avérer problématique pour des applications en culture cellulaire.

L'étape suivante a alors été l'adaptation de la technique du wet spinning pour l'impression 3D. Pour cela un montage spécial a été mis en place qui a permis la déposition contrôlée du gel sur une surface grâce à une platine motorisée (Figure 14). La surface en question consistait en une lame de verre sur laquelle était fixée une membrane en polycarbonate, matériau sur lequel le gel a relativement une bonne adhésion.

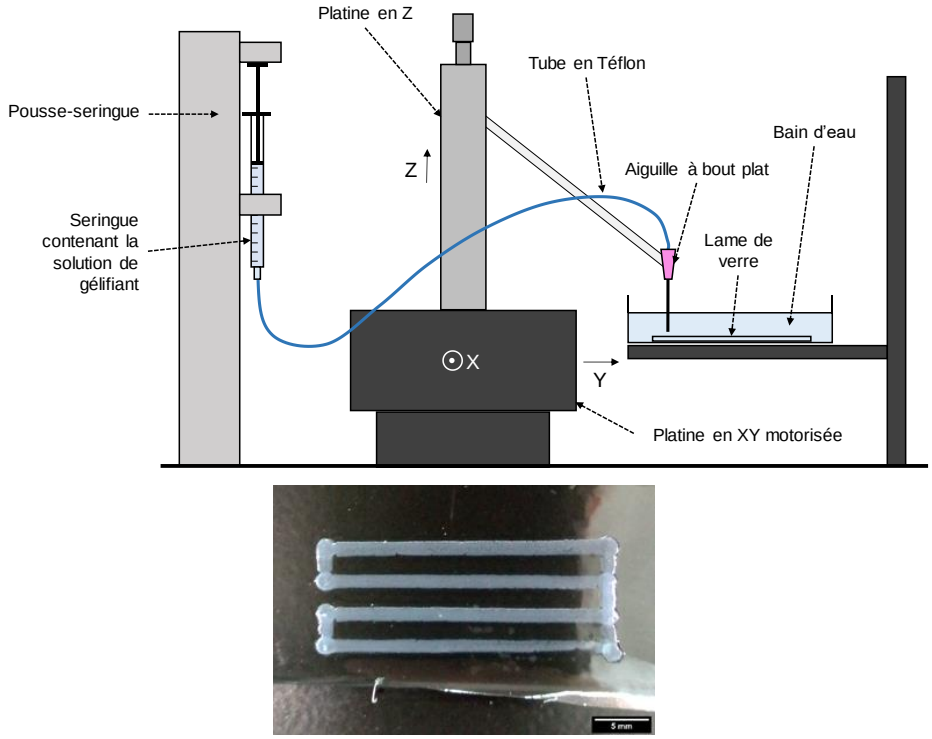

Figure 14 : Haut : dispositif expérimental utilisé pour l'impression 3D de gel de gal-C7. Bas : photo d'un dépôt de gel de Gal-C7 déposé en impression 3D (échelle : 5 mm).

Les conditions permettant l'adhérence du gel déposé sur la membrane ont également été recherchées, en jouant toujours sur le débit et la taille d'aiguille, mais aussi sur la vitesse de la platine ainsi que sur la distance entre l'aiguille et la surface de dépôt. En effet, ces conditions influent sur la vitesse de gélification du gel, qui elle-même influe sur l'adhérence du gel : plus le gel gélifie tôt, moins il aura adhérera à la surface. Les tailles des dépôts en fonction de ces conditions ont également été mesurées par microscopie optique ainsi que l'épaisseur des dépôts. Les largeurs des dépôts peuvent atteindre plus d'1 mm alors que leur épaisseur est d'environ 50 µm. Lorsque deux couches sont superposées, l'épaisseur du dépôt est doublée. Ceci ouvre donc les portes de l'impression 3D pour la technique du wet spinning, bien qu'il faille encore améliorer la dispersion et l'adhérence du gel sur la surface de dépôt.

Conclusion

Au cours de cette thèse, nous avons pu trouver une nouvelle classe de gélifiants de faible poids moléculaire adaptés à la croissance et à la différenciation des cellules souches neurales humaines. Ces gélifiants sont de simples molécules dérivées des glucides, relativement faciles à synthétiser à l'échelle du gramme et à purifier. Parmi les molécules de différentes familles, les alkylgalactonamides se sont révélés biocompatibles. De manière surprenante, un incrément d'un carbone dans la chaîne alkyle des gélifiants a considérablement modifié les propriétés des hydrogels et leur biocompatibilité. En particulier, le *N*-heptyl-D-galactonamide (Gal-C7) a donné des hydrogels avec une structure et des propriétés compatibles avec son application finale. Celui-ci a donc été choisi pour être testé pour la culture de cellules souches neurales humaines et s'est avéré être un très bon support pour leur croissance et leur différenciation en neurones ainsi qu'en cellules gliales après 7 jours *in vitro*. Malheureusement, il est difficile d'étudier les hydrogels pendant plus d'une semaine car ils se dégradent rapidement dans des conditions de culture cellulaire. Dans un deuxième temps, nous avons réussi à trouver une technique pour injecter, extruder et façonner les hydrogels de Gal-C7 qui sont normalement assez difficiles à manipuler à cause de la synérèse. Cette méthode est basée sur la gélification par échange de solvant et est appelée filage en voie humide ou « wet spinning ». Grâce à elle, des filaments d'hydrogel composés de 97% en poids d'eau et de 3% en poids de gélifiant peuvent être obtenus avec une structure microscopique assez différente de celle des gels obtenus par rampe de température. Les fibres qui composent l'hydrogel sont beaucoup plus minces, presque monodisperses en largeur et s'organisent radialement à l'intérieur du filament. De plus, nous avons pu adapter le processus de wet spinning à l'impression 3D. Les hydrogels peuvent ainsi être déposés sur un substrat de manière contrôlée et plusieurs couches peuvent être superposées pour augmenter la hauteur des dépôts. L'adhérence des gels à la surface n'est pas encore optimale, mais ce procédé est très prometteur pour l'application de gélifiants de faible poids moléculaire à l'impression 3D.

Les gélifiants d'alkylgalactonamide de bas poids moléculaire constituent donc des molécules très intéressantes pour la création de supports de culture cellulaire grâce à leur structure microscopique et leurs propriétés mécaniques particulières. Des travaux supplémentaires devraient être effectués pour améliorer leur stabilité dans les conditions de culture cellulaire, en particulier pour leur utilisation comme implants *in vivo*. La réticulation pourrait être une solution, mais la plus grande partie du travail ici serait de trouver le bon agent de réticulation qui ne nuirait pas aux propriétés mécaniques natives de l'hydrogel, qui sont essentielles à la croissance et à la différenciation des cellules. Une autre stratégie consisterait à coupler les hydrogels d'alkylgalactonamide à un autre matériau plus résistant, tel qu'un scaffold en polymère. En outre,

les filaments obtenus par wet spinning doivent être d'avantage testés en conditions de culture cellulaire et pour cela leur stabilité doit d'abord être améliorée, chose qui pourraient également être obtenue par réticulation. De plus, les gels obtenus par rampe de température et ceux par wet spinning ont été étudiés purs. Cependant, il est possible de jouer sur différents paramètres. Par exemple, l'incorporation d'additifs peut modifier leurs propriétés. L'organisation anisotrope des hydrogels doit être encore développée pour obtenir un alignement des neurones à l'intérieur des échafaudages. Poser simplement les filaments macroscopiques obtenus en wet spinning les uns à côté des autres pourrait représenter une solution potentielle à ce problème.

Abstract

Nowadays, repairing brain lesions is still one of the main challenges of tissue engineering. Meanwhile, work still has to be done for the creation of representative *in vitro* brain tissue models, especially when it comes to the biomaterials used to support cell growth. This present work consists in the development of a hydrogel as a biomaterial for the survival and growth of human neural stem cells. These (supra)molecular gels, the property of which is to form by self-assembly, may present many advantages for this kind of application. Indeed, their mechanical properties, their bioavailability and their microstructure – among others – make them interesting candidates for neuron culture. One family of supramolecular gelators have thus been synthesized, characterized and tested as cell culture scaffolds. Those gelators are alkylgalactonamides, which means they are derived from a sugar – the galactose – and an alkyl fatty chain. They form hydrogels by cooling down to room temperature after a first dissolution at high temperature. The cooling provokes the self-assembly of the molecules resulting in the formation of the fibers. During their preparation, it has been found that a controlled cooling rate enabled the formation of more homogeneous and more stable hydrogels that are compatible with cell culture conditions and with longer fibers. These hydrogels have shown a good biocompatibility as well as a good cell survival and a three-dimensional growth of human neural stem cells. The latter grew long neurites and expressed markers of neuronal (β3-tubulin) and glial differentiation (GFAP), especially on one of the hydrogels. The last part of this work was to use new 3D material structuring techniques in order to further construct well-defined centimetric scaffolds with these hydrogels. A technique of wet spinning based on solvent exchange was developed and enabled the direct and controlled extrusion of the hydrogel at room temperature. Thin and regular hydrogel filaments composed of monodisperse nanometric fibers can thus be obtained. Trials have also been done to apply this method to 3D printing. In the end, this project shows that some molecular gels can display properties particularly adapted for tissue engineering, especially with neural stem cells, and it also opens perspectives for the shaping of these delicate materials.

Keywords: Matrix for cell culture, Low molecular weight hydrogel, Self-assembly, Neuron, Fiber, Wet spinning

Résumé

La réparation de lésions cérébrales reste de nos jours un grand challenge de l'ingénierie tissulaire. De même, l'établissement de modèles *in vitro* représentatifs du tissu cérébral est un sujet qu'il reste à explorer, surtout du point de vue des biomatériaux à utiliser pour soutenir la croissance cellulaire. Ce travail consiste donc au développement d'un biomatériau de type hydrogel adapté à la survie et la croissance de cellules souches neurales humaines. Les gels de type (supra)moléculaires, qui ont la particularité de se former par auto-assemblage, pourraient présenter de nombreux avantages pour ce type d'application. En effet, ils possèdent entre autres des propriétés mécaniques, une biodisponibilité et une structuration aux échelles micro et nanométriques originale qui font de ces gels des supports intéressants pour la culture de neurones. Une famille de gélifiants supramoléculaires a donc été synthétisée, caractérisée et étudiée en tant que support de culture cellulaire. Ces gélifiants sont de type alkylgalactonamide, c'est-à-dire dérivés d'un sucre – le galactose – et d'une chaîne grasse de type alkyle. Ils forment des hydrogels par refroidissement jusqu'à température ambiante d'une solution de gélifiant préalablement portée à haute température. Le refroidissement entraîne la formation de fibres micrométriques par auto-assemblage des molécules. Il a été établi qu'un contrôle précis du refroidissement lors de leur préparation permettait l'obtention d'hydrogels plus homogènes, plus résistants, qui sont compatibles avec les conditions de culture cellulaire et avec des fibres plus longues. Ces hydrogels se sont révélés être biocompatibles, avec une survie et une croissance en trois dimensions des cellules souches neurales humaines en leur sein. Ces dernières développent de longs neurites et expriment des marqueurs de la différentiation neuronale (β3-tubuline) ou gliale (GFAP), notamment sur l'un des hydrogels. Le dernier aspect de ce travail a consisté à l'utilisation de nouvelles techniques de structuration en 3D des matériaux afin de construire avec ces hydrogels des supports centimétriques avec une forme bien définie. Une technique de filage en voie humide basée sur l'échange de solvants (wet spinning) a alors été mise au point permettant d'extruder l'hydrogel de façon contrôlée et directement à température ambiante. Elle permet d'obtenir de fins filaments de gel très réguliers soutenus par des fibres nanométriques de largeur monodispersée. Des essais ont également été effectués pour appliquer cette technique à l'impression 3D. Au final, ce projet démontre que certains gels moléculaires peuvent présenter des propriétés particulièrement adaptées pour l'ingénierie tissulaire notamment avec des cellules souches neurales et ouvrent également des perspectives dans le domaine de la mise en forme de ces matériaux délicats.

Mots-clés : Matrice pour culture cellulaire, Hydrogel moléculaire, Auto-assemblage, Neurone, Fibre, Wet spinning